Miguel Patrick Marx

BS Geologia

A new specimen of *Cardiocorax mukulu* with a nearly complete cranium from Angola

Dissertação para obtenção do Grau de Mestre em

Paleontologia

Orientador: Octávio Mateus, Prof. Associado com Agregação
FCT-UNL

19 May 2020

FACULDADE DE CIÊNCIAS E TECNOLOGIA
UNIVERSIDADE NOVA DE LISBOA

May 2020

Miguel Patrick Marx

BS Geologia

A new specimen of *Cardiocorax mukulu* with a nearly complete cranium from Angola

Dissertação para obtenção do Grau de Mestre em Paleontologia

Orientador: Octávio Mateus, Prof. Associado com Agregação FCT-UNL

Acknowledgments

Firstly, I would like to thank my advisor, Octávio Mateus, for allowing me to work on this incredible specimen, guiding me throughout the process of this work, and being an incredible mentor and friend. I would like to thank Mike Polcyn and Louis Jacobs for their generous advice, mentorship, and for introducing me to the two rules. I want to also thank Ricardo Araújo for the advice on how to measure plesiosaur vertebrae. I am immensely grateful to Projecto PaleoAngola for funding my stay in Angola for the 2019 summer excavation, and the Institute of Study for Earth and Man at SMU for funding my trip to Dallas in Dec. of 2017, providing financial aid for my visit in Nov. of 2019, and funding the CT scan of the cranium from MGUAN PA278. I also thank Chris Beard and Megan Sims for organizing my collection visit to the University of Kansas and Ross Seacord, George Corner, and Shane Tucker for accommodating my visit to the University of Nebraska- Lincoln in April of 2019. I would also like to thank Elliot Smith for providing a photograph of the skull of *Thalassomedon haningtoni* (UNSM 50132).

My friends and colleagues in Portugal are the best. Starting with Lourinhã, a big thanks to everyone at the Museu da Lourinhã for being so kind to me the past five years. I have learned a lot from my master's, PhD, and postdoc colleagues during my time in Portugal and I want to thank all of them for helping me develop as a scientist. I want to also thank Alex Guillaume, Andre Saleiro, João Russo, João Pratas, Hugo Campos, Darío Estraviz-Lopez, João Muchagato, Vincent Cheng, Francisco Costa, Cátia Ribeiro, Miguel Moreno-Azanza, Eduardo Puértolas and Filippo Rotatori for all the laughs and memories. Alexandra Fernandes (gurl!) for the amazing time spent together in the classroom and the field across three continents, and Roberto Pereira, Helena Oliveira, Andre Bonito, and Pedro Fialho for the great times we shared in class and during fieldtrips. A big thanks to Miguel Moreno-Azanza and Eduardo Puértolas for helping with the systematics portion of this work. Another big thanks to the Dream Team, Isabel, Celso, Euridice, and Simão for an amazing time excavating in Angola. I also want to thank Maciej Ruciński and Bruno Costa for making the Caparica PaleoHouse a great place to live and for the late nights playing Catan and Street Fighter. João Russo, Alexandra Fernandes, and Maciej Ruciński all helped prepare the flip jacket for the skull block, Bruno Costa helped mechanically prepare the mandible block, and Melanie Lex helped prepare the propodial block. Lastly, I need to thank my parents for their love and support, making this thesis possible at all.

Abstract

We report a plesiosaur specimen that includes the most well complete skull of an Elasmoaurid plesiosaurian from Sub-Saharan Africa. The new specimen, MGUAN PA278 from the Maastrichtian outcrops of Bentiaba, Angola includes fully preserved semicircular canals, both hyoids, a nearly complete mandible, seventeen cervical vertebrae, a rib and rib fragment, a propodial, and paddle elements. A CT scan of the cranium was performed at UTCT in Austin, TX to visualize all aspects of the cranium and to produce a digital model of the skull and casts of the endosseous labyrinths. The cranium was segmented at SMU using AMIRA software and compared to other well preserved elasmosaurid plesiosaurian skulls from collection visits and from the literature. MGUAN PA278 is diagnosed as *Cardiocorax mukulu* based on the morphology of the middle cervical neural spines. *C. mukulu* is returned from a phylogenetic analysis as a basal elasmosaurid outside of the Elasmosaurinae-Aristonectinae clade and the sister taxon of *Libonectes morgani*. The compact morphology of the endosseous labyrinth in MGUAN PA278 may be an adaptation to living in a pelagic environment.

Keywords: Africa, Angola, Maastrichtian, cranium, endosseous labyrinth

Resumo

Reportamos aqui o crânio mais completo dos plesiossauros de África Subsaariana. O novo espécime, MGUAN PA278, dos afloramentos maastrichtianos de Bentiaba, Angola inclui um crânio quase completo, incluindo canais semicirculares totalmente preservados, ambos hióides, uma mandíbula quase completa, dezessete vertebras cervicais, um fragment de costela e uma costela, um fêmur e elementos das barbatanase. Uma tomografia computadorizada do crânio foi realizada na UTCT em Austin, Texas, para visualizar todos os aspectos do crânio e produzir um model digital do crânio e moldes dos labirintos interósseos. O crânio foi segmentado na SMU usando o software AMIRA e comparado a outros crânios dos plesiossauros elasmosaurídeos bem preservados, através de visitas a coleções e da literatura. MGUAN PA278 é diagnosticado como *Cardiocorax mukulu* com base na morfologia dos espinhos neurais cervicais. C. mukulu é retornado de uma análise filogenética como um elasmosaurídeo basal fora do clado Elasmosaurinae-Aristonectinae e o táxon irmão de *Libonectes morgani*. A morfologia compacta do labirinto endósseo em MGUAN PA278 pode ser uma adaptação à vida em um ambiente pelágico.

Palavras-chave: África, Angola, Maastrichtian, crânio, labirinto interósseo

Graphical Abstract

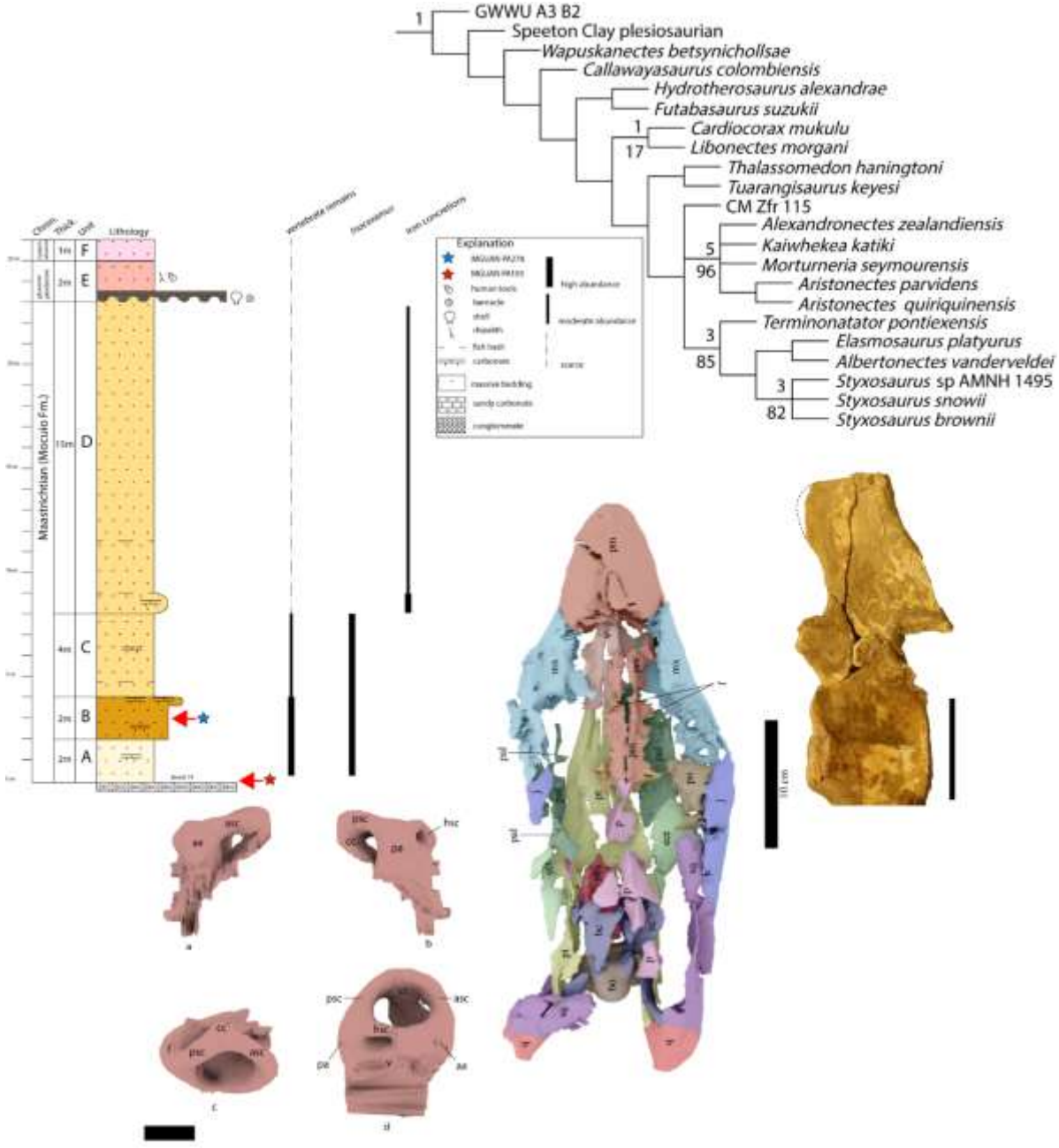

Table of Contents

Acknowledgements ii
Abstract iii
Resumo iv
Graphical abstract v
Anatomical and institutional abbreviations 5
1. Introduction 6
1.1 A history of Plesiosauria in paleontology 6
1.2 Angolan and southern hemisphere elasmosaurids 9
1.3 Geological setting of Bentiaba, Angola 17
1.4 Classification and Systematics of Plesiosauria 22
1.5 A review of the systematics of Elasmosauridae 33
2. Methods 41
3. Stratigraphic provenance of MGUAN PA278 44
4. Taphonomy 46
5. Results 54
5.1 Systematic paleontology, material, revised diagnosis of *Cardiocorax mukulu* 54
5.2 Craniofacial skeleton description 64
5.3 Palate description 86
5.4 Braincase and basicranium description 89
5.5 Endosseous labyrinth digital cast description 98
5.6 Mandible description 100
5.7 Dentition description 110
5.8 Axial skeleton description 114
5.9 Appendicular skeleton description 132
6. Phylogenetic analysis 137
7. Discussion 150
7.1 Amended diagnosis of *Cardiocorax mukulu* with comments on MGAUN PA103 150
7.2 Phylogenetic affinity of *Cardiocorax mukulu* 157
7.3 Sensory adaptations of *Cardiocorax mukulu* 161
8. Conclusion 163
Bibliography 164
Annex I- Elasmosaurid centrum measurements from literature 181
Annex II- Character scoring 190

Annex III- New character description 191
Annex IV- OBJ file of *Cardiocorax mukulu* (MGUAN PA278) digital model 192

Table of Figures

Figure 1.1.1: *Plesiosaurus dolichodeirus* holotype 7
Figure 1.2.1: Araújo et al., (2015a) figure of cervical vertebrae from MGUAN PA103 12
Figure 1.2.2: Araújo et al., (2015a) pectoral and pelvic girdle from MGUAN PA103 13
Figure 1.2.3: Araújo et al., (2015b) aristonectine elasmosaurid cervical series 14
Figure 1.2.4: Araújo et al., (2015b) histology sections of aristonectine propodials 15
Figure 1.3.1: Mateus et al., (2019) geologic map of Angola 19
Figure 1.3.2: Stratigraphic relationship of formations in Bentiaba, Angola 20
Figure 1.3.3: Close-up of Ombe basalt 20
Figure 1.3.4: Sandstone layers capped by carbonate benches 21
Figure 1.3.5: Strganac et al., (2014) stratigraphic section of Bentiaba, Angola 23
Figure 1.4.1: O'Keefe (2001) cladogram of Plesiosauria 25
Figure 1.4.2: Druckenmiller and Russell (2008) cladogram of Plesiosauria 26
Figure 1.4.3: Ketchum and Benson (2010) phylogeny of Plesiosauria 28
Figure 1.4.4: Benson and Druckenmiller (2014) phylogeny of Plesiosauria 30
Figure 1.5.1: Otero et al., (2018) cladogram of Elasmosauridae 39
Figure 1.5.2: O'Gorman (2020) phylogeny of Elasmosauridae 40
Figure 3.1.1: Local stratigraphy above Bench 19 (Bentiaba, Angola) 44
Figure 3.1.2: Excavation site of MGUAN PA278 45
Figure 4.1.1: Fauna associated with MGUAN PA278 48
Figure 4.1.2: Excavation of MGUAN PA278 with blocks arranged in in-situ arrangement 49
Figure 4.1.3: Excavation of MGUAN PA278 line drawing 50
Figure 4.1.4: Field sketch of MGUAN PA278 excavation 51
Figure 4.1.5: Line drawing of skull block in dorsal view 52
Figure 4.1.6: Photo of skull block in dorsal view 53
Figure 5.2.1: Skull of MGUAN PA278 in dorsal view 59
Figure 5.2.2: Skull of MGUAN PA278 in dorsal view with labels and elements outlined 60
Figure 5.2.3: Posterior view of MGUAN PA278 skull 61
Figure 5.2.4: Temporal bar of MGUAN PA278 62-63
Figure 5.2.5: Exposed dorsal surface of premaxillae 66
Figure 5.2.6: 3D model of MGUAN PA278 with and without labels 71-78

Figure 5.2.7: CT sections of skull 79-82
Figure 5.2.8: Right lateral view of *S. snowii* holotype (KUVP 1301) 83
Figure 5.2.9: Left lateral view of *S. snowii* holotype (KUVP 1301) 84
Figure 5.2.9.1: Left lateral view of *T. haningtoni* (UNSM 50132) 85
Figure 5.2.9.2: Exposed upper and lower tooth rows of *S. snowii* (KUVP 1301) 86
Figure 5.3.1: Cross-section of the basicranium and pterygoids 89
Figure 5.4.1: Anterior view of sella turcica and associated structures of the parabasisphenoid 95
Figure 5.4.2: Parasagittal section of braincase with cranial nerve openings in view 95
Figure 5.4.3: Parasagittal section of braincase with dorsum sellae and sella turcica in view 96
Figure 5.4.4: Plexus basilaris 96
Figure 5.4.5: CT sections of endosseous labyrinth 97-98
Figure 5.5.1: Endosseous labyrinth digital cast of MGUAN PA278 99
Figure 5.6.1: Right retroarticular process 104
Figure 5.6.2: Right coronoid process 105
Figure 5.6.3: Left retroarticular process 105
Figure 5.6.4: Dorsal view of mandible block 106
Figure 5.6.5: Dorsal view of mandible block with labels 107
Figure 5.6.6: Medial margin of right ramus of the mandible 108
Figure 5.6.7: Medial margin of right ramus of the mandible with line drawing 109
Figure 5.6.8: Articular suture in *S. snowii* (KUVP 1301) 110
Figure 5.7.1: Isolated teeth associated with MGUAN PA278 111
Figure 5.7.2: Mandibular symphysis 112
Figure 5.7.3: Close-up of tooth crown 113
Figure 5.8.1: Left lateral view of atlas-axis complex 116
Figure 5.8.2: Posterior view of atlas-axis complex 117
Figure 5.8.3: Ventral view of atlas-axis complex 117
Figure 5.8.4: Anterior cervical vertebra 1 120
Figure 5.8.5: Anterior cervical vertebra 2 120
Figure 5.8.6: Anterior cervical vertebra 4 121
Figure 5.8.7: Anterior cervical vertebra 6 121
Figure 5.8.8: Anterior cervical vertebrae 5 and 3 122
Figure 5.8.9: Anterior cervical vertebra 7 122
Figure 5.8.9.1: Proximal cervical vertebra 1 123
Figure 5.8.9.2: Proximal cervical vertebra 2 124
Figure 5.8.9.3: Proximal cervical vertebra 2 with neural spine attached 124

Figure 5.8.9.4: Proximal cervical vertebra 3 125
Figure 5.8.9.5: H-index graph 126
Figure 5.8.9.6: Cervical vertebrae series from MGUAN PA103 129
Figure 5.8.9.7: Posterior cervical vertebrae from MGUAN PA271 130
Figure 5.8.9.8: Rib fragment of MGUAN PA278 131
Figure 5.9.1: Figure of propodial 133
Figure 5.9.2: Figure of fibulare 134
Figure 5.9.3: Figure of distal tarsal element 135
Figure 5.9.4: Figure of phalanges block 136
Figure 6.1: Serratos et al., (2017) consensus tree 143
Figure 6.2: Replicated consensus tree of Serratos et al., (2017) 144
Figure 6.3: Consensus tree of Serratos et al., (2017) matrix including MGUAN PA278 144
Figure 6.4: Consensus tree of Serratos et al., (2017) matrix including *C. mukulu* hypodigm 145
Figure 6.5: Replicated consensus tree of Otero et al., (2018) 145
Figure 6.6: Consensus tree of Otero et al., (2018) 146
Figure 6.7: Otero et al., (2018) consensus tree with *E. carinognathus* pruned 146
Figure 6.8: Otero et al., (2018) consensus tree with MGUAN PA278 included 147
Figure 6.9: Otero et al., (2018) consensus tree with *C. mukulu* hypodigm included 147
Figure 6.9.1: O'Gorman (2020) with MGUAN PA103 included 148
Figure 6.9.2: Sachs et al., (2015) consensus tree with *C. mukulu* hypodigm included 149
Figure 6.9.3: Allemand et al., (2017) consensus tree with *C. mukulu* hypodigm included 149
Figure 7.1.1: Left scapula, left clavicle, and interclavicle from *C. mukulu* holotype (MGUAN PA103) 155
Figure 7.1.2: Pectoral girdle of *C. mukulu* holotype (MGUAN PA103) 156
Figure 7.2.1.: Cervical vertebrae morphotypes of Otero (2016) 159
Figure 7.2.2: Biogeographic distribution of elasmosaurid morphotypes from Otero (2016) 160

Table Index

Table 1: Plesiosaurian clade definitions 32
Table 2: Cranium measurements of MGUAN PA278 70
Table 3: Mandible measurements of MGUAN PA278 103
Table 4: Cervical centrum measurements of MGUAN PA278 125

Anatomical abbreviations

aa, anterior ampulla
aac, atlas-axis complex
an, angular
ar, articular
asc, anterior semicircular canal
atic, atlas intercentrum
atna, atlas neural arch
atr, atlas rib
axc, axis centrum
axna, axis neural arch
axr, axis rib
bc, braincase
bo, basioccipital
bs, basisphenoid
bpp, basipterygoid process
c, centrum
cc, crus communis
cl, clavicle
cor, coronoid
ct, crista trabecularis
d, dentary
ect, ectopterygoid
en, external nares
epi, epipterygoid
exo-op, exoccipital-opisthotic
f, frontal
fs, foramina subcentralia
hr, hypophyseal ridge
hsc, horizontal semicircular canal
icf, intercoracoid fenestra
icl, interclavicle
j, jugal
llr, lateral longitudinal ridge
ms, medial sinus
mx, maxilla
na, neural arch
nc, neural canal
ns, neural spine
p, parietal
pa, posterior ampulla
pal, palatine
pbs, parabasisphenoid
pm, premaxilla
po, postorbital
pof, postfrontal
poz, postzygapophysis
pr, prootic
pra, prearticular
prf, prefrontal
prz, prezygapophysis
ps, parasphenoid
psc, posterior semicircular canal
pt, pterygoid
q, qudrate
r, rib
sa, surangular
sc, scapula
scl, sclerotic ring
so, supraoccipital
spl, splenial
st, sella turcica
sq, squamosal
v, vomer
vk, ventral keel
vn, ventral notch;
vs, vestibule
qpt quadrate process of pterygoid

Institutional abbreviations

AMNH, American Musuem of Natural History, New York City, New York, U.S.A.; **ANSP**, Academy of Natural Sciences, Philadelphia, U.S.A.; **BMNH**, Natural History Museum, London, England; **CM**, Canterbury Museum, Christchurch, New Zealand; **FCT/UNL**, Faculdade de Ciências e Tecnologia da Universidade Nova de Lisboa, Caparica, Portugal (FCT/UNL); **GNS**, Geological National Survey (New Zealand), Lower Hutt, New Zealand; MGUAN, Museu Geologico da Universidade Agostinho Neto, Luanda, Angola; **GWWU**, Geomuseum, University ofMünster,Münster, Germany; **MLP**, Museo de la Plata, La Plata, Argentina; **MOZ**, Museum of New Zealand, Te Papa Tongarewa, Wellington, New Zealand; **ML**, Museu da Lourinhã, Lourinhã, Portugal; **MOR**, Museum of the Rockies, Bozeman, Montana, U.S.A.; **ROM**, Royal Ontario Museum, Toronto, Ontario, Canada; **SDSM**, South Dakota School of Mines and Technology, Rapid City, South Dakota, U.S.A.; **SGO.PV**, Paleontología de Vertebrados, Museo Nacional de Historia Natural, Santiago, Chile; **SGU**, Saratov State University, Saratov, Russia; **SMNK-PAL**, Staatliches Museum für Naturkunde Karlsruhe, Karlsruhe, Germany; **SMNS**, Staatliches Museum für Naturkunde, Stuttgart, Germany; **SMU SMP**, Southern Methodist University Shuler Museum of Paleontology, Dallas, Texas, U.S.A.; **TTU**, Museum of Texas Tech University, Lubbock, Texas, U.S.A.; **UCMP**, University of California Museum of Paleontology, Berkeley, California, U.S.A.; **KUVP**, University of Kansas Vertebrate Paleontology Collection, Lawrence, Kansas, U.S.A.; **UNSM**, University of Nebraska State Museum, Lincoln, Nebraska, U.S.A.; **UTA**, University of Texas at Austin, Austin, Texas, U.S.A.

Introduction: A history of Plesiosauria in paleontology

Plesiosaurians are a diverse clade of secondarily aquatic diapsid reptiles with a cosmopolitan distribution and a fossil record that extends from the Norian to the end of the Maastrichtian (Sennikov and Arkhangelsky, 2010; Benson and Druckenmiller, 2014; O'Gorman and Coria, 2016; Otero et al., 2018). Plesiosauria is a clade within Sauropterygia, the precise phylogenetic placement of Sauropterygia is ambiguous among reptile lineages. The general consensus among phylogenetic analyses suggests Sauropterygia is nested within Neodiapsida either outside of the archosauromorph-lepidosauromorph split or shares a more recent common ancestor with Lepidosauromorpha than with Archosauromorpha (Benton, 1985; Sues, 1987; Rieppel, 1989; Rieppel, 1994; Rieppel, 1999; Rieppel and Reisz 1999; Müller, 2004; Liu et al., 2011; Lee, 2013; Neenan et al., 2013; Benton, 2015; Sues, 2019).

Plesiosaurians and other marine reptiles were significant in establishing vertebrate paleontology as a scientific discipline (Buffetaut, 1987; Taylor, 1997). The first published study on plesiosaurs was done by Henry De la Beche (1796-1855) and Anglican cleric Reverend William Conybeare (1787-1857) (Taylor, 1997). It was in 1821 when De la Beche and Conybeare were reviewing ichthyosaur material when they realized that some of the bones did not match morphologically with identifiable ichthyosaur material (De la Beche and Conybeare, 1821). De la Beche and Conybeare determined that the new bones represented a form that was intermediate between ichthyosaurs and reptiles such as the crocodile, thus naming the new form *Plesiosaurus* from Greek meaning, "nearer reptiles" (Taylor, 1997). Conybeare's 1822 publication on both ichthyosaurs and plesiosaurs would feature the first known skull of a plesiosaur (plate 19 from Conybeare, 1822) and shortly after, in December of 1823, Mary Anning (1799-1847) would discover the first complete skeleton of a plesiosaur from the Sinemurian-aged Lower Lias Group, near Lyme Regis, England (Torrens, 1995; Taylor, 1997; Vincent & Taquet, 2010). This specimen (BMNH 22656) would become the holotype for *Plesiosaurus dolichodeirus* (Conybeare, 1824). Additional well-complete plesiosaurian skeletons were excavated from the Toarcian aged outcrops of Baden-Württemberg, Germany (Dames, 1895; Bardet et al., 1999; Benson et al., 2012). French anatomist, Henry de Blainville (1777-1850) named the order Plesiosauria in 1835 based on general features of plesiosaurian anatomy that are distinguishable from other known reptiles (Blainville, 1835; von Huene, 1921; Ketchum and Benson, 2010).

Figure 1.1.1. The holotype of *Plesiosaurus dolichodeirus* Conybeare 1824 (BMNH 22656) on display at the Natural History Museum (London).

Outside of Europe, progress on plesiosaurian research would initiate in the U.S., starting at the mid-nineteenth century. American paleontologist, Joseph Leidy (1823-1891), would name and describe the first plesiosaur specimens from the U.S., *Cimoliasaurus magnus* from Late Cretaceous glauconitic outcrops in New Jersey, and *Discosaurus vestus* from the Cretaceous of Alabama (Leidy, 1851; Welles, 1962; Ebersol and Dean, 2013). Both of which are now considered *nomina dubia*. Excavations in the western interior of the U.S. would reveal the first large-bodied, long-necked plesiosauroids (Cope, 1868, 1869; Williston, 1890, 1903, 1906, 1914, 1925, Williston and Moodie, 1913, 1917; Welles, 1943). The western interior of the U.S. encompasses the Graneros Shale, Greenhorn Limestone, Carlile Formation, Niobrara Formation, and the Pierre Formation which represent transgression and regression events of the Western Interior Seaway during the radiation and diversification of Xenopsaria and its sub-clades (Welles, 1943, 1952, 1962; Carpenter, 1996, 1997, 1999; Schumacher and Everhart, 2005; Benson and Druckenmiller, 2014; Otero, 2016). From the late 19th century to mid-20th century, plesiosaurians from the western interior of the U.S. were recovered that would provide significant contributions toward understanding their taxonomy and evolutionary history (Cragin, 1888; Cope, 1869; Williston, 1890; Williston, 1903; Welles, 1943, 1959; Carpenter, 1996, 1997, 1999; Otero 2016; Sachs et al., 2015, 2018). The anatomical descriptions made by American paleontologists, Samuel W. Williston and Samuel P. Welles would be significant toward understanding the taxonomy of Western Interior Basin plesiosaurians and establish a comparative framework for future studies (Williston 1903, 1906; Welles 1943, 1949, 1952, 1962).

Globally, plesiosaur research has advanced, allowing for the discovery and description of new specimens that have significantly enhanced our understanding of plesiosaur systematics, paleobiology, and biogeography. This includes important contributions from Australia (Romer and Lewis, 1959; Thulborn and Turner, 1993; Cruickshank et al., 1999; Kear, 2002a, 2002b, 2003, 2004, 2005a, 2005b, 2006, 2007, 2016), New Zealand (O'Gorman et al., 2017b; Otero et al., 2016), Japan (Sato and Storrs, 2000; Sato et al., 2006; Obata et al., 2007; Shimada et al., 2010; Sato et al., 2012; Utsunomiya, 2019), Russia (Averianov and Popov, 2005; Sennikov and Arkhangelsky, 2010; Berezin, 2011; Zverkov et al., 2017; Fischer et al., 2017; Berezin, 2018), the Middle East (Werner and Bardet, 1996; Bardet and Pereda-Suberbiola, 2002; Kear et al., 2008; Bardet, 2012; Rabinovich et al., 2014), Norway (Knutsen et al., 2012a; Knutsen et al., 2012b; Druckenmiller and Knutsen, 2012; Liebe and Hurun, 2012), Portugal (Smith et al., 2012), Spain (Bardet et al., 2008; Bardet et al., 2018; Quesada et al., 2019), Greenland (Marzola et al., 2018), Canada (Kubo et al., 2012; Sato et al., 2011), Columbia (Noè et al., 2003; Páramo et al., 2016; Páramo et al., 2018; Páramo et al., 2019), Argentina (Lazo and Cichowolski, 2003; Gasparini et al., 2003; Gasparini et al., 2007; O'Gorman et al., 2010; O'Gorman et al., 2015a), Chile (Otero et al., 2012) , and even Antarctica (Chatterjee et al., 1989; Kellner et al., 2011; Martin et al., 2007; O'Gorman et al., 2019a, 2019b). The worldwide distribution of plesiosaurs, and their long temporal duration during the Mesozoic has allowed for the discovery of plesiosaurian remains on every continent and in dozens of additional countries.

The fossil record of plesiosaurians however, on the entire continent of Africa has remained quite poor overall. There are certain geologic and environmental conditions that are responsible for a significant lack of not only plesiosaur material, but Mesozoic amniote fossils in general (Jacobs et al., 2006; Mateus et al., 2019, figure 4.2). An extensive metamorphic plateau that traverses much of the interior of Africa, and younger overlying layers of rock makes access to Mesozoic outcrops difficult (Jacobs et al., 2006; Mateus et al., 2019). There are only seven total taxa that have been named and described from the continent of Africa, with one being a *nomen dubium* (Andrews, 1911; Cruickshank, 1997; Arambourg, 1952; Bardet et al., 2003; Buchy et al., 2005; Buchy et al., 2006; Vincent et al., 2011; Lomax and Wahl, 2013; Sachs and Kear, 2017; Allemand et al., 2018; Allemand et al., 2019). Plesiosaurian fossil material is scare throughout Africa but is highly abundant in the Lower Maastrichtian outcrops of Bentiaba, Angola (Jacobs et al., 2006; Mateus et al., 2012; Araújo et al., 2015a; Araújo et al., 2015b). African plesiosaurians diagnosable to the species level have only been reported from Morocco, Angola, and South Africa. Isolated and fragmentary remains of plesiosaurs have been found in other localities in Africa, however many are not diagnosable to the intrafamilial level (Cruickshank, 1997; Benton et al., 2000).

Angolan and southern hemisphere elasmosaurids

Plesiosaur remains have been recovered from various localities in Angola, but Iembe in Bengo Province and Bentiaba in Namibe Province stand out as being particularly rich localities (Jacobs et al., 2006; Mateus et al., 2012; Araújo et al., 2015a; Araújo et al., 2015b). Early reports of vertebrate remains from Namibe provence in Southern Angola do not entail detailed descriptions, but rather notes of interest. The earliest report of Mesozoic marine amniote fossils in Namibe (historically named Moçamedes) comes from Nascimento (1898), where he writes on a layer with "a large amount of calcified bones mixed with shells and other sea creatures" north of the Carcavalho Lagoon in Moçamedes. Choffat (1905) focuses on the invertebrate fossil record and does not comment on vertebrate remains. Dartevelle and Casier (1943-1959) mistook a fragment of a plesiosaur rib for a dinosaur tooth (figured in Mateus et al., 2012). Multiple discoveries of plesiosaur fossils would come to light throughout the second half of the 20th century (Antunes, 1961, 1964, 1970; Neto, 1960, 1964; Lapão, 1972). However, none of these specimens would be described in detail. Antunes (1961) published on reptile remains collected by Mascarenhas Neto (1960) in Iembe, and reported plesiosaur vertebrae and girdle elements from Iembe, as well as isolated plesiosaur teeth and vertebrae from Maastrichtian-aged outcrops in Cambota, Cabinda, Barra do Dande, the Moçamedes Basin, Ambrizete, and Bentiaba, and teeth from Fazenda dos Cavaleiros (Antunes, 1964, 1970). Neto (1964) reports the occurrence of reptile teeth from the Maastrichtian of Bentiaba (formerly São Nicolau). South of Sumbe (formerly Novo Redondo), Lapão (1972) documented vertebrae from a Maastrichtian outcrop, designating them to *Plesiosaurus*. However, the genus *Plesiosaurus* is constrained to the Lower Jurassic of Europe, and thus any taxonomic designation for it in the Cretaceous is dubious.

Paleontological fieldwork in Angola would come to a halt in the mid-1970s, with the fight for independence, followed by a civil war which would continue until 2002. Recent paleontological fieldwork was thus only possible near the start of the 21st century. In 2005, the first field-based paleontological exploration since the end of the Angolan Civil War would be led by the International Projecto PaleoAngola team, composed of paleontologists and geologists from The United States (Louis Jacobs and Michael Polcyn), Portugal (Octávio Mateus), the Netherlands (Anne Schulp), and Angola. A total of 14 excavations between 2005 and 2019 have yielded several plesiosaur specimens and one new taxon (Araújo et al., 2015a).

The most complete elasmosaurid skeletons are recovered from a bonebed above the 'Bench 19' sandy carbonate layer at Bentiaba, Angola. The elasmosaurid, *Cardiocorax mukulu* Araújo, Polcyn, Schulp, Mateus, Jacobs, Gonçalves, Morais, 2015a was described based on a series of five 'posterior' cervical vertebrae and one isolated anterior cervical vertebra, one dorsal vertebra, fragments of dorsal ribs, nearly complete pectoral and pelvic girdles and a forelimb that includes a humerus, radius, ulna and

isolated phalanges (Figure 1.2.1. and 1.2.2.) (Araújo et al., 2015a). Autapomorphies diagnosing *C. mukulu*, as strictly mentioned in Araújo et al., 2015a, include: (1) bilateral ventral buttress of the coracoid asymmetrical (2) a highly reduced dorsal blade of the scapula (3) medial contact between the scapulae and clavicles that extends along the entire medial surface (4) the shaft of the scapula is ellipsoid in cross-section and splays anteriorly (5) The ventral area of the clavicles is almost as broad as the ventral area of the scapulae (6) There is medial contact between the clavicles along the entire medial length (7) The neural spines of the posterior cervical vertebrae exhibit an angled apex (8) the neural spines of the posterior cervical vertebrae almost touch adjacent neural spines (9) The neural spines of the cervical vertebrae are transversally broad; the length of the neural spine base is only slightly smaller than the length of the centrum.

C. mukulu is unique among elasmosaurids in having a highly reduced dorsal blade of the scapula and an expansive surface area on the ventral side of the coracoids; it is hypothesized in Araújo et al. (2015a) that atrophy of the muscles associated with abduction of the forelimbs and an expansion of the muscles associated with adduction (expanded attachment sites on the ventral surface of the coracoids, scapulae and clavicles) suggest a protraction-retraction based movement of the limbs rather than the "underwater flying" method hypothesized by other plesiosaur researchers (Araújo et al., 2015a; Robinson, 1975). The humerus of *C. mukulu* is also proximodistally short relative to its distal width and suggests an increase in mechanical advantage associated with limb movement. There is a general trend within Sauropterygia for a reduction in the dorsal blade of the scapula and shortening of the humerus in more derived forms through the Mesozoic (Araújo et al., 2015a).

Aristonectine plesiosaur material gen. et. sp. indet. is also reported from the 'Bench 19' section of Bentiaba, although a moderately well-complete individual has yet to be discovered (Figure 1.2.3.). Taxonomic assignment to Aristonectinae is based on the anterior-middle cervical vertebrae being approximately as long as high (Benson & Druckenmiller, 2014, ch153:1; Araújo et al., 2015b). Araújo et al., 2015b further unite the Angolan aristonectine material with the New Zealand specimens (MONZ R1526, GNS CD427-429 and GNS CD428) based on the v-shaped neurocentral suture in lateral view of the anterior to middle cervical vertebrae (Benson & Druckenmiller, 2014, 172:1). Araújo et al., (2015b) report the character separating the Angolan and New Zealand aristonectines from *Aristonectes* and *Khaiwhekea* is the presence of the lateral ridges on the anterior cervical centra on the latter two taxa in their phylogenetic analysis (Benson & Druckenmiller, 2014, 154:1).

The Angolan aristonectine material was determined to also be morphologically indiscriminate from aristonectine material from Patagonia, not diagnosable to the species level (Araújo et al., 2015b). Histological sectioning from two specimens (MGUAN PA85 and MGUAN PA550) suggested an adult ontogenetic stage (Araújo et al., 2015b) (Figure 1.2.4.). A mid-diaphyseal section from MGUAN PA85 exhibits primary and secondary osteons with three lines of arrested growth, and haversian remodeling along the interior region of the cortical bone. The metaphyseo-diaphysis section from MGUAN PA85 also exhibits three lines of arrested growth in the cortices with secondary osteons in the deep regions of the cortices, and a highly remodeled medullary spongiosa. A metaphyseo-diaphyseal section from MGUAN PA550 exhibits only one line of arrested growth and a highly cancellous cortex. The external morphology of the aristonectine material suggests a juvenile ontogenetic stage based on the lack of articular facets on the propodials, lack of a scapular and glenoid facet on the coracoid, and unfused neural arches and ribs on the cervical vertebrae. Araújo et al., 2015b place the Angolan aristonectine material as a ‘Brown juvenile’ (Brown, 1981) and a ‘Wiffen adult’ (Wiffen et al., 1995), thus suggesting paedomorphism.

Figure 1.2.1. (A) Cervical vertebrae series (B) anterior cervical vertebra (C) dorsal rib (D) dorsal vertebra centrum from the holotype of *Cardiocorax mukulu* (MGUAN PA103) Araújo et al., (2015a). Fig. 2 from Araújo et al., (2015a).

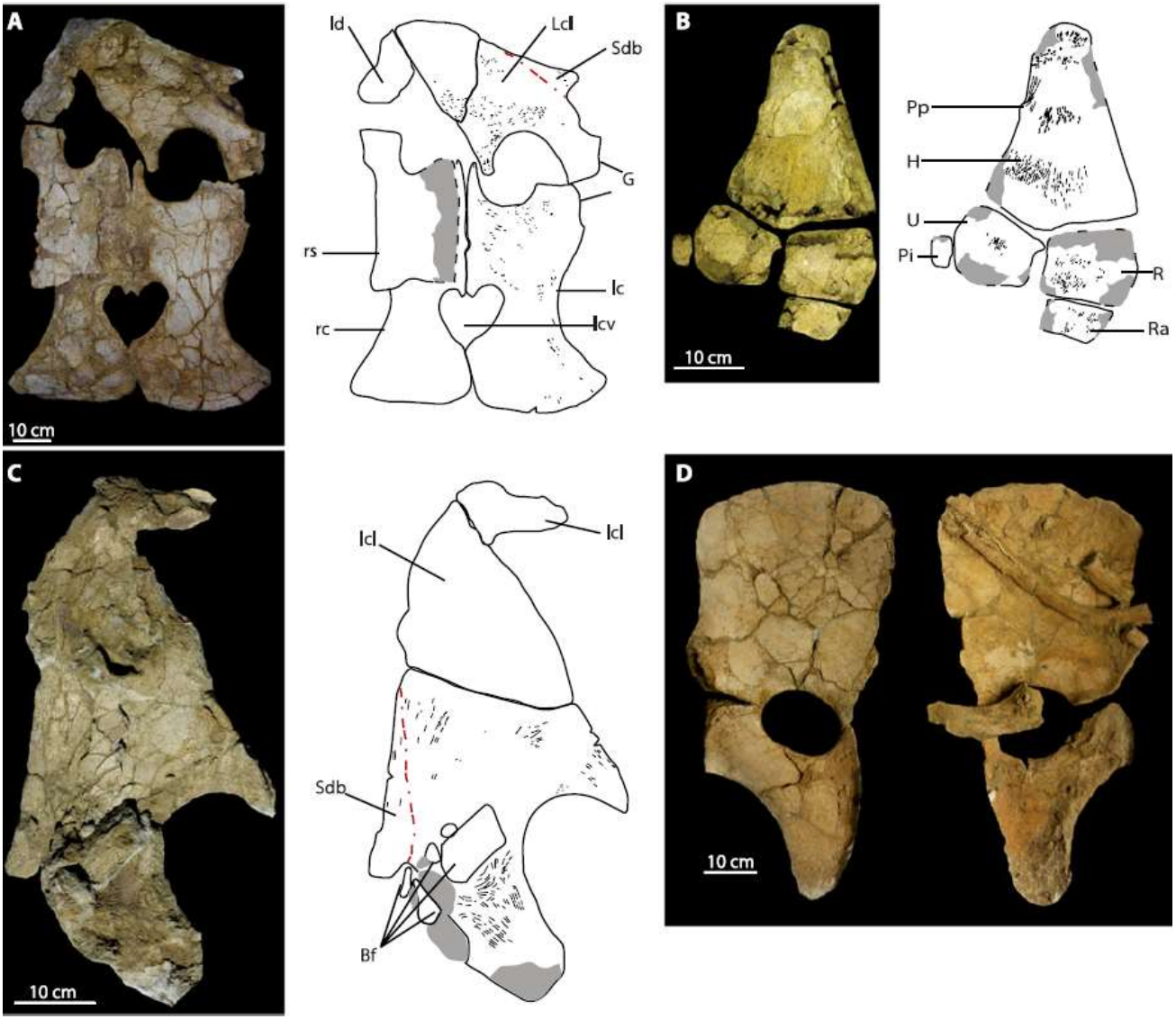

Figure 1.2.2. Girdle and limb elements from *C. mukulu* (MGUAN PA103) (A) pectoral girdle (B) humerus with radius, ulna, radiale and supernumerary element articulated (C) left scapula, clavicle, and interclavicle (D) left half of pelvic girdle in dorsal (left side) and ventral view (right side). Fig 3 from Araújo et al., (2015a).

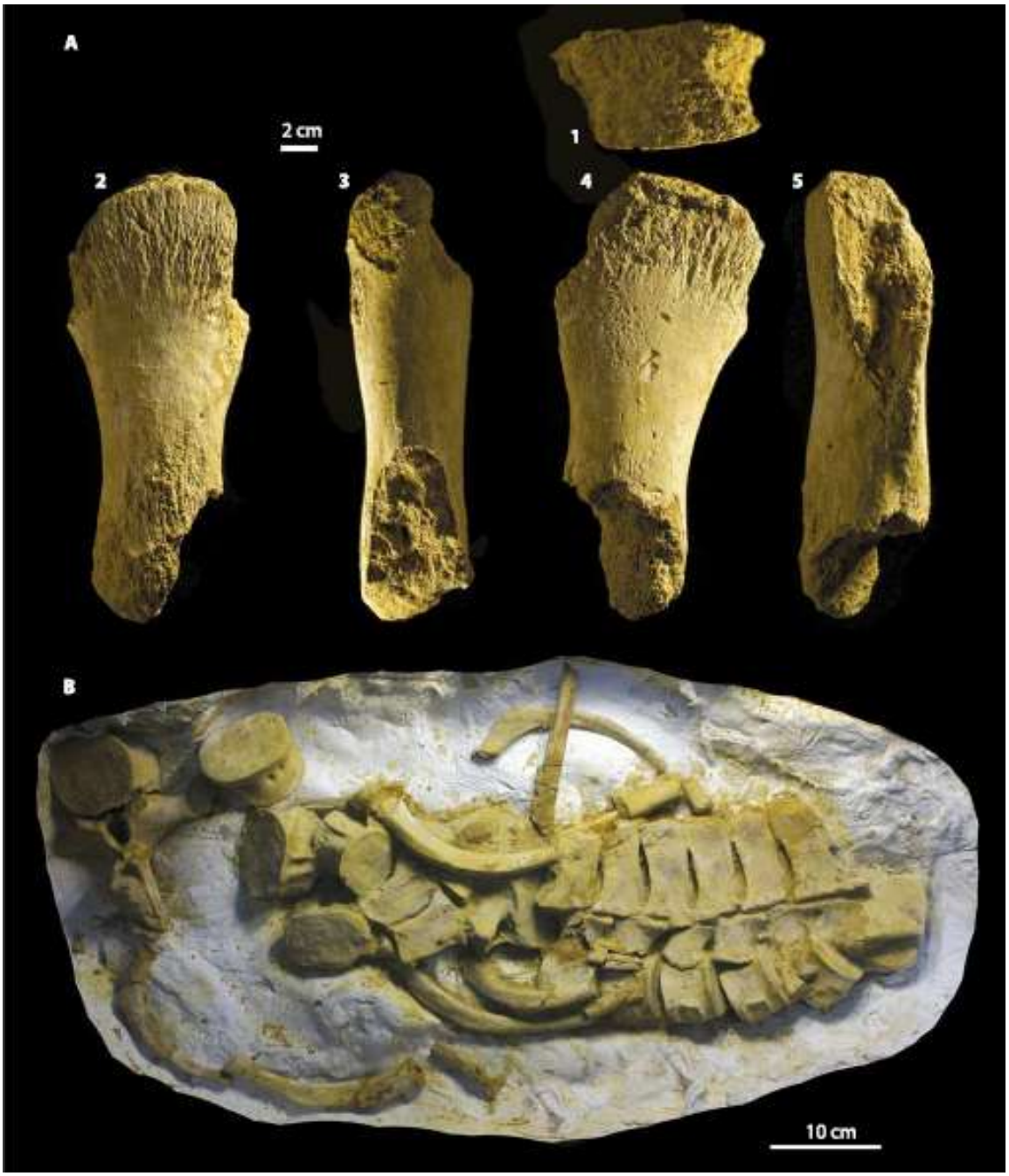

Figure 1.2.3. Aristonectine elasmosaurid (MGUAN PA85) (A) propodial in proximal (1) dorsal (2) preaxial or postaxial view (3) ventral (4) preaxial or postaxial view (5). (B) cervical and pectoral vertebrae series. Fig. 1 from Araújo et al., (2015b).

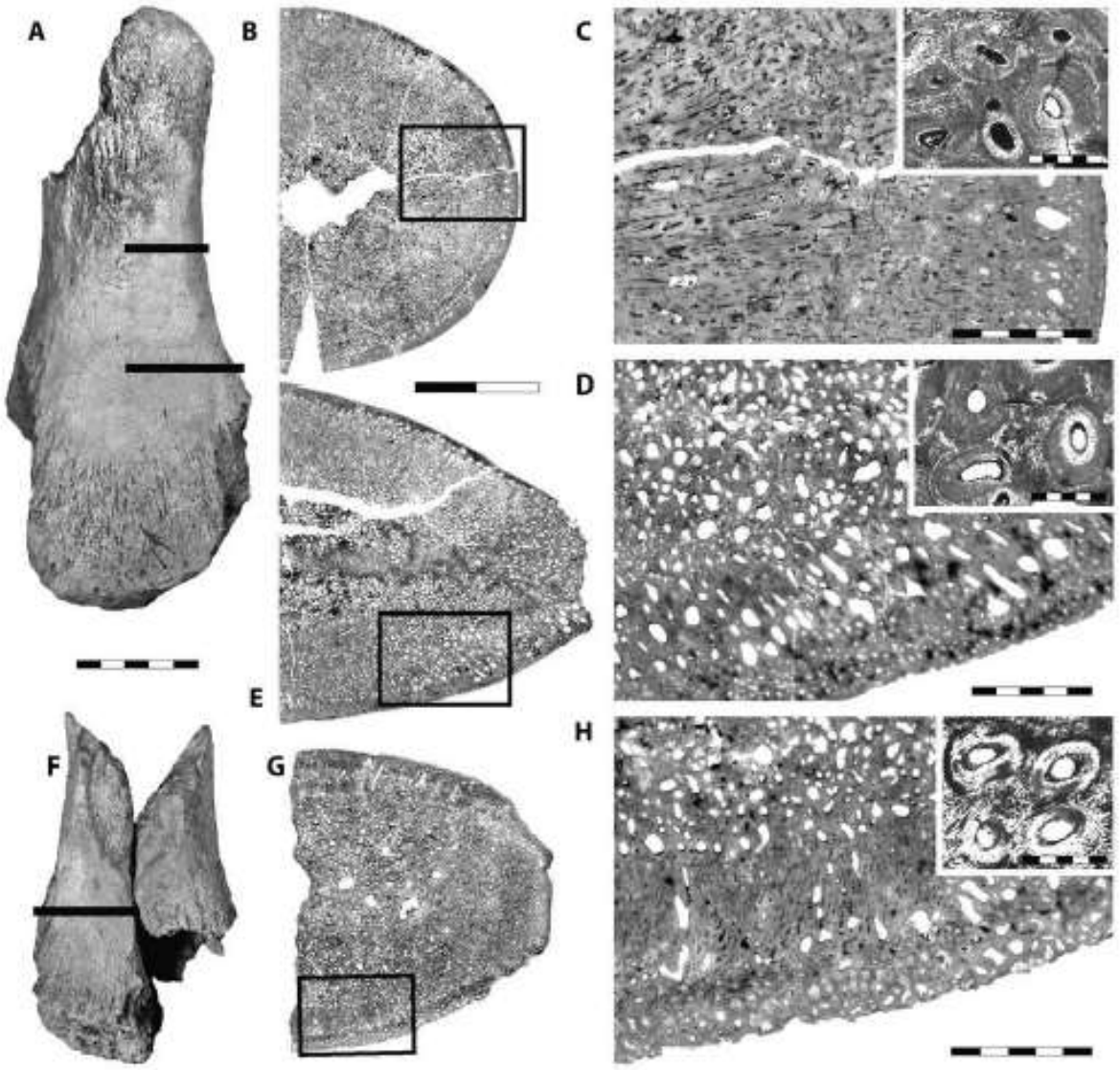

Figure 1.2.4. Aristonectine elasmosaurid histology samples. (A) location of propodial sections from MGUAN PA85 (B-C) histology section from the diapophysis (D-E) histology section between the diapophysis and epiphysis (F) location of propodial section from MGUAN PA550 (G-H) histology section between the diapophysis and epiphysis. Fig. 8 from Araújuo et al., (2015b).

Southern Hemisphere elasmosaurids have received less scientific attention relative to their Northern Hemisphere counterparts. However, the Weddellonectian Biogeographic province, as defined by Zinsmeister 1979 to be Patagonia, Western Antarctica and New Zealand, has emerged as a region of concentrated interest for elasmosaurid research (Otero et al., 2012; O'Gorman and Coria, 2016; O'Gorman et al., 2017b; Otero et al., 2018; O'Gorman, 2020). Within the Southern Hemisphere, recent phylogenetic analyses have found support for two clades: Weddellonectia O'Gorman and Coria, 2016 and Aristonectinae O'Keefe and Street, 2009. Weddellonectia was recently defined in the large-scale phylogenetic analysis of O'Gorman (2020) as the most inclusive clade within Elasmosauridae that contains *Aristonectes quiriquinensis* Otero, O'Gorman, Moisley, Terezow, and McKee, 2018 but not *Elasmosaurus platyurus* Cope, 1868. Weddellonectia is a clade that radiated within the Late Cretaceous and is comprised of both aristonectine and non-aristonectine elasmosaurids from the Southern Hemisphere and circum-Pacific (O'Gorman and Coria, 2016; O'Gorman, 2020). *Kawanectes lafquenianum* O'Gorman, 2016, *Vegasaurus molyi* O'Gorman, Salgado, Olivero, and Marenssi, 2015b, *Aphrosaurus furlongi* Welles, 1943, *Morenosaurus stocki* Welles, 1943, and two elasmosaurid specimens not diagnosable to the genus level from Antarctica (MLP 14-I-20-16 and MLP 15-I-7-48) comprise the Weddellian non-aristonectine elasmosaurids (O'Gorman and Coria, 2016; O'Gorman, 2020). *Futabasaurus suzukii* Sato, Hasegawa, and Manabe, 2015, and *Tuarangisaurus keyesi* Wiffen and Moisley 1986 may not be included in the clade, Weddellonectia (O'Gorman and Coria, 2016; O'Gorman et al., 2017b; Otero et al., 2018). Weddellian non-aristonectine elasmosaurids from the upper Maastrichtian of Antarctica (MLP 14-I-20-16 and MLP 16-I-7-48) reveal the survival of non-aristonectine elasmosaurids in the Weddellian biogeographic province across a possible faunal turnover event between the lower Maastrichtian and upper Maastrichtian (Consoli and Stilwell, 2009; Otero et al., 2015; O'Gorman and Coria, 2016).

Within Weddellonectia is the derived clade, Aristonectinae, which is distinct from all other elasmosaurid plesiosaurains based on a unique cranial morphology, a high tooth count in the maxillae and dentary, and distinctly short cervical vertebrae (ex. *A. parvidens*, *Kaiwhekea katiki* Cruickshank and Fordyce, 2002) (O'Gorman, 2015). Aristonectines achieved the largest estimated body sizes for Elasmosauridae, and their unique "oral battery", and mandible morphology has been hypothesized to be used for filter feeding (O'Keefe et al., 2017). Both the time and place of origin for Aristonectinae remains ambiguous. *Futabasaurus suzukii* (Santonian in age from Japan) has been recovered as an aristonectine in previous phylogenetic analyses (Otero et al., 2012; Otero et al., 2014; Otero et al., 2016) and not in others (O'Gorman, 2016; O'Gorman, 2020). If *S. suzukii* is a true Aristonectine, it would be the earliest known aristonectine, and could suggest a Northern Hemisphere origin (O'Gorman, 2015). The remains of

extremely ‘long-necked’ elasmosaurids (Elasmosaurines) have been documented in the Southern Hemisphere, thus elasmosaurines are not endemic to the Western Interior Seaway (Otero et al., 2015).

Within the southern hemisphere, Australia is also rich in terms of elasmosaurid plesiosaurian remains. However, remains of individual specimens are fragmentary, with historical species now considered *nomina dubia* (Kear, 2003). The Aptian-Albian aged epicontinental deposits of the Eromanga Basin are particularly rich in plesiosaur and other marine reptile remains (Kear, 2003). *Eromangasaurus australis* Sachs, 2005 was recovered from the lower Cretaceous Eromanga Basin, and is the only elasmosaurid species from Australia that includes a well-complete cranium and mandible (Kear, 2005). *E. australis* is one of the earliest known elasmosaurid species and exhibits primitive characters, including circular dentition, and the possible presence of a pineal foramen, possibly indicating a basal position within Elasmosauridae (Kear, 2016). The only other elasmosaurid plesiosaurian that is diagnosable to the species level, is *Opallionectes andamookaensis* Kear, 2006 from the lower-middle Aptian section of the Bulldog Shale, Eromanga Basin, which has not been utilized in any phylogenetic analysis (Kear, 2006).

Geologic Setting of Bentiaba, Angola

The formation of the fossiliferous outcrops along the coast of Angola are the product of a rifting process, that began between the southern tips of Africa and South America during the Late Jurassic (Nurnbergy and Muller, 1991). Rifting of the South Atlantic may have developed along The Walvis Ridge, and progressively traveled north (Standlee et al., 1982; Jacobs et al., 2006; Gaina et al., 2013; Jacobs et al., 2016). Oceanic floor formed along the coast of Angola by the Barremian, with oceanic surface circulation between the South Atlantic and North Atlantic occurring in the Albian (Jacobs et al., 2006; Ogg and Smith, 2004; Reyment and Dingle, 1987; Maisey, 2000).

Off-shore seismic and sediment core data suggest that after the synrift sequence, there is a massive unit of sandstone layers 200 meters thick; this can be interpreted as the first event of deposition on the Angolan coast (Jacobs et al., 2006; Ala and Selley, 1997; Marton et al., 2000). Above the massive sandstone layers is a Lower Aptian unit is composed of evaporites and suggests a period of isolation from open ocean circulation. After the evaporite section are massive carbonate and clastic units that extend through the Late Cretaceous and Paleogene and represent an established connection between the South and North Atlantic (Jacobs et al., 2006; Brognon and Verrier, 1966a, b; Gerrard and Smith, 1982). The continent of Africa experienced uplift throughout the Cenozoic, resulting in the exposure of Mesozoic marine deposits (Jacobs et al., 2006; Bond, 1978; Sahagian, 1988; Lunde et al., 1992; Nyblade and Robinson, 1994).

The stratigraphic section from Bentiaba ranges in age from Cenomanian to Late Maastrichtian, based on carbon isotope analyses, magnetostratigraphy, and $^{40}Ar/^{39}Ar$ dating, with most marine amniote fossils being located in the Late Campanian and Maastrichtian horizons (Strganac et al., 2014). The stratigraphy from Bentiaba was described in detail by Strganac et al., (2014) and is summarized here in order to provide an understanding of the lithology of the rock units at Bentiaba and changes in the environment through time. The base of the measured stratigraphic section is in contact with the Piambo Fm., approximately 20 m in thickness, formed by red sandstone and conglomerate. Above the Piambo Fm., the Salinas Fm. is 60 m in thickness and represents a shallow-marine unconformity that overlies this base. The lower 24 m section of the Salinas Fm. is composed of blue-grey sandstone with conglomerate channels intercalating the sand beds. Two coquina layers are present within the Salinas Fm., with the upper-most coquina layer below the lowest tan-yellow fine sandstone and siltstone in the whole section (Figure 1.3.5.). The top 10 meters of the exposed Salinas Fm. contain Late Turonian-Early Coniacian ammonite remains and correlate with beds I through IX in Cooper (2003).

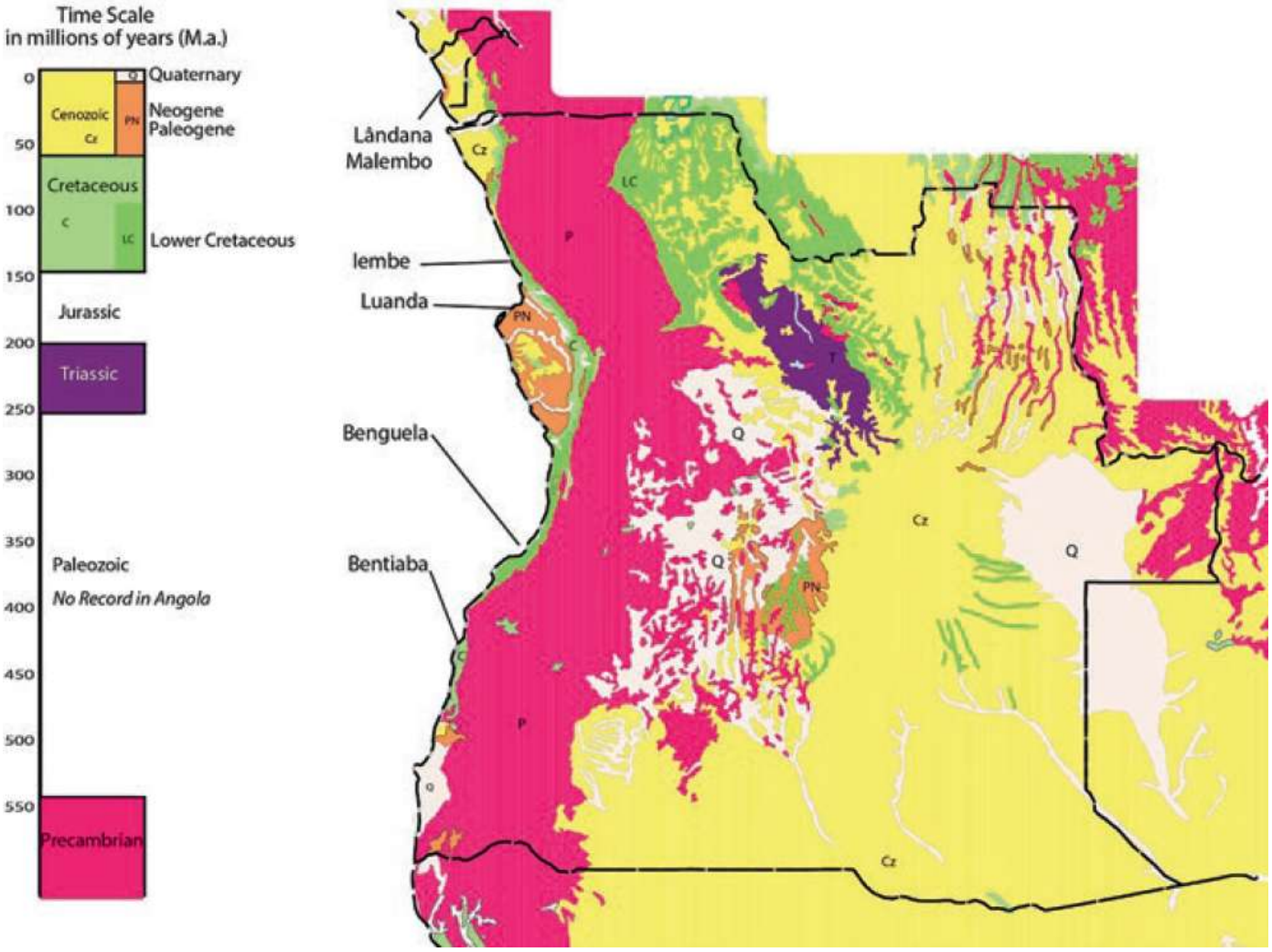

Figure 1.3.1. Geologic map of Angola. Scale: ~1:30,000,000 (U.S. Geological Survey, 2002). Along the coast of Southern Angola are Cretaceous-aged rock outcrops. Fig 4.2 from Mateus et al., (2019), Chapter 4 in *Biodiversity of Angola Science & Conservation: A Modern Synthesis*.

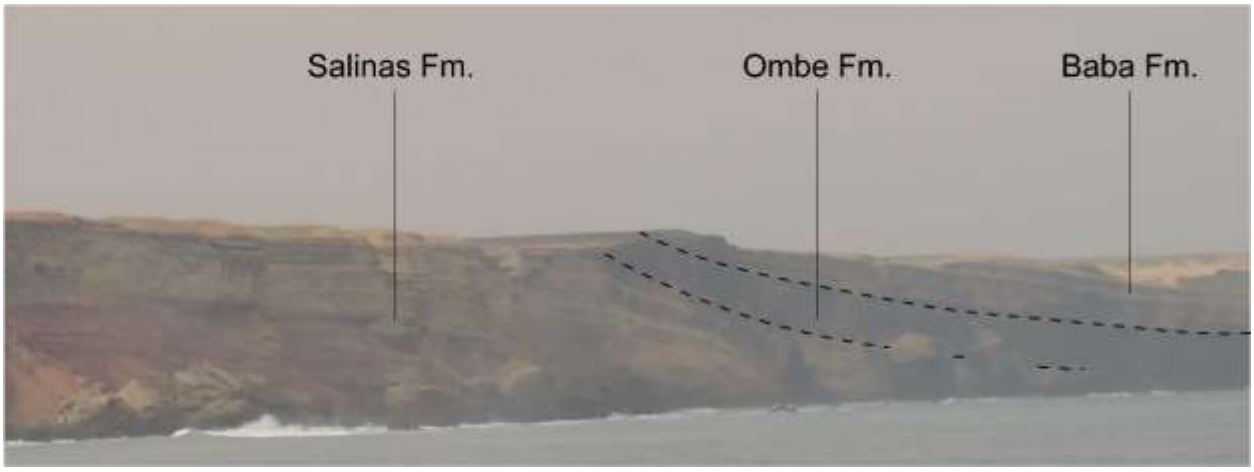

Figure 1.3.2. Stratigraphic relationship of formations at Bentiaba, Namibe, Southern Angola (Mocuio Fm. not pictured).

Figure 1.3.3. Ombe basalt with vertical columnar dikes apparent. Baba Fm. cropping out above Ombe basalt pictured.

Figure 1.3.4. Sandstone layers capped by limestone benches in Baba Fm.

Above the Salinas Fm., there is a 6-meter thick basalt flow from the Ombe Fm. On the western section of the Ombe Fm., pillow basalt and hyaloclastites are evident along the modern shoreline, while the eastern exposure of the Ombe Fm. exhibits baked and weathered marine sediment below the basalt. This indicates the basalt erupted along the Cretaceous coastline. Basalt samples provide an age estimation of 84.6 Ma (Santonian) for the Ombe Fm. based on $^{40}Ar/^{39}Ar$ dating. This dating is significant, as the age of the basalt provides an age anchor for the rest of the section. The Ombe Fm. is followed by the Baba Fm., a 45 m section that is composed of alternating units of thick fine-grained sandstones and sandstone layers composed of a limestone cement, 5- 10 cm in thickness. Bivalve shells are present throughout this section but most densely in the limestone-cemented layers. In the lower 10 m of the Baba Fm., ammonites have been found that can be designated a biostratigraphic age of Middle Santonian to Early Campanian (Cooper, 2003).

The contact between the Baba Fm., and the above Mocuio Fm is indicated by a 5 cm coquina. The sedimentology between the Baba Fm. and the Mocuio Fm. is similar in that both are composed of soft fine sandstone intervened with harder carbonate-cemented sandstones, although the lower 20 m of the exposed Mocuio Fm. differs from the Baba Fm. in having sandstone beds that are much less thicker (maximum of 2 m in thickness). It is above the 19th carbonate bench from the base of the Mocuio Fm. at Bentiaba, 'Bench 19', where a bonebed of vertebrate fossils is located (Schulp et al., 2008; Polcyn et al., 2010; Mateus et al., 2012; Strganac et al., 2014). The top of the Mocuio Fm. is composed of 10 m of massive friable sandstone and includes vertebrate remains, although it is less fossiliferous than the first four meters above Bench 19 (Mateus et al., 2012).

The bonebed above Bench 19 is rich in marine amniote remains (Mateus et al., 2012; Araújo et al., 2015a; Araújo et al., 2015b). The fossil richness of the locality can be credited to the highly narrow continental shelf the fossils were deposited on, which received influxes of fine sand derived from proximal granitic shield rocks (Jacobs et al., 2016). The age of Bench 19 was determined by correlation of its magnetostratigraphy to chron C32n.1n, designating the time interval of the bench to be between 71.4 to 71.64 Ma (Strganac et al., 2014). The dense concentration of fossils along with the high taxonomic diversity present at this site reflects the productivity of the shallow marine environment at Bentiaba; a possible result of the Benguela upwelling system (Shannon 1985; Jacobs et al., 2009a; Jacobs et al., 2009b; Mateus et al., 2012).

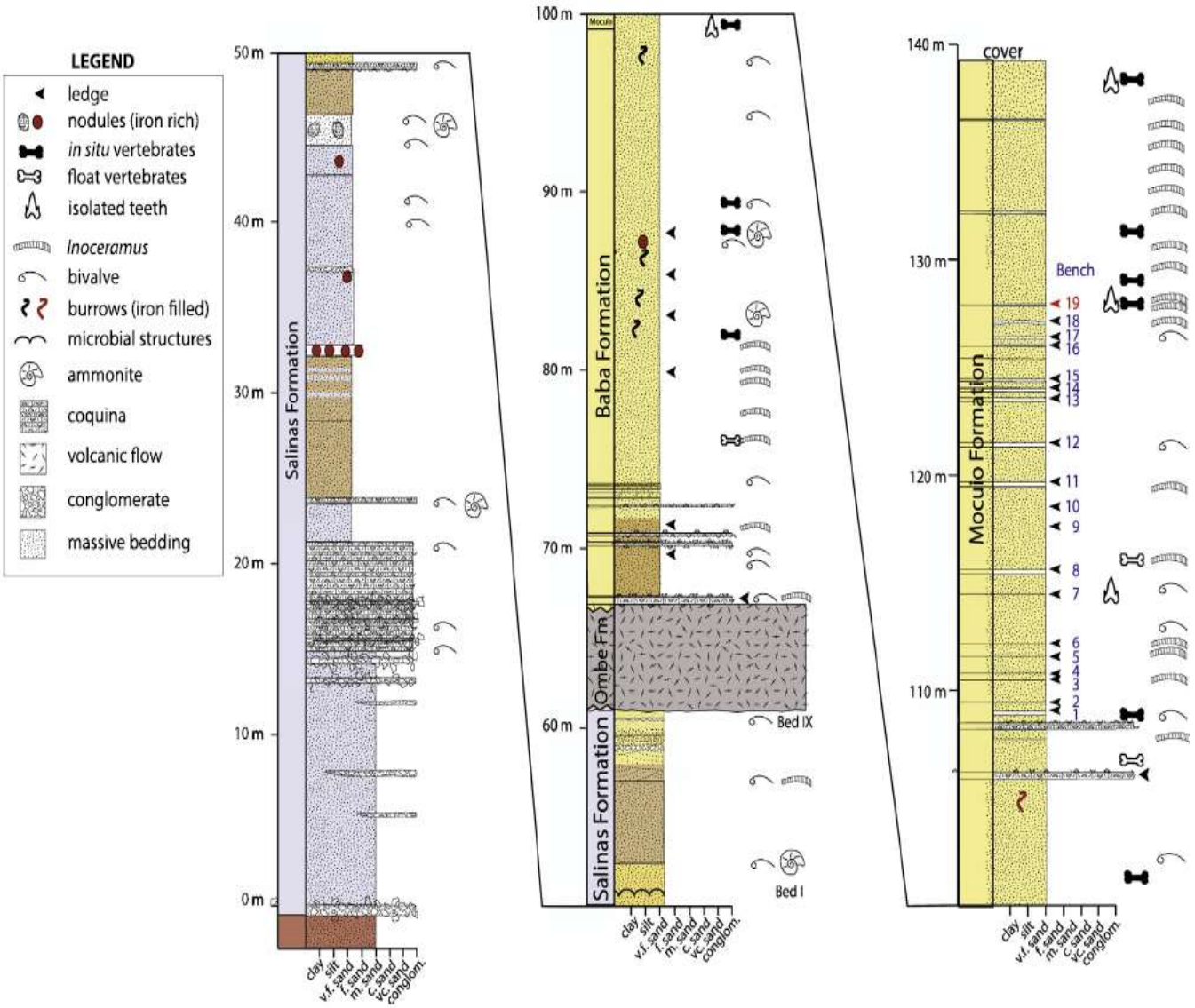

Figure 1.3.5. Stratigraphy of Bentiaba, Angola. Bench 19 is indicated in red (second column from left). Fig. 2 from Strganac et al. (2014).

Classification and Systematics of Plesiosauria

Sauropterygia Owen 1860 is a monophyletic clade of secondarily aquatic diapsids that originated in the Late Permian and includes the subclades, Placodontia, Pachypleurosauria, Nothosauria and Pistosauria, with Plesiosauria being a subclade of Pistosauria (Ketchum and Benson, 2010; Neenan et al., 2013; Sues, 2019). Plesiosauria has been recovered as a monophyletic taxon since its naming (Storrs, 1991; O'Keefe, 2001, 2004; Druckenmiller & Russell, 2008; Ketchum and Benson, 2010; Benson and Druckenmiller, 2014) and has long been divided into two subgroups: the small-headed and long-necked plesiosauromorphs (Plesiosauroidea Welles, 1943) and the large-headed, short-necked pliosauromorphs (Pliosauroidea Welles, 1943), although there is a continuum between the two forms with the pliosauromorph form evolving independently at least twice within Plesiosauria (Andrews, 1910, 1913; Welles, 1943, 1952; Tarlo, 1960; Persson, 1963; Brown, 1981; Williston, 1907; White, 1940; Bakker, 1993; Carpenter, 1997). The pliosauromorph and plesiosauromorph body plans were apparent by the Early Jurassic, when plesiosaurian diversity was high but disparity was low (Benson et al., 2012). Plesiosaurian disparity would increase throughout the Early-Middle Jurassic, drop near the Jurassic-Cretaceous boundary, and then increase again throughout the Cretaceous (Benson et al., 2012; Benson and Druckenmiller, 2014). Large-scale phylogenetic analyses have been integral toward understanding broad evolutionary patterns in Plesiosauria, while others are more focused on a single lineage (Ketchum and Benson, 2010). A historical overview of systematic studies on the Plesiosauria will not be provided here, but rather a synopsis of the most relevant and recent publications concerning higher-level plesiosaurian systematics. A historical summary of plesiosaurian systematics is provided by Ketchum and Benson (2010) and highlights the main issues in plesiosaurian phylogenetic analyses, which typically include a low number of characters, low number of taxa, poor outgroup selection, exclusion of important characters, and inadequate in-group taxa selection.

As reviewed by Ketchum and Benson (2010) the first published phylogenetic analysis of Plesiosauria from a wide stratigraphic and taxonomic range was by O'Keefe (2001), who used 31 ingroup taxa, three outgroup taxa (*Simosaurus*, *Cymatosaurus* and Pistosauridae were constructed to be paraphyletic in reference to the ingroup taxa) and 166 characters:107 from the skull and 59 postcranial characters. Parsimony analysis of the data matrix resulted in twelve most-parsimonious trees (MPTs), all with a length of 432. The MPTs had a consistency index (CI) of 0.47, a Rescaled Consistency Index (RCI) of 0.34 (uninformative characters were excluded), and a Retention Index (RI) of 0.72. The strict consensus tree from the twelve MPTs was produced, with a bootstrapping of the characters (1000 replicates) and a calculation of decay rate for each node within Plesiosauria. In the resulting phylogeny, a monophyletic Plesiosauria contained the traditional superfamilies: Pliosauroidea and Plesiosauroidea.

Within Pliosauroidea, *Thalassiodracon* formed an outgroup to a polytomy formed by *Eurycleidus*, *Attenborosaurus*, Pliosauridae and Rhomaleosauridae. Both Pliosauridae and Rhomaleosauridae were recovered as monophyletic, but the internal relationships of Rhomaleosauridae received very low support (decay index of one and bootstrap support <50%). In Plesiosauroidea, *Plesiosaurus* was the outgroup taxon to a new monophyletic taxon, Euplesiosauria O'Keefe, 2001. Euplesiosauria in turn is composed of a polytomy formed by Cryptocleidoidea, *Microcleidus* and Elasmosauridae (although it is stated by O'Keefe, 2001 that *Microcleidus* is a problematic taxon and removal of morphometric characters recovered *Microcleidus* as the sister taxon to Cryptocleidoidea and Elasmosauridae). O'Keefe (2004) would follow up to this study with the inclusion of a new taxon, *Plesiopterys* to the original three outgroup taxa and 31 ingroup taxa of O'Keefe (2001). Four new characters were also added to the original matrix of 166 characters. *Plesiopterys* was recovered as the sister taxon to Plesiosauroidea and the general pattern recovered in O'Keefe (2001) was maintained.

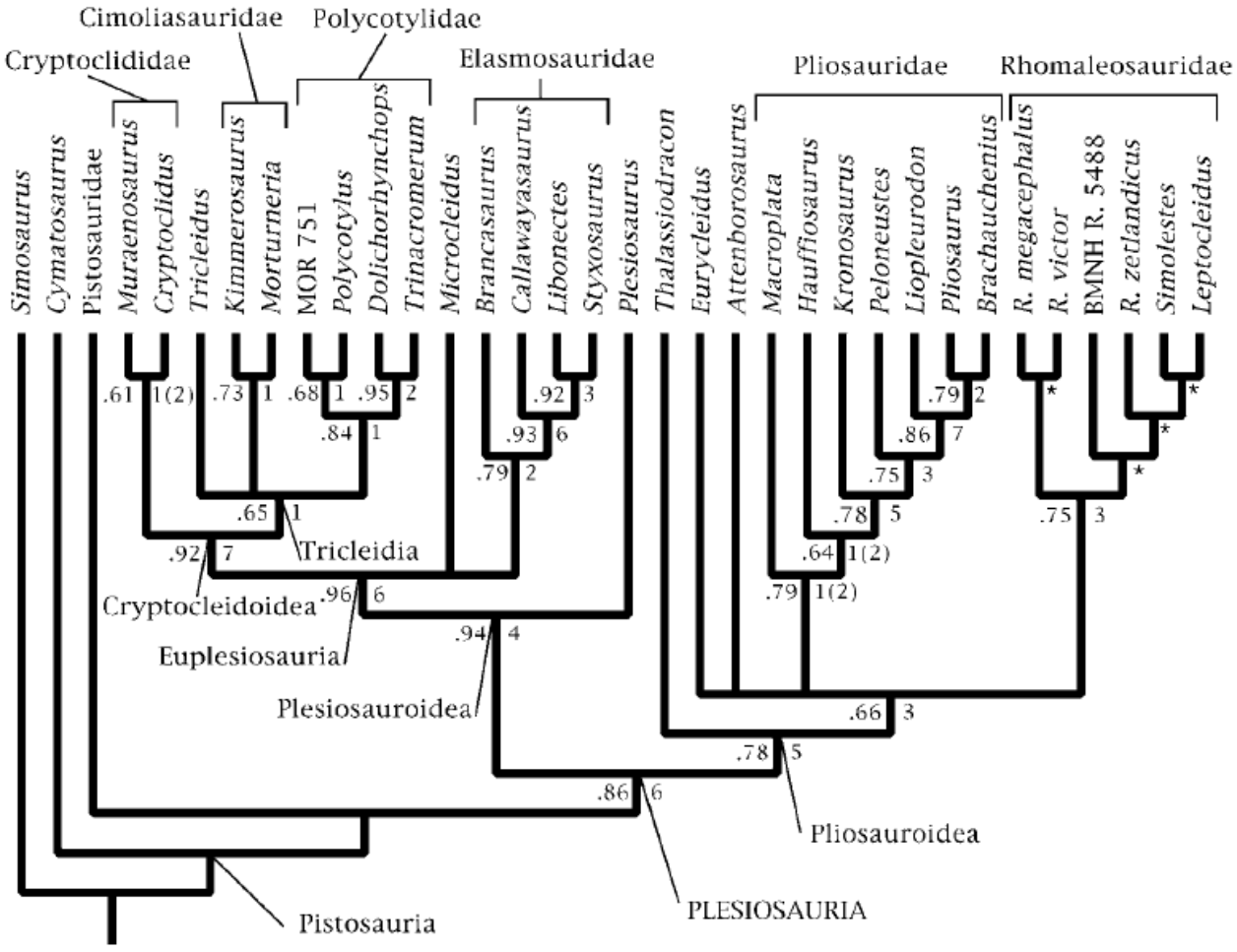

Figure 1.4.1. Cladogram of the Plesiosauria. Fig. 20 from O'Keefe (2001).

Following O'Keefe (2001, 2004), Druckenmiller & Russell (2008) would also publish a phylogenetic analysis with the purpose of resolving the classification and phylogenetic position of *Leptocleidus* by analyzing higher-level plesiosaurian systematics, which would utilize 28 taxa and 152 characters. The analysis found that *L. capensis* and *L. superstes* form a clade (Leptocleididae) that is the sister taxon to Polycotylidae. Both Leptocleididae and Polycotylidae formed the clade, Leptocleidoidea, which is the sister taxon to Pliosauridae, with a paraphyletic Rhomaliosauridae. Plesiosauroidea formed a large polytomy composed of *Thalassiodracon hawkinsi*, *Plesiosaurus dolichodeirus*, *Plesiosaurus wildi*, Elasmosauridae, BMNH R.1336 and BMNH 49202. The results of O'Keefe (2001, 2004) are at obvious odds with Druckenmiller and Russell (2008) concerning the relationship of polycotylids and leptocleidids with other plesiosaurians.

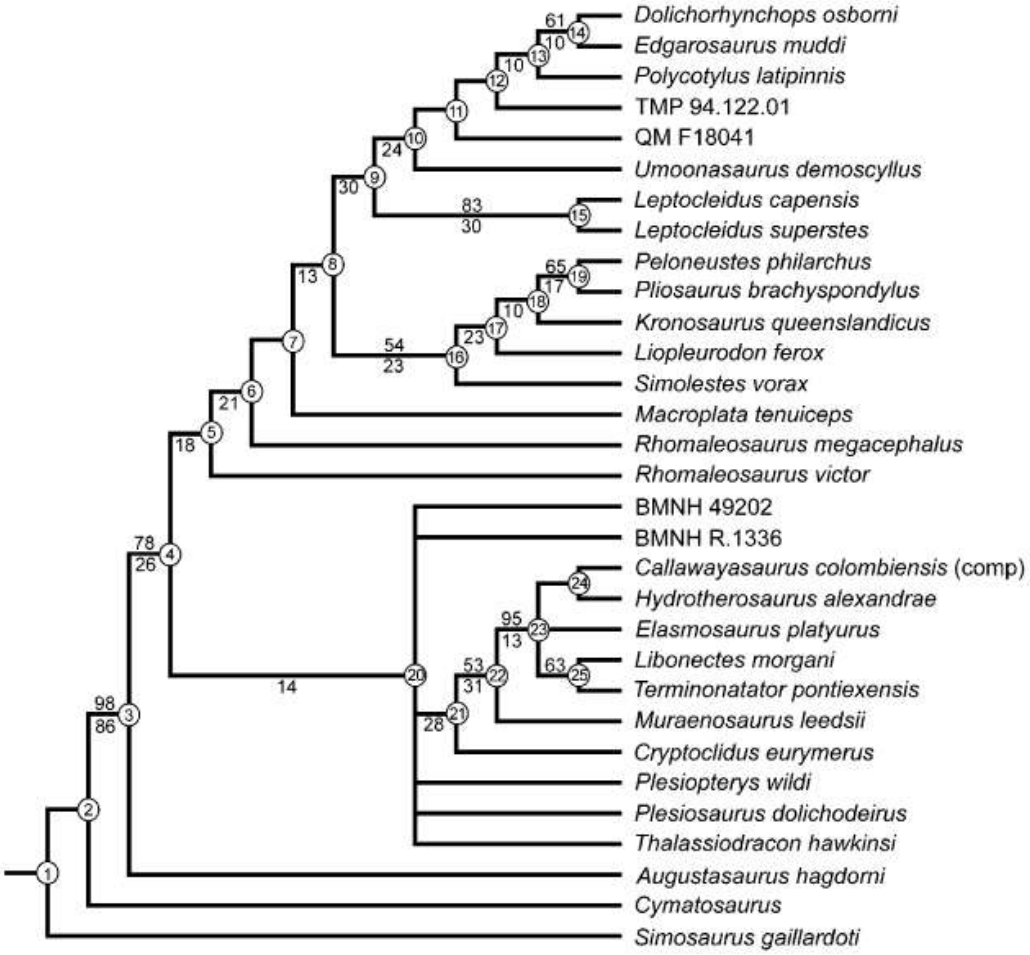

Figure 1.4.2. Hypothesis of relationships within Plesiosauria. Fig. 14 from Druckenmiller & Russell (2008).

The large-scale phylogenetic analysis of Ketchum and Benson (2010) utilizes 66 taxa and 178 characters (113 cranial, 25 axial and 40 appendicular) and was important in critiquing issues in past phylogenetic studies and providing a character matrix and taxon dataset aimed at resolving contentious higher-level plesiosaurian relationships and providing branch-based definitions for the purpose of stabilizing plesiosaurian classifications. A strict consensus tree with a CI of 0.3277, RI of 0.6007, and RCI of 0.2014 was recovered and resulted in the placement of *Attenborosaurus conybeari*, '*Plesiosarus*' *macrocephalus*, and a clade composed of *Archaeonectrus rostratus*, *Macroplata tenuiceps*, and BMNH 49202 outside of the traditionally defined Plesiosauria. In order to maintain the congruence of these mentioned taxa within Plesiosauria, a new clade, Neoplesiosauria Ketchum and Benson (2010), was created to encompass the clade composed of Plesiosauroidea and Pliosauroidea, with Plesiosauria moved to a more basal position to include *A. conybeari*, '*P'. macrocephalus*, *A. rostratus*, *M. tenuiceps*, and BMNH 49202. The analysis recovered Rhomaleosauridae as being monophyletic and the sister taxon to Pliosauridae. Polycotylidae and Leptocleididae are sister taxa and form the clade Leptocleidia within Plesiosauroidea. Leptocleidia is the sister taxon of a clade composed of *Cryptoclidus eurymerus*, *Kimmerosaurus langhami*, *Muraenosaurus leedsii*, and *Tricleidus seeleyi* which together form the clade, Cryptoclidia. Cryptoclidia is the sister taxon of Elasmosauridae and the clade formed by Cryptocledia and Elasmosauridae is the sister taxon to Plesiosauridae, with basal plesiosauroid taxa just outside of the ((Plesiosauridae) (Elasmosauridae + Cryptoclidia)) node. These results suggest that the pliosauromorph body plan evolved twice within Plesioauria, highlighting the plasticity of the cranium in plesiosaurians and variation in the number of vertebrae in the vertebral column. Important definitions to plesiosaurian taxonomic groups utilized stem-based definitions in order to maintain taxon concepts despite changes to plesiosaurian phylogenetic hypotheses.

The PhD thesis of Evans (2012), although unpublished, is an important work in that it took into consideration the biases outlined in Ketchum and Benson (2010) and utilized the largest compiled character dataset known (339 qualitative and quantitative characters) with 107 taxonomic units. The purpose of the study was to test the evolutionary affinity of the lower Jurassic plesiosaur, *Raptocleidus blakei* Evans, 2012. The characters were selected from past studies and included based on biases outlined by Ketchum and Benson (2010). A ratchet analysis (Parsimony Ratchet of Nixon (1999)) was run on the dataset using PAUPRat (Sikes and Lewis, 2001) followed by a heuristic search with TBR and the "Multrees" option selected. The resulting strict consensus tree provided the statistics: CI: 0.245, RI: 0.636, and RCI: 0.156. The most striking result from the strict consensus tree was the placement of Leptocleidomorpha (Leptocleididae + Polycotylidaea) in a polytomy with *Stretesaurus taylori* Benson, Evans, and Druckenmiller 2012 and Pliosauridae, contra O'Keefe (2001, 20014) but congrument with

Druckenmiller and Russel (2008). Within Plesiosauroidea, Elasmosauridae was recovered as the sister taxon to Cryptocleididae. Interestingly, Evans (2012) recovered Leptocleidia as the sister group to Elasmosauridae in 3/20 ratchet analysis replicates of the data set.

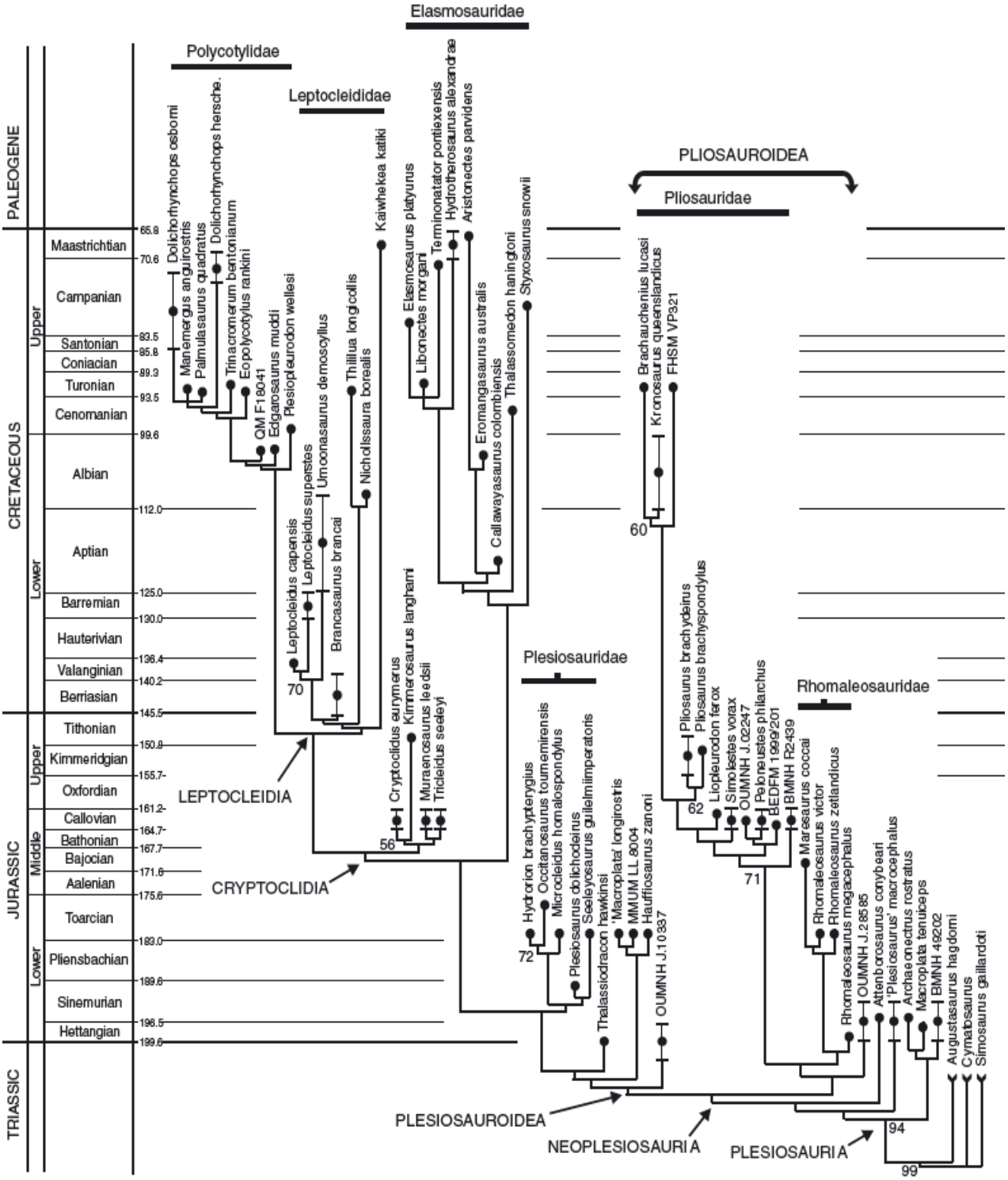

Figure 1.4.3. Phylogeny of the Plesiosauria. Fig. 6 from Ketchum & Benson (2010).

The character matrix and OTUs that are widely used by many plesiosaurian researchers since its original publication, is that by Benson and Druckenmiller (2014) with 270 characters and 80 OTUs. The main purpose of this study was to test for a possible faunal turnover event near the Jurassic-Cretaceous boundary in Plesiosauria and compare these findings with data from other tetrapod groups across the Jurassic-Cretaceous boundary. The character matrix for this study was an extension of an earlier publication by Benson et al., (2012) which assessed the phylogeny and disparity of Early Jurassic plesiosaurians from the Lias Group of the U.K. and the Holzmaden from Germany (Benson et al., 2012). Thus, the study focuses on Middle Jurassic- Early Cretaceous plesiosaurians. The character matrix was developed from a review of characters used in O'Keefe (2001, 2004), Sato (2002), Druckenmiller and Russell (2008), Smith and Dyke (2008), Ketchum and Benson (2010, 2011) and Benson et al., (2012), with 24 new characters added. Gap weighting was not employed (continuously varying characters were not scored quantitatively) in order to encourage the use of the matrix for future phylogenetic studies and 'wildcard' taxa were removed in order to increase resolution of strict reduced consensus tree.

The analysis by Benson and Druckenmiller (2014) reported failure in elucidating phylogenetic relationships between the major plesiosaurian clades: Plesiosauroidea, Pliosauroidea, and Rhomaleosauridae, and identified new monophyletic groups, including Thalassophonea, Brachaucheninae (a clade of Cretaceous pliosaurids) and Xenopsaria, which includes most Cretaceous plesiosauroids (Elasmosauridae, Leptocleididae, and Polycotylidae). The strict consensus of the shortest-length trees recovered from the full dataset in Fig.2 of Benson & Druckenmiller (2014) was pruned for wildcard taxa: '*Pistosaurus* skull', *Macroplata*, *Eurycleidus*, *Pliosaurus funkei*, *Pliosaurus irgisensis*, and *Eromangasaurus* to provide higher resolution to the strict reduced consensus tree in Fig.3 of Benson & Druckenmiller (2014). In the strict consensus, before pruning, a massive polytomy is formed by Pliosauridae, Rhomaleosauridae, *Eoplesiosaurus*, *Strateosaurus*, and even the pistosaurid outgroup taxa. The strict reduced consensus after pruning wildcard taxa reveals a large polytomy from the node of Plesiosauria formed by Plesiosauroidea, Pliosauridae, Rhomaleosauridae, *Eoplesiosaurus* and *Strateosaurus* (Figure 1.4.4.). Within Plesiosauroidea, Elasmosauridae is the sister taxon to Leptoclidia and together form the clade, Xenopsaria, which is the sister taxon to Cryptoclididae. Together, these two clades form Cryptoclidia. *Abyssosaurus* from Cryptoclididae, the Xenopsaria lineage and the Brachaucheninae lineage would cross the Jurassic, into to the Cretaceous period. This suggests that a total of three pleiosaurian lineages crossed the Jurassic-Cretaceous boundary, although cryptoclidians would go extinct shortly after (Benson and Druckenmiller, 2014).

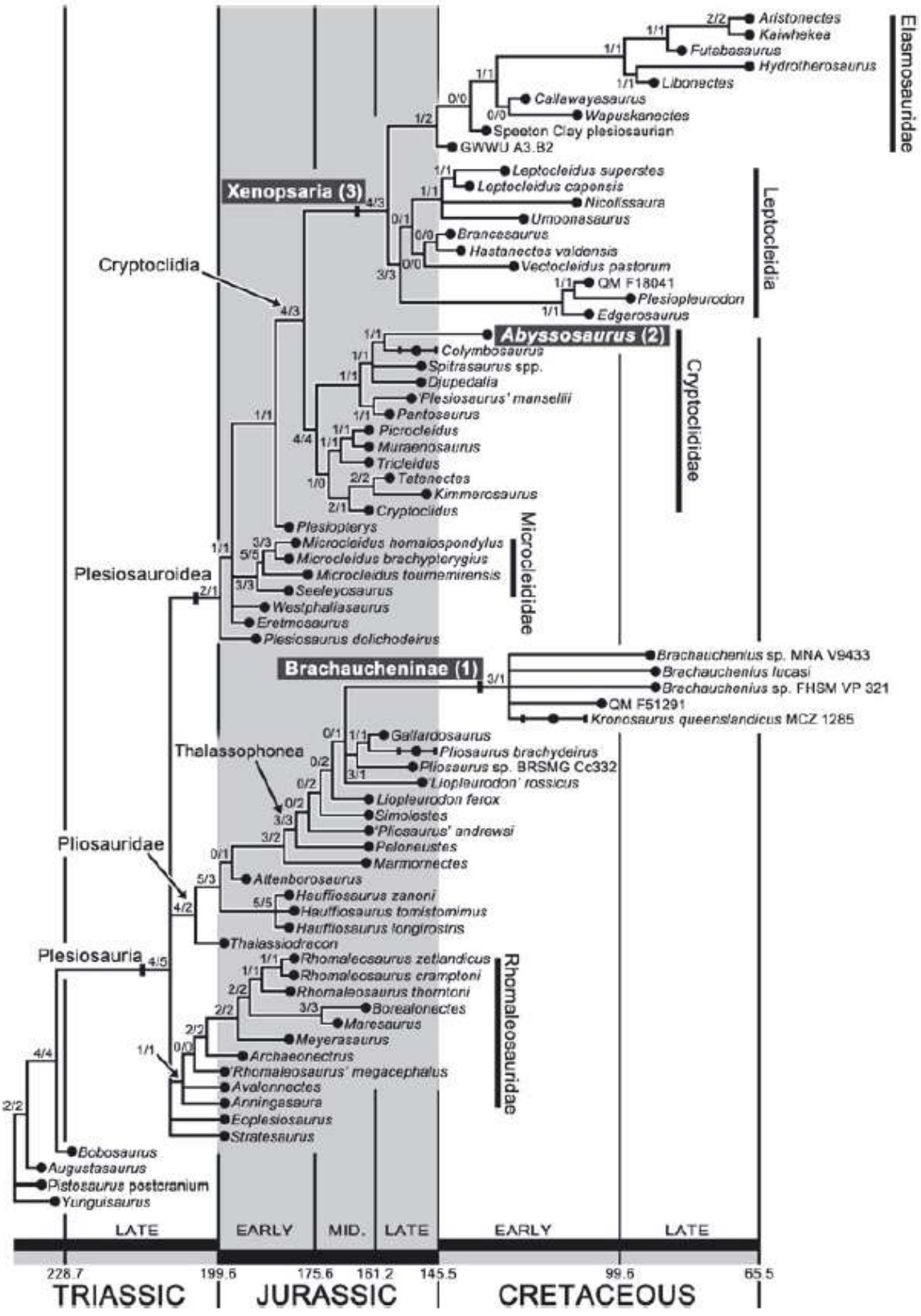

Figure 1.4.4. Phylogeny of the Plesiosausria. Fig. 3 from Benson & Druckenmiller (2014).

The results of Benson and Druckenmiller (2014) cast some uncertainty on the basal relationships of Plesiosauria among the major taxonomic groups, which is interesting considering the sampling of early plesiosaurians in the Lower Jurassic Lagerstätten-rich localities in Europe. The polytomy produced by Benson and Druckenmiller (2014) suggests that Rhomaleoasauridae may be a third major clade within Plesiosauria. However, as noted by Benson & Druckenmiller (2014), the uncertain basal relationships may have been a product of 'wildcard' taxa. Benson and Druckenmiller (2014) concluded that a monophyletic Pliosauroidea is exclusive to a monophyletic Neoplesiosauria. It seems that additional Triassic- Early Jurassic plesiosaurian taxa will be needed to break the polytomies. Subsequent research on plesiosaurian systematics has utilized the character matrix and OTU dataset of Benson and Druckenmiller (2014) for phylogenetic analyses, even for phylogenetic studies of elasmosaurids despite the fact that the original OTUs of Benson & Druckenmiller (2013) only includes nine elasmosaurids. The clade Elasmosauridae is one of the least resolved clades within Plesiosauria, as is evident by inconsistent topologies among different researchers (Druckenmiller and Russell, 2008; Vincent et al., 2011; Serratos et al., 2017; Sachs et al., 2018).

Table 1. List of modern plesiosaurian clade definitions pertinent to this work and supported by recent and comprehensive phylogenetic analyses.

Clade	Definition	References
Plesiosauria De Blainville 1835	All taxa more closely related to *Plesiosaurus dolichodeirus* and *Pliosaurus brachydeirus* than to *Augustosaurus hagdorni*.	Ketchum & Benson, 2010
Neoplesiosauria Ketchum and Benson 2010	The most recent common ancestor of *Plesiosaurus dolichodeirus* and *Pliosaurus brachydeirus* and all of its descendents	Ketchum & Benson, 2010
Plesiosauroidea Welles 1943	All taxa more closely related to *Plesiosaurus dolichodeirus* than to *Pliosaurus brachydeirus*.	Ketchum & Benson, 2010
Cryptoclidia Ketchum and Benson 2010	The most recent common ancestor of *Cryptocleidus eurymerus* and *Polycotylus latipinnis* and all of its descendents.	Ketchum & Benson, 2010
Xenopsaria Benson and Druckenmiller 2014	All taxa more closely related to *Elasmosaurus platyurus*, *Polycotylus latipinnis*, and *Leptocleidus superstes* than to *Cryptoclidus eurymerus*, *Plesiosaurus dolichodeirus*, *Rhomaleosaurus cramptoni*, or *Pliosaurus brachydeirus*.	Benson & Druckenmiller, 2014
Elasmosauridae Cope 1869	All taxa more closely related to *Elasmosaurus platyurus* than to *C. eurymerus*, *L. superstes*, *Plesiosaurus dolichodeirus* or *Polycotylus latipinnis*	Ketchum & Benson, 2010
Aristonectinae O'Keefe and Street, 2009	The most recent ancestor of *Kaiwhekia katiki* and *Aristoneces* and all of its descendents.	O'Keefe and Street, 2009; Otero, 2012
Styxosaurinae Otero 2016 = Elasmosaurinae Cope 1869	The most inclusive clade that contains *Elasmosaurus platyurus*, but no *Aristoneces parvidens*.	Otero, 2016; O'Gorman, 2020

A review of the systematics of Elasmosauridae

The taxon, *Elasmosaurus platyurus* Cope, 1868, for which the family Elasmosauridae (Cope, 1869) was named, is represented by a single specimen (ANSP 10081) and provides a well-complete axial skeleton (72 cervical vertebrae including the atlas-axis complex; 103 total centra) but only fragments of the skull and the anterior end of the snout along with isolated rib fragments (Cope, 1869; Sachs, 2005a; Sachs et al., 2013). The specimen originally included the pectoral and pelvic girdles, but both have been lost (Welles, 1943; Carpenter, 1997; Sachs, 2005a). It is suspected that the girdle elements of *E. platyurus* were destroyed by vandals in the New York City workshop of Waterhouse Hawkins, who had prepared to make molds of the plesiosaur girdles for display in the new Paleozoic Museum in New York's central park (Davidson and Everhart, 2018). Elasmosauridae was originally defined on the presence of a prominent median pectoral bar (Cope, 1869; Carpenter, 1997). However, this character in the type specimen, ANSP 10081, can only be extrapolated based on a drawing of the pectoral girdle from Cope (1869). Despite the completeness of the axial skeleton, the lack of girdle and limb elements, and the fragmentary remains of the skull make *E. platyurus* a poor type specimen to base a family on. As mentioned by Carpenter (1997) the taxon *E. platyurus* should be restricted to the holotype. The interrelationships of taxa within Elasmosauridae are currently not well understood (Vincent et al., 2011; Serratos et al., 2017; Sachs et al., 2018). A general review of cladistical studies focused on the development of Elasmosaurid systematics and how it has reached our modern concept of Elasmosauridae and its subfamilies is provided.

The first study of elasmosaurid systematics using cladistical methods was undertaken by Carpenter (1999). His review of North American elasmosaurids would help clarify the taxonomy of elasmosaurids, which during the late 90s was confusing due primarily to poor type material, and the paucity of preserved elasmosaurid crania (Carpenter 1997, 1999). Carpenter's 1999 review of North American elasmosaurids found only five genera to be valid, following the methodology used by English plesiosaur researchers (Tarlo, 1960; Brown, 1981; Taylor, 1992; Taylor and Cruickshank 1993; Storrs, 1997) who showed that intraspecific variation and ontogenetic differences can mislead systematic evaluations. The cladistic analysis of Carpenter (1999) considered only taxa from Plesiosauroidea with a total of 15 taxa and 20 characters. Carpenter's diagnosis for Elasmosauridae is based on the presence of 36 or more cervical vertebrae, anterior mid-cervical vertebrae are elongated, and the presence of lateral ridges on cervical vertebrae. Carpenter defined Elasmosauridae as the most recent common ancestor of *Brancasaurus brancai* Wegner, 1914 and *Tuarangisaurus keyesi* and all its descendants.

In early cladistical studies, Jurassic taxa were often included in the clade Elasmosauridae. This includes taxa such as *Muraenosaurus leedsi*, *Microcleidus*, and *Occitanosaurus tournemirensis* (Bardet et al., 1999; Gasparini et al., 2003). As reviewed by Ketchum and Benson (2010), the lack of Early and Late Cretaceous plesiosauroid taxa in these cladistic analyses creates a bias where Jurassic taxa are included in Elasmosauridae. Additionally, Cryptoclididae was often recovered as the sister taxon to Elasmosauridae, although this relationship would change with future studies (Carpenter et al., 1999, Bardet et al., 1999, Gasparini et al., 2003).

The work of O'Keefe (2001) in the first large-scale phylogenetic study of Plesiosauria would provide a high number of characters (166) and result in the taxa: *Brancasaurus brancaii* Wegnar, 1914, *Callawayasaurus colombiensis* Welles, 1962, *Libonectes morgani* Welles, 1949, and *Styxosaurus snowii* Williston, 1890, being included within Elasmosauridae. *Microcleidus* and *Muraenosaurus* were not designated as elasmosaurids contra past studies (Andrews 1910; Carpenter, 1999; Bardet et al., 1999). Elasmosauridae is supported with a bootstrap value of 79 and a decay rate of one with morphometric characters included and two with the elimination of morphometric characters (O'Keefe, 2001). O'Keefe (2001) defines Elasmosauridae as a taxon including *Brancasaurus*, *Styxosaurus*, their most recent common ancestor, and all descendants.

Soon after the large-scale cladistic analysis of O'Keefe (2001), the PhD thesis of Sato (2002) would focus on the evolutionary relationships of elasmosaurid plesiosaurians, with a character matrix of 215 characters (qualitative and quantitative characers with multistate coding), and 34 terminal units (including plesiosauroids not within Elasmosauridae). The phylogenetic analysis of Sato (2002) is a thorough study that included a high number of taxa previously diagnosed and defined as elasmosaurids, and analyzed the effects of taxon and character selection (Welles, 1943; Welles, 1962; Brown, 1993; Carpenter, 1999; O'Keefe, 2001). Sato (2002) categorized taxa into "splitter" (specimens scored individually), "composite" (combined character scores for specimens of the same species), and "less missing data", where only taxa that were considered well-complete were included in the analysis. Characters were divided into categories: "all characters" (includes all characters), "qualitative only" (excludes quantitative characters), and "selected characters" (removes characters interpreted to be homoplastic). In total, Sato (2002) ran nine analyses with combinations of the above conditions. Sato returned a monophyletic Elasmosauridae, however, this clade was distinct from that of Brown (1981, 1993) which included Jurassic and Cretaceous taxa: *Muraenosaurus*, *Occitanosaurus*, and *Brancasaurus*. The definition of Elasmosauridae sensu O'Keefe (2001) applied to the phylogenetic analysis of Sato (2002) would include Cryptocleididae and most of the plesiosaurian taxa included in the analysis, even *Plesiosaurus dolichodeirus*, and *Leptocleidus*. This wide inclusion of plesiosaurians into the definition of

Elasmosauridae sensu O'Keefe (2001) is due to the basal position of *B. brancaii* in Sato (2002). In four out of the nine analyses for which "Pleo-morpha", Cry-morpha", and "Ela-morpha" are resolved, "Pleo-morpha" (the most inclusive clade containing *P. dolichodeirus* but not *C. eurymerus*) is the sister taxon to the clade formed by "Ela-morpha" (the most inclusive clade containing *E. platyurus* but not *C. eurymerus*) and "Cry-morpha" (the most inclusive clade including *C. eurymerus* but not *E. platyurus*). Elasmosauridae only received a bootstrap value greater than 50% when "less missing data" was combined with "all" characters and "qualitative only" characters, excluding *B. brancaii*. Sato (2002) defines Elasmosauridae as the least inclusive clade containing *E. platyurus, T. haningtoni*, and *C. colombiensis*.

The large dataset of Druckenmiller & Russell (2008) recovered Elasmosauridae with the taxa: *Callawayasaurus columbiensis*, *Hydrotherosaurus alexandrae* Welles, 1943, *Elasmosaurus platyurus*, *Libonectes morgani*, and *Terminonatator pointiexensis* Sato, 2003 (*Muraenosaurus leedsii* was not included in Elasmosauridae) in the strict consensus of tree of three most parsimonious trees (tree length = 5802 steps; CI = 0.543; RI = 0.568; RC = 0.309). Elasmosauridae is recovered with a bootstrap value of 95 and a bremer support of 13 which indicates strong support for a monophyletic clade. *Brancasaurus* was not included in the cladistic analysis of Druckenmiller & Russell (2008) who define Elasmosauridae as the most recent common ancestor of *Callawayasaurus colombiensis* and *Elasmosaurus platyurus* and all its descendants

Cimoliasauridae, a family named by DeLair (1959), based on the ambiguous genus *Cimoliasaurus* was referred to as a junior synonym of Elasmosauridae by O'Keefe and Street (2009) after reviewing the osteological morphology of *Cimoliasaurus* which indicated an elasmoaurid affinity. O'Keefe and Street (2009) also erected the family, Aristonectidae for austral Cretaceous cryptocleidoids. The clade referes *Aristonectes parvidens* to a group outside of Elasmosauridae, contra Gasparini et al., 2003. *A parvidens* would be reclassified as an elasmosaurid in the large phylogenetic analysis of Plesiosauria by Ketchum and Benson (2010). Elasmosauridae in the phylogenetic analysis of Ketchum and Benson (2010) is composed of *E. platyurus, L. morgani, T. pontiexensis, H. alexandrae, A. parvidens, E. australis, C. columbiensis*, and *T. haningtoni*. Ketchum & Benson (2010) provide a stable branch-based definition for Elasmosauridae, which this thesis accepts as the functional definition: All taxa more closely related to *Elasmosaurus platyurus* than to *C. eurymerus, L. superstes, P. dolichodeirus* or *Polycotylus latipinnis*.

Description and phylogenetic analysis of *Zarafasaurua oceanis* Vincent, Bardet, Pereda Suberbiola, Bouya, Amaghzaz, and and Meslouh, 2011 from the Maastrichtian phosphate mines of

Morocco by Vincent et al., (2011) utilized 22 taxa and 67 characters, with a branch-and-bound search for the most parsimonious trees. The analysis resulted in three parsimonious trees with a strict consensus yielding a length of 154, CI (excluding uninformative characters) = 0.49 and RI = 0.63. Interestingly, *Kaiwhekea* and *Tuarangisaurus* formed the sister clade to Polycotylidae (*Nichollssaura* (*Thililua*, *Dolichorynchops*)). As reviewed by Vincent et al., 2011, *Kaiwhekea*, has been assigned to different family-level taxonomic groups in past analyses including Crytoclididae (Cruickshank and Fordyce, 2002), Cimoliasauridae (O'Keefe, 2004), and Aristonectidae (O'Keefe and Street, 2009). Additionally, Vincent et al., (2011) found that *Microcleidus* is a basal elasmosaurid, which goes against the analyses of O'Keefe (2001), Ketchum and Benson (2010), Bardet et al., (1999) and Gasparini et al., (2003). Vincent et al., (2011) note that character states for many elasmosaurid taxa are unknown, thus resulting in significant difficulties toward resolving elasmosaurid phylogeny and unstable nodes. Kubo et al., (2012) in the description and phylogenetic analysis of *Albertonectes vanderveldei* Kubo, Mitchell, Henderson, 2012 would include more elasmosaurid taxa than any published analysis previously (18 taxa). Although, Kubo et al., (2012) echo the same issue regarding a lack of consensus on the intrafamilial phylogenetic relationships of Elasmosauridae.

A phylogenetic analysis by Otero et al., (2012), which included a well-preserved postcranial skeleton of an elasmosaurid from the Maastrichtian of Chile revealed diagnostic characters that include this specimen into a sub-group of Cretaceous Southern Hemisphere elasmosaurids from the Weddellian Biogeographic Province. The subfamily clade Aristonectinae is proposed by Otero et al., (2012), as Aristonectidae was found to be polyphyletic. The phylogeny of 22 taxa yielded three most parsimonious trees with CI = 0.52, RI = 0.68 and a length of 246 with low-resolution nodes within Elasmosauridae. The phylogeny revealed a general dichotomy in Elasmosauridae between the exceptionally long-necked elasmosaurids from North America and the shorter-necked elasmosaurids from the Weddellian Biogeographic Province. Aristonectinae is diagnosed by: skull length not reduced or drastically enlarged in comparison to the body length, moderately large neck, and the presence of more than 25 maxillary teeth (characters 1, 2, and 48 in O'Keefe and Street, 2019, respectively) and can be defined as the most recent common ancestor of *Kaiwhekia katiki* and *Futabasaurus suzukii*, and all its descendants (Otero, 2012).

Benson and Druckenmiller (2014) would compile a large plesiosaurian taxon and character matrix (270 unordered characters and 80 OTUs), which has since been utilized and modified by elasmosaurid researchers as the standard for cladistic analysis. The study by Benson and Druckenmiller (2014) recovered Elasmosauridae as the sister taxon of Leptocleidia, which together form the clade, Xenopsaria. The clade Xenopsaria is remarkable in that it represents a major radiation of plesiosauroids

after the Jurassic-Cretaceous transition (Benson and Druckenmiller, 2014). Xenopsaria is well supported with a bremer index of three with 'unstable taxa' and four with 'unstable taxa' removed. Cryptocleididae, which had previously been hypothesized to be the sister taxon of Elasmosauridae is instead outside of Xenopsaria, with the taxa of leptocleididae and polycotylidae composing the sister taxon of Elasmosauridae.

Otero (2016) would again recognize a clear distinction between two distinct lineages of elasmosaurids. The southern hemisphere Weddellian biogeographic province elasmosaurids with anteroposteriorly short cervical vertebrae and the northern hemisphere Western Interior Seaway elasmosaurids with elongated and relatively low cervical vertebrae. Otero (2016) describes two Late Cretaceous North American elasmosaurids, which he assigns to *Styxosaurus* (both previously assigned to *Hydralmosaurus*, now a *nomen dubium*), and establishes the subfamily Styxosaurinae. Syxosaurinae is diagnosed as a clade of Campanian elasmosaurids from the Western Interior Seaway that are characterized by: 60 cervical vertebrae or more; mid-cervical centra are anteroposteriorly elongated (two-thirds to two-times the width); mid-cervical centra are as broad as high ("can-shaped"); neck is much longer than the trunk; skull is less than one-tenth the cervical series length; plesiomorphic number of 17-19 dorsal vertebrae. Syxosaurinae is defined *sensu* Otero (2016) as *Terminonatator, Styxosaurus* (='*Hydralmosaurus*'), *Albertonectes*, *Elasmosaurus*, their most recent common ancestor and all descendants.

O'Gorman (2016) recovered a monophyletic Elasmosauridae and Aristonectinae when adding *Kawanectes lafquenianum* using the character matrix of Benson and Druckenmiller (2014). The analysis confirmed the hypothesis of an earlier phylogenetic study by O'Gorman et al., 2015, suggesting a close relationship between Late Cretaceous aristonectine and non-aristonectine elasmosaurids from Patagonia, Antarctica, and the Pacific coast of North America. O'Gorman and Coria (2016) would establish the clade Weddellonectia to encompass this more inclusive clade, diagnosable by a postaxial accessory ossicle that articulates with the humerus and a 180° separation between epipodial facets and defined by O'Gorman and Coria (2016) as *Aristonectes*, *Kaiwhekea*, *Morenosaurus*, *Vegasaurus*, *Kawanectes*, their most recent common ancestor, and all descendants. The addition of a new specimen from the upper Maastrichtian López de Bertodano Fm. (MLP 14-I-20-16) and a redescription of historical elasmosaurid specimens would expand the clade of Weddellonectia *sensu* O'Gorman and Coria (2016) with the inclusion of *Aphrosaurus furlongi* (O'Gorman et al., 2017b). The close phylogenetic affinities of some southern hemisphere and Circum-Pacific Late Cretaceous elasmosaurid plesiosaurians thus seems to be well-supported (O'Gorman, 2016b; O'Gorman and Coria, 2016; O'Gorman et al., 2017a).

Serratos et al., (2017) would describe and perform a phylogenetic analysis incorporating *Nakonanectes bradti* using the dataset of Benson and Druckenmiller (2014) to include 270 characters and 92 taxa. The consensus tree recovered polytomies at the node of Xenopsaria, however the two sub-clades Aristonectinae and Styxosaurinae were returned. Serratos et al., (2017) conclude that the differences between the topology in their study compared to Otero (2016) is due to a smaller body of studies focused on elasmosaurid comparative anatomy, thus affecting character scores. Serratos et al., (2017) found that not all members of Styxosaurinae necessarily are forms with the absolute longest necks. Interestingly, *Kawanectes lafquenianum*, *Mauisaurus haasti*, *Vegasaurus molyi*, and *Hydrotherosaurus alexandrae* were also included in Styxosaurinae. Serratos et al., (2017) defined Styxosaurinae as all taxa more closely related to *S. snowii* than to *A. parvidens* [or *E. australis*, *C. colombiensis*, *W. betsynichollsae* and the 'Speeton Clay Plesiosaurian'].

A redescription of the highly important holotype specimen of *Styxosaurus snowii* Williston 1890 (KUVP 1301) was done by Sachs et al., (2018) along with a phylogenetic analysis. This redescription was in grave need due to the important anatomical and morphological characters in *S. snowii* and its obvious importance in understanding internal relationships within Styxosaurinae and Elasmosauridae. Phylogenetic analysis was run with both the Serratos et al., (2018) and Otero (2016) datasets (based off the character and taxon matrices of Benson and Druckenmiller, 2014). Sachs et al., (2018) found that Styxosaurinae *sensu* Otero, 2016 and Serratos et al., 2017 is not a usable taxon. Serratos et al. (2017) removed *E. platyurus* from their analysis as it was found to be a wildcard taxon, however, Sachs et al. (2018) did not find *E. platyurus* (internal specifier of senior synonym, Elasmosaurinae Cope, 1869) to be a wildcard taxon. Thus, the interrelationships within Elasmosauridae remained highly unresolved as there is very little consensus between phylogenetic studies.

Cladistical studies focused on southern hemisphere elasmosaurid taxa have begun to build robust systematic hypotheses. Otero et al., (2018), with the addition of the taxon *Aristonectes quiriquinensis*, would add three new apomorphies to diagnose Aristonectinae: opening of the foramen magnum is at a low angle (~60°), an 'A-shaped' midline notch of the squamosal in dorsal view, the presence of a horizontal 'chamber' between the secondary teeth and primary teeth on the dentary (Otero et al., 2018). The consensus tree from Otero et al., (2018) shows support for Styxosaurinae as a subfamily (Figure 1.5.1.). O'Gorman (2020) presents the most up-to-date phylogeny for elasmosaurid plesiosaurians, with new characters and additional taxa added to the character and OTU matrix of Benson and Druckenmiller (2014), providing 283 characters, and 98 OTU. O'Gorman, 2020 synonymizes Styxosaurinae with Elasmosaurinae and establishes a new clade, Euelasmosaurida O'Gorman, 2020 based on the following characters: ventral margin of orbit convex (Ch.5, 0 → 1), sagittal crest high and rising above the cranial

table (Ch.50, 2→3), ventral notches on articular faces of anterior and middle cervical centra (Ch.155, 0→1), anterolateral margin of the scapula is flat or gently convex (Ch.202, 1→0), and tibia length/width ratio is between 0.8 and 1 (Ch.255, 1→2). O'Gorman 2020 also utilized additional elasmosaurid taxa that were not included in the analysis of Serratos et al., (2017), including *C. mukulu*. In the consensus tree, *C. mukulu* is returned as a basal elasmosaurid taxon outside of Elasmosaurinae and Weddellonectia, with *L. morgani* branching just basal to *C. mukulu*, within Euelasmosauria (Figure 1.5.2.).

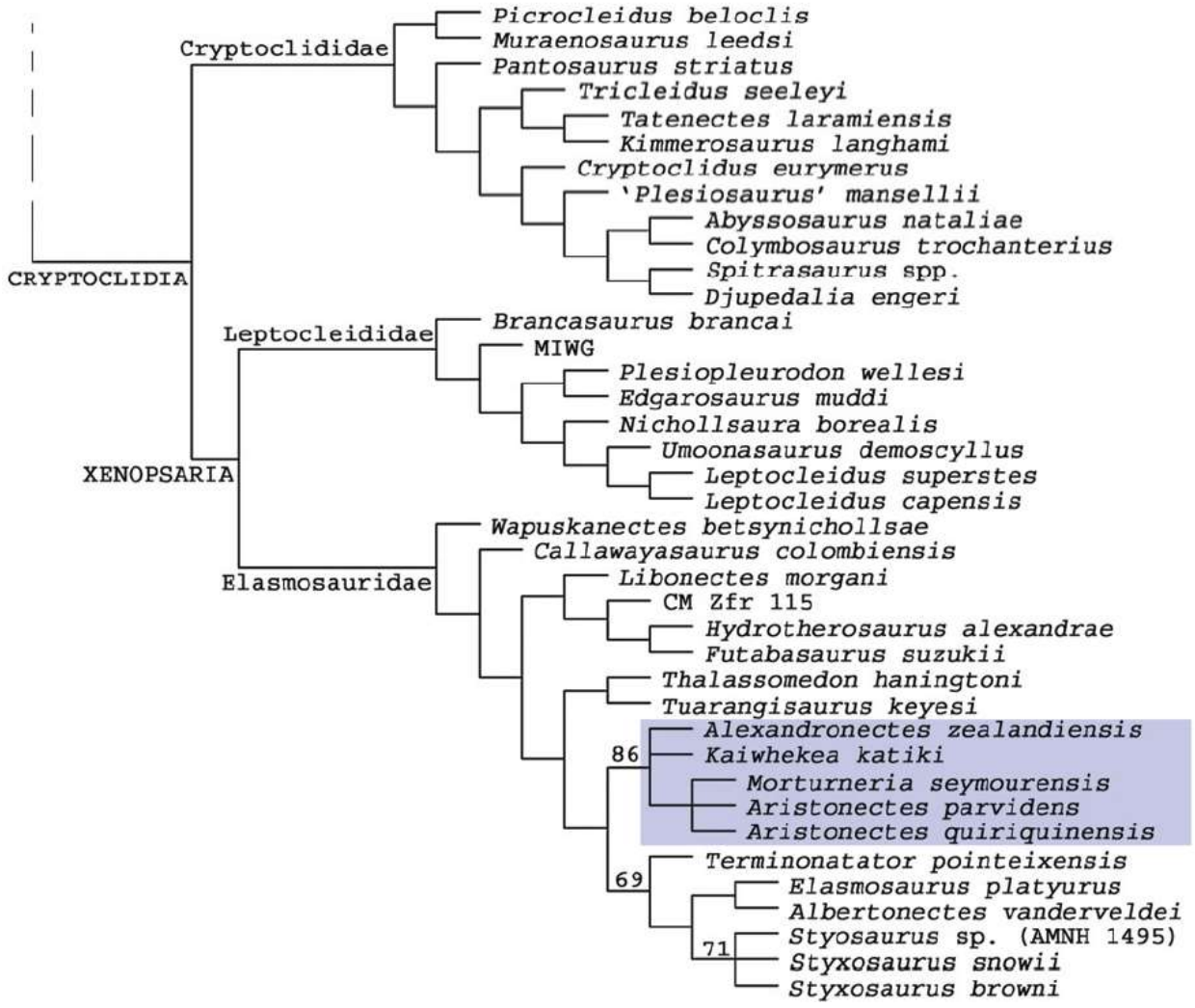

Figure 1.5.1. Cladogram showing elasmosaurid plesiosaurian evolutionary relationships. Aristonectinae is highlighted by the gray box. Figure 12 from Otero et al., (2018).

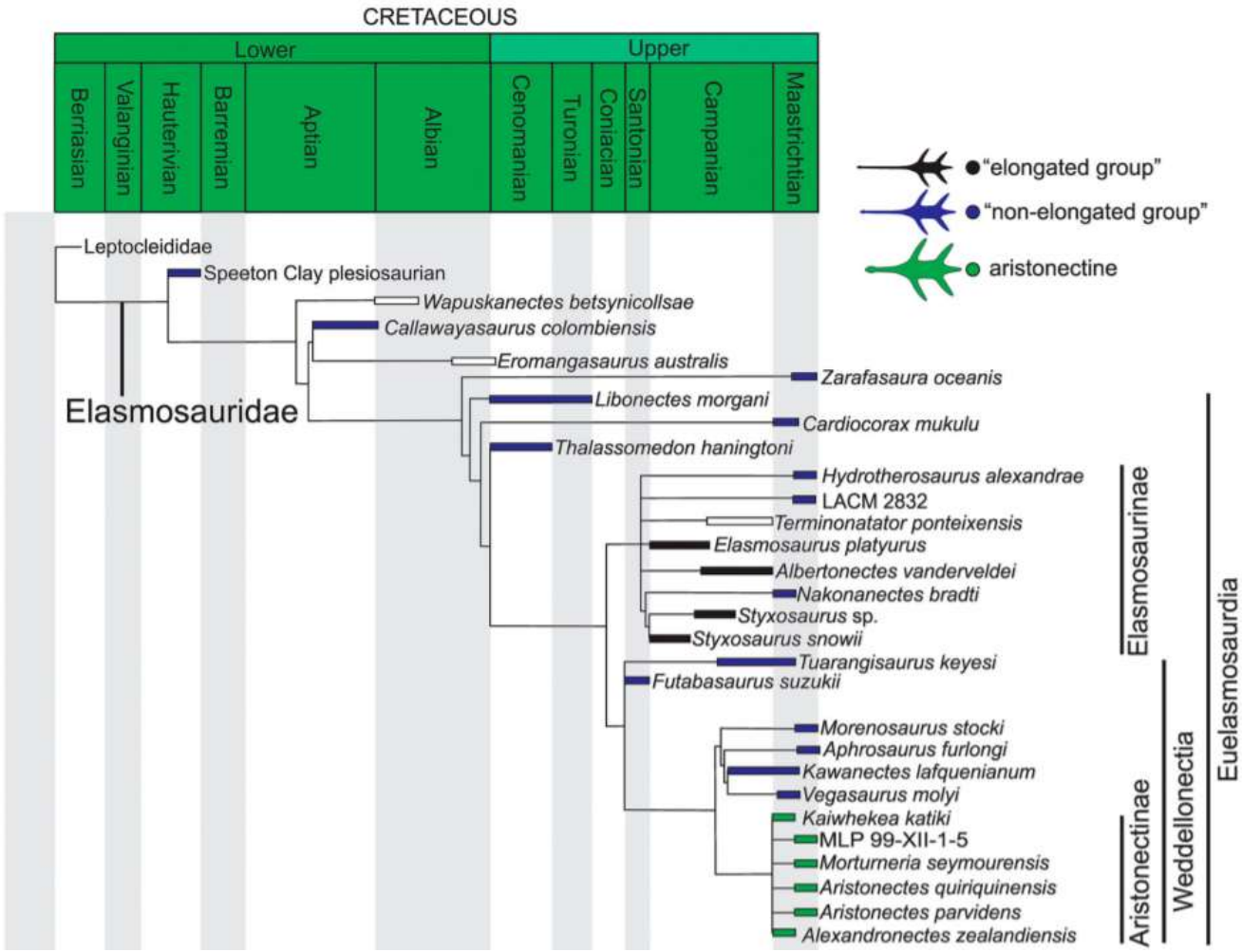

Figure 1.5.2. Phylogeny of Elasmosauridae, including *C. mukulu*. Figure 14 from O'Gorman, (2020).

Methods

The new elasmosaurid specimen from Angola, MGUAN PA278, was mechanically prepared at the Universidade Nova de Lisboa (FCT/UNL) in the macropaleontology laboratory using airscribe, metal and wooden picks to remove rock matrix surrounding bone. Water and acetone were used to soften the fine sandstone matrix. Photographs of the specimen blocks were taken to keep a record of preparation progress and taphonomic data. Sediment that was removed during preparation was collected in plastic bags for future sieving. A photogrammetry of the block containing the skull and the block containing the mandible was performed to map the location of bone elements. The surface of the propodial block was prepared and the jackets containing the rib fragment and posterior cervical vertebra were opened to catalog all of the material associated with MGUAN PA278. Fully prepared and partially prepared elements were described, although further preparation is needed to completely expose all elements associated with MGUAN PA278. The skull was isolated and plaster-jacketed for transport to The University of Texas at Austin High-Resolution CT Facility (UTCT). The skull was CT-scanned overnight for eight hours on a helical non-continuous CT scan.

Scan parameters: NSI scanner, GE Small Spot source, 300 kV, 0.75mA, 4 brass filter, Perkin Elmer detector, 0.25 pF gain, 2 fps, 1 x 1 binning, no flip, source to object 670.0 mm, source to detector 1086.0mm, helical non-continuous CT scan, vertical extent 590.9 mm, pitch 98.467 mm, 6 revolutions, 3 sets, helical sigma 0.0, 4 frames averaged, 0 skip frames, 18005 projections, 5 gain calibrations, 15 mm calibration phantom, data range [-0.5, 5.5] (grayscale adjusted from NSI defaults), beam-hardening correction = 0.45. Voxel size = 141.9 μm. Total slices = 3449. An 8bit jpg version of the 16bitTIFF images was also created.

The 16bitTIFF images were used for segmentation of the cranial bones and the endosseous labyrinth using the software program, AMIRA, at Southern Methodist University (SMU). The raw digital model of the skull on AMIRA was then texturized on MeshLab using the Laplacian filter at 10 smoothing steps reduced from 3,367,985 polygons to 1,000,000 polygons and an additional Laplacian filter at 3 smoothing steps. The braincase was rendered with a Laplacian filter at 10 smoothing steps reduced from 1,578,782 polygons to 500,000 polygons. The semicircular canals were rendered with a Laplacian filter at 10 smoothing steps with no reduction. Perpendicular views of the cranium and semicircular canals were figured using the software, LightWave 11.6.3.

Six collection visits were done by M.M. to compare the skull and postcrania of MGUAN PA278 with other elasmosaurid taxa. In Dec. of 2017, the skull of the holotype of *Libonectes morgani* (SMU SMP 69120), the femur of *Cardiocorax mukulu* specimen, MGUAN PA270, and isolated cranial elements from Bentiaba, Angola were studied and photographed at the Shuler Museum of Paleontology (SMP) at SMU.

In Nov. of 2018, M.M. visited SMP SMU a second time to catalog and photograph plesiosaur cranial and postcranial material from Bentiaba, Angola. Photographs of the skull of the holotype specimen of *Callawayasaurus colombiensis* at UTCT were also taken while the cranium of MGUAN PA278 was being CT-scanned in Nov. of 2018. In April of 2019, M.M. visited the University of Kansas (KU) to redescribed and perform character analysis and photogrammetry on the skull of the holotype specimen of *S. snowii* (KUVP 1301). M.M. also visited the University of Nebraska State Museum (UNSM) for character analysis and description of *T. haningtoni* (UNSM 50132). Additional plesiosaur specimens in the collections at UNSM were studied and photographed. In October of 2019, the holotype of *C. mukulu* was redescribed, scored for characters in a phylogenetic analysis, and photographed at the Museu da Lourinhã in Portugal. A final collection visit by M.M. was done in Dec. of 2019 at SMP SMU, cataloging and photographing every Angolan plesiosaur specimen from Bentiaba, Angola in the SMU SMP collection. MGUAN PA278 was compared to the studied specimens during collection visits and with elasmosaurid specimens from the literature.

Phylogenetic analysis of the new elasmosaurid specimen (MGUAN PA278) and a composite of *Cardiocorax mukulu* was done using five different matrices (Sachs et al., 2015, Allemand et al., 2017, Serratos et al., 2017, Otero et al., 2018, and O'Gorman 2020) using the software, TNT v.1.5 (Goloboff and Catalano, 2016). Serratos et al., 2017, Otero et al., 2018, and O'Gorman, 2020 are recent data sets with a large number of elasmosaurid taxa. Additionally, Serratos et al., 2017 added two new characters to the Benson and Druckenmiller character matrix that are specific to elasmosaurid plesiosaurins. Otero et al., (2018) and O'Gorman (2020) introduced multiple new characters and scored several taxa first-hand. The composite of *Cardiocorax mukulu* was returned in Otero et al., 2018 as the sister taxon to *L. morgani*. To further test the evolutionary affinity between *C. mukulu* and *L. morgani*, the dataset of Allemand et al., 2017 (containing three specimens attributed to *L. morgani*) and Sachs et al., 2015 (first-hand coding for the holotype of *L. morgani*) were run with the composite of *C. mukulu*. Details on the phylogenetic analyses are provided in the phylogeny section (Section 6.).

Measurements of the cranium were taken with Dragonfly 4.1 [Computer software] Object Research Systems ORS Inc, Montreal, Canada, 2018; software available at http://www.theobjects.com/dragonfly and with the software, Meshlab. Three cervical vertebrae attached to the skull block were also measured using Dragonfly 4.1. All other vertebrae that were exposed from preparation were measured with a digital caliper. Height of the centra was measured from the anterior articular facet, length was measured as the maximum anteroposterior distance across the cervical centrum, and width was measured as the maximum distance across the anterior end of the centrum, as standardized by Welles (1952). Smith and Araújo (2017) also define width and height on the anterior facet of the cervical vertebrae, and in this work, we

follow this standardization. Measurements of the propodial from MGUAN PA278 were taken with measurement tape, and dimensions of the paddle elements were done with a digital caliper. Stratigraphic and field data on MGUAN PA278 was collected by Octávio Mateus during the 2017 and 2019 excavations in Bentiaba, Angola. The height index (HI; height/length ratio), as standardized by Welles (1952) for cervical centra was measured for a single cervical centrum associated with the holotype of *C. mukulu* (MGUAN PA103), as it was the only well-exposed centrum in the cervical vertebrae series, and ten well-exposed cervical vertebrae associated with MGUAN PA278. Centrum measurements used to construct the graph of HI values against cervical vertebra position were taken from measurements of selected aristonectine (*Aristonectes parvidens* and *Aristonectes quiriquinensis*), elasmosaurine (*Styxosaurus brownii*, *Hydralmosaurus serpentinus* = *Styxosaurus* sp.) , and '*Cimoliasarus*'-grade elasmosaurid taxa (*Hydrotherosaurus alexandrae*, *Thalassomedon haningtoni*, and *Libonectes morgani*) from Welles (1943, 1949), Otero (2016), Otero et al., (2014a), and O'Gorman (2015). Centrum measurements and height indices of the holotype of *Styxosaurus snowii*, Williston 1890 (KUVP 1301) were measured by M.M. during a collection visit to the University of Kansas in April of 2019.

Stratigraphic provenance of MGUAN PA278

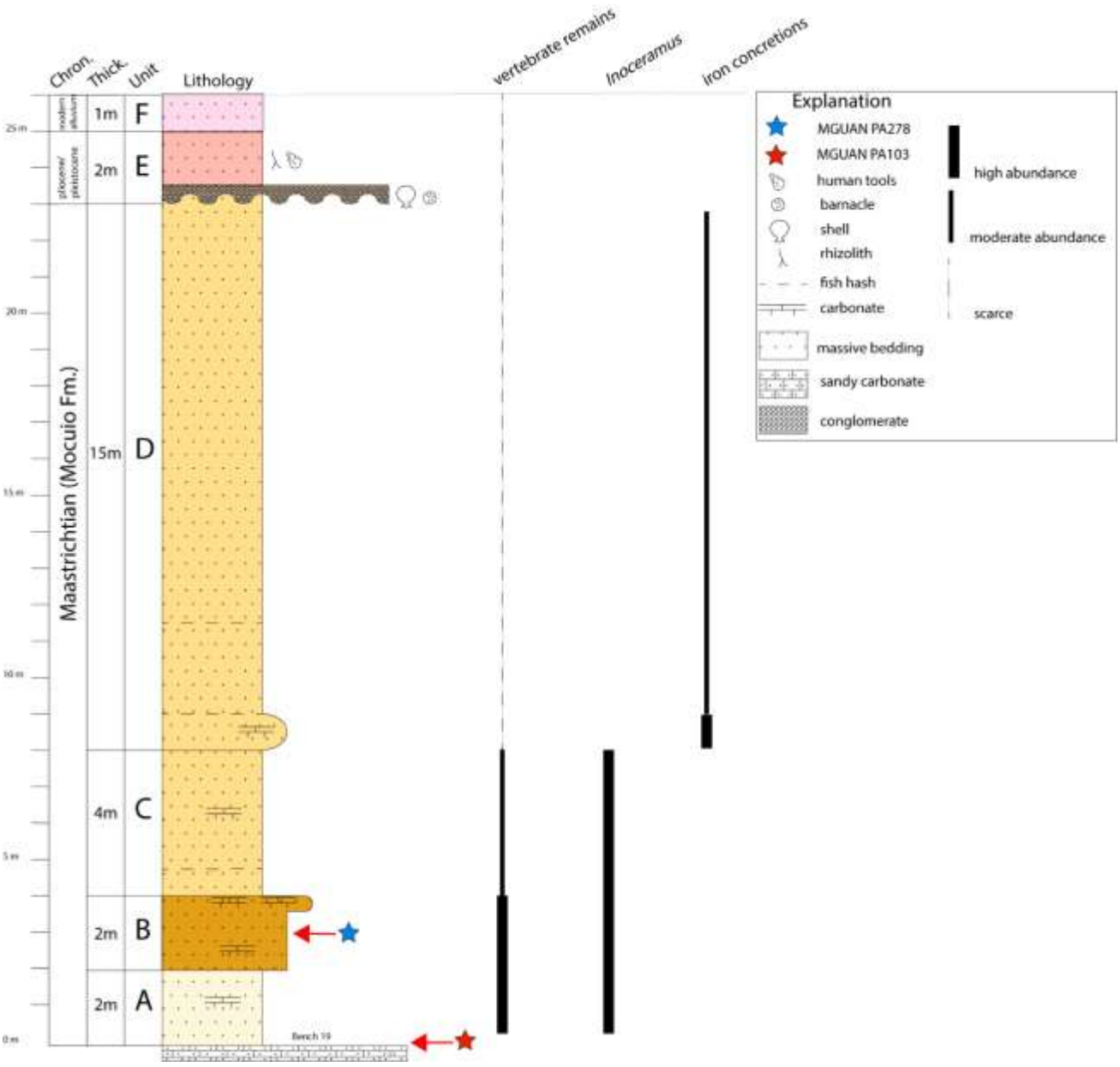

Figure 3.1.1. Stratigraphic column above Bench 19 within the Mocuio Fm. The new plesiosaur specimen (MGUAN PA278) was recovered three meters above Bench 19. Chron. = chronostratigraphy, Thick.= thickness.

MGUAN PA278 was recovered approximately three meters above Bench 19 in the Mocuio Formation of Bentiaba, Angola (figure 3.1.1.). The specimen was within Unit B; this layer is differentiated from other layers by an tannish color and a greater amount of carbonate than the underlying whittish sandstone (Unit A) and the overlying Unit C layer. Within Unit B, shell fragments of *Inoceramus* are found concentrated at the top of the layer. The holotype of *C. mukulu* was recovered just above Bench 19, in Unit A. *Inoceramus* shells are present in the lower three units, but disappear in Unit D. Unit D is

chracterized by the presence of abundant iron concretions thoughout the layer. Two thin layers dense with fish bones (fish hash in the column) are present in Unit D and one is apparent in Unit C. The Mocuio Fm. is capped by a 0.5 m conglomerate with fossils of bivalves and barnacles. The conglomerate and the light colored pinkish sandstone layer in Unit E are Pliocene-Pleistocene in age, with the top-most layer being modern alluvium.

Figure 3.1.2. Excavation site of *C. mukulu* (MGUAN PA278) within the Unit B section above Bench 19.

Taphonomy

The elements associated with MGUAN PA278 include a well-complete cranium and mandible, thirteen teeth, two hyoids, an atlas-axis complex, and at least fifteen postaxial cervical vertebrae. These remains indicate that the anterior-most end of the animal was preserved, in addition to a propodial, metapodial elements, 33 phalanges, and two rib fragments. Erosion is observable on all vertebrae within the rock layer, suggesting the vertebrae were worn before burial. Plastic shearing deformation is observable in one centrum. The cranium is dorsoventrally compressed, with the best-preserved regions being the occiput, the right posterolateral side of the skull, and the anterior end of the snout. These areas were the least affected by compressional, shearing, and erosional forces. Thus, these areas retain most of their original three-dimensional morphology. The left-lateral side of the skull, in contact with four cervical vertebrae, is significantly distorted. There is clear evidence of bioturbation in the rock matrix containing the skull, with two separate calcified burrows visible; one in the right orbit and a second going through the left orbit. These burrows exhibit a branching pattern inside the sandstone matrix. Part of the skull roof in the antorbital region of the cranium, and the parietal crest in the posterior-half of the cranium, had already been eroded before the animal was buried. The obvious evidence of erosion in the cranium and the absence of all primary teeth in the skull, and only two remaining in the mandible, suggests erosion of bone elements on the bottom of the continental shelf and decay of tooth ligaments before burial.

The right ramus of the mandible is tilted, with the dorsal margin facing medially, while the left ramus is oriented in approximately life position. The right lateral surface of the mandible was exposed in the field and is significantly weathered, especially on the coronoid process and the surangular. Five phalanges are partially articulated while all the rest are disarticulated. Two phalanges adjacent to the articulated set were replaced as casts by a carbonaceous matrix. Limb elements are highly dispersed. Modern weathering had caved-in the head of the propodial, exposing trabeculae coated in halite crystals. The two rib fragments associated with MGUAN PA278 are compressed.

The bone elements of MGUAN PA278 are highly disarticulated and mixed with the skeletal remains and teeth of mosasaurs, bony fish, sharks, and even the phalanx of a turtle (Figure 4.1.1.). Mosasaur vertebrae recovered with the blocks containing MGUAN PA278 align to form a series, suggesting that the mosasaur vertebrae belong to a single individual (Figure 4.1.2.). The disarticulated elements of MGUAN PA278 and associated fauna suggests perturbation on the shelf floor and a slow burial time (figure 4.1.2., 4.1.3., 4.1.4.). The disarticulated condition of the skeletal elements from MGUAN PA278 indicates that the soft tissue connection between the bones had been decomposed or scavenged before burial. Only one bite mark from a carnivorous vertebrate is observed on an anterior

cervical vertebra. The gouge from the tooth mark is shallow in depth. *Squalicorx pristodontis* is most associated with bite marks on plesiosaur bones from Bentiaba (Araújo et al., 2015b). No evidence of healing on the bone is apparent and suggests scavenging rather than an attack bite (Dortangs et al., 2002). The recovered plesiosaur remains can confidently be assigned to a single individual based on the association and proximity of the elements, all coming from an adult elasmosaurid plesiosaurian without duplicates, and with the same style of preservation.

The bone layer in which the elements of MGUAN PA278 are preserved is greater than 10 cm in thickness. In terms of lithology, the sediment matrix surrounding the bones is a fine immature feldspathic sandstone with a clay cement (Araújo et al., 2015b). There is a carbonaceous residue that covers many of the larger bone elements of MGUAN PA278, such as the propodial, mandible, cranium, and vertebrae. This carbonaceous residue effectively acts as a glue and is especially apparent where the skull is bonded to four separate cervical vertebrae, that are in turn adhered to each other and surrounding cervical vertebrae.

Six mosasaur vertebrae, and four mosasaur teeth were found associated with MGUAN PA278 (Figure 4.1.1., 4.1.2.). Three of the isolated teeth are from *Globidens*, and one is likely from *Prognathodon*. Several small shark teeth were recovered during preparation, in addition to shark teeth found on-site during the excavation of MGUAN PA278. There is a large shark centrum on top of the propodial of MGUAN PA278 that can be tentatively ascribed to *Squalicorax pristidontus*, based on the size. The blocks included many isolated bony fish elements. A large tooth from *Enchodus* is present at the anterior end of the mandible of MGUAN PA278 (Figure 4.1.3.).

Overall, it can be inferred that the environment at Bentiaba during the Early Maastrichtian (71.4-71.64 Mya) was a productive locality, with a high diversity and abundance of macropredaceous vertebrates (Mateus et al., 2012; Araújo et al. 2015a, 2015b; Polcyn et al., 2010; Schulp et al., 2006, 2007, 2013). MGUAN PA278 includes the anterior-most end of the animal and a limb. Pre-burial erosion is evident on the vertebrae, mandible and skull, with only two observable primary teeth remaining in the mandible, indicating a relatively slow burial time at approximately 50-100m in depth on the continental shelf (Strganac et al., 2014, 2015). The presence of only a single bite mark on one cervical vertebra may suggest an overall absence of regular scavenging by large-bodied sharks on the observed skeletal material. Other plesiosaur specimens exhibit a high degree of scavenging by *Squalicorax pristodontus* (Araújo et al., 2015b, M.M. pers. obs.) This lack of scavenging may have been crucial toward the preservation of the plesiosaur specimen and the well-complete nature of the cranium and mandible.

Figure 4.1.1. Vertebrate remains recovered from the *C. mukulu* (MGUAN PA278) excavation site in Bentiaba, Angola. Top row, a phalanx from a chelonid turtle. Second row, isolated teeth from *Globidens*; last tooth in the row is likely from *Prognathodon*. Third row, neonate mosasaur remains: an isolated vertebra followed by two humeri. Fourth row, isolated teeth from the large macrophagous shark, *Squalicorax*. Fifth row from the left side, isolated teeth from *Cretolamna biarculata*, *Carcharias* (?), isolated sawfish tooth, and an isolated shark centrum. Scale is equal to 2 cm.

Figure 4.1.2. Blocks with associated elements from *C. mukulu* (MGUAN PA278) arranged according to *in situ* relationship. Color differences between blocks reflect different lighting environments and usage of different cameras. The spatial relationships of the blocks is approximated based on the excavation notes of Octávio Mateus.

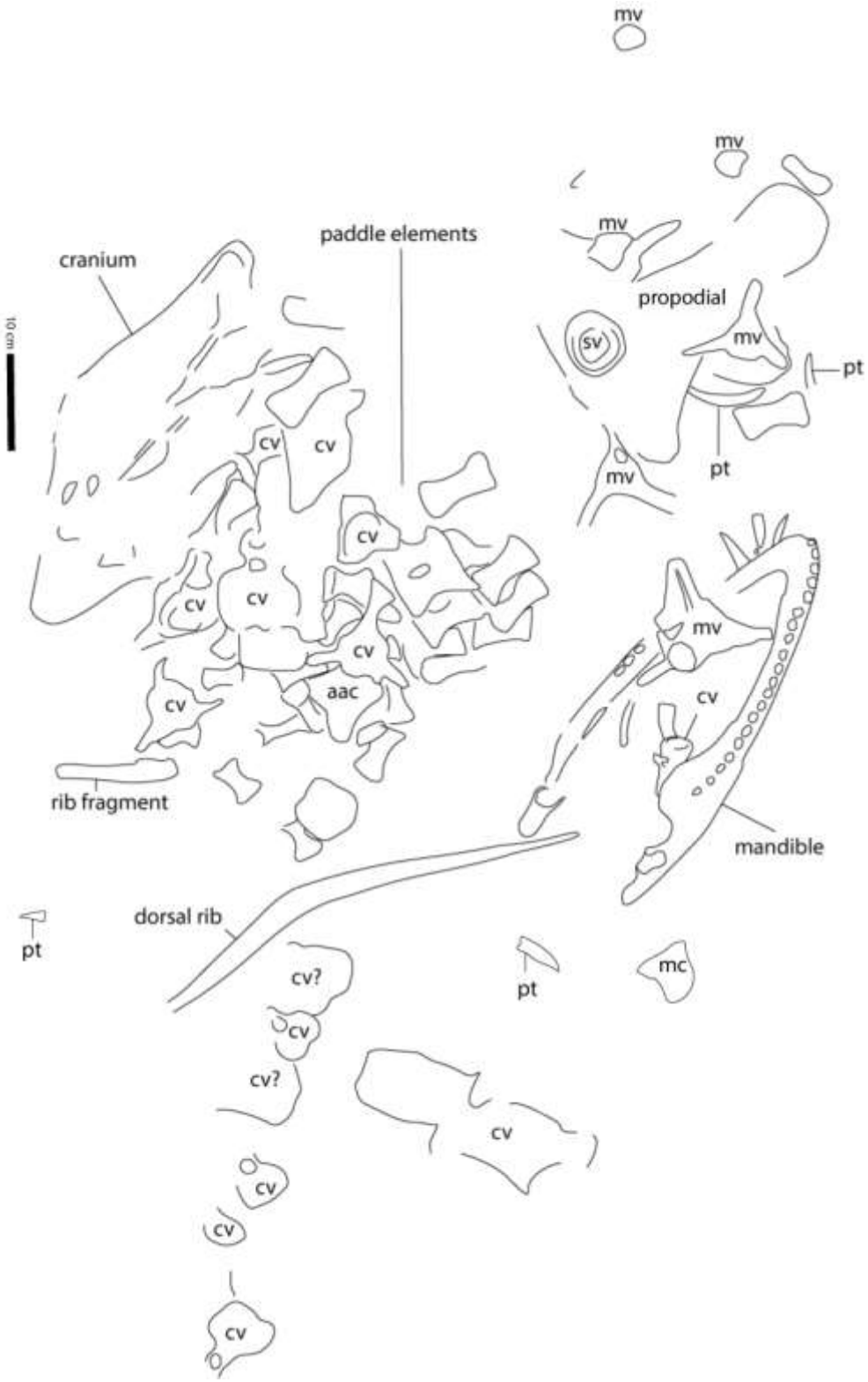

Figure 4.1.3. Quarry map of *C. mukulu* (MGUAN PA278). **Abbreviations**: aac, atlas-axis complexe; cv, cervical vertebra from MGUAN PA278; mv, mosasaur vertebra; sv, shark vertebra; mc, metacarpal; pt, plesiosaur tooth. The spatial relationships of the blocks is approximated based on the excavation notes of Octávio Mateus.

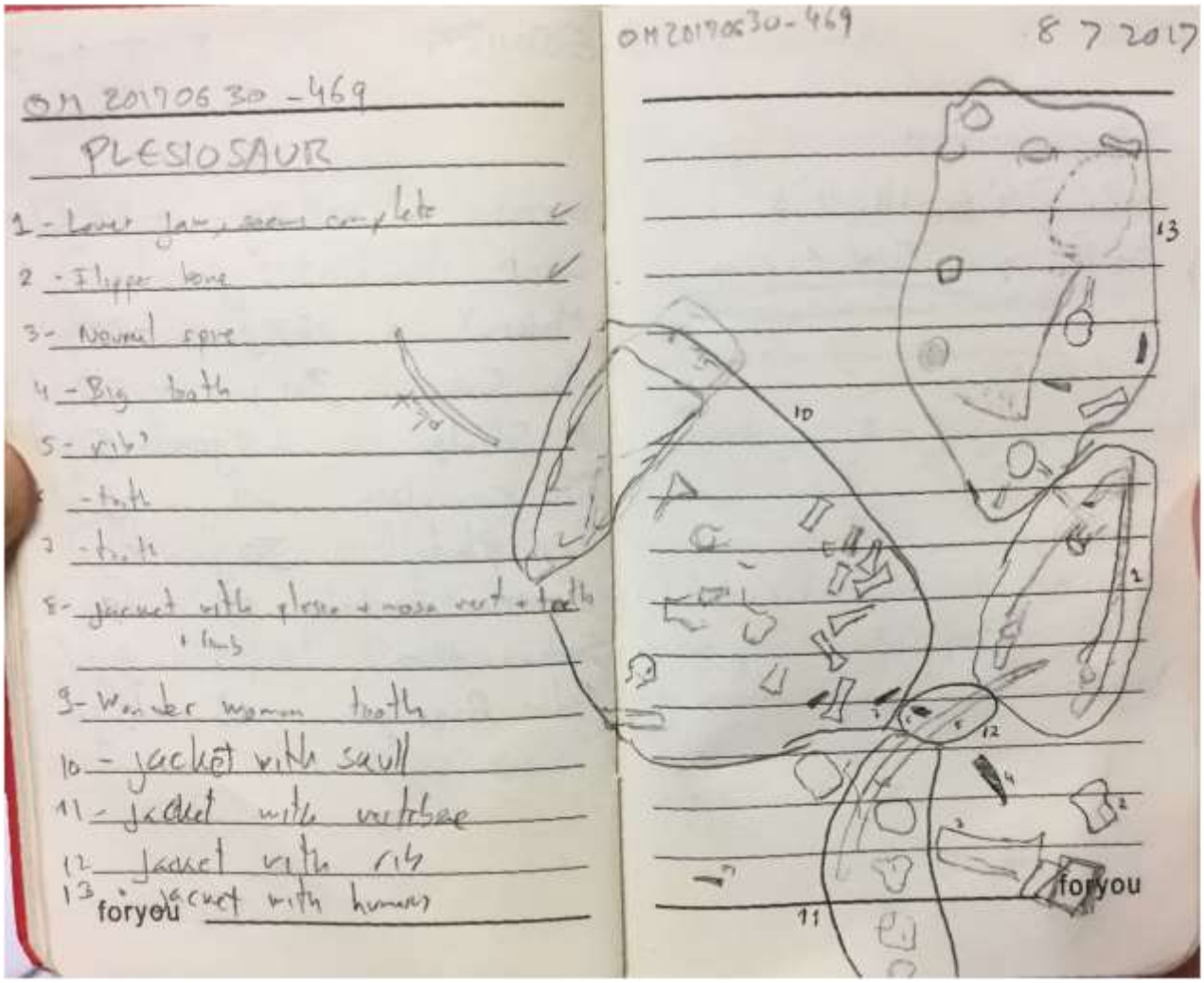

Figure 4.1.4. Sketch and notes of Octávio Mateus from the excavation site of *Cardiocorax mukulu* (MGUAN PA278); July 2017.

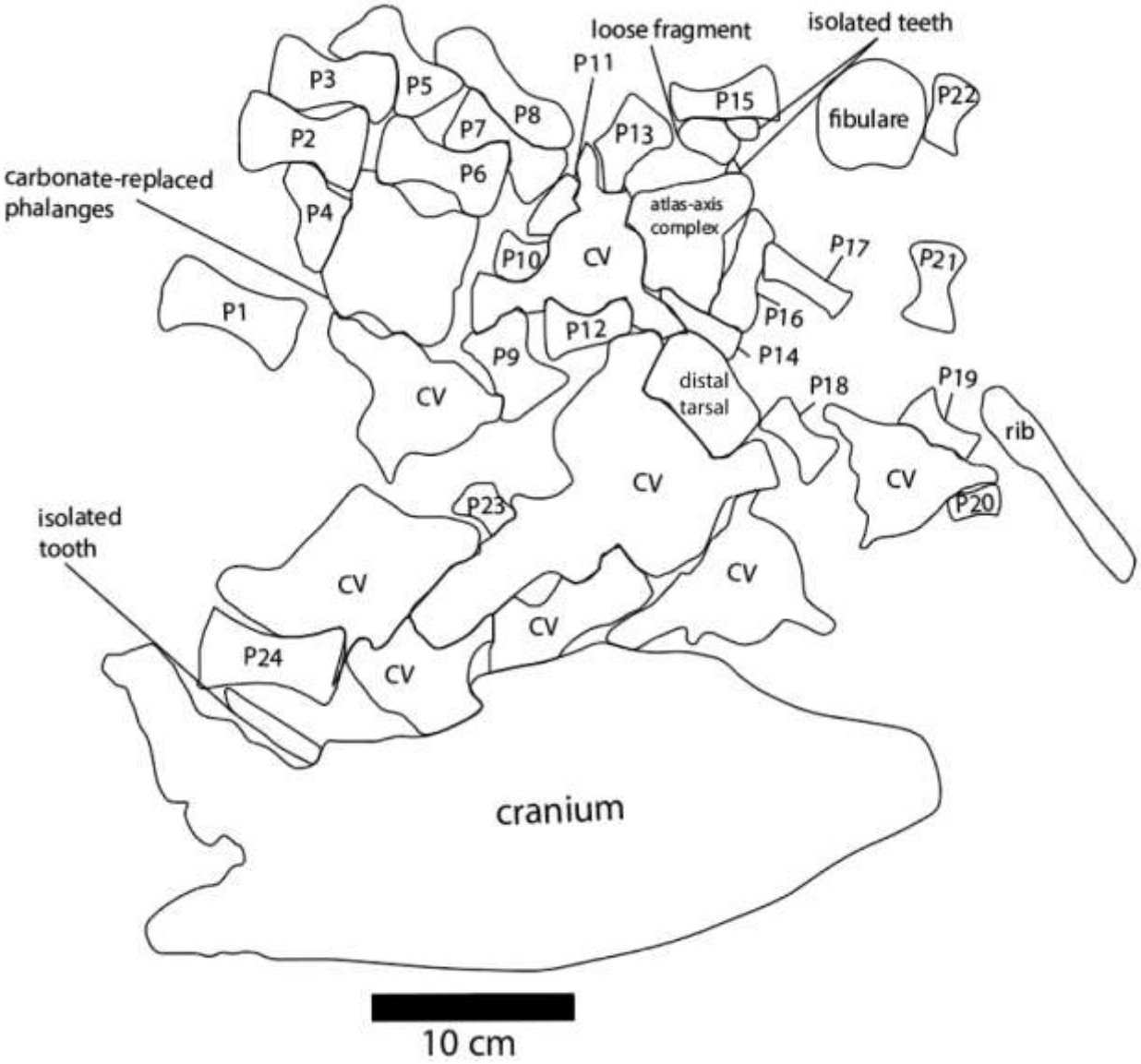

Figure 4.1.5. Line drawing with labels of elements from the skull block of *Cardiocorax mukulu* (MGUAN PA278).

Figure 4.1.6. Photo of the skull block from *Cardiocorax mukulu* (MGUAN PA278) during preparation in dorsal view.

SYSTEMATIC PALEONTOLOGY

REPTILIA Linnaeus, 1758

DIAPSIDA Osborn, 1903

SAUROPTERYGIA Owen, 1860

PLESIOSAURIA de Blainville, 1835

XENOPSARIA Benson & Druckenmiller, 2014

ELASMOSAURIDAE Cope, 1869

***Cardiocorax mukulu* Araújo et al. 2015**

Horizon:

The Unit B fine yellowish sandstone layer above Bench 19 of Strganac et al., (2014). Part of the Mocuio Formation in the São Nicolau Group

Age:

Early Maastrichtian (71.4- 71.64 Ma) (Strganac et al., 2015)

Locality:

Bentiaba, Moçamedes Municipality, Namibe Province, Angola. General geographic coordinates:

S 14.2° E 12.3°

Material:

New specimen of *Cardiocorax mukulu* reported here: MGUAN PA278

A nearly complete cranium and mandible. Thirteen associated teeth outside of the cranium and mandible, and two hyoids. A nearly complete atlas-axis complex and at least 15 postaxial cervical vertebrae. Two dorsal/pectoral rib fragments, one propodial, at least two mesopodial elements, one metapodial element, and 33 phalanges.

Specimens referable to *Cardiocorax mukulu*:

Holotype: MGUAN PA103

Other specimens: MGUAN PA270, MGUAN PA271

Etymology: the genus name is based off the heart-shaped intercoracoid fenestra, derived from Latinised Greek *Kardia* and Latinised Greek *corax* ("crow" from which the word coracoid is derived from). The word '*mukulu*' translates to 'ancestor' in Angolan Bantu dialects (Araújo et al., 2015a).

Revised diagnosis of *Cardiocorax mukulu* Araújo et al., (2015a)

New unique combination of characters used to diagnose *C. mukulu*:

Maxilla, a dorsal ramus of the maxilla that forms the majority of the anterior margin of the orbit; premaxilla and maxilla, an unambiguous count of five premaxillary alveoli and seventeen maxillary alveoli in the upper tooth row; internal nares, internal nares exhibit an ellipsoidal shape in palatal view; pterygoids, an absence of medial contact between the pterygoids beneath the basioccipital; coracoids, posterolateral cornua of the coracoids extends lateral to the glenoid of the pectoral girdle; exoccipital-opisthotic, three distinct cranial nerve openings (one jugular and two foramen for branches of nerve XII) on the lateral and medial surface of the exoccipital-opisthotic; clavicles, clavicles contact each other along entire medial margin; vertebrae, middle cervical neural spines exhibit a sinusoidal outline along the anterior margin in lateral view.

Autapomorphies retained from original diagnosis (Araújo et al., 2015a) of *C. mukulu*:

Clavicles, clavicular ventral area nearly as broad as scapular ventral area; scapula, proximodistal extent of the dorsal blade is significantly less than the anteroposterior extent of the scapula, scapular shaft is ellipsoidal in cross-section broadly splaying anteriorly, medial contact between scapulae extending along entire medial surface; coracoids, asymmetrical ventral buttress of the coracoids.

Unique combination of characters from Otero (2016) and Otero et al., (2018) to diagnosis *C. mukulu* (parent matrix: Benson and Druckenmiller, 2014): ch.13.1, the alveolar margin of upper jaw in lateral view is undulating or 'scalloped'; ch.52.0, anterior extension of the parietal extends to the level of the temporal bar; ch.61.1, dorsal portion of the posterior margin of the squamosal is inflected abruptly anterodorsally; ch.98.0, the pterygoids form a loose, overlapping contact with the basicranium; ch.132.1, heterodont posterior premaxillary dentition, reduced distalmost alveolus; ch.136.1, an absence of enamel 'striations'; ch.165.1, the presence of a rounded median ventral keel on the cervical centra; ch.207.2, posterolateral cornua of the coracoid extend lateral to the glenoid.

Description of MGUAN PA278

Cranial skeleton

The anteroposterior length of the skull of MGUAN PA278 was not significantly affected by taphonomic processes and measures 390.4 mm from the tip of the premaxillae until the occipital condyle. From the posterior-most end of the cranium (right quadrate) until the anterior tip of the premaxillae, the skull length is 445.5 mm. Due to mediolateral compression, the width of the skull and temporal fenestrae could not be determined accurately. The right temporal fenestra measures 174.2 mm anteroposteriorly. The anteroposterior length of the right orbit (better preserved than its left counterpart) measures 68.2 mm, although the right postorbital bar is worn and not in complete articulation. Thus, this measurement should be considered more of an approximation. Distortion of the skull in and around the area of the orbits prevents accurate determination of orbit dimensions.

The preorbital portion of the premaxillae between the fifth alveolus of the upper tooth row and the tip of the snout exhibits relatively low distortion, with the left premaxilla being slightly displaced ventrally and laterally as made evident by a large crack running posteromedially from the anterior end of the left premaxilla, to parallel the dorsal suture between both premaxillae (Figure 5.2.1. and 5.2.2.). The posterodorsal extension of the premaxillae on the skull roof is highly worn between the fifth alveolus of the upper tooth row and the orbitonasal bar. Past the orbitonasal bar, the posterior extensions of the premaxillae are well preserved. The left maxilla is particularly worn and tilted to where maxillary alveoli four through seven face laterally. Within the left maxilla, alveoli past alveolus seven are not discernable. The right maxilla is preserved in good condition. Calcareous rock matrix resides within most of the alveoli in the upper tooth row. The posterior portion of the left maxilla and the left jugal, which contribute to the ventral border of the left orbit are rotated horizontally, with the dorsal margin of the left maxilla and jugal facing medially and the ventral margin facing laterally. The posterior extension of the left

maxilla on the temporal bar is missing. The dorsal ramus of the right maxilla is preserved, but the dorsal ramus of the left maxilla is fractured near its base, with the distal end tilted medially. The palate is exposed in dorsal view of the cranium, between the fifth alveolus of the premaxillae and the orbitonasal bars, due to severe erosion along the skull roof. The right postorbital bar, formed by the postorbital and frontal, is dorsoventrally compressed along with most of the right temporal bar.

In dorsal view of the left half of the cranium, the postorbital bar is mostly worn away, the temporal bar is missing, and the quadrate and squamosal are rotated to where the dorsal margin of the left squamosal faces medially and the condyles of the left quadrate face laterally. The right temporal bar is slightly bowed medially. The occiput and the right posterolateral corner of the skull that encompasses the posterior half of the jugal, the squamosal, quadrate, right paroccipital process, and quadrate process of the pterygoid exhibit a low degree of distortion and are one of the best-preserved areas of the skull with respect to three-dimensional articulation (Figures 5.2.3. and 5.2.4.). The dorsal rami of both squamosals are missing. In dorsal view, the parietal can be traced along the midline of the skull, medial to the temporal fenestrae. The anterior-most extent of the parietal forms an interdigitating suture with the posterior extensions of the premaxillae between the orbits. Posterior to the parietal-premaxillary suture, a fragment from the anterior portion of the parietal is offset from the midline of the skull. Posterior to this fragment, most of the remaining fragments from the parietal are realigned along the midline of the skull. The posterior-most fragment of the parietal is displaced toward the right half of the skull. The distal margin of the parietal crest has mostly worn away, although the base of the crest remains. The supraoccipital is fragmented with its lateral portions located overtop the prootics and exoccipital-opisthotics, while the median portion is floating in matrix above the basioccipital.

In ventral view of the skull, the palate is highly fractured and bows dorsally, although sutures between different palatal elements can still be discerned. Significant dorsoventral compression of the skull is evident in and around the area of the orbits, to the point where the frontals contact the palate in some areas. The left ectopterygoid and palatine are displaced with the lateral margins of these elements facing upward, a likely result of distortion along the left side of the cranium. The right subtemporal fenestra is only slightly distorted, with the lateral margin bowed medially. The anteroposterior length of the right subtemporal fenestra is preserved.

The parasphenoid and basisphenoid are articulated together, although a narrow space separates the basisphenoid from the basioccipital. Morphological details of thin and fragile features of the basicranium including the clinoid processes and the ventral keel of the parasphenoid are clearly visible. The prootics are detached from the basicranium and are floating in the rock matrix. The semicircular canals in the right half of the braincase are clearly visible between the prootic, exoccipital-opisthotic, and

the supraoccipital. Although, the semicircular canals from the left-half of the cranium are not entirely preserved due to breakage of braincase elements. The base of the right exoccipital-opisthotic remains articulated with the basioccipital, while the left exoccipital-opisthotic is partly displaced from its contact with the basioccipital.

Two calcified burrows are visible in the skull block of MGUAN PA278, with one located just lateral to the left frontal and a second going through the center of the right orbit. The burrow in the right half of the skull block forms branches that off-shoot in different directions within the rock matrix. Calcareous residue is apparent throughout much of the surface of the cranial elements and is most concentrated in the alveoli of the upper tooth row, and the ventral margin of the basioccipital. Despite the noted distortion, the skull of MGUAN PA278 overall retains exceptional three-dimensional preservation and thus provides significant morphological and anatomical insight.

Figure 5.2.1. Cranium of *Cardiocorax mukulu* (MGUAN PA278) in dorsal view.

Figure 5.2.2. Cranium of *C. mukulu* (MGUAN PA278) in dorsal view with exposed cranial elements labeled and illustrated.

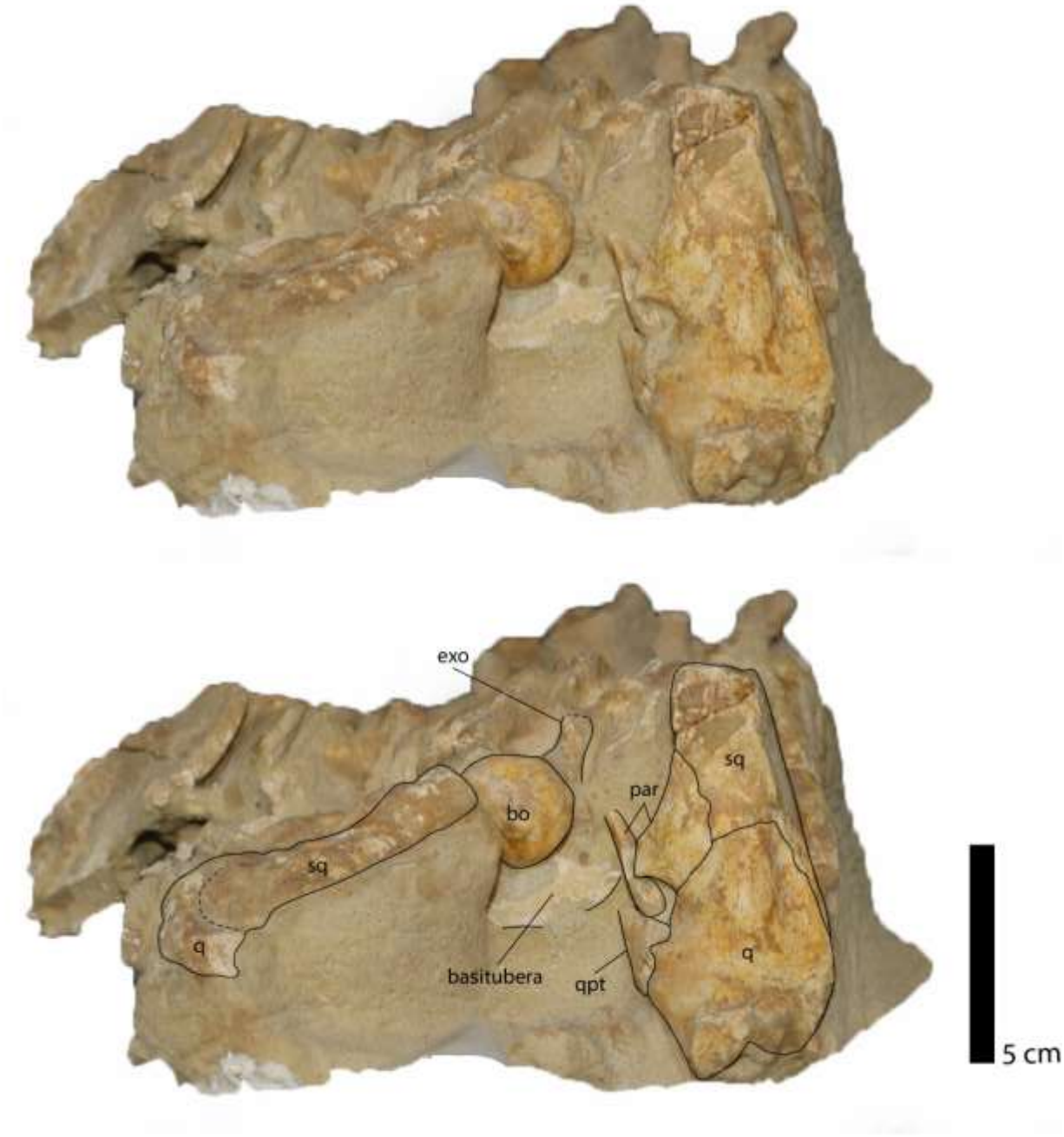

Figure 5.2.3. Exposed occiput of *C. mukulu* (MGUAN PA278) cranium.


5 cm

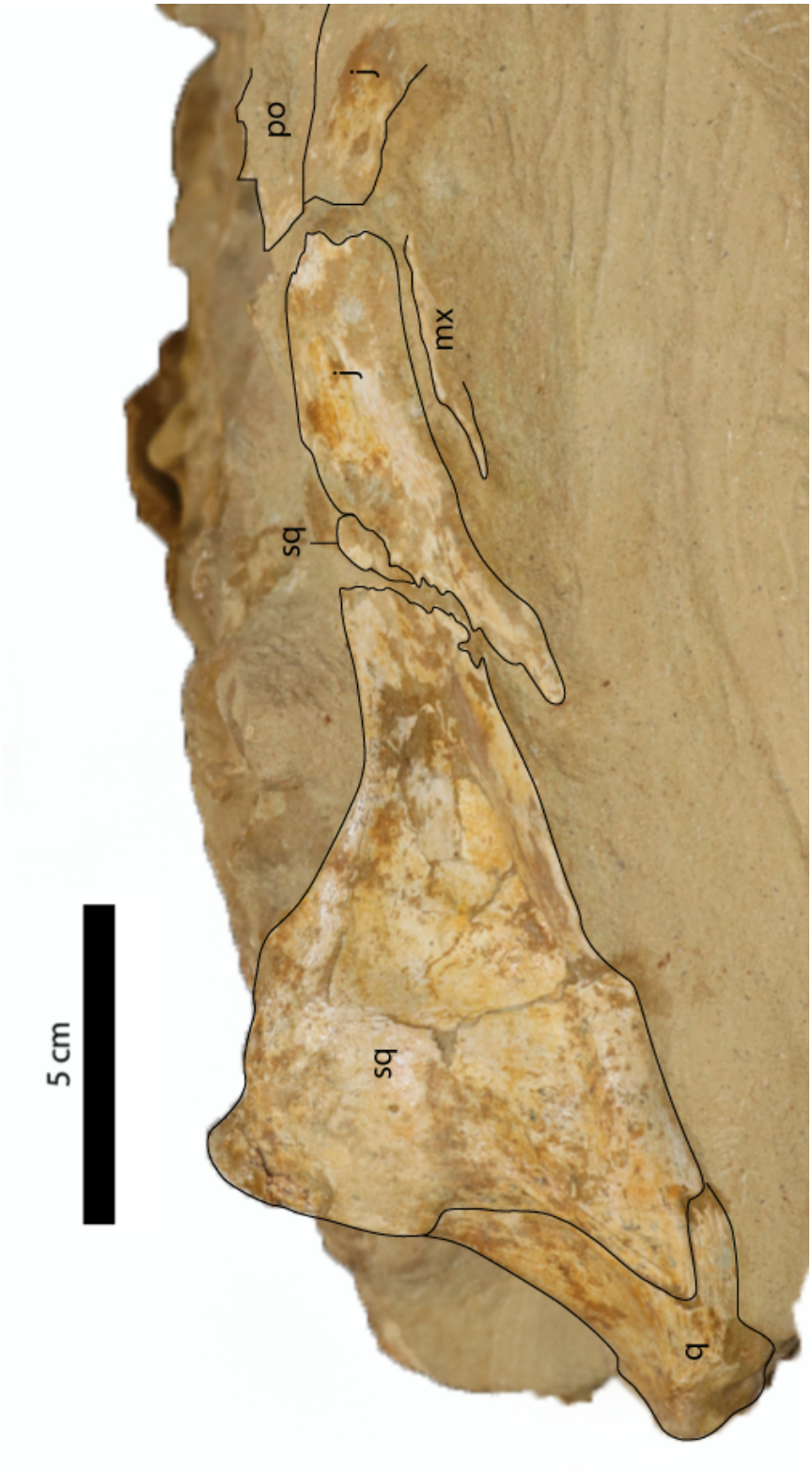
po
j
j
mx
sq
sq
q
5 cm

Previous pages (62-63): Figure 5.2.4. *C. mukulu* (MGUAN PA278) with exposed right temporal bar and right temporal bar labeled with cranial elements outlined.

Craniofacial Skeleton

The **premaxillae** are large, broad elements that form the anterior end of the skull (figure 5.2.5.). The suture between the premaxillae is straight and visible in dorsal view of the skull. A dense network of foramina is apparent across the dorsal and lateral surface of the premaxillae, making the snout highly vascularized. Anteriorly, the snout forms a rounded and blunt tip. A dorsomedian process is present along almost the entire dorsal margin of the premaxillae (Figures 5.2.6., 5.2.7.). This dorsomedian process is expressed as a subtle ridge at the anterior-most end of the premaxillae. The dorsal process flattens above the third premaxillary alveolus but becomes prominent as a broad ridge, triangular in cross-section posterior to the third premaxillary alveolus until the fifth premaxillary alveolus. Beyond the fifth alveolus of the premaxillae, the posterior extensions of the premaxillae are extremely weathered. The broad triangular dorsomedian ridge from the snout transitions to form a lower, and sharper ridge between the orbits. A dorsomedian ridge is a character that is common within Elasmosauridae, specifically *S. snowii*, *T. haningtoni*, *N. bradti*, *T. keyesi*, *E. australis*, *T. ponteixensis*, and *F. suzukii*, but not *A. parvidens*, *H. alexandrae*, *Z. oceanis*, *C. colombiensis*, and *Lagenanectes richterae* Sachs, Hornung, and Kear, 2017 (Welles, 1943; Gasparini, 2003; Kear, 2005; Sato, 2003, 2006; Vincent et al., 2011 Sachs et al., 2017; Sachs, 2018; O'Gorman, 2020, M.M. pers. obs.). This process has not been mentioned or described in *S. brownii* or *K. katiki* (Welles, 1952; Carpenter, 1999; Otero, 2016; Cruickshank & Fordyce, 2002).

In dorsal view, a slight bulge of the premaxillae anteromedial to the orbitonasal bars in MGUAN PA278 is suggestive of a premaxillary 'boss', observable in *S. snowii*, *S. brownii*, and *T. haningtoni* but not *L. morgani*, *T. keyesi* or *C. colombiensis* (Figure 5.2.8., 5.2.9., 5.2.9.1.) (Otero, 2016; O'Gorman et al., 2017b, M.M. pers. obs.). However, the weathered nature of the premaxillae in this area makes this interpretation difficult for MGUAN PA278. Narrow posterior extensions of the premaxillae along the dorsal midline of the skull form the dorsomedial margin of the external nares. The suture between the premaxillae and the maxillae arises from behind the fifth alveolus of the premaxillae and curves posteromedially until it reaches the anterior margin of the external nares. The maxillae contribute to the lateral margin of the external nares anterior to the orbitonasal bar. The external nares of MGUAN PA278 are located anterior to the orbitonasal bars however the precise outline of the external nares cannot be assessed due to compression of the skull and damage along the posterior extensions of the premaxillae.

The dorsomedian process is expressed as a low transversely compressed ridge medial to the orbits. The highly compressed dorsomedian process is asymmetric in that the ridge is expressed exclusively by the right premaxilla (Figure 5.2.7.). This suggests some sort of taphonomic effect, where the dorsomedian ridge on the left premaxilla has worn away. The posterior extensions of the premaxillae overlap and divide the frontals between the orbits, as is the case in most elasmosaurids. The ventral margin of the premaxillae and the medial margins of the frontals form the olfactory sulcus between the orbits. The posterior termination of the premaxillae in MGUAN PA278 is located medial to the postorbital bar. The junction between the premaxillae and the parietal forms an interdigitating suture and is transversally broad. The broad suture and spatulate morphology of the parietal at its interface with the posterior extensions of the premaxillae is observable in MGUAN PA278 and is informative regarding elasmosaurid skull anatomy, as this area is often one of the most difficult areas to interpret due to taphonomic distortion or ambiguous areas of contact between the premaxillae and parietal (Welles, 1943; Carpenter, 1997; O'Gorman, 2017b; Sachs and Kear, 2017; Sachs, 2018).

Both premaxillae contain the same number of primary alveoli (5) as *S. snowii*, *L. morgani*, *T. haningtoni*, and *C. colombiensis*, but differs from *E. platyurus* (6), *E. australis* (3), and the aristonectines *K. katiki* (7) and *A. parvidens* (13) (Cruickshank and Fordyce, 2002; Sachs, 2005a; Kear, 2007; O'Gorman, 2015a; Sachs et al., 2018) . The anterior-most pair of premaxillary teeth in MGUAN PA278 is the smallest in the premaxillae. Pairs of premaxillary teeth become sequentially larger posteriorly in MGUAN PA278, as determined by the diameters of the alveoli in palatal view. In the left premaxilla, a replacement tooth can be seen transitioning into the first primary alveolus. A second replacement tooth in the left premaxilla is entering the third primary alveolus. In the right premaxilla, replacement teeth can be seen transitioning into the second and fourth primary alveoli. In total, four replacement teeth are present in the premaxillae, with no primary teeth remaining. Replacement teeth at the anterior-most end of the premaxillae are more procumbent than the more posteriorly positioned replacement teeth. In palatal view the premaxillary alveoli are ovate in shape with the long axis oriented along the labiolingual axis (Figure 5.2.6.). Secondary alveoli are situated medial to the primary alveoli within indented channels. The premaxillae do not contribute to the palate. A narrow opening between the premaxillae medial to primary alveoli pairs two through three is identified as the 'vomeronasal fenestra', although O'Gorman et al., (2017b) questions this homology. The 'vomeronasal fenestra' is also seen in *L. morgani* and in *E. platyurus* (Carpenter, 1997; Sachs, 2005; MM pers. obs.).

Figure 5.2.5. Exposed surface of the premaxillae of *C. mukulu* (MGUAN PA278).

The alveoli of the **maxillae** are oriented more vertically as opposed to the procumbent alveoli of the premaxillae. In the right-half of the skull, maxillary alveoli one through six are sub-vertical in orientation, while maxillary alveoli seven through seventeen exhibit a straight, vertical orientation. The maxillary alveolus with the greatest dimensions and root depth is the third alveolus, located within the orbitonasal bar, which accommodates a large tooth, sometimes referred to as the 'maxillary fang' in the literature (Carpenter, 1999; Sachs et al., 2018). The depth of the third maxillary alveolus in the right maxilla is approximately 48.8 mm. The anteroposterior length of the third alveolus, seen in ventral view, is 18.6 mm long (measured perpendicular to the labiolingual axis) with a width of 16.0 mm (measured parallel to the labiolingual axis). The length and width of the maxillary alveoli in palatal view and their tooth depth decreases in the posterior direction of the upper tooth row. A total of 17 primary alveoli are discernable in the right maxilla. Only the first seven maxillary alveoli are discernable in the left maxilla, as this left element is significantly more distorted than its right counterpart. A count of 17 maxillary

alveoli contrasts with maxillary tooth counts of 15 visible complete and fragmented teeth in the better-exposed right maxilla of *S. snowii* (KUVP 1301) (Figure 5.2.9.2.) (Sachs et al., 2018 counts 10 preserved teeth in the right maxilla and 13 in the left maxilla, but a personal visit by M.M. does not substantiate this count) (Otero, 2016; M.M. pers. obs.). *L. morgani* (SMU SMP 69120) exhibits 13 teeth in the left maxilla and 14 in the right maxilla (Carpenter, 1997; M.M. pers. obs.), SMNS 81783 (*L. morgani*) has 15 maxillary alveoli in the left maxilla (the right maxilla is damaged) (Allemand et al., 2017). In MGUAN PA278 the upper tooth row on the right side of the skull terminates at approximately the halfway point of the supratemporal fenestra. In palatal view, the maxillary alveoli are more circular in outline and less ovate than the premaxillary teeth.

A dorsal extension of the maxillae anterior to the orbits contributes to the orbitonasal bar. This dorsal extension of the maxillae is also present in *L. morgani*, *L. 'atlansense'*, *N. bradti*, *T. keyesi,* and *K. katiki,* but not in *S. snowii,* and *T. haningtoni* (Cruickshank and Fordyce, 2002; Sachs et al., 2017; Serratos et al., 2017; O'Gorman et al., 2017b, M.M. pers. obs.). In MGUAN PA278, this dorsal ramus of the maxillae exhibits concave anterior and posterior margins. The anterior margin of the orbitonasal bar demarcates the posterior-most extent of the external nares in MGUAN PA278. On the left maxilla, the base of the orbitonasal bar remains but its dorsal half is broken off and dips into the palate. There is a concavity posterior to the orbitonasal bar on the dorsal margin of both maxillae that precedes a prominent convexity along the posteroventral border of the orbits. The suture between the maxilla and the jugal below the orbit is best preserved on the left half of the cranium and divides the posteroventral convexity of the orbit to form an inclined interdigitating suture (Figure 5.2.6.). The convexity makes the orbit of MGUAN PA278 reniform in shape, a common feature of many elasmosaurids, such as *L. morgani, S. snowii, S. browni, T. haningtoni T. keyesi, C. colombiensis,* and *K. khatiki* but not *F. suzukii* (Carpenter, 1997, Cruickshank & Fordyce, 2002; Sato, 2003; Otero, 2016; O'Gorman et al., 2017b; M.M. pers. obs.). Posterior to the left orbit, the left maxilla is missing. The right maxilla tapers posteriorly along the ventral margin of the temporal bar. Contact between the maxilla and the squamosal is inhibited by the jugal. In view of the palate, the maxillae extend medially to contribute to the lateral margin of the internal nares. In cross-section of the right maxilla, neurovascular canals oriented anteroposteriorly form a network for branches for the trigeminal nerve.

Ventral to the posterior processes of the premaxillae are the **frontals** that demarcate the dorsomedial border of the orbits. The frontals are elongated, contributing to the dorsal margin of the orbitonasal bars, separating the external nares from the orbits, and the formation of the postorbital bar. In cross-section of the interorbital region the frontals are triangular with processes that extend ventrally, laterally and medially (Figure 5.2.7.). The ventral extensions of the frontals increase in depth posteriorly,

until two partial walls are formed along the posteromedial margins of the orbits. These partial walls are also present in *L. morgani* (Carpenter, 1997) but difficult to identify in specimens with compressed crania. A frontal foramen, identified in polycotylid plesiosaurians and even the elasmosaurid *T. keyesi*, is not present in MGUAN PA278 (Carpenter, 1997; Bardet et al., 2003; O'Gorman et al., 2017b). The identification of the **prefrontals** is difficult to confirm in MGUAN PA278, although a loose triangular fragment of bone located above the right orbitonasal bar, posterior to the right external naris, may be a prefrontal (Figure 5.2.2.).

The **jugal** is an elongated element in MGUAN PA278 that contributes to the posteroventral margin of the orbits, bordered ventrally by the maxilla and dorsally by the **postorbital**. The postorbital (missing in the left half of the skull) restricts the jugal from the dorsal margin of the temporal bar. The suture between the jugal and the squamosal forms a sharp interdigitating pattern and is inclined anterodorsally-posteroventrally (Figure 5.2.4.). In lateral view of the right half of the cranium, the jugal is broken along the middle by a crack running dorsoventrally. The jugal appears slightly more elongated and shallower than some other elasmosaurid plesiosaurians with a more robust jugal that is rhomboidal in outline, such as *L. morgani*, *S. snowii* or *T. haningtoni* (M.M. pers. obs.) (Figures 5.2.6., 5.2.8., 5.2.9., and 5.2.9.1.). However, the overall shape of the jugal may have been affected taphonomically in MGUAN PA278. The jugal separates the maxilla from the squamosal in MGUAN PA278, as it does in almost all elasmosaurid plesiosaurians, except *N. bradti* (Serratos et al., 2017). The postorbital is a triangular element with a posterior process that forms part of the dorsal margin of the temporal bar posterior to the orbit. The postorbital also forms the posterior border of the orbit and the anterior margin of the temporal fenestra. The postorbital extends posteriorly along the dorsal margin of the temporal bar and terminates before the mid-point of the temporal fenestra (Figure 5.2.6.).

Thus, in MGUAN PA278 the orbit is reniform in outline and encompassed by the maxilla along most of its ventral and anterior margin. The jugal forms the posteroventral corner of the orbit, the postorbital contributes to the posterior margin along with the frontal, and the frontal delimits the dorsomedial and anteromedial margin. A loose triangular fragment of bone, located posterior to the external naris and medial to the dorsal ramus of the maxilla in MGUAN PA278 is tentatively referred to as the prefrontal (Figure 5.2.2.). This prefrontal would have contributed to the anteromedial margin of the orbit. The presence of a postfrontal is difficult to discern as this element may have been lost before burial of the animal. Comparatively, the postfrontal should contribute to the posterior margin of the orbit as it does in other plesiosaurian taxa (Welles, 1962; Carpenter, 1997; Cruickshank and Fordyce, 2002; Kear, 2007; Vincent et al., 2011; Otero, 2016; Sachs et al., 2017; Serratos et al., 2017; O'Gorman et al., 2017b; Sachs et al., 2018).

The **parietal** is fragmented into five separate pieces along the dorsal midline of the skull. The anterior-most piece is a flat and transversally broad anterior process that articulates with the premaxillae along the same plane as the postorbital bar (Figure 5.2.6.). The majority of elasmosaurid taxa with three dimensionally preserved crania exhibit the premaxillary-parietal suture at approximately the mid-point of the orbits along the skull roof (*L. morgani*, *T. haningtoni*, *S. snowii*, *T. keyesi*, *K. katiki*, and *E. australis*) (Fordyce and Cruickshank, 2002; Kear, 2007; O'Gorman, et al., 2017b; M.M., pers. obs.). However, *Z. oceanis* shares with MGUAN PA278 a premaxilla-parietal contact at the level of the postorbital bar (Vincent et al., 2011). From the anterior margin, the parietal transitions posteriorly, to become mediolaterally compressed and then triradiate in cross section. A crest is expressed dorsally on the parietal posterior to the anterior contact with the premaxillae that is narrow at the base and thins toward the top. The apex of the crest has eroded away, although the base remains. At the anterior end, the preserved crest is low and broad but becomes a narrower and slightly higher above the braincase. The posterior-half of the parietal is situated above the braincase and contacts the supraoccipital ventrally. A pineal foramen is not evident.

The **squamosals** are large elements that encompasses the posterior and posterolateral margins of the temporal fenestrae. The right squamosal is used for description, as this element is in complete articulation with surrounding cranial elements and is much better preserved than the left squamosal. The anterior ramus of the squamosal forms a highly interdigitating and inclined suture with the jugal. A clear suture is also seen along the squamosal-quadrate interface. Together, the squamosal and postorbital form the dorsal margin of the temporal bar, which appears to be straight and does not present any ridges or processes, as it does in *S. browni* (Otero, 2016). The posterior margin of the squamosal is slightly convex and juts out posteriorly above the quadrate in right lateral view (Figure 5.2.6.). The dorsal rami of both squamosals are missing in MGUAN PA278. The right paroccipital process of the exoccipital contacts the squamosal medially. The **quadrate** articulates with the squamosal and the quadrate process of the pterygoid, with partial contact from the paroccipital process along its dorsomedial margin. Two condyles are evident on the distal end of the quadrates for articulation with the mandibular glenoid. A shallow sulcus separates the condyles of the quadrate, which extends 55 mm posterior to the occipital condyle in the better-preserved right quadrate.

The antorbital length of the skull of MGUAN PA278 measures 141.39 mm from the tip of the premaxillae until the anterior margin of the orbit (identified as the posterior border of the preorbital bar). This provides MGUAN PA278 with a 'beak-index' (measured by dividing the antorbital region of the skull by the length of the skull from the tip of the snout to the occipital condyle; Welles, 1952) of 36.2%, compared to 40.5%, 45%, and 42% in *L. morgani* specimens SMU SMP 69120, D1-8213, and SMNS

81783, respectively, 34% in *T. keyesi*, 33% in *N. bradti*, 35% in *T. ponteixensis*, 31% in *Z. oceanis*, 26% in *K. katiki*, and 40.8% in *E. australis* (Wiffen and Moisley, 1986; Carpenter, 1999; Cruickshank and Fordyce, 2002; Sato, 2003; Kear, 2005; Vincent et al., 2011; Serratos et al., 2017; Allemand et al., 2017; Allemand et al., 2018). A beak-index of approximately 40% is common in non-aristonectine elasmosaurids (Sato, 2003; Allemand et al., 2017; Allemand et al., 2018). The proportion of the temporal fenestra length relative to the skull length, measured from the tip of the snout to the occipital condyle is 44.6% in MGUAN PA278. Proportionally, the temporal fenestrae are longer than that of *N. bradti* (40%), and *L. morgani* (37%) (Serratos et al., 2017; Allemand et al., 2018). The orbit to skull length ratio for MGUAN PA278 is 17.5% and is similar to values for *N. bradti* (17%) and *L. morgani* (22%) (Serratos et al., 2017).

Table 2. Measurements from cranium of *C. mukulu* (MGUAN PA278)

Cranial measurements of *C. mukulu (* MGUAN PA278)	
length of cranium from tip of premaxillae to occipital condyle	390.4 mm
length of cranium from tip of premaxillae to right quadrate (better preserved quadrate)	445.5 mm
anteroposterior length of right temporal fenestra	174.2 mm
anteroposterior length of the right orbit	68.17 mm
Depth of third maxillary alveolous (maxillary fang)	48.8 mm
anteroposterior length of the third maxillary alveolous (maxillary fang) in palatal view	18.6 mm
mediolateral width of the third maxillary alveolous (maxillary fang) in palatal view	16.0 mm
length of vertical process of the left (better preserved) pterygoid	28.5 mm
anteroposterior length of the sella turcica	33.6 mm
mediolateral width of the sella turcica	18.6 mm

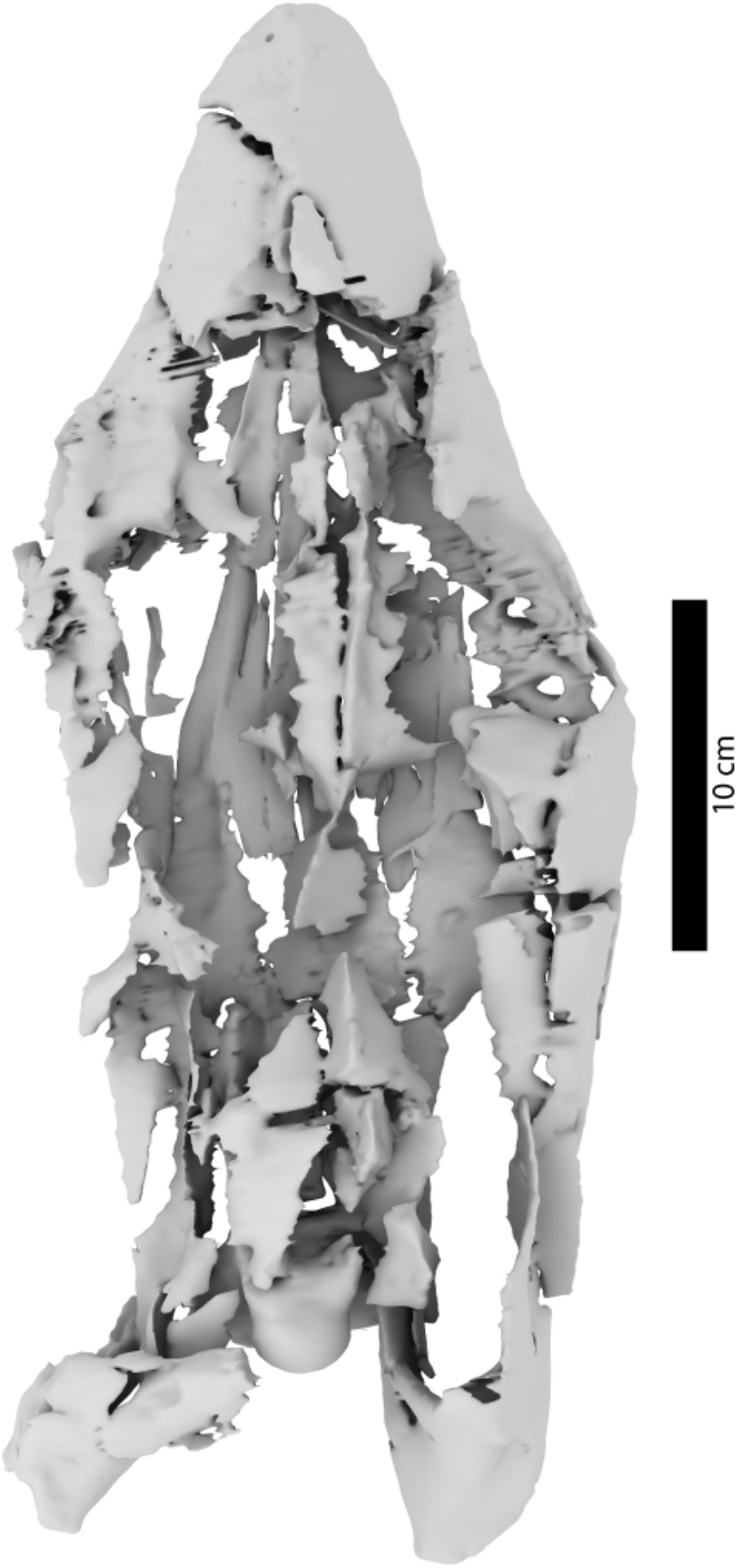
10 cm

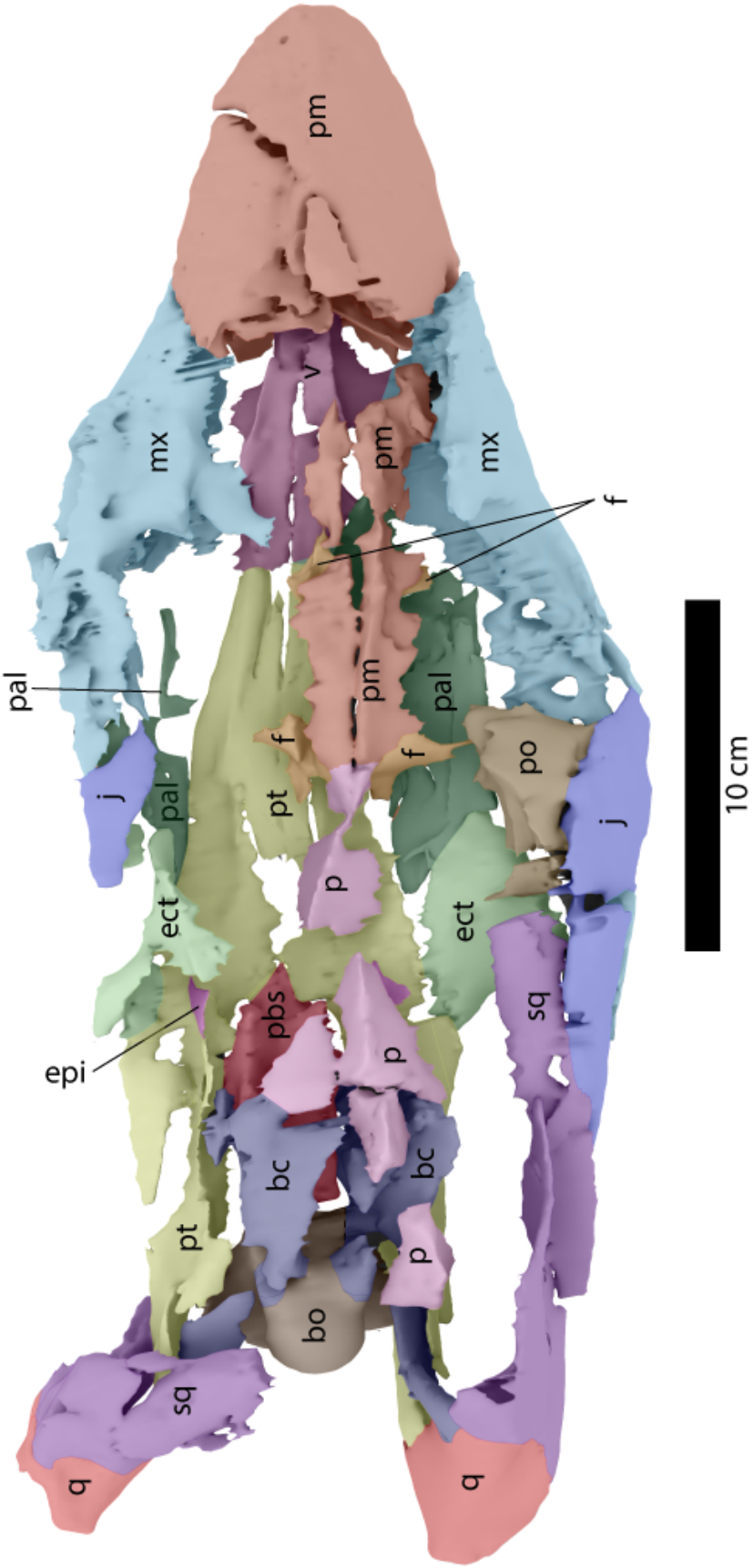
pm
v
mx
pm
mx
f
pal
pm
pal
f
f
po
pal
j
pt
p
ect
ect
j
sq
pbs
epi
p
bc
bc
pt
p
bo
sq
q
q
10 cm

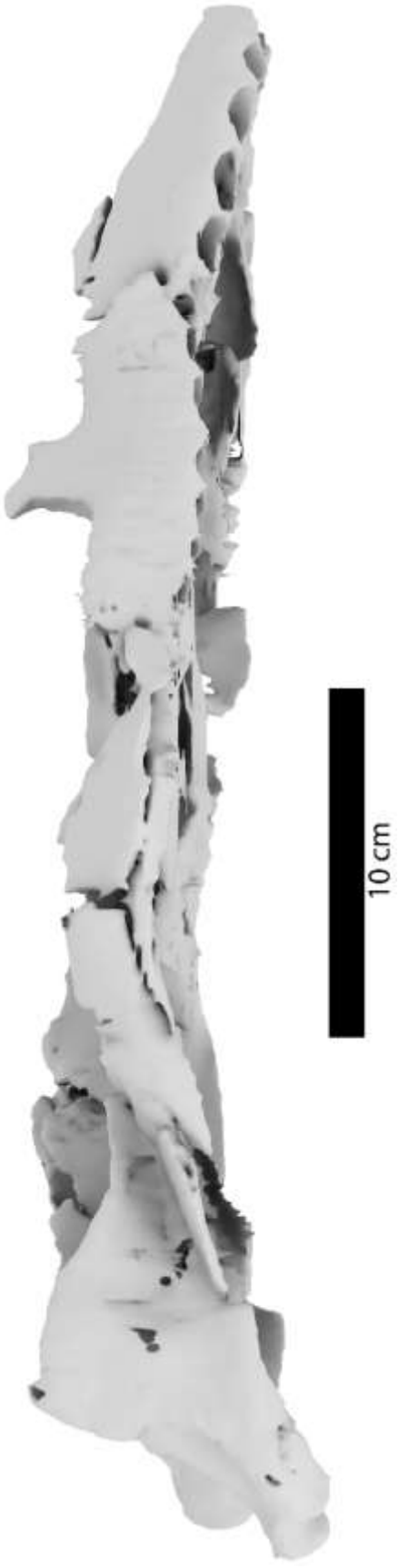
10 cm

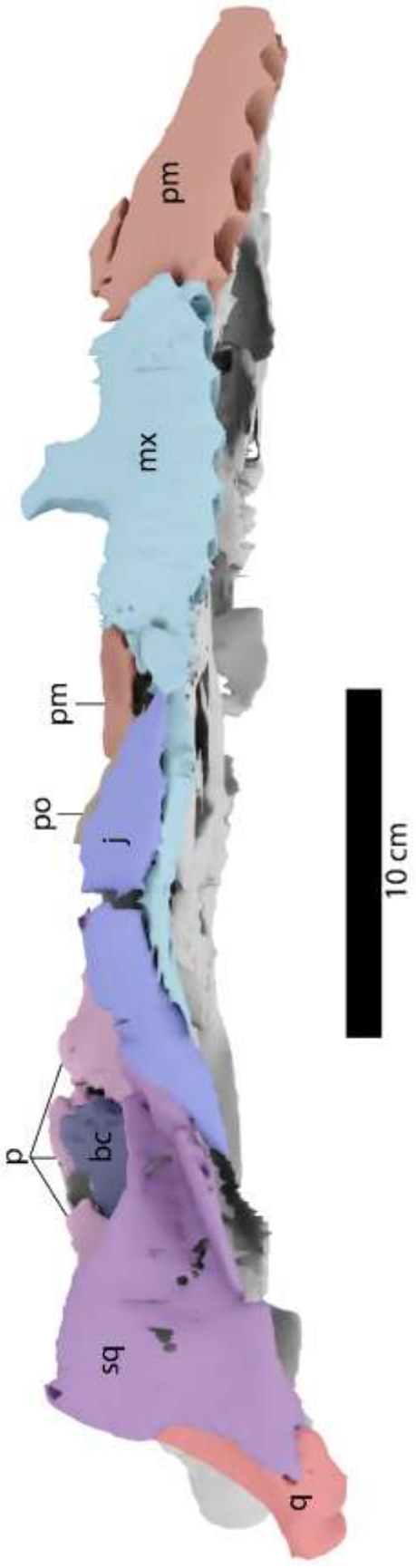
pm
mx
pm
po
j
p
bc
sq
q
10 cm

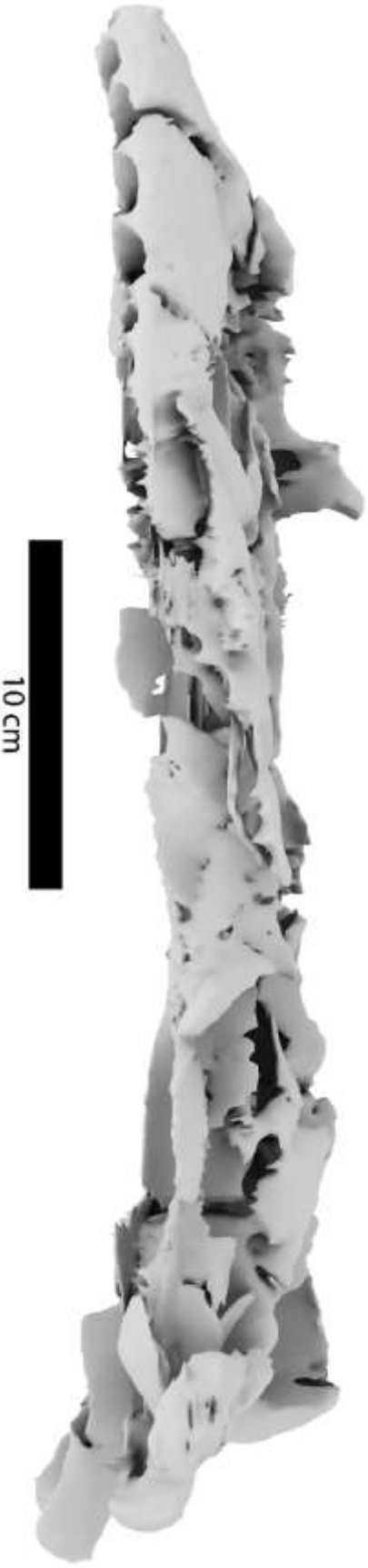
10 cm

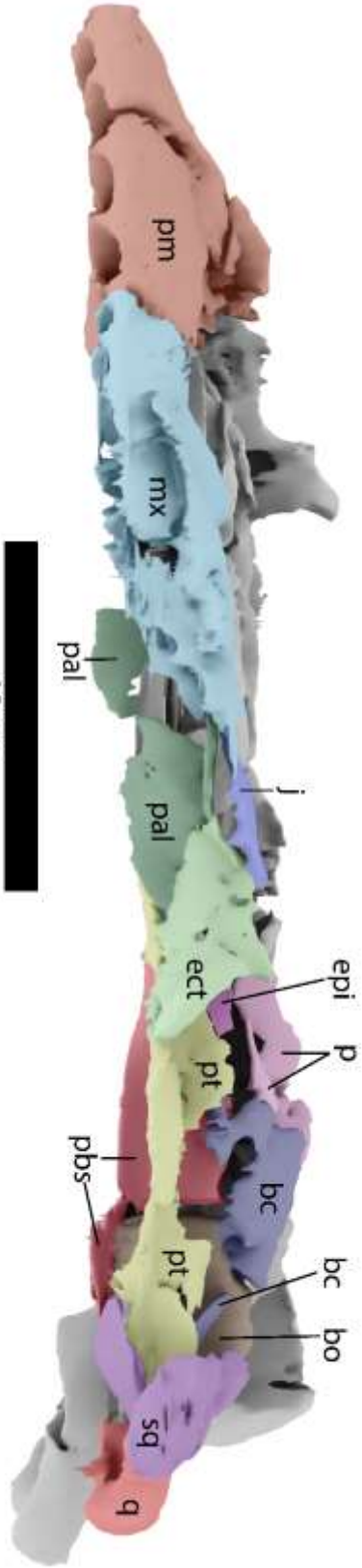
pm
mx
pal
10 cm
pal
j
ect
epi
p
pt
pbs
bc
pt
bc
bo
sq
q

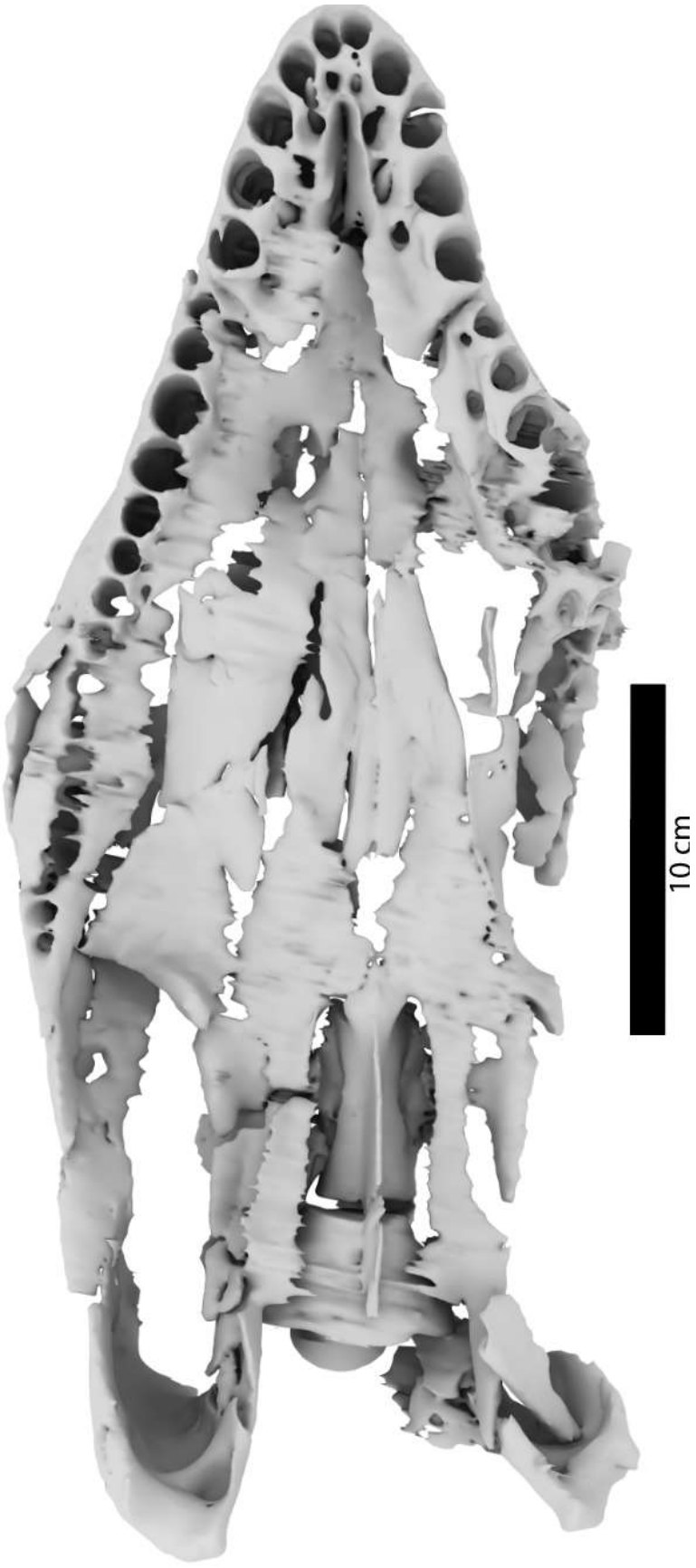
10 cm

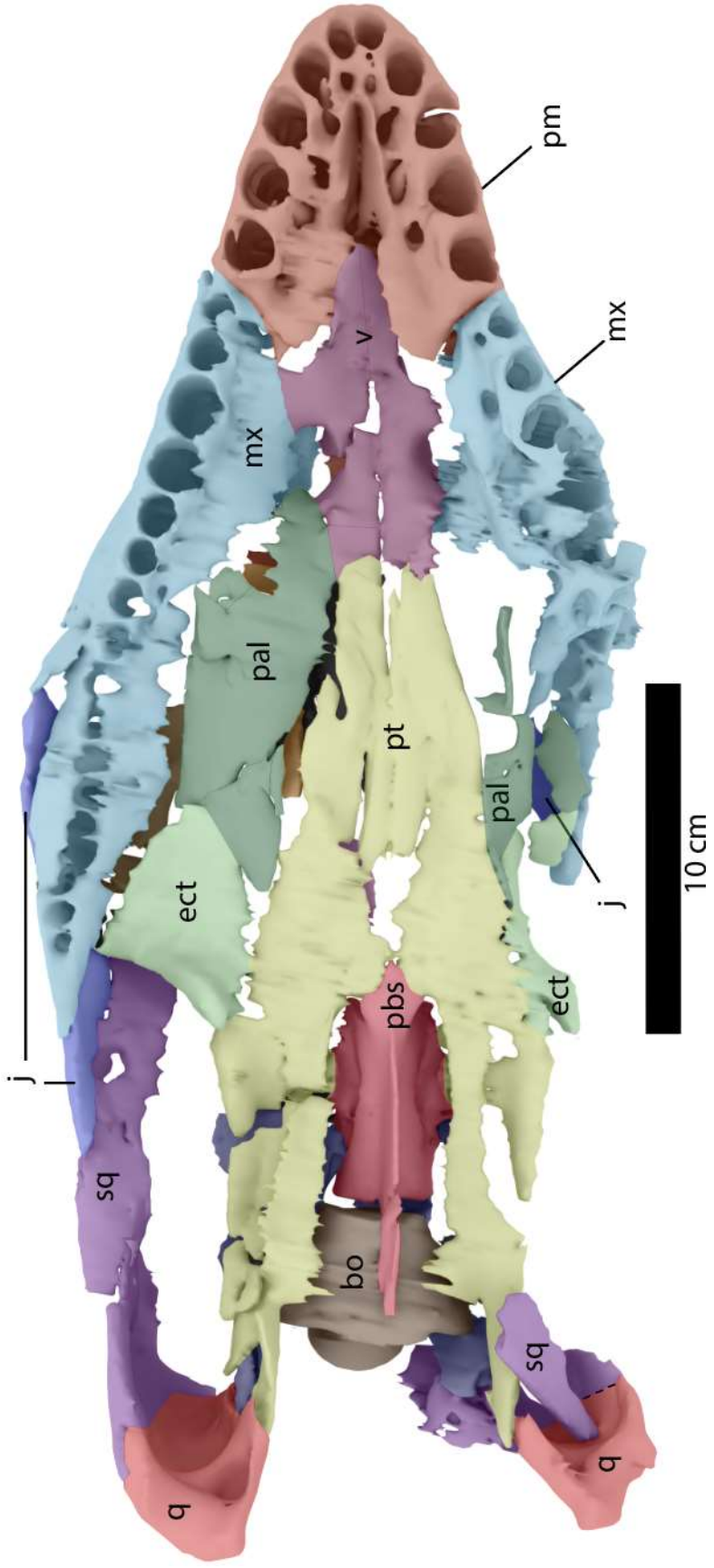
pm
mx
v
mx
pal
pt
pal
ect
j
10 cm
j
ect
pbs
sq
bo
sq
q
q

Figure 5.2.6. Previous page (pg.71- 78): Three-dimensional model of the cranium of *Cardiocorax mukulu* (MGUAN PA278) in dorsal, right lateral, left lateral, and ventral views. The dashed line between the left squamosal and left quadrate in ventral view of the cranium indicates the approximate contact between these two elements, as this suture was difficult to determine with the CT data.

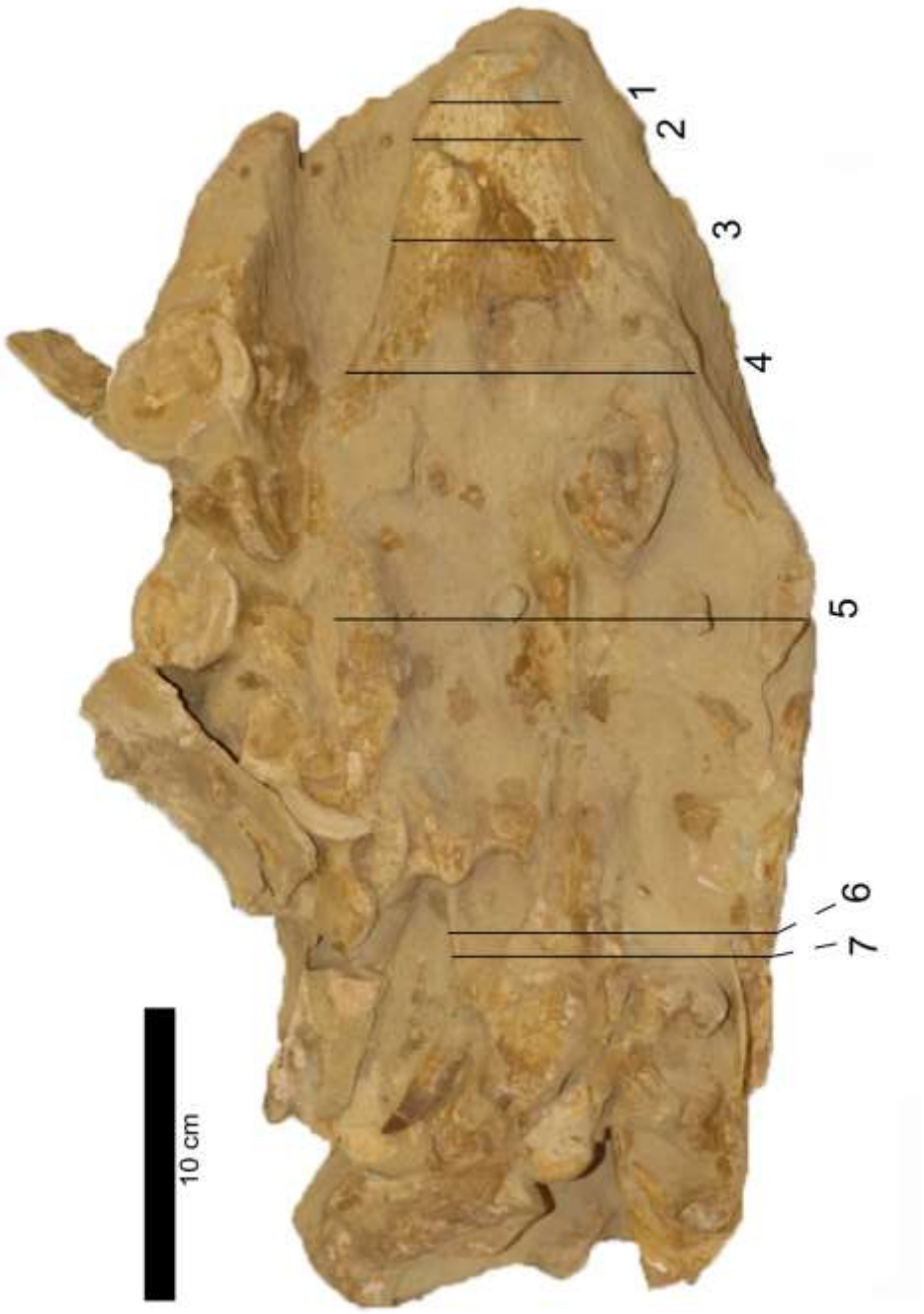

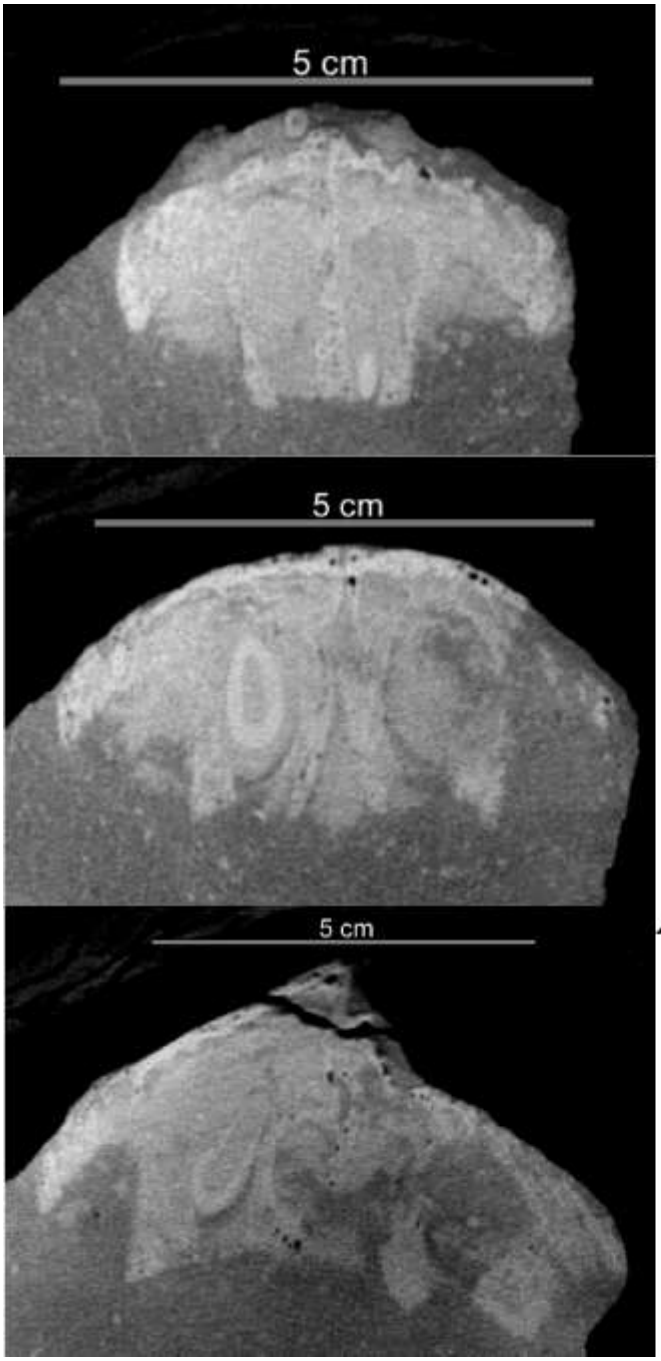
5 cm
5 cm
5 cm

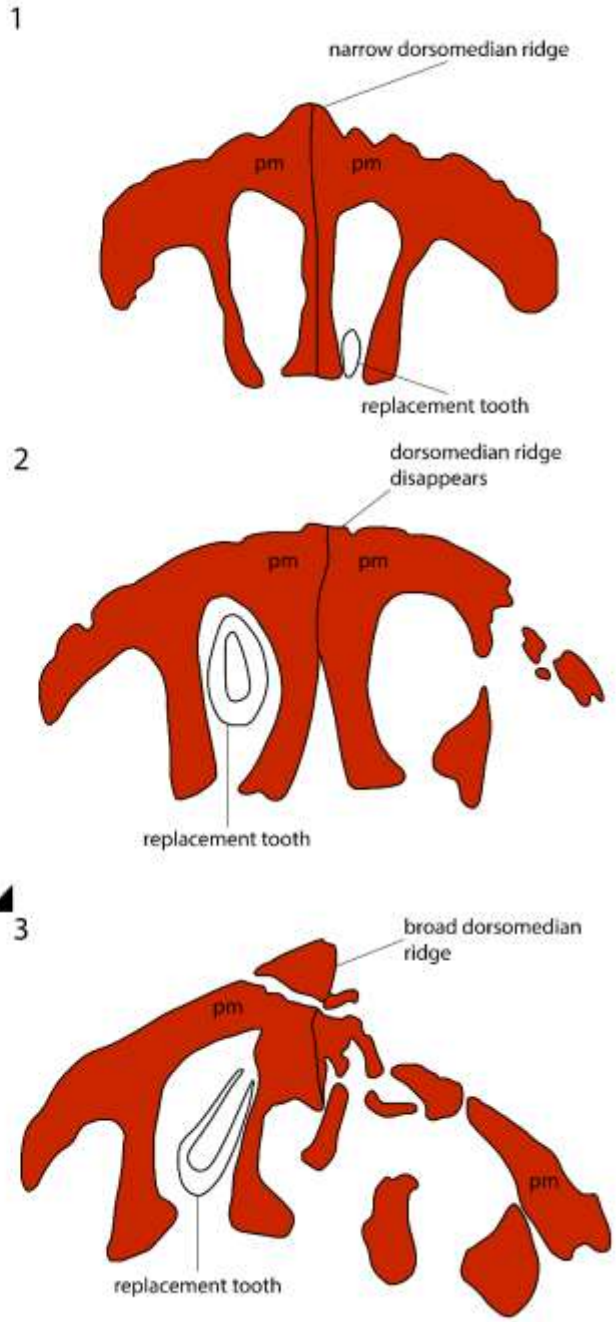
1
narrow dorsomedian ridge
pm
pm
replacement tooth
2
dorsomedian ridge
disappears
pm
pm
replacement tooth
3
broad dorsomedian
ridge
pm
pm
replacement tooth

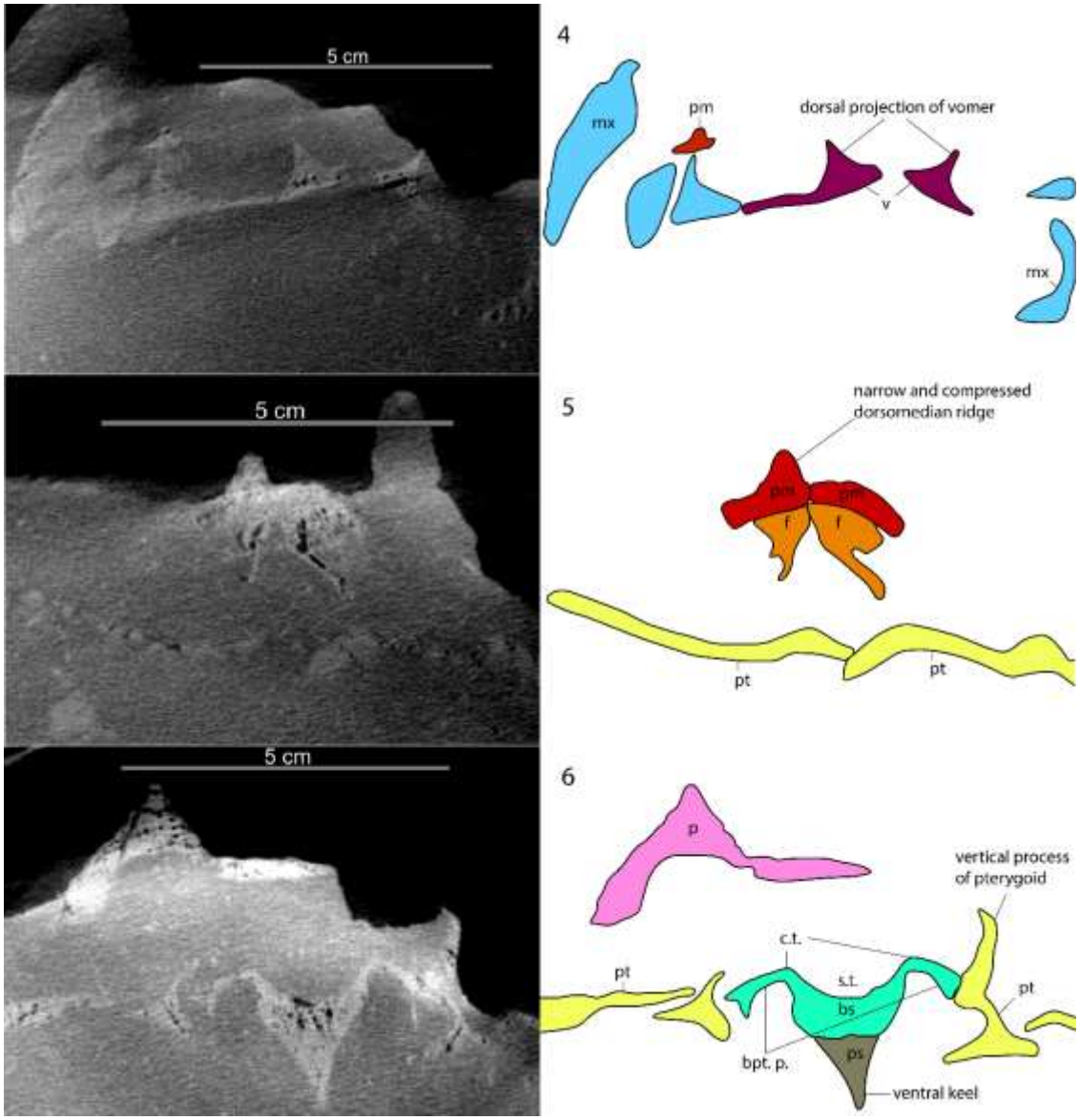
5 cm
5 cm
5 cm
4
mx
pm
dorsal projection of vomer
v
mx
5
narrow and compressed
dorsomedian ridge
pm
pm
f
f
pt
pt
6
p
vertical process
of pterygoid
c.t.
pt
s.t.
bs
pt
bpt. p.
ps
ventral keel

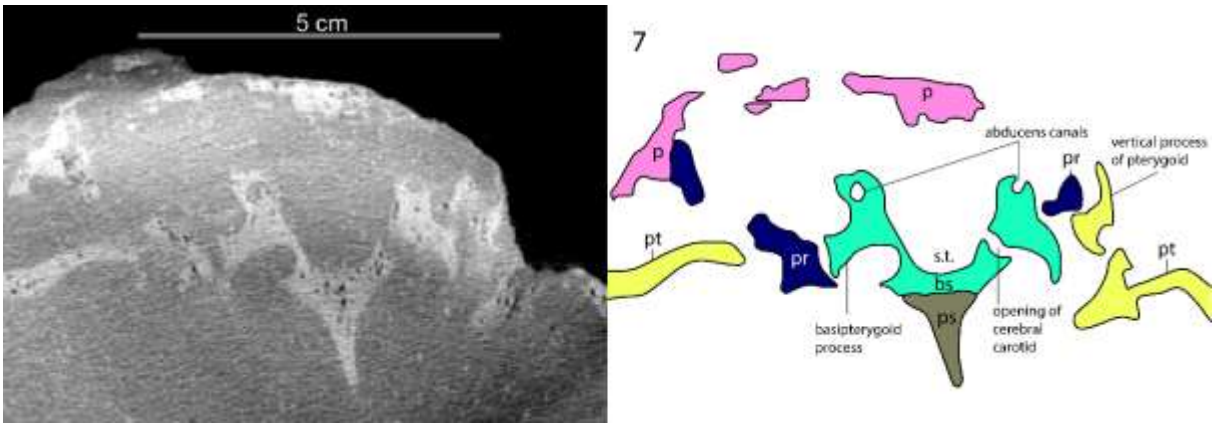

Figure 5.2.7. Previous pages (pg. 79-82) Skull CT sections of *Cardiocorax mukulu* (MGUAN PA278).

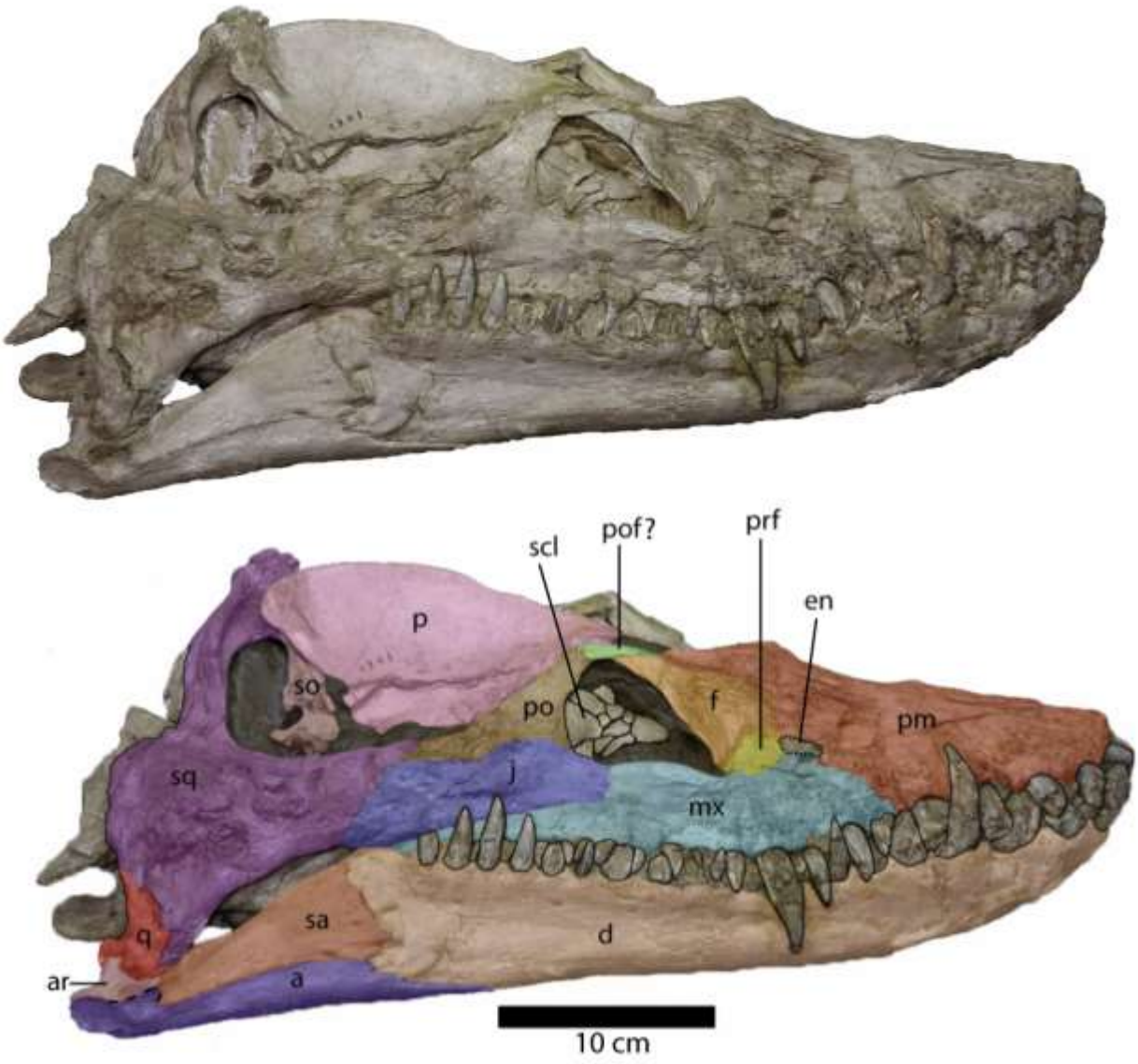

Figure 5.2.8. Right lateral view of the holotype of *Styxosaurus snowii* (KUVP 1301); used for comparison with MGUAN PA278. The dashed line between the articular and angular, and the angular and surangular indicate uncertain contacts between elements.

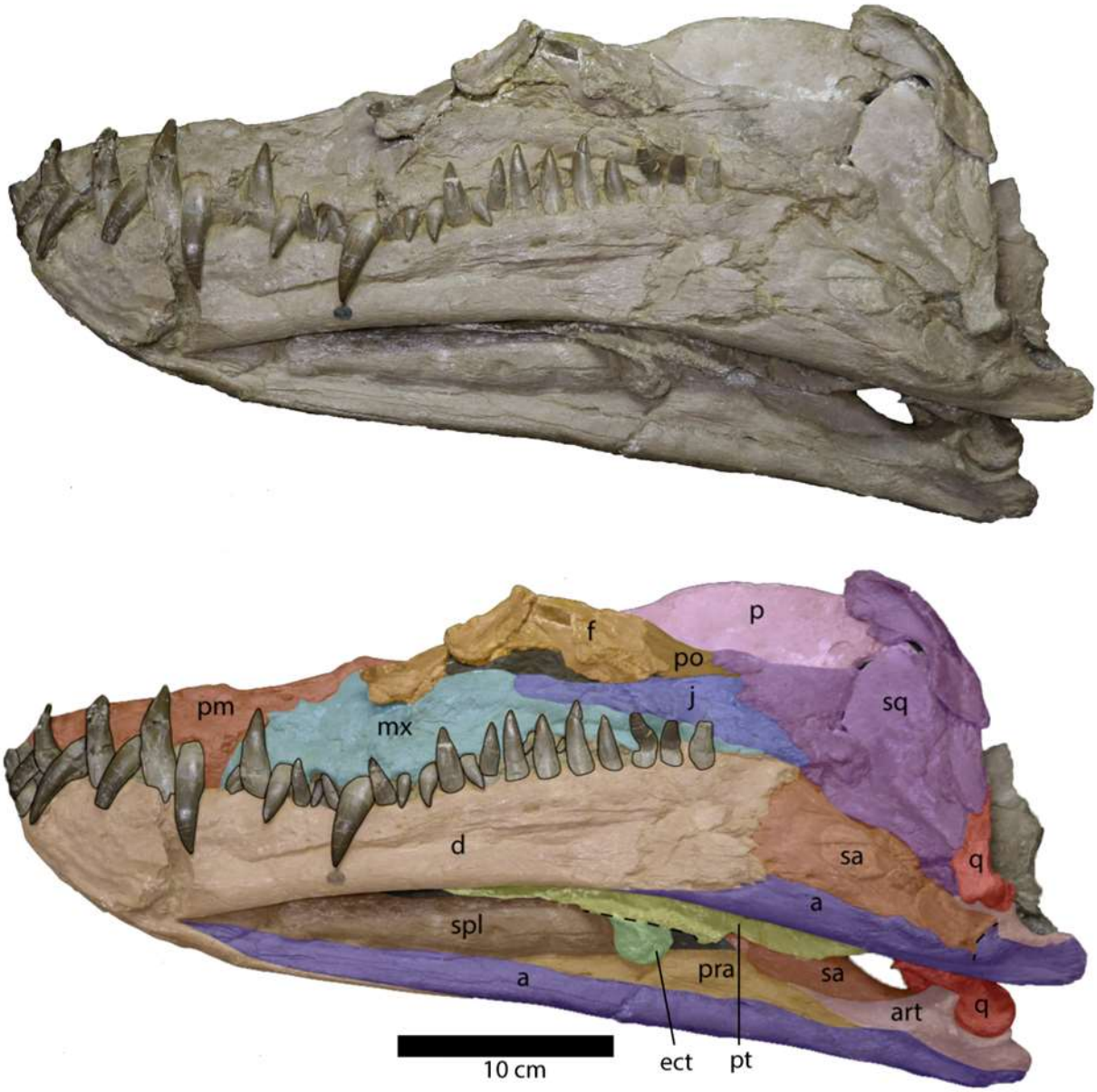

Figure 5.2.9. Left lateral view of the holotype of *Styxosaurus snowii* (KUVP 1301). The dashed line between the pterygoid and the ectopterygoid indicates an uncertain boundary between these two elements. A dashed line is also present between the left angular and surangular.

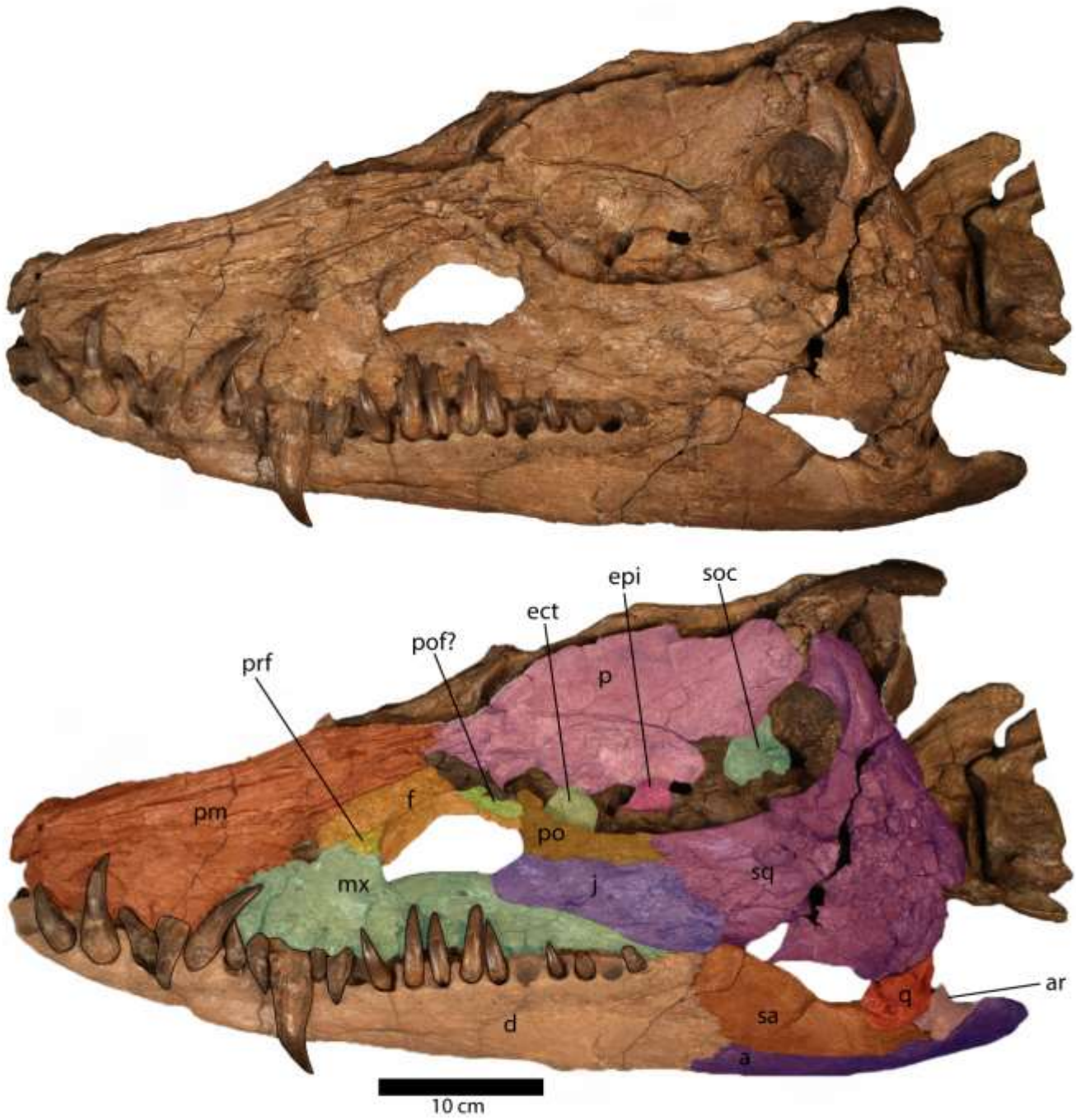

Figure 5.2.9.1 Left lateral view of *Thalassomedon haningtoni* (UNSM 50132) used for comparison with MGUAN PA278. Photo courtesy of Elliot Armour Smith.

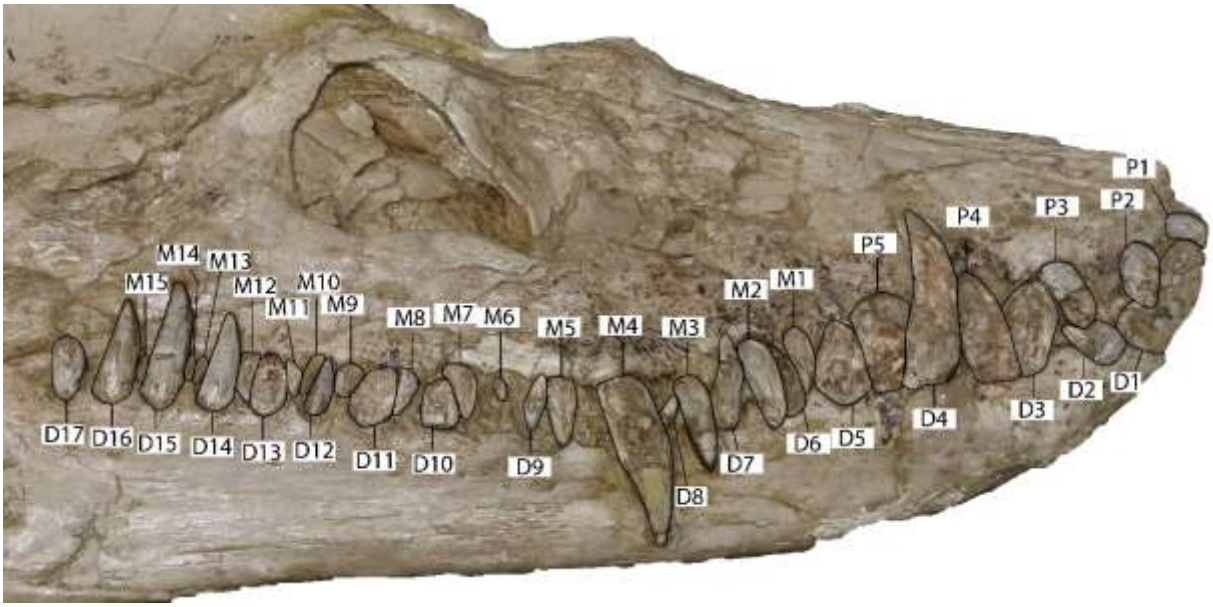

Figure 5.2.9.2. Right lateral view of the cranium of *S. snowii* (KUVP 1301) with observable fragmented and preserved teeth in the upper and lower tooth row labeled. P, premaxillary; M, maxillary; D, dentary.

The palate

At the anterior-most end of the palate is a narrow slit that is identified as the vomeronasal fenestra. This fenestra is proceeded by a pair of **vomers**. The anterior margin of the vomers forms a wedge. The vomers contact the medial borders of the premaxillae and become constricted between the internal nares. In cross-section, the vomers are dorsoventrally flat elements at the anterior end, but become triradiate in shape between the internal nares, with a sharp ridge along the dorsal surface that parallels the medial contact between the pair (Figure 5.2.7.). A similar morphology is noted in an *L. morgani* specimen from Morocco (D1-8213), where dorsal extensions of the vomers form a "gutter' in dorsal view of the palate (Allemand et al., 2018). The vomers contribute to the anterior and medial border of the internal nares, while the lateral margin of the internal nares is bordered by palatal extensions from the maxillae. In ventral view, the vomers do not show evidence of a ventral ridge along or near their medial interface, as in *L. morgani* (D1-8213) (Allemand et al., 2018). The internal nares are ovate in outline with the long axis oriented anteroposteriorly. The morphology of the internal nares in *L. morgani* and *F. suzukii* are different in being tear-drop shaped, with a rounded posterior margin and a sharp anterior margin (Carpenter, 1997; Sato, 2006; MM pers. obs.). The location of the internal nares cannot easily be identified in *C. colombiensis* despite full exposure of the palate in ventral view (MM pers. obs.). The internal nares of MGUAN PA278 are also different from *L. morgani*, in that they are located directly

beneath the external nares, as opposed to being located anterior to the external nares. The vomers extend posteriorly beyond the internal nares approximately 17 mm.

Posterior to the vomers, the **pterygoids** can be visualized as large paired elements that are bordered laterally by the **palatines** (Figure 5.2.6.). The palatines are sub-rectangular in shape, provide a small contribution to the posterior border of the internal nares and contact the maxillae**.** The pterygoids are morphologically complex elements that form an elongated wedge along the midline of the palate, contact the basicranium, and extend to the quadrates. The pterygoids of MGUAN PA278 do not separate the vomers along the midline, similar to *Z. oceanis*, but unlike *L. richterae* (Vincent et al., 2011; Sachs et al., 2017). In cross-section, the pterygoids are flat elements anterior to the interpterygoid fenestra (Figure 5.2.7.). The parasphenoid separates the pterygoids at the anterior end of the interpterygoid fenestra, making the pterygoids laterally straddle the basicranium. There is no anterior interpterygoid fenestra, as in all elasmosaurids, but common in polycotylids and leptocleidids (Carpenter, 1997; O'Keefe, 2001). Lateral to the basisphenoid, the pterygoids exhibit vertical processes, which taper to a sharp end and contact the basicranium medially via the basipterygoid processes (Figure. 5.2.7.). The vertical process of the left pterygoid is better preserved and extends for approximately 28.5 mm lateral to the basicranium. The vertical processes of the pterygoids are curved, with the medial side concave and the lateral side convex.

Posterior to the sella turcica, the processes of the basipterygoid terminate and the vertical processes of the pterygoids significantly decrease in height to form a low dorsal ridge. Thus, the pterygoids appear as narrow triradiate bars that parallel the basicranium, separating the interpterygoid fenestra from the subtemporal fenestra (Figure 5.2.6.). The pterygoids extend medially posterior to the interpterygoid fenestra but do not contact each other beneath the basitubera (Figure 5.2.6.). The keel of the parasphenoid is elongate in MGUAN PA278 and prevents medial contact between the pterygoids posterior to the interpterygoid fenestra (Figure 5.3.1.). This contrasts strikingly with *L. morgani*, *C. colombiensis*, and *L. richterae* where there is contact between the pterygoids posterior to the interpterygoid fenestra (Welles, 1962; Carpenter, 1997; Sachs et al., 2017; MM pers. obs.). The lack of medial contact between the pterygoids under the basicranium is not unique to MGUAN PA278 among elasmosaurid plesiosaurians, as this condition is also present in *T. keyesi* (O'Gorman et al., 2017b). The quadrate processes of the pterygoids extend posterolaterally to contact the quadrate along the medial margin. Contributions to the medial margin of the quadrate via the quadrate processes of the pterygoid are modest in MGUAN PA278 compared to *L. morgani* (SMU SMP 69120) where the pterygoid contributes to the entire medial margin of the quadrate and squamosal. Comparatively, the quadrate processes of the pterygoid from SMU SMP 69120 transition into exceptionally expanded processes dorsoventrally. No

other known elasmosaurid plesiosaurian exhibits a quadrate process of the pterygoid that contacts the entire medial margin of the quadrate and squamosal and this may be an autapomorphy for *L. morgani*. Posterior to the ectopterygoid and lateral to the interpterygoid fenestra, the pterygoids present processes that are extremely thin toward the interpterygoid fenestra but thicken along the medial margin of the subtemporal fenestra. The lateral portions portion of the pterygoids, along the subtemporal fenestrae, was significantly affected taphonomically. In *L. morgani* (D1-8213 and SMNS 81783), the lateral margin of the pterygoids is curved ventrolatrally (Allemand et al., 2017; Allemand et al., 2018). The same condition may have once been present in MGUAN PA278 but has since been deformed.

In cross-section of the palate, the left **epipterygoid** appears as a vertically high and thin element that sutures with the anterior end of the vertical process of the pterygoid. The dorsal apex of both epipterygoids is oriented anterodorsally. Within elasmosaurid plesiosaurian literature, there is very little descriptive work on the epipterygoids, as these thin fragile elements are often broken or obscured. In *L. morgani* the distal margin of the element appears broken and thus its morphology cannot be described, although Carpenter (1997) restores the epipterygoids with an anterodorsal orientation. In *T. haningtoni*, the epipterygoids exhibit a more smoothly convex distal margin. The epipterygoids have a triangular in outline *T. keyesi* (O'Gorman et al., 2017b). In *L. morgani* (SMNP 18783), the epipterygoids are most similar to MGUAN PA278 in being triangular with an apex oriented anterodorsally (Allemand et al., 2017). It cannot be determined if the epipterygoid contacted the parietal, as taphonomic distortion has altered the location of the parietal. Contact between the epipterygoid and parietal has been noted in other plesiosaurians (Noè et al., 2003).

The **ectopterygoids** are situated posterior to the palatines and lateral to the pterygoids to form the anterior margin of the subtemporal fenestrae (Figure 5.2.6.). The right ectopterygoid is better preserved than the left ectopterygoid and exhibits a clear ventral flange. Flanges of the ectopterygoids are present in some western interior seaway elasmosaurids, such as *S. snowii*, *N. bradti*, and *L. morgani* (Serratos et al., 2017; M.M. pers. obs.). A flange from the palate is sometimes produced by both the ectopterygoid and pterygoid in some elasmosaurid taxa, such as *N. bradti* and possibly *S. snowii* (Serratos et al., 2017; Sachs et al., 2018), however, in MGUAN PA278, this process is located entirely on the ectopterygoid. A ventral flange formed only by the ectopterygoid is also present in *L. morgani* (D1-8283) (Allemand et al., 2018). A dorsolateral extension of the ectopterygoid contacts the medial surface of the maxilla and the jugal in MGUAN PA278. In cross-section, the dorsolateral extension is a dorsoventrally thin bone that gradually thickens toward the palate.

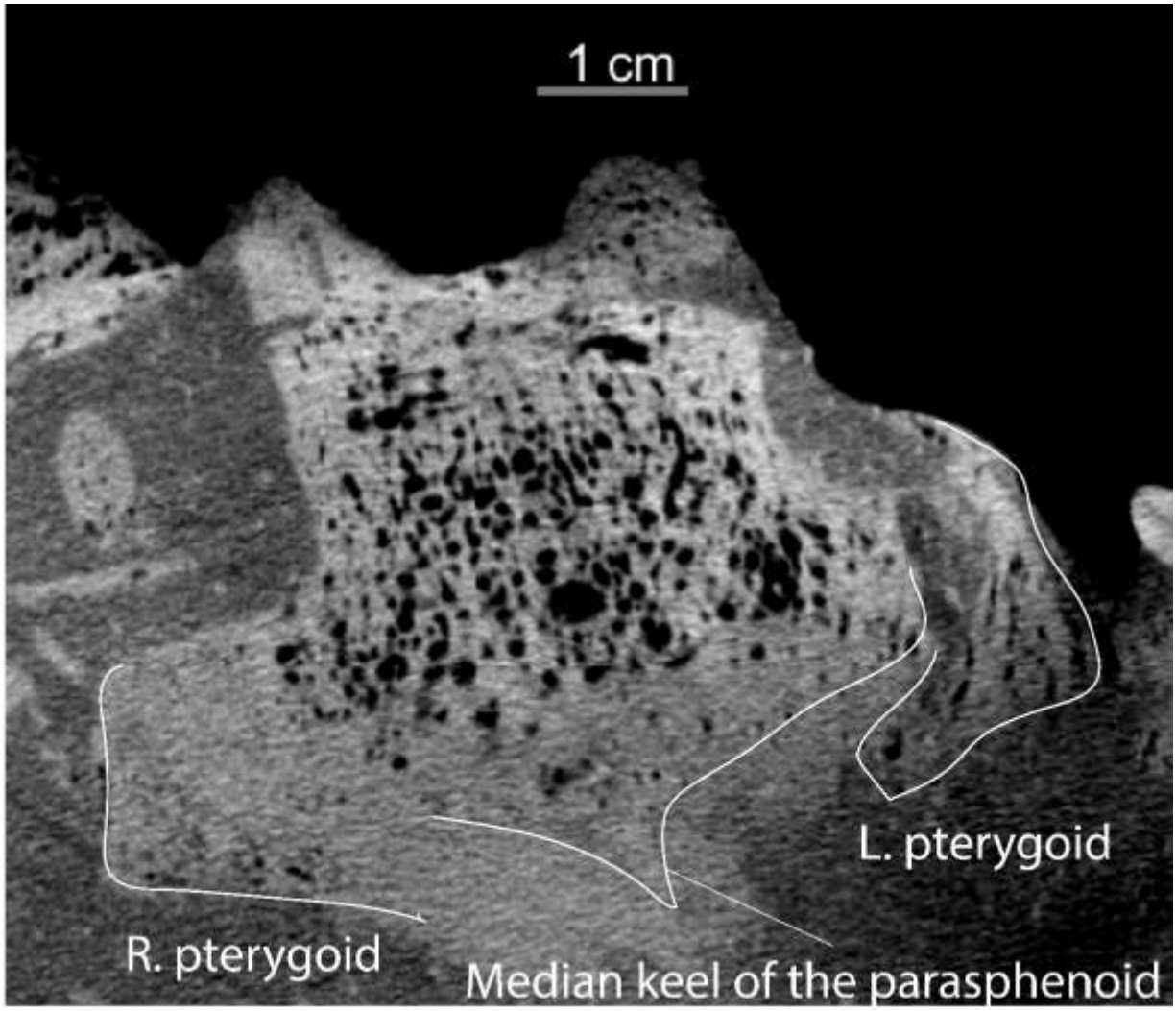

Figure 5.3.1. Cross-section of the basicranium, showing the lack of medial contact between the pterygoids in *Cardiocorax mukulu* (MGUAN PA278).

The braincase and basicranium

The anterior-most end of the basicranium is expressed as a wedge formed by the elongated cultriform process of the parasphenoid, separating the pterygoids medially just before the interpterygoid fenestra (Figure 5.2.6.). The cultriform process of the parasphenoid is dorsoventrally flat in cross-section. Posteriorly, the parasphenoid presents a prominent ventral keel within the interpterygoid fenestra. The ventral keel of the parasphenoid divides the interpterygoid fenestra evenly and terminates beneath the basitubera of the basioccipital. The basisphenoid is situated above the parasphenoid and anterior to the basioccipital. At the anterior end of the basisphenoid are anterodorsal extensions which in the literature of

elasmosaurid plesiosaur anatomy have been termed the ‘lower cylindrical processes’ or ‘pila metoptica’ (Carpenter, 1997; Zverkov et al., 2017; Allemand et al., 2017). The pila metoptica is however a cartilaginous structure, and ‘lower cylindrical process’ is not an anatomical term, but rather, a term introduced by Carpenter (1997). The anterodorsal extension of the basisphenoid bone lateral to the sella turcica in MGUAN PA278 and other plesiosaurians is homologous to the basisphenoidale (Paluh and Sheil, 2013). The basisphenoidales are slightly sinusoidal in anterior view and meet each other ventromedially to form a v-shaped outline. Posteriorly, the basisphenoidales merge with the crista trabeculares, which forms low walls lateral to the sella turcica.

The basipterygoids are short lateral extensions along the entire lateral surface of the crista trabeculares and contact the vertical processes of the pterygoids. A groove that extends along the lateral surface of the parabasisphenoid merges with a foramen on the lateral surface of the basisphenoid where the branch of the cerebral carotids would have entered, posterior to the basipterygoid processes. The sella turcica is elongated (length: 33.6 mm, width: 18.6 mm) and forms a shallow medial depression that deepens posteriorly. MGUAN PA278 exhibits the greatest sella turcica length to width ratio for any known plesiosaurian currently (Zverkov et al., 2017 supplementary data). A length to width ratio greater than 1 is also shared by *L. morgani*, while non-elasmosaurid plesiosaurians, including aristonectines, exhibit sella turcica length to width ratios near a 1:1 ratio (Zverkov et al., 2017 supp. data). In dorsal view, the anterior margin of the sella turcica forms a u-shape, with a distinct notch at its mid-width, similar to a Russian elasmosaurid braincase, SGU 251/1 (Zverkov et al., 2017).

At the posterior end of the sella turcica are two openings for the passage of the left and right cerebral carotid arteries into the pituitary gland (Figure 5.4.1.). Separated openings for the cerebral carotid arteries is also shared with *L. morgani* (SMU SMP 69120). *A. zealandiensis*, and an elasmosaurid basicranium from the Campanian of Russia (SGU 251/1) exhibit a single opening in the back of the sella turcica for the entrance of the cerebral carotids (Otero et al., 2016; Zverkov et al., 2017). As noted by Zverkov et al. (2017) the single opening for the cerebral carotid arteries at the back of the sella turcica is a derived condition within Sauropterygia, although also present in some derived ichthyosaur, testudine, squamate, and archosaur taxa (Albrecht, 1976; Baumel & Witmer, 1993; Maish & Matzke 2000; Witmer & Ridgely, 2009; Zverkov et al., 2017). Interestingly, the opening for the left cerebral carotid is located more anteriorly on the basisphenoid than its right counterpart and presents an asymmetry in the morphology of the basicranium.

Dorsal to the opening for the cerebral carotids is the dorsum sellae. Anterolateral to the dorsum sellae are the clinoid processes which have in the past been referred to as the ‘upper cylindrical processes’ by Carpenter (1997), although correctly referred to as the clinoid processes by O’Keefe (2006) and

Zverkov et al., (2017) as these structures are homologous broadly in Reptilia (Romer, 1976). The clinoid processes are triangular in lateral view with transversely narrow but anteroposteriorly elongated bases. The clinoid processes are oriented at a low angle, approximately 17.5° anterodorsally from the horizontal plane. A foramen runs through the base of the clinoid processes and is oriented straight anteroposteriorly. This foramen would have housed the abducens nerve (VI) in life. Between the clinoid processes, there are no openings that pierce the dorsal surface of the basicranium and enter the basisphenoid, unlike the perforations seen in the basicranium of the Maastrichtian Russian elasmosaurid, SGU 251/1, and are likely openings for artery branches (Zverkov et al., 2017). At the posterior end of the basisphenoid, there is no clivus (notch at the posterior end of the basisphenoid).

Posterior to the clinoid processes, the prootics are broken away from the basisphenoid at the base and are thus not in articulation. Shearing of the braincase is evident, as the left prootic is tilted medially, and the right prootic and exoccipital-opisthotic are tilted laterally, to the right. The bases of the prootics are mediolaterally compressed and elongated anteroposteriorly. The prootics in MGUAN PA278 articulate dorsally with the supraoccipital and posterodorsally with the exoccipital-opisthotic. Carpenter (1997) cites the presence of the canal for the lateral head vein in *L. morgani* (SMU SMP 69120). An opening for cranial nerve VII is reported in the prootics of *L. morgani* specimens from Morocco, and *Dolichorhynchop*s sp. (ROM 29010) (Sato et al., 2011; Allemand et al., 2017; Allemand et al., 2018; Allemand et al., 2019).

The endosseous labyrinth is shared between the prootic, exoccipital-opisthotic, and supraoccipital. The exact location of the sutures between the elements of the braincase could not confidently be identified in view of the CT data. Even in plesiosaur braincases free from rock matrix and clearly visible, the sutures between elements is sometimes not obvious due to complete co-ossification (Andrews, 1913; O'Keefe, 2006; Sato et al., 2011; Ketchum and Benson, 2011; O'Gorman et al., 2017b). In Allemand et al., (2019) a brain endocast from *L. morgani* (D1-8213) exhibits an area for the presence of cranial nerve V, exiting from the 'prootic fenestra'. In MGUAN PA278, there are no fenestra or canals evident in either of the prootics. The fact that both elements are disarticulated from the basisphenoid may have obscured any such foramen (V and VII) if they were present.

The right endosseous labyrinth is better preserved than its left counterpart, which is generally well preserved except for the region encasing the anterior semicircular canal and the anterior ampulla. The semicircular canals, crus communis and the regions corresponding to the ampullae are thick and bulbous in morphology, typical of known elasmosaurid plesiosaurians (Figure 5.4.5.) (Neenan et al., 2017). The canals are smoothly arched and not sinusoidal. An interesting feature in both endosseous labyrinths is the presence of a sinus that contacts the crus communis and extends to the medial margin

between the anterior and posterior ampullae. A sinus within the endosseous labyrinth has not been figured in any known elasmosaurid endosseous labyrinth cast, and is not a result of taphonomic distortion or bioerosion, as the bone containing the sinus is continuous with the surrounding walls of the endosseous labyrinth, and this sinus is present in both the left and right halves of the braincase. A similar sinus is also present in *Nothosaurus marchicus*, and is identified by Voeten et al., (2018) as a paratympanic sinus or middle cerebral vein. The endosseous labyrinth opens ventrally above the fenestra ovalis, which presents an opening between the base of the prootic and the exoccipital-opisthotic. The anterior amupulla is located within the prootic, likely along with the anterior semicircular canal and part of the horizontal semicircular canal, although it is difficult to assess exactly which parts of the endosseous labyrinth are present in which braincase element, as sutures are not visible. However, in other preserved elasmosaurid prootic and exoccipital-opisthotics ,where the semicircular canals can be visualized, the posterior semicircular canal passes through the exoccipital-opisthotic and supraoccipital, the anterior semicircular canal passes through the prootic and supraoccipital, and the horizontal semicircular canal is shared between the prootic and exoccipital-opisthotic (Chatterjee and Small, 1989; O'Keefe et al., 2017; Allemand et al., 2017; Allemand et al., 2018). This pattern is seen more broadly within plesiosauria and is the assumed condition in MGUAN (O'Keefe, 2006; Sato and Wu, 2011). The fossae for the ampullae and ultricus are widely open in MGUAN PA278, as in *L. morgani* (D1-8213, SMNS 81783) (Allemand et al., 2017; Allemand et al., 2018).

The exoccipital-opisthotics articulate with the dorsal surface of the basioccipital and at the base of the left exoccipital-opisthotic are three distinct nerve openings. The right exoccipital-opisthotic is partly damaged along its base and does not show the same number as a consequence. The jugular foramen is located between the suture of the exoccipital and opisthotic in MGUAN PA278 and would have allowed passage for the glossopharyngeal nerve (IX), the vagus (X), and accessory nerve (XI), as these nerves pass through foramen within the metotic fissure broadly in amniotes (Rieppel, 1994; Voeten et al., 2018). Posterior to the jugular canal, two additional nerve canals are visible and housed branches of the hypoglossal nerve (XII) in MGUAN PA278. The two hypoglossal canals of MGUAN PA278 clearly pierce the exoccipital along its mediolateral axis and are present on both the medial and lateral surface of the exoccipital. *L. morgani* specimen, SMNS 81783, exhibits two nerve openings on the medial side of the exoccipital-opisthotic (IX and X + XI), while D1-8213 exhibits four on the medial side (X + XI, IX and two openings for XII), and two on the lateral surface (IX and X + XI) (Allemand et al., 2017; Allemand et al., 2018). Carpenter (1997) illustrates four neural canal openings on the lateral surface of the exoccipital-opisthotic (IX, X + XI and two openings for XII) and five on the medial surface for *L. morgani* (IX, X + XI, and three openings for XII) (SMU SMP 69120). The isolated elasmosaurid basicranium from the Campanian of Russia exhibits three hypoglossal canals present on both the medial

and lateral side of the exoccipital. *Mauisaurus haasti* (CM Zfr 115) exhibits two nerve openings on the lateral surface of the exoccipital-opisthotic (IX + X + XI, and XII) and three on the medial surface (IX + X, XI, and XII) (Hiller et al., 2005). In the aristonectine elasmosaurid taxa, *T. keysei* and *Alexandronectes zealandiensis*, only two distinct nerve openings are visible in lateral aspect of the exoccipital-opisthotics (IX+X+XI and XII in *T. keysei*, IX+X and XII in *A. zealandensis*) (Otero et al., 2016; O'Gorman et al., 2017b). O'Keefe et al., (2017) reports one jugular canal and two hypoglossal canals openings on the lateral surface of the right exoccipital-opisthotic in *Morturneria seymourensis* (TTU 9219); in medial view of the right exoccipital-opisthotic of TTU 9219 (provided in figure 8 of Chatterjee and Small (1989)), there are three canals for the hypoglossal nerve branches and an extensive metotic fissure that would have housed nerve IX+X+XI and a branch of the jugular vein (Chatterjee and Small, 1989). Interestingly, there is an asymmetry in TTU 9219, where the left exoccipital-opisthotic exhibits two hypoglossal foramina on the medial surface of the left exoccipital-opisthotic (Chatterjee and Small, 1989). Aside from instances of asymmetry, the branching pattern of the cranial nerves might be of phylogenetic significance (noted by Zverkov et a., 2017) and informative taxonomically.

The right paraoccipital process of the exoccipital-opisthotic in MGUAN PA278 is better preserved than its left counterpart and extends ventrolaterally to contact the squamosal and quadrate, with a very light trace of a suture evident. In cross-section, the paroccipital process is oval in outline at its base on the opisthoitic. Distally, the paroccipital process becomes significantly deeper dorsoventrally and compressed anteroposteriorly. The contact with the squamosal and quadrate is dorsoventrally expansive, similar to *L. morgani* (SMU SMP 6912) (Carpenter, 1997; M.M., pers. obs). Due to mediolateral compression in the posterior-half of the skull, the exact orientation of the paroccipital processes cannot be determined exactly.

The supraoccipital caps the prootic and exoccipital-opisthotic (Figure 5.4.2.). In MGUAN PA278, this single element is split between the left and right halves of the braincase, with a single midline fragment floating in the rock matrix. The supraoccipital also contributes to the dorsal margin of the endosseous labyrinth in reptiles, although the sutures between the supraoccipital, prootic, and exoccipital-opisthotic cannot be identified due to tight suturing (Romer, 1976). Adjusting the braincase elements to correct for the shearing would provide the supraoccipital with a smooth concave ventral margin, a convex dorsal margin, with lateral extensions to cover the prootic and exoccipital-opisthotic. At the posterior end of the supraoccipital is a posteromedian process, similar to *L. morgani*, that projects posteriorly (Carpenter, 1997; M.M. pers. obs.). The supraoccipital does not appear to be complete enough for assessing the presence of a posteromedian ridge that extends dorsoventrally along the posterior margin of the supraoccipital above the foramen magnum, as in *T. ponteixensis* (Sato, 2003).

In cross-section of the basicranium, a slight separation is evident between the basisphenoid and the basioccipital that is filled by carbonate (Figure 5.4.3.). Within the basioccipital, two canals are evident oriented straight anteroposteriorly within the basioccipital and may be remnants of the notochord. There is no evidence of a 'medial foramen' near the ventral surface of the basioccipital, as there is in the aristonectine, *A. zealandiensis* and other plesiosaurians, *Cryptocleidus* and *Hauffiosaurus tomistomimus* (Andrews, 1910; Benson et al., 2011; Otero et al., 2016). Due to taphonomic separation between the basioccipital and basisphenoid, it could not be determined if a fontanelle was present between the suture of these two elements.

On the dorsal surface of elasmosaurid basioccipitals, between the facets for the exoccipital-opisthotics is an anteroposteriorly short and shallow fossa (Andrews, 1910; Wegner, 1914; Carpenter, 1997; Druckenmiller, 2002; Sato et al., 2011; Zverkov et al., 2017, MM pers. obs.). Zverkov et al., (2017) identify the fossa as accommodation for the plexus basilaris. The same fossa is identifiable in MGUAN PA278 approximately 30 mm anterior to the posterior margin of the occipital condyle. The fossa is shallow and takes up a small surface area on the floor of the basioccipital (Figure 5.4.4.).

The basitubera are located ventrolateral to the occipital condyle and are oriented posterolaterally. Between the basitubera is a broad sheet of bone that is continuous between the basitubera. On the ventral side of the basioccipital, the parasphenoid extends to nearly the posterior end of the ventral surface of the basioccipital. The ventral keel of the parasphenoid is located at mid-width on the ventral surface of the basioccipital and separates the medial expansion of the pterygoids. The parasphenoid does not develop cristae ventrolaterales (posterolateral extensions of the parasphenoid that cover the basitubera) beneath the basibuera, as it does in lower Jurassic plesiosaurians, *T. hawkinsi* and *E. arcuatus* (O'Keefe, 2006). There is a smoothly rounded ridge along the ventral margin of the occipital condyle. The occipital condyle is slightly cordiform in shape (the dorsal-half is slightly wider than the ventral-half) with no evidence of a notochordal pit. The neck of the occipital condyle is highly constricted along its ventral margin, but only moderately so on the dorsal surface, with no contribution from the exoccipital-opisthotics. There is a shallow concavity anterior to the dorsal margin of the occipital condyle in MGUAN PA278, which is also present in SGU 251/2 (Zverkov et al., 2017). On the elasmosaurid basicranium from the Campanian of Russia (SGU 251/2), Zverkov et al., (2017) reports a canal on the anterior margin of the basitubera that is referred to by the authors as part of the eustacian canal. The same structure is not present in MGUAN PA278 and doesn't appear to be present in *L. morgani* (SMU SMP 69120). There is no evidence of stapes in MGUAN PA278, as is usual among elasmosaurids, aside from *T. keyesi* (O'Gorman et al., 2017b).

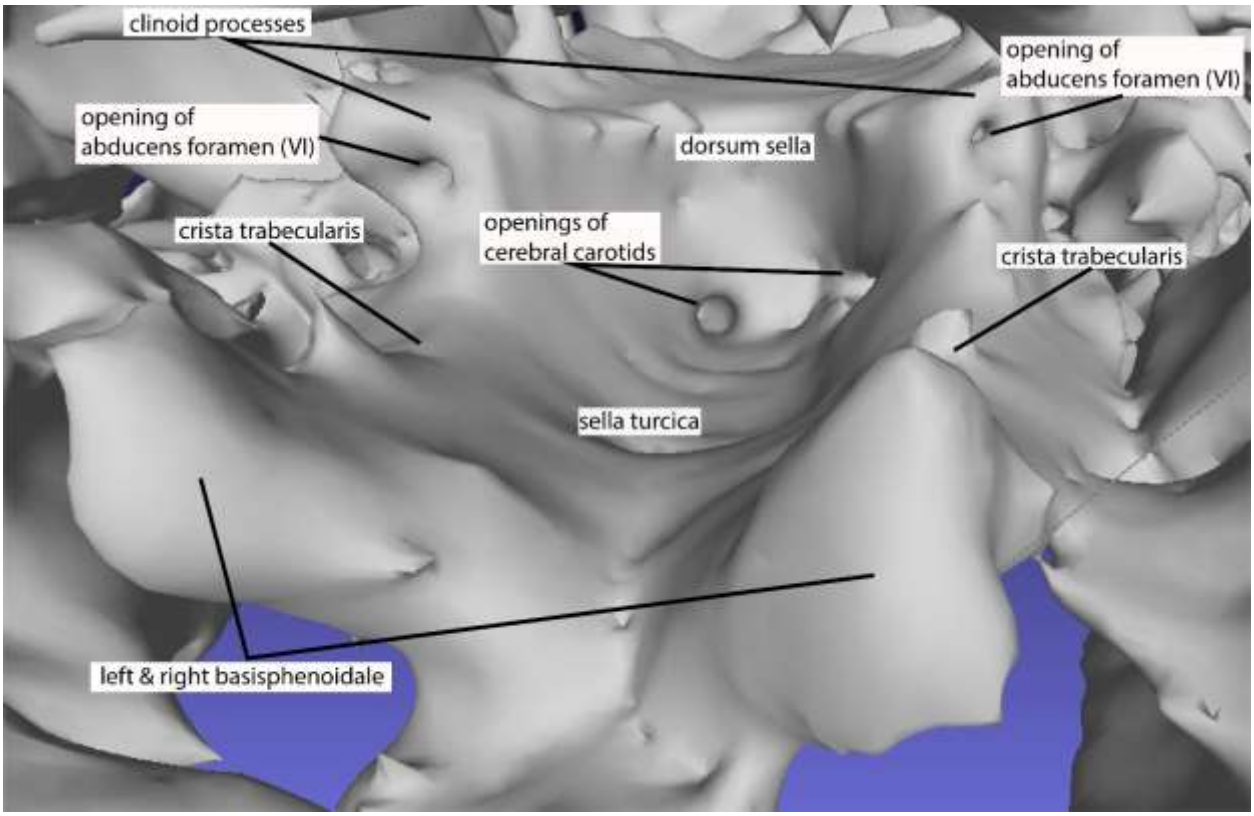

Figure 5.4.1. Anterior view of the sella turcica and structures of the parabasisphenoid. Image from 3D model of *Cardiocorax mukulu* skull (MGUAN PA278) in MeshLab.

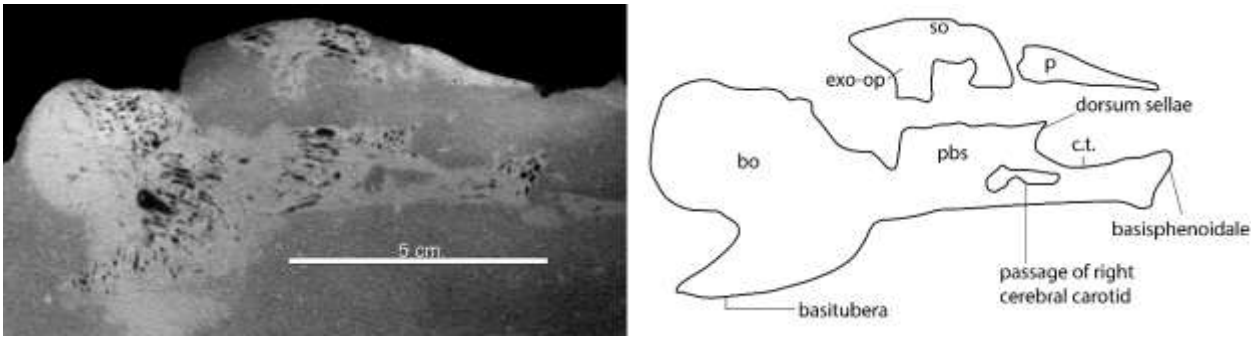

Figure 5.4.2. Parasagittal section of braincase showing the basisphenoidale, dorsum sellae, and opening of right cerebral carotid from *C. mukulu* (MGUAN PA278).

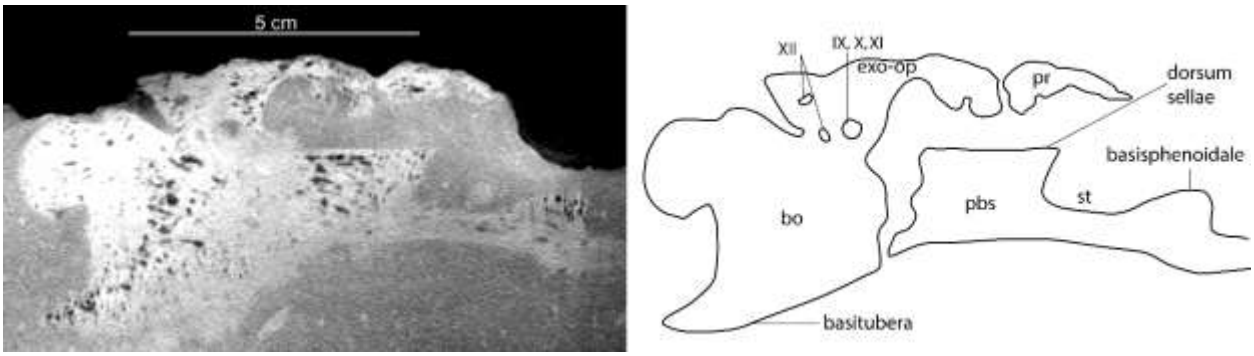

Figure 5.4.3. Parasagittal section of braincase exposing cranial foramen of *C. mukulu* (MGUAN PA278)

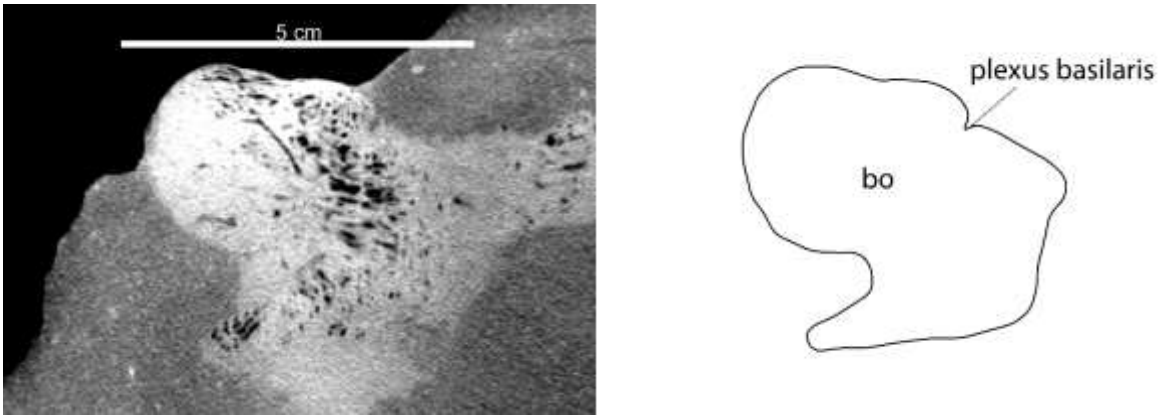

Figure 5.4.4. Plexus basilaris exposed on basioccipital of *C. mukulu* (MGUAN PA278).

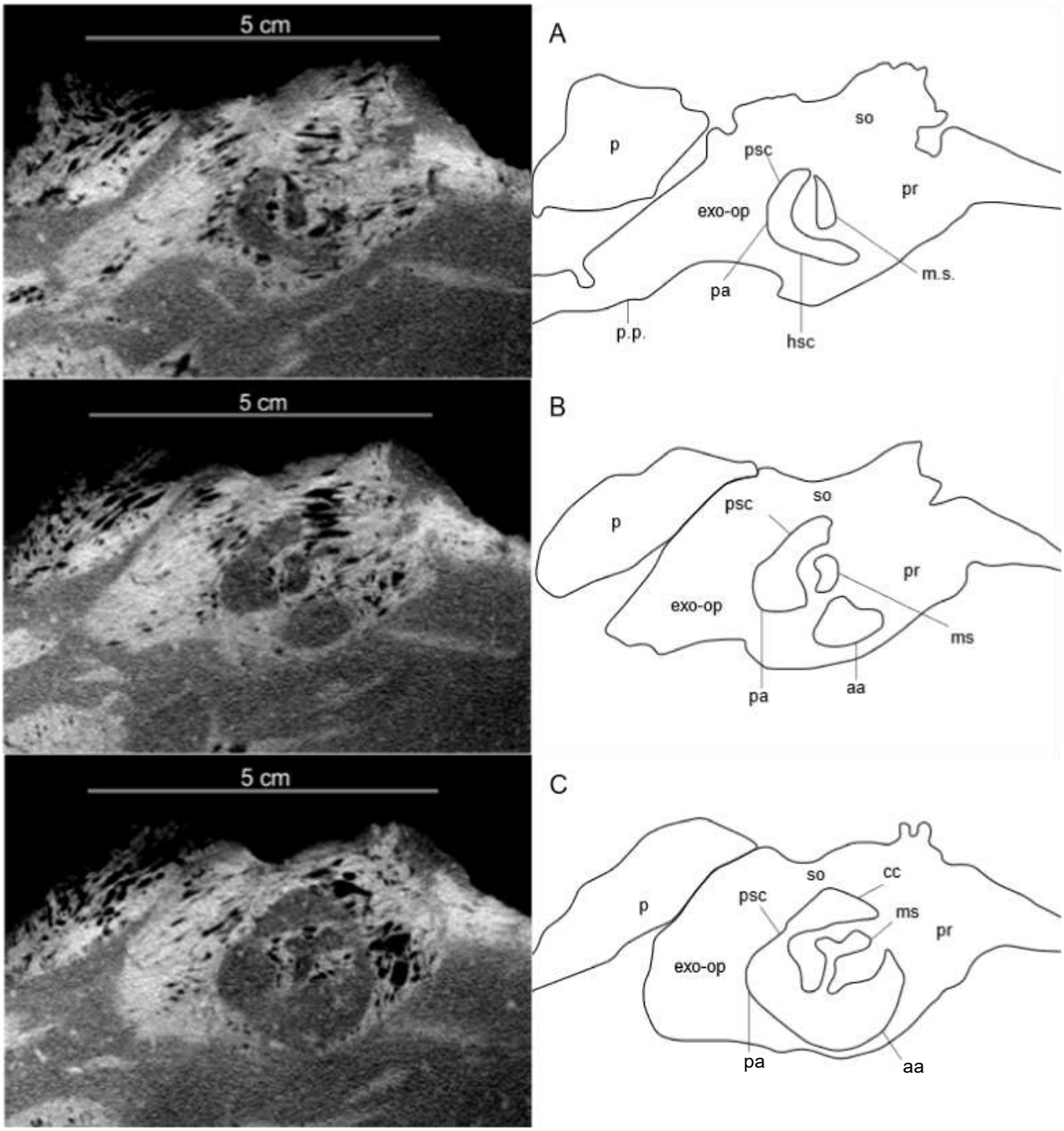
5 cm
5 cm
5 cm
A
p
so
psc
pr
exo-op
m.s.
pa
p.p.
hsc
B
p
psc
so
pr
exo-op
ms
pa
aa
C
p
so
cc
psc
ms
pr
exo-op
pa
aa

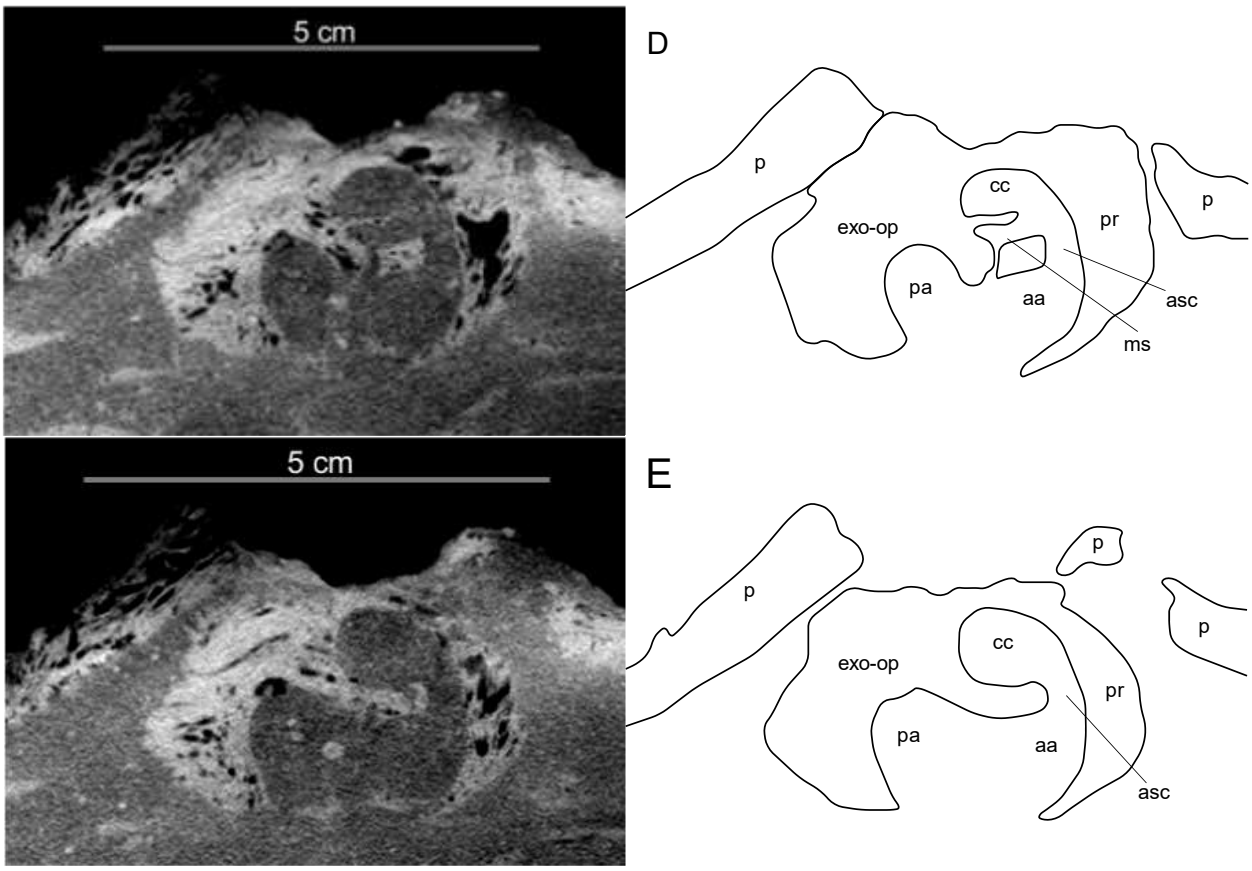

Figure 5.4.5. CT slices of endosseous labyrinth (pg. 97- 98) from the dorsal margin (A) to the ventral margin (E) of *C. mukulu* (MGUAN PA278). Slices A-E are progressively transitioning from the apex of the endosseous labyrinth to its ventral-most extent.

Description of the Endosseous labyrinth digital cast

The endosseous labyrinth is almost completely preserved in the right half of the braincase, although the vestibule not entirely preserved. The left endosseous labyrinth is missing most of the anterior ampulla and the lagena. The overall morphology of the endosseous labyrinth in MGUAN PA278 is rotund and globular, similar to the endosseous labyrinth cast of SMU SMP 69120 (Neenan et al., 2017). The morphology of the endosseous labyrinth digital cast is distinct from that of *B. brancaii* (Sachs et al., 2016a). The semicircular canals of *B. brancaii* appear more gracile and exhibit wider dorsoventral extent than the more compact morphology of MGUAN PA278 (Sachs et al., 2016a). Only three other endosseous labyrinth casts have been made for elasmosaurid plesiosaurians, one for *C. colombiensis* and two for *L. morgani* (SMU SMP 69120 & D1-8213) (Neenan et al., 2017; Allemand et al., 2019). The endosseous labyrinth of *C. mukulu* is distinct in being more compact in overall shape than SMU SMP

69120. The anterior and posterior semicircular canals are circular in cross-section and curve smoothly to meet at the apex of the crus communis. The crus communis is also rounded in cross-section and is short dorsoventrally; barely extending further dorsally than the ampullae (Figure 5.5.1.). The endosseous labyrinth of *C. mukulu* is thus short dorsoventrally, more so than *C. colombiensis* and D1-8213 (*L. morgani*) (Neenan et al., 2017; Allemand et al., 2019). The openings between the semicircular canals are constricted, similar to SMU SMP 69120 (Neenan et al., 2017). The ampullae of *C. mukulu* are incredibly enlarged. Between the ampullae, the vestibule is continuous with the surface of the ampullae. In lateral view, the horizontal semicircular canal is almost entirely absorbed into the lateral surface of the endosseous labyrinth. This condition contrasts sharply with all known sauropterygian otic capsules but is similar to SMU SMP 69120 (Neenan et al., 2017). The middle sinus (Figure 5.4.5.), which is present in both left and right endosseous labyrinth of MGUAN PA278, is interpreted as a paratympanic sinus or middle cerebral vein, based on its homologous location to that of the middle sinus from *Nothosaurus marchicus* (Voeten et al., 2018).

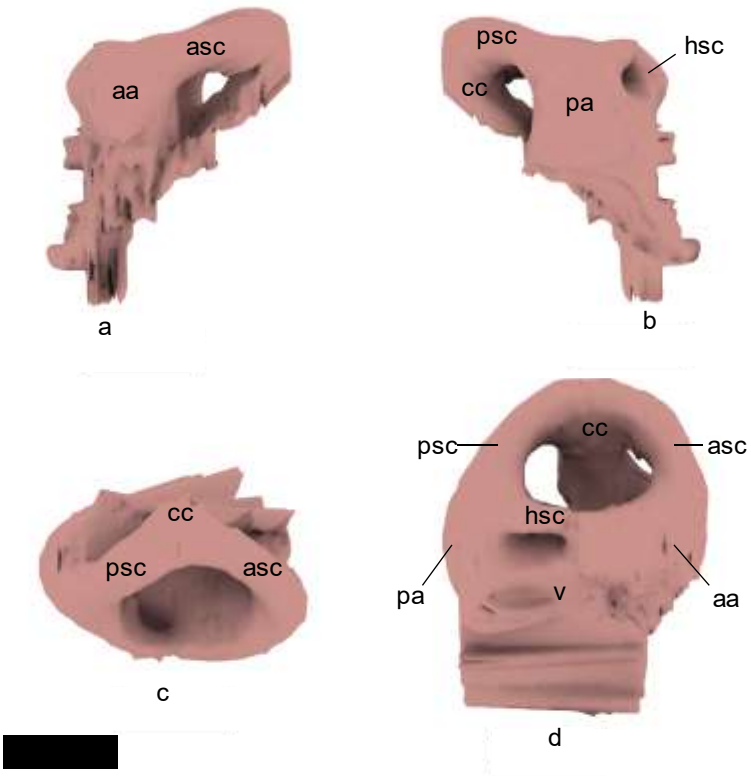

Figure 5.5.1. Right endosseous labyrinth digital cast of *Cardiocorax mukulu* (MGUAN PA278) in anterior (top left corner), posterior (top right corner), dorsal (bottom left corner), and lateral (bottom right corner) views.

The Mandible

The mandible is overall weathered but is not compressed and retains exceptional three-dimensional articulation between bone elements. The maximum anteroposterior length of the mandible is 453 mm from the preserved anterior margin of the symphysis to the right retroarticular process. The left ramus of the mandible measures 445 mm from the symphysis to the left retroarticular process. The maximum length measured from the right ramus is accepted as the total length of the mandible in MGUAN PA278, because the left ramus is broken underneath the centrum of an overlying mosasaur vertebra which may influence the anteroposterior length. The coronoid process on the left ramus is almost completely worn away. The right ramus of the mandible was also subject to erosional processes, with the coronoid process being particularly weathered along the lateral surface. The right ramus is slightly tilted, with the ventral margin facing slightly laterally, while the orientation of the left ramus is preserved more vertically in life position. The anterior margin of the symphysis is worn. Three alveoli are situated adjacent to the mandibular symphysis on the right ramus of the mandible. Two primary functional teeth are observable remaining in the alveoli at the anterior end of the mandible. Eleven replacement teeth are visible in the mandible either within replacement alveoli or transitioning into primary alveoli.

On the right ramus of the mandible, the retroarticular process is well-exposed and allows detailed description (figure 5.6.1, 5.6.2.). The retroarticular process is wider than high (width: 22.2 mm; height: 17.4 mm) and is formed by the articular dorsally and angular ventrally posterior to the mandibular glenoid, making the process sub-circular in cross-section. The right retroarticular process is 37.50 mm long, measured from the posterior end of the process until the posterior end of the right mandibular glenoid, and is longer than the mandibular glenoid (17.5 mm). At the posterior end of the retroarticular process, the bone is highly rugose. Along the dorsal and ventral surface, the texture of the retroarticular process is striated. The lateral surface of the right retroarticular process presents an anteroposteriorly oriented ridge of bone that is chipped at approximately its mid-length (Figure 5.6.1.). The long axis of the retroarticular process projects straight posterodorsally and is not inflected medially, as it is in *N. bradti* (Serratos et al., 2017). The left retroarticular process is only exposed along its dorsal surface but is the same morphologically as its right counterpart in what is observable.

In contrast, the retroarticular processes of *S. snowii* (KUVP 1301), *T. haningtoni* (UNSM 50132), and *N. bradti* are dorsoventrally deep and mediolaterally narrow (Serratos et al., 2017; Sachs et al., 2018; M.M. pers obs). A surface roughening, corresponding to the insertion of the *M. depressor mandibulae,* is present at the distal ends of the retroarticular processes of both *S. snowii* and *T. haningtoni*, but the

surface is particularly rugose in MGUAN PA278 (Druckenmiller 2002; Taylor, 1992). The retroarticular processes of *L. morgani*, *S. browni*, *C. colombiensis*, *T. ponteixensis*, *E. australis*, and *A. parvidens* are damaged (Sato, 2003; Kear, 2005; O'Gorman, 2015a; Otero, 2016; M.M. pers. obs.). There is no sulcus evident on the dorsal surface of the retroarticular process in MGUAN PA278, as is present in *N. bradti* (Serratos et al., 2017). Additionally, *N. bradti* is distinct in having a concave distal end on the retroarticular processes (Serratos et al., 2017). The retroarticular processes of MGUAN PA278 are morphologically most similar to *Aristonectes quiriquinensis* (SGO.PV.975) which exhibits a retroarticular process that is dorsoventrally compressed (W>H) (Otero et al., 2014). Although, in *A. quiriquinensis* the retroarticular processes is curved dorsally and slightly angled dorsomedially (Otero, et al., 2014). The retroarticular process of *K. khatiki* is oriented approximately straight posterior to the mandibular glenoid and appears to have a height and width that is sub-equal, but this process not been described in enough detail to supplement additional comparison (Cruickshank and Fordyce, 2002). The retroarticular processes of the holotype of *L. morgani* (SMU SMP 69120) are figured in Welles (1949) (plate 1 and 3). While today both retroarticular processes are damaged, the left retroarticular process was intact at the time of the holotype description of *L. morgani*, and the figures and drawings provided by Welles (1949) show that the left retroarticular process of *L. morgani* was similar to MGUAN PA278 in being oriented straight posteriorly, with the long axis pointed slightly posterodorsally.

The mandibular glenoid of MGUAN PA278 is divided into two cotyles on its articular surface, one medially and a second laterally, with pronounced anterior and posterior borders that are expressed as high flanges of bone as is common in all elasmosaurid plesiosaurians (figure 5.6.3.). The anterior flange curves slightly inward towards the center of the glenoid, while the posterior flange is oriented straight vertically. The medial cotyle is separated from the lateral cotyle on the mandibular glenoid by a low and smooth ridge oriented anteromedially-posterolaterally. The lateral cotyle is located almost completely on the lateral surface of the mandible. These cotyles on the glenoid would receive the condyles of the quadrate, with the sulcus separating the condyles on the quadrate fitting with the low ridge on the mandibular glenoid. Below the glenoid, in lateral view, is the presence of a depression that is bordered ventrally by a low mound of bone formed by the angular. This mound is continuous anteriorly with a subtle ridge that is approximately 18 mm long and runs anteroposterioly along the lateral interface of the surangular and angular ventral to the mandibular glenoid. This depression bordered ventrally by a ridge is also evident in the mandible of *S. snowii* and *T. haningtoni* (Sachs et al., 2018; M.M. pers. obs.). The contacts between the articular, surangular, and angular in lateral view can be discerned based on the light traces of the sutures observable (these elements are tightly co-ossified, making sutures less obvious). The articular bone in reptiles contributes to the formation of the mandibular glenoid and can also contribute to areas of the mandible outside of the mandibular glenoid, such as the retroarticular process (Romer, 1976;

Sues, 2019). In Plesiosauria, the articular contributes to the medial margin of the mandible, in addition to the dorsal margin of the retroarticular process (Brown, 1981; Taylor and Cruickshank, 1993; Carpenter, 1997; Storrs, 1997; Druckenmiller, 2002; Smith and Dyke, 2008; Smith and Vincent, 2010; Ketchum and Benson, 2011). In our interpretation of the extent of the articular on the mandible, the articular conforms to the border created by the mandibular glenoid and extends posteriorly to cover the dorsal margin of the retroarticular process (Figure 5.6.2.). The extent of the articular was similarly interpreted to follow this pattern of contributing to the dorsal margin of the retroarticular process in *S. snowii* (Figure 5.2.8., 5.2.9., 5.6.8.) and *T. haningtoni* (Figure 5.2.9.1.), although damage along the lateral surface of the mandible makes our interpretation of the lateral extent of the articular on the mandible approximate. The description of this element in elasmosaurid plesiosaurian literature is lacking or not figured; our interpretation of the articular of *S. snowii* (KUVP 1301) differs from that of Sachs et al., (2018) who do not indicate the presence of the articular on the dorsal margin of the retroarticular process.

The mandible is deepest from the apex of the coronoid process to the ventral margin of the mandible below the coronoid process. The coronoid process is weathered and thin in the right ramus, while the coronoid process on the left ramus is almost completely gone due to severe erosion (figure 5.6.4, 5.6.5.). In lateral view of the left ramus of the mandible, there does not appear to be a lateral depression on the preserved angular, as is present in *B. brancaii* (Sachs et al., 2016a). The maximum dorsoventral depth of the right ramus along the coronoid process is 82.5 mm. In what is preserved, the right coronoid process is formed medially by the coronoid and splenial, while the lateral side is formed by the dentary and surangular. Due to severe erosion along the lateral surface of the right coronoid process it cannot be determined if the dentary or the surangular contributed principally to the lateral margin of the coronoid process. The posterior opening of the meckelian canal is well exposed on the medial surface of the right ramus and presents a narrow opening formed by the splenial, and prearticular (Figure 5.6.6., 5.6.7.). The medial margin of the right ramus is exposed enough to permit general description (Figure 5.6.6., 5.6.7.). Anterior to the articular, the prearticular is located dorsal to the angular and medial to the surangular. Much of the medial surface of the surangular is not exposed due to incomplete cleaning and an anterior cervical vertebra that is attached to the medial surface of the right ramus of the mandible by rock matrix. The coronoid is an elongated element that contributes significantly to the dorsal margin of the coronoid process and extends anteriorly.

The dentary and angular are elongated elements in MGUAN PA278 that are slightly bowed out laterally in dorsal view of the mandible. The right dentary is better exposed than the left dentary and retains at least 20 primary tooth alveoli. This count contrasts with 19 dentary alveoli in *L. morgani* (SMU SMP 69120), at least 18 in *T. haningtoni* (UNSM 50132), at least 16 in *S. snowii* (KUVP 1301), at least

19 in *N. bradti* (MOR 3072), 17-18 in *T. ponteixensis*, 42-44 in *K. khatiki*, approximately 50 in *A. quiriquinensis*, and 63-65 in *A. parvidens* (Cruickshank and Fordyce, 2002; Sato, 2003; Sato et al., 2014a; O'Gorman, 2016; Serratos et al., 2017). *F. suzukii* shares with MGUAN PA278 20 dentary alveoli and *T. keyesi* exhibits 20-21 dentary alveoli (Sato, 2003; O'Gorman, 2017b). The dentary alveoli of MGUAN PA278 are slightly ellipsoidal in shape, with compression along the labio-lingual axis. The primary alveoli are aligned close to each other, with only a slim border of dentary bone four millimeters or less present between adjacent alveoli. A row of secondary alveoli is present medial to the primary row on the rami. Crushed and broken fragments of primary teeth can also be seen in twelve alveoli in the right dentary. The crowns of eleven secondary replacement teeth are visible in the preserved mandible. On the right ramus, the row of primary alveoli extends from the symphysis to approximately the mid-point of the coronoid process. It is not known if the angular and splenial contribute to the formation of the mandibular symphysis in MGUAN PA278. Without further preparation or a CT scan, the presence or absence of a symphyseal keel cannot be verified. The ventral and medial surfaces of the symphysis are obscured by matrix, making description of this area difficult.

Table 3. Measurements from the mandible of *C. mukulu* (MGUAN PA278).

Mandible measurements of *C. mukulu* (MGUAN PA278)	
anteroposterior length of the mandible	453 mm
anteroposterior length of right (better exposed) retroarticular process	37.53 mm
mediolateral width of the right (better exposed) retroarticular process	22.2 mm
dorsoventral height of the right (better exposed) retroarticular process	17.4 mm
length of right mandiblar glenoid	17.48 mm
maximum dorsoventral depth along the right coronoid process	82.53 mm

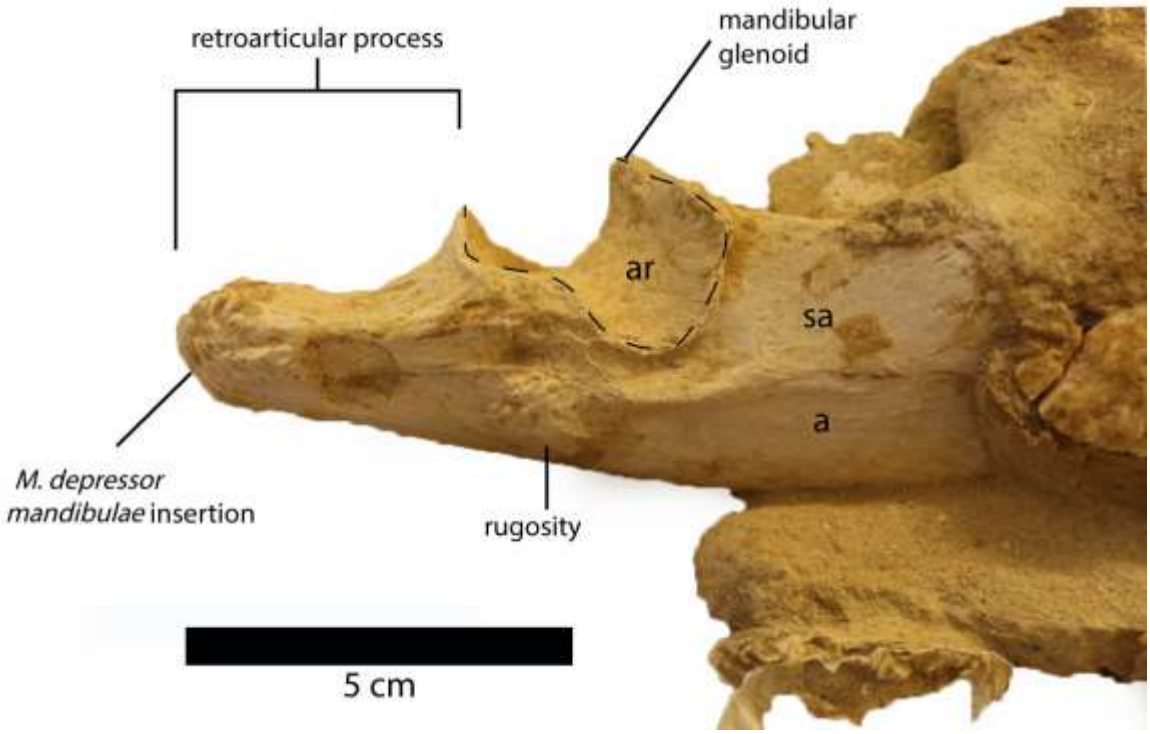

Figure 5.6.1. Right retroarticular process of *Cardiocorax mukulu* (MGUAN PA278) in right lateral view.

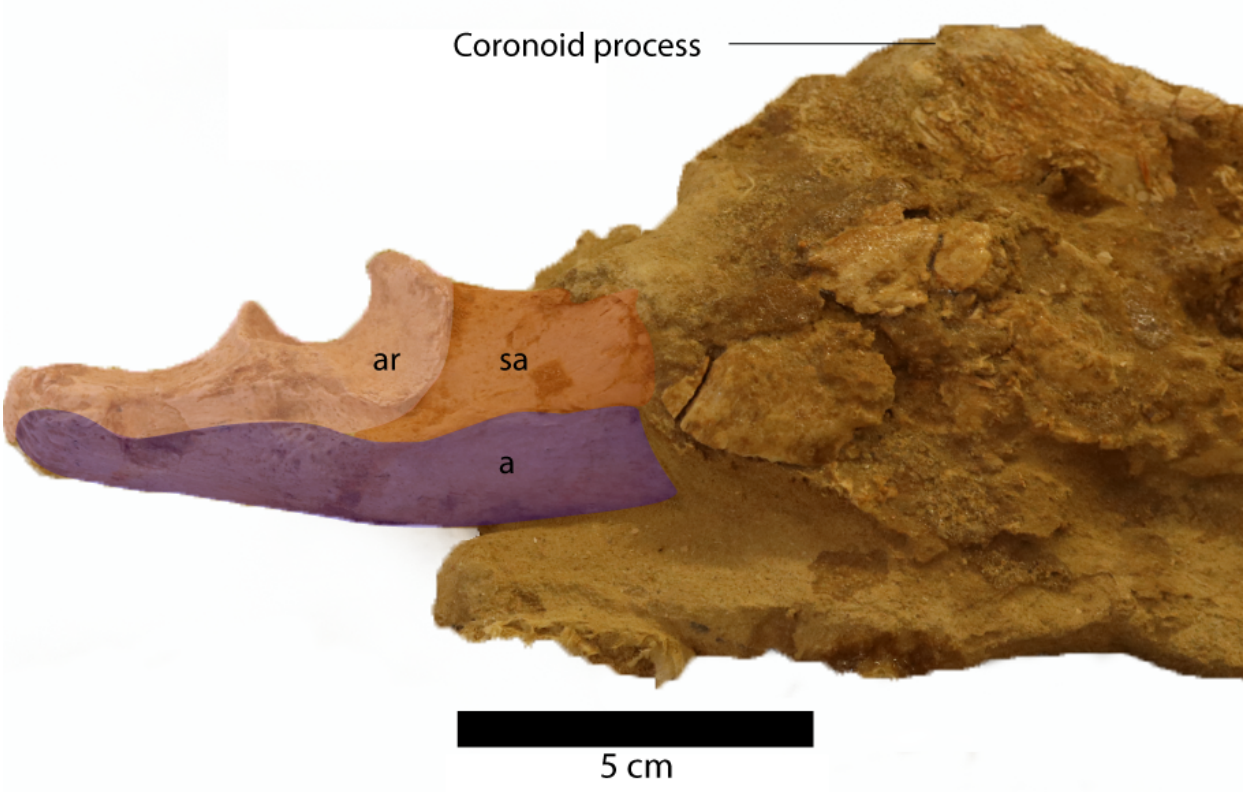

Figure 5.6.2. Right retroarticualr process from *Cardiocorax mukulu* (MGUAN PA278) in right lateral view with labeled mandible elements and coronoid process.

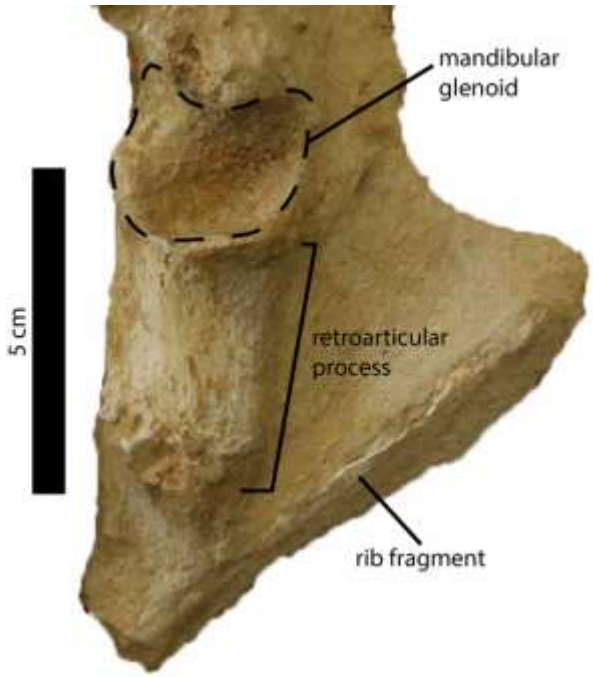

Figure. 5.6.3.. Left retroarticular process from *Cardiocorax. mukulu* (MGUAN PA278) in dorsal view.

Figure 5.6.4. Dordsal view of mandible from *Cardiocorax mukulu* (MGUAN PA278).

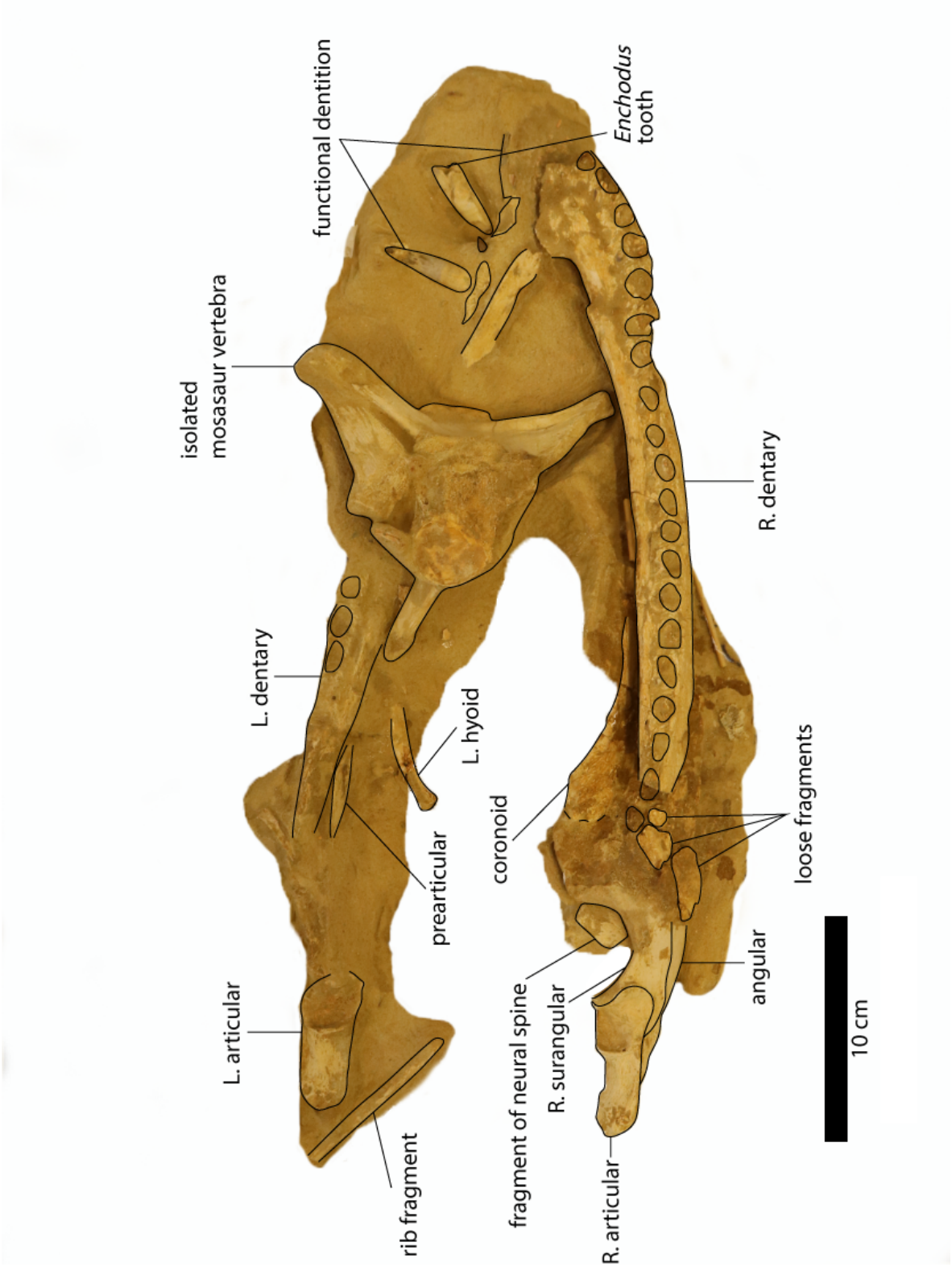

Figure 5.6.5. Dorsal view of mandible from *Cardiocorax mukulu* (MGUAN PA278) with bones labeled.

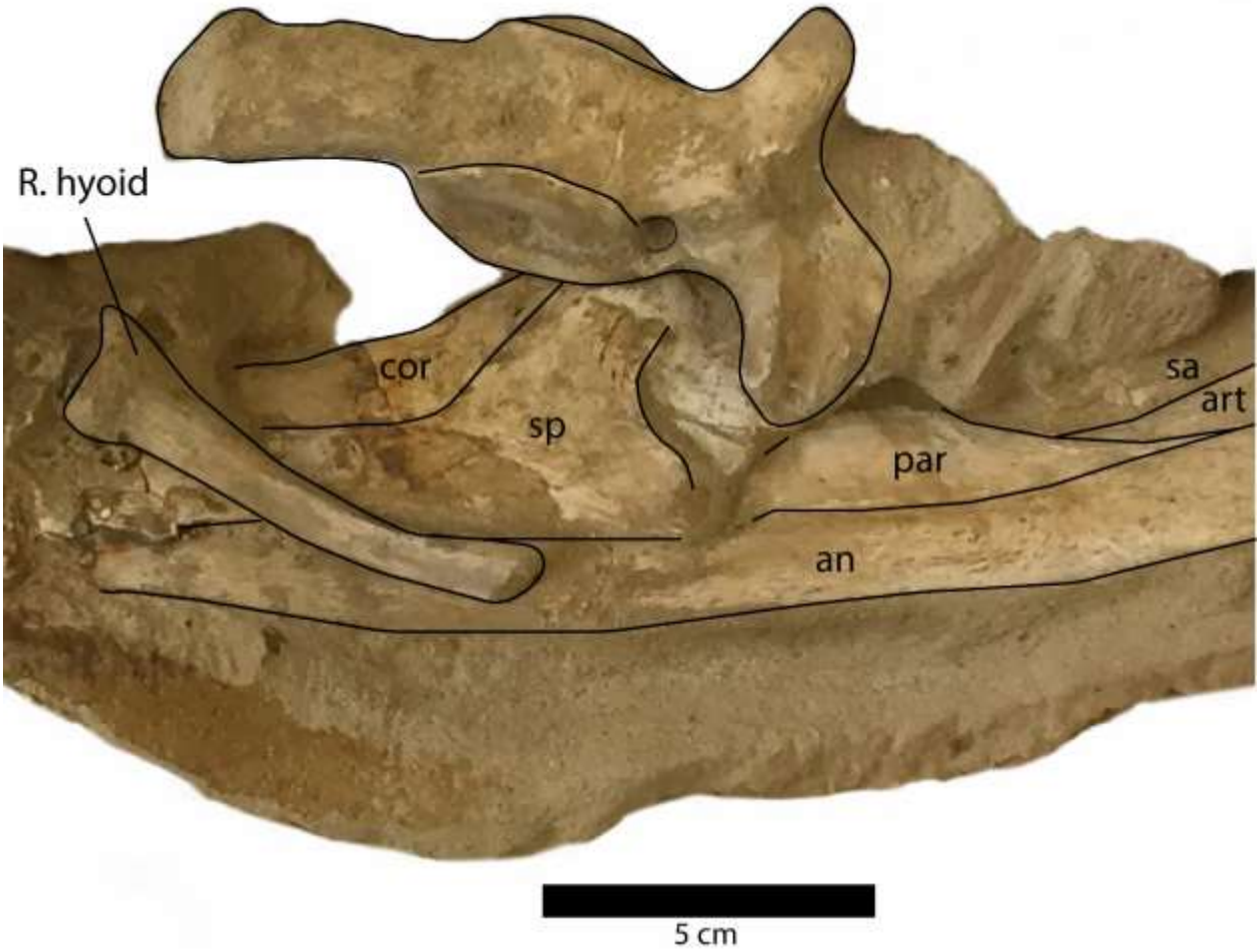

Figure 5.6.6. Medial view of right mandibular ramus of *Cardiocorax mukulu* (MGUAN PA278).

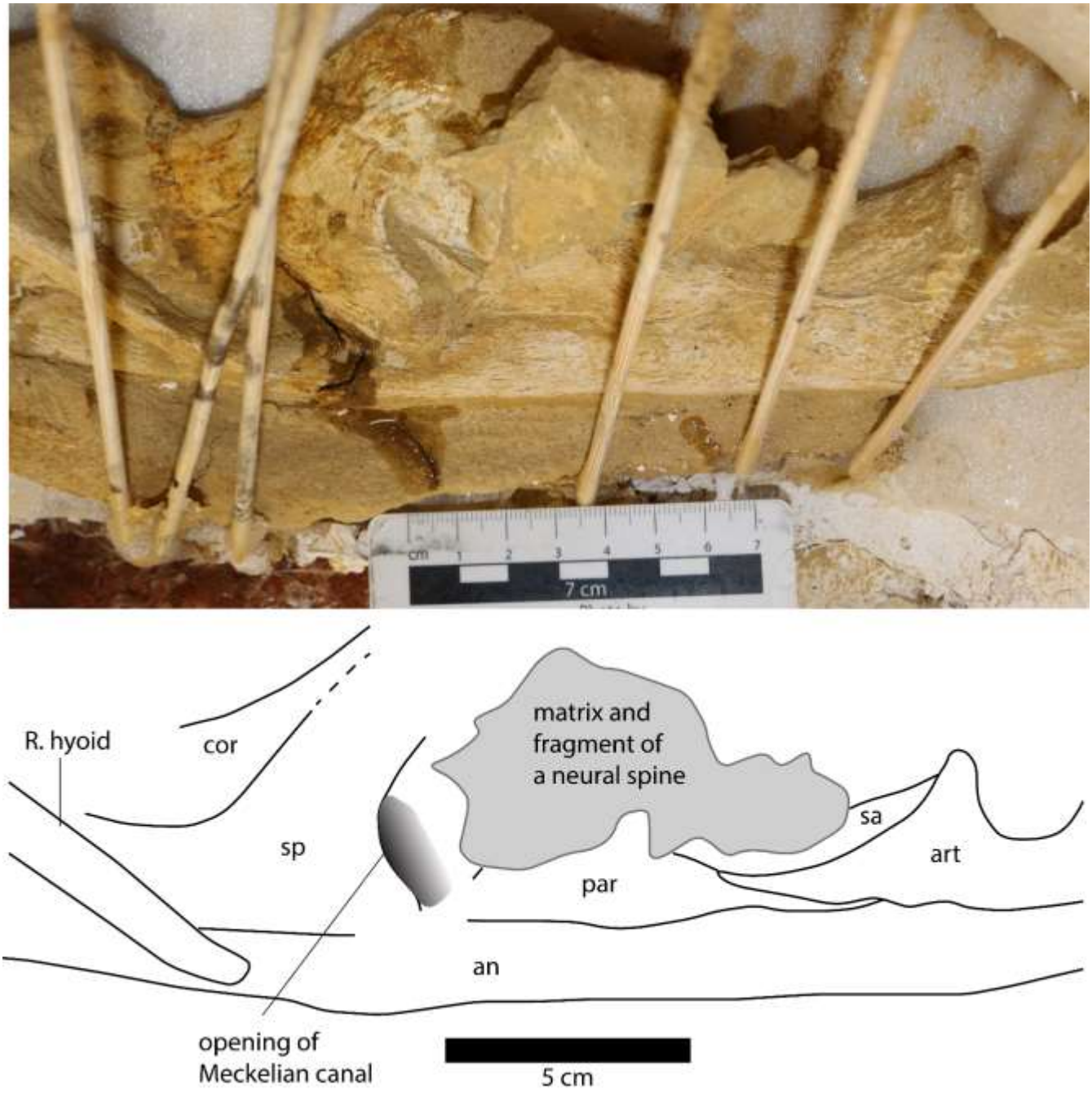

Figure 5.6.7. Medial view of right ramus of the mandible of *Cardiocorax mukulu* (MGUAN PA278).

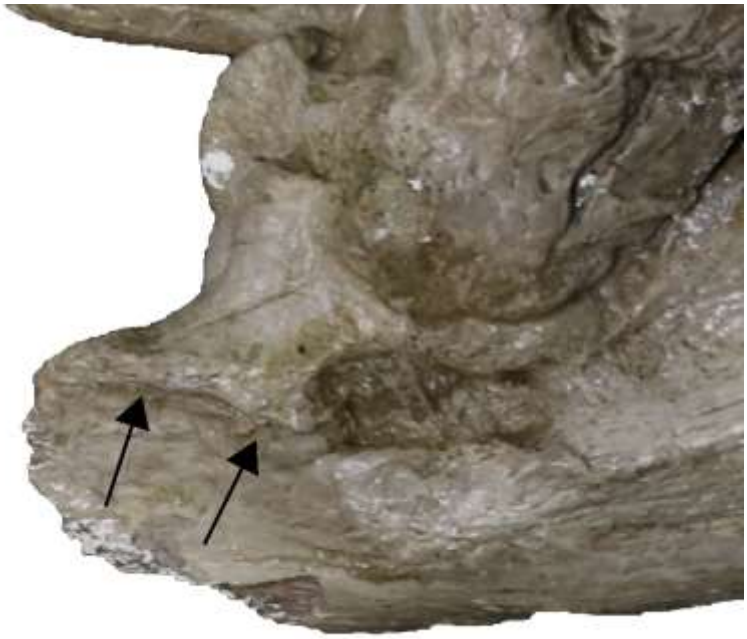

Figure 5.6.8. Preserved portion of right retroarticular process of *S. snowii* (KUVP 1301) in lateral view. Arrows indicate articular-angular suture.

Dentition

Thirteen teeth are associated with MGUAN PA278 outside of the skull and mandible; the best-preserved teeth outside the cranium and mandible preserve the crowns (Figure 5.7.1.). There is a total of four teeth remaining in the skull of MGUAN PA278, all are replacement teeth of the premaxillae. Two observable primary teeth remain in the alveoli of the mandible, with one located along the mandibular symphysis and a second at the anterior end of the left ramus (figure 5.7.2.). The crowns of eleven replacement teeth are observable in the mandible along with the crushed and fragmented remains of primary teeth within twelve primary alveoli. The teeth are anisodont with respect to size and shape. All teeth are compressed along one axis and exhibit striae on the enamel that is oriented apicobasally (Figure 5.7.1 and 5.7.3.). Compressed dentition is a common feature of elasmosaurids (Welles, 1962; Sato, 2003; Sachs and Kear, 2015; Allemand et al., 2017; Sachs et al., 2018; Allemand et al., 2018). In all observable teeth, the striae run subparallel to each other and taper just before the tip of the crown. Two different tooth curvature directions are evident in the preserved teeth. the symphyseal teeth of the mandible are curved lingually and compressed labiolingually, thus curvature is perpendicular to the direction of compression. The second morphology observed shows curvature aligned more parallel to the direction of

compression. This can be observed in the replacement teeth of the premaxillae and in associated loose tooth elements (Figure 5.7.3.).

The symphyseal teeth preserved in the mandible of MGUAN PA278 and the morphology of the alveoli in the skull and mandible suggest that the premaxillary teeth and the symphyseal teeth were procumbent, with the orientation of the teeth becoming more vertical in the posterior direction of the upper and lower tooth rows. The largest alveoli identified in MGUAN PA278 are primary alveoli 3-5 of the premaxillae and 6-9 of the maxillae. There is a trend of decreasing alveoli size in the posterior direction of the upper and lower tooth row. There is a total of 17 alveoli in the right maxilla and at least 20 observable alveoli in the right dentary of MGUAN PA278.

Figure 5.7.1. Tooth crowns associated with *Cardiocorax mukulu* (MGUAN PA278).

Figure 5.7.2. Functional tooth and crown of replacement tooth near mandibular symphysis of *Cardicorax mukulu* (MGUAN PA278).

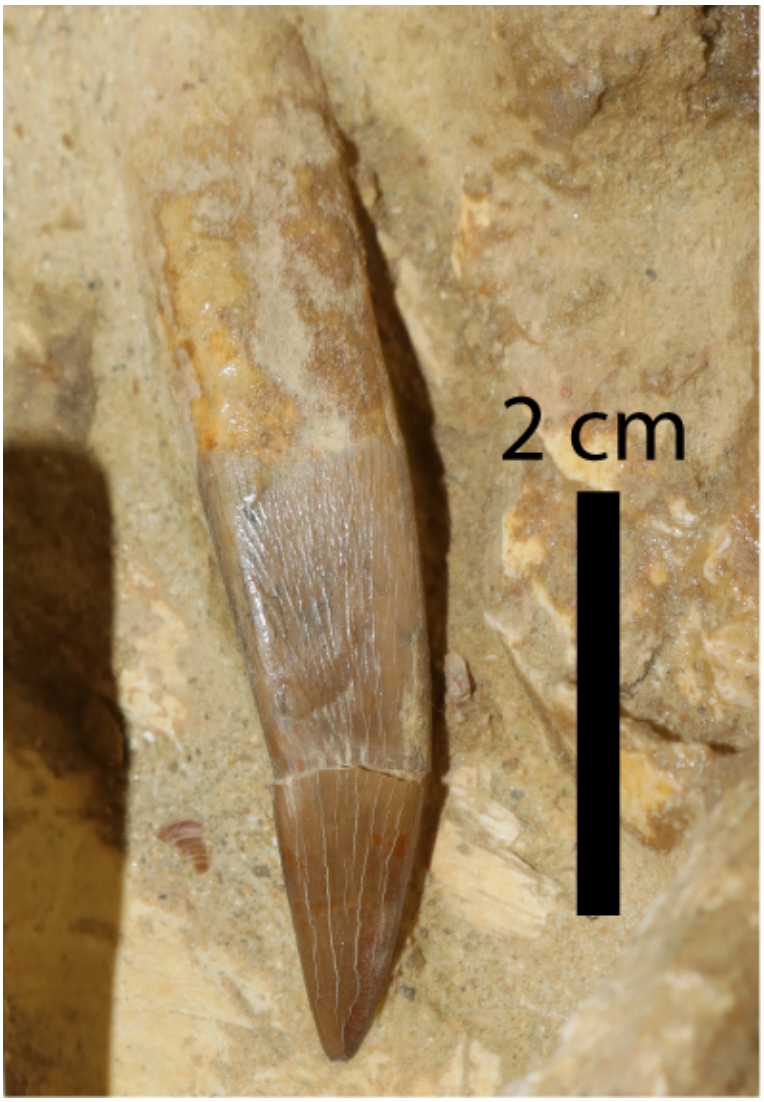

Figure 5.7.3. Tooth associated with *Cardiocorax mukulu* (MGUAN PA278).

Hyoid

Two hyoids are present in MGUAN PA278 and are located medial to the mandible (Figure 5.6.5. and 5.6.7.). The left hyoid is mostly obscured, with only the posterior margin visible. The right hyoid is adhered to the medial side of the right ramus of the mandible. The right hyoid is sub-straight, as opposed to the more sigmoidal hyoid seen in *N. bradti* (Serratos et al., 2017). The hyoid appears most similar *to E. australis*, in being straight (Kear, 2005). The hyoids are not prepared enough to allow detailed description.

Axial Skeleton

A mostly complete atlas-axis complex, in addition to at least 15 postaxial cervical vertebrae from the anterior and middle region of the cervical series are associated with MGUAN PA278. The relative location of the cervical vertebrae in the vertebral column is determined by the absolute size of the centra, the height of the neural spine relative to the height of the centrum, and the morphology of the prezygapophyses. None of the vertebrae are fully prepared and thus descriptions are made where possible. Overall, the vertebrae are well-preserved with the neural spines and cervical ribs being the most commonly damaged in all the vertebrae. One cervical vertebra exhibits shear-like plastic deformation. Calcareous residue covers all the observable cervical vertebrae. The calcareous reside, when removed off the vertebrae, sometimes leaves an etching mark on the surface of the bone. The carbonate acts as a cement that connects bone elements that are in close proximity to each other. One bite mark is observable in an anterior cervical vertebra and is the only evidence of vertebrate feeding on MGUAN PA278 (figure 5.8.4.). None of the vertebrae formed an articulated series in-situ and are dispersed throughout the specimen blocks.

Vertebrae

Atlas-axis complex

MGUAN PA278 includes a nearly complete atlas-axis complex, only the neural spines of the atlas and axis are partly damaged, mostly along the dorsal margin (figure 5.8.1.). Incomplete preparation prevents accurate dimensional measurements of the centrum complex. The atlas and axis vertebrae are completely fused without any trace of a suture, although the atlas and axis portions of the centrum unit can be delineated by a u-shaped notch formed at approximately mid-length of the atlas-axis complex between the neural arch of the atlas vertebra and the neural arch of the axis vertebra in lateral view (Figure 5.8.1.). This notch delineates the ventral margin of a fenestra that separates the neural arches. This foramen is present in *N. bradti* (Serratos et al., 2017) *L. morgani* (Carpenter, 1997; Sachs et al., 2017), *T. haningtoni* (MM. pers. obs.), *E. platyurus* (Sachs, 2005), and *Albertonectes vanderveldi* Kubo, Mitchell, and Henderson, 2012 (Kubo et al., 2012), but not *S. snowii* (Sachs et al., 2018; MM pers. obs.). The pedicles of the axial neural arch extend dorsally and transition into the postyzygapophyses. The postzygapophyses are obscured and prevent description. The neural arches of the atlas and axis are both completely fused to their respective centra without any noticeable suturing.

The articular facet of the axis is amphicoelous, wider than high (W>H) and exhibits a thickened articular rim that is constricted by a shallow depression. The neural canal forms a shallow excavation along the dorsal margin of the axial centrum, making the dorsal margin of the axial articular facet bilobate in shape. The morphology of the axis articular facet is distinct from *S. snowii*. The axial facet of *S. snowii* (KUVP 1301) is sub-platycoelous and is dorsoventrally deep, 38.1 mm high and 30.18 mm wide, as opposed to being binocular in shape. An articular rim is present along the margins of the articular facet of the axis in KUVP 1301, however, this rim is not as strongly convex as what is seen in MGUAN PA278. The morphology of the axis articular facet in MGUAN PA278 is most similar to *L. morgani* and *T. haningtoni*. Both taxa exhibit an axial facet that is wider than high (W>H) with a thickened articular rim (figure 5.8.2.). The dorsal margin of the axial articular facet in *L. morgani* presents a shallow notch, making the axial facet appear slightly binocular in shape.

There is a significant constriction between the articular facet of the axis and the axis centrum in MGUAN PA278. Additionally, the lateral surface of the constricted axis centrum is rugose and grooved, with low ridges of bone oriented in a subparallel fashion anteroposteriorly. A subtle swelling is present on the lateral surface of the axis centra in *S. snowii* (KUVP 1301) and *T. haningtoni* (UNSM 50132) that is not present in MGUAN PA278 (M.M. pers. obs.). The articular facet of the atlas is obscured by matrix, although it is narrower than the facet for the axis vertebra. The atlas does not present a swelling, which can be seen in the atlas vertebrae of *E. platyurus*, and *T. haningtoni* (Sachs, 2005; Sachs et al., 2016b).

In ventral view, the hypophyseal ridge is a very prominent process that spans the entire anteroposterior length of the atlas-axis complex in MGUAN PA278 (figure 5.8.3.). The hypophyseal ridge is transversely thick at its anterior end and reaches its greatest depth just anterior to the mid-point of the atlas-axis complex. In ventral view, a swelling or 'boss' can be seen at the anterior end of the hypophyseal ridge. The anterior extent of the hypophyseal ridge splays laterally to merge with the articular facets of the atlas; the posterior end of the hypophyseal ridge merges with the articular facet of the axis (Figure 5.8.3.). In *N. bradti*, the hypophyseal ridge is dorsoventrally deep beneath both the atlas and axis, as opposed to just the atlas (Serratos et al., 2017). The hypophyseal ridge exhibits a ventral boss and extends along the entire anteroposterior length of the atlas-axis complex in *L. morgani*, *A. vanderveldi*, *N. bradti*, and perhaps in *A. parvidens*, but not in *T. keyesi* or *S. snowii* (Sato et al., 2012; Sachs et al., 2015; O'Gorman, 2016; Serratos et al., 2017; O'Gorman et al., 2017b; Sachs et al., 2018; M.M. pers. obs.). In MGUAN PA278, the atlas-axis ribs are clearly visible and are oriented posteroventrally and posterolaterally with a narrow slit separating the atlas rib from the axis rib. The atlas rib is narrow and rod-like, while the axis rib is morphologically distinct in presenting a broad articulation with the axis centrum that tapers distally. In all elasmosaurids, the axis rib forms a broad articulation with

the axis centrum and is in close contact with the atlas rib. Both the atlas and axis ribs extend beyond the axial articular facet, as it does in all elasmosaurid plesioaurians except *L. morgani* (Sachs et al., 2015).

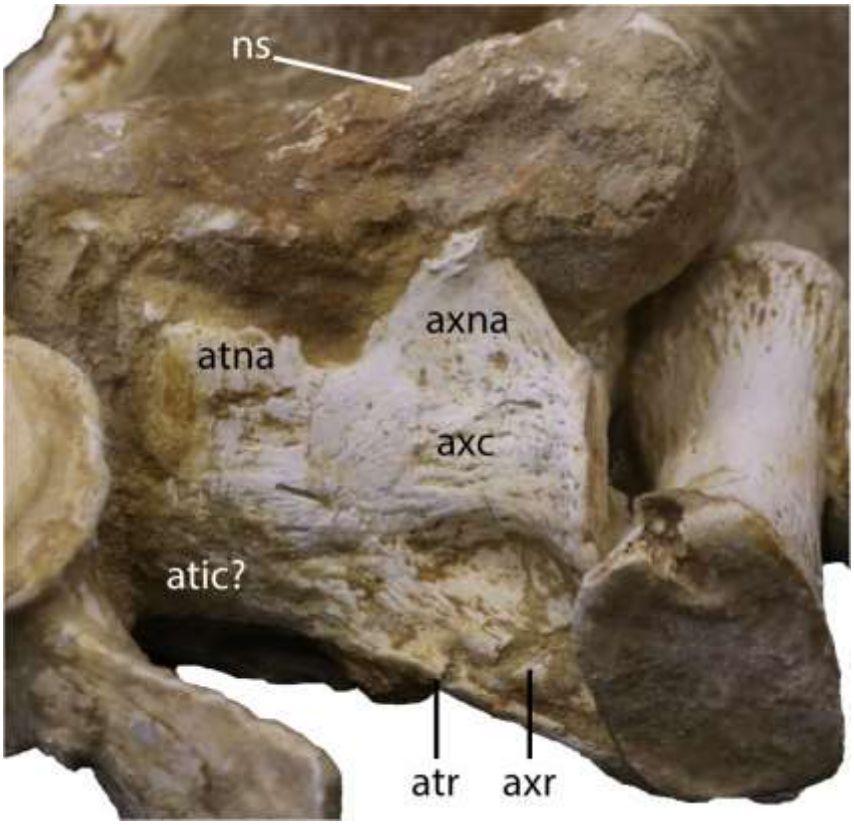

Figure 5.8.1. Left lateral view of the atlas-axis complex from *Cardiocorax mukulu* (MGUAN PA278).

Figure 5.8.2. Exposed posterior view of atlas-axis complex from *Cardiocorax mukulu* (MGUAN PA278).

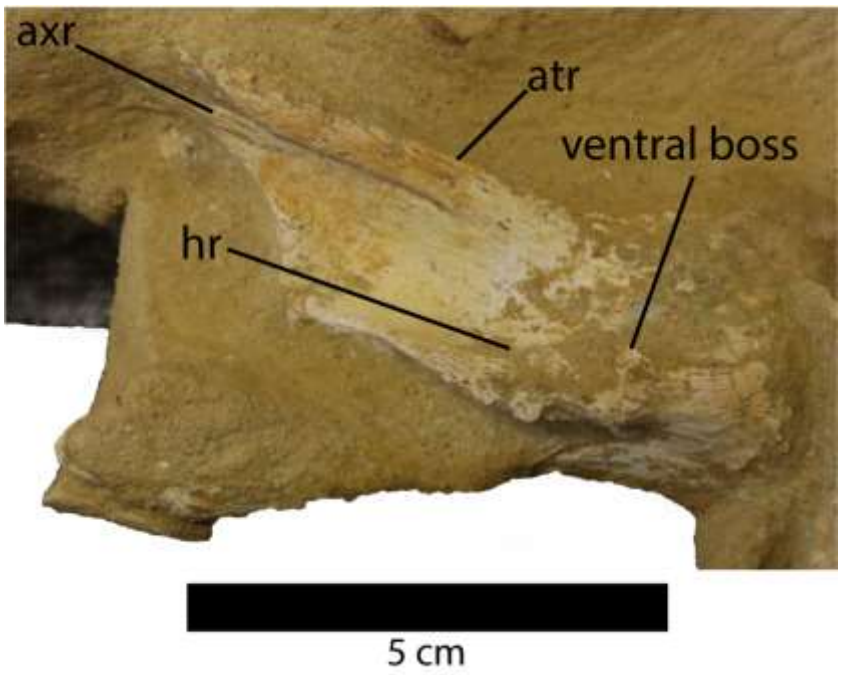

Figure 5.8.3. Exposed ventral view of the atlas-axis complex from *Cardiocorax mukulu* (MGUAN PA278)

Postaxial cervical vertebrae

Cervical vertebrae are provided number designations based on their placement in the cervical column relative to each other, and not their actual location which cannot be assessed with MGUAN PA278, as a complete and articulated cervical column was not recovered with the specimen. Thus, the anterior-most cervical vertebra associated with MGUAN PA278 is 'anterior cervical vertebra 1', and the next largest cervical vertebra is 'anterior cervical vertebra 2', etc. (Table 4). This method of labeling is used simply to organize associated vertebrae. Altogether, there are seven anterior cervical vertebrae, and three vertebrae from a more proximal region of the cervical that allow for general description. Additional vertebrae are preserved in the rib block of MGUAN PA278, however incomplete preparation has left these vertebrae mostly obscured, and thus these vertebrae were not included in the description here (Figure 4.1.2. and 4.1.3.). The posterior-most cervical vertebra ('proximal cervical vertebra 3') only exposes the left lateral surface, the neural spine, and part of the anterior articular facet.

The articular facets of all described anterior cervical centra (except the unprepared posterior cervical vertebra) exhibit a shallow excavation along their dorsal margin, formed by the neural canal, and a second shallow concavity along the ventral margin at mid-width, making the centra binocular in shape. Two of the three proximal cervical vertebrae also exhibit articular facets with a binocular shape, while the articular facets of the posterior-most cervical vertebra ('proximal cervical vertebra 3') is obscured by matrix. The articular facets of all observable cervical vertebrae are sub-amphicoelous with a shallow concavity situated in the center of the articular facet and exhibit a thickened articular rim that is constricted by a shallow depression. The exposed anterior articular facet of 'proximal cervical vertebra 3' is more platycoelous.

Lateral longitudinal ridges are present slightly above mid-height on the lateral surface of the centra. In ventral aspect, a pair of foramina subcentralia are present at about mid-length of the centra and laterally straddle a prominent ventral keel that extends anteroposteriorly between the articular facets across the entire length of the centra. At the interface between the keel and the articular facets, the keel splays laterally and merges with the ventral rim of the articular facets. The foramina subcentralia are circular in shape and are situated within sulci. All observable centra are constricted between the anterior and posterior articular facets. The neural arches and cervical ribs are fully fused to the centra. The cervical ribs, while being damaged in some fashion in almost all the observable vertebrae, present a hatchet-shaped morphology, with anterior and posterior projections at the distal end of the ribs. Only 'cervical vertebra 1' (Figure 5.8.4.) exhibits cervical ribs without an anterior projection at the distal end. Rather, the cervical rib of the anterior-most cervical vertebra is smoothly convex along its anterior margin, concave along the posterior margin, and oriented posterolaterally. The cervical ribs are all single-

headed without a trace of a suture in MGUAN PA278. Overall, the general morphology of the cervical vertebrae expressed by MGUAN PA278 is shared with the majority of elasmosaurid plesiosaurians. Elasmosaurid vertebrae have been typically diagnosed by platyceolous articular, however, as noted by Sachs et al. (2014) and observations made by M.M., an amphicoelous condition is expressed, at least within local regions of the cervical column. Elasmosaurid taxa with amphicoelous cervical vertebrae include *L. morgani*, *E. platyurus*, *A. vanderveldi*, *S. snowii*, *H. alexandrae*, *C. colombiensis*, and AMNH 1495 (*Styxosaurus* sp.) (Sachs, 2005; Kubo et al., 2012; Sachs et al., 2015).

None of the cervical vertebrae form an articulated or semi-articulated series. However, the small size of the cervical vertebrae and their proximity to the skull indicates that the majority of the cervical vertebrae are from the anterior region (Table 4). Three cervical vertebrae are larger than the anterior-most cervical vertebrae and may be middle cervical vertebrae (Table 4). Aside from absolute size, the height of the neural spines relative to the height of the centra is greater in the more proximal cervical vertebrae than the anterior-most cervical vertebrae.

In the anterior cervical vertebrae, the prezygapophyses merge medially to form an inset surface that is divided by a thin ridge of bone that smoothly transitions to the neural spine dorsally (figure 5.8.5.). This same ridge dividing the prezygapophyses and transitioning to the neural spine was noted in the anterior cervical vertebrae of *Mauisaurus haasti* Hector, 1874 (Hiller et al., 2005). The postzygapophyses are all obscured by matrix in the anterior cervical vertebrae. The mediolaterally compressed morphology of the neural spines from the anterior cervical vertebrae is preserved, along with the expression of a straight anterior margin of the neural spine. The height of the neural spine in the anterior cervical vertebrae is less than that of the centrum. None of the anterior cervical vertebrae present ‘axial striations’ on the lateral and ventral sides of the articular facets, as is present in AMNH 1495 (*Styxosaurus* sp.) (Otero, 2016).

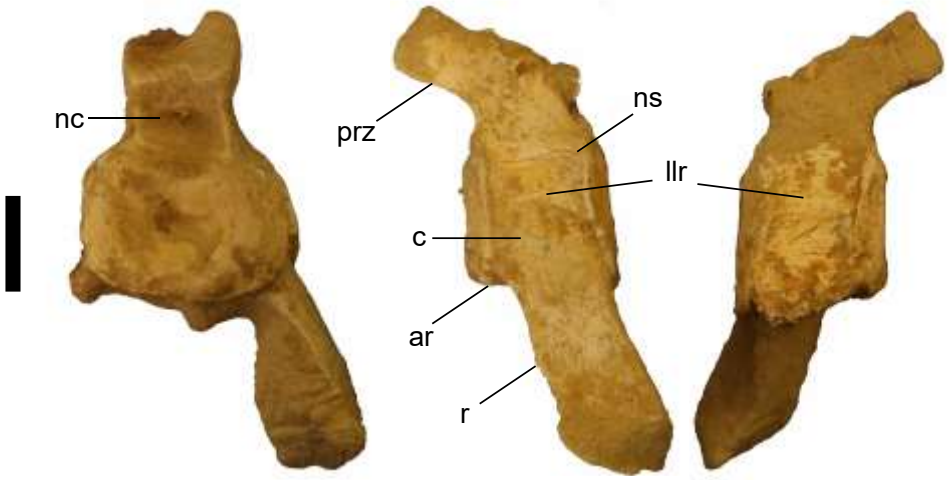

Figure 5.8.4. Anterior, left lateral, and right lateral views of the anterior-most cervical vertebra associated with *C. mukulu* (MGUAN PA278), 'anterior cervical vertebra' 1. ar is articular rim for vertebrae figures. Scale is 2 cm.

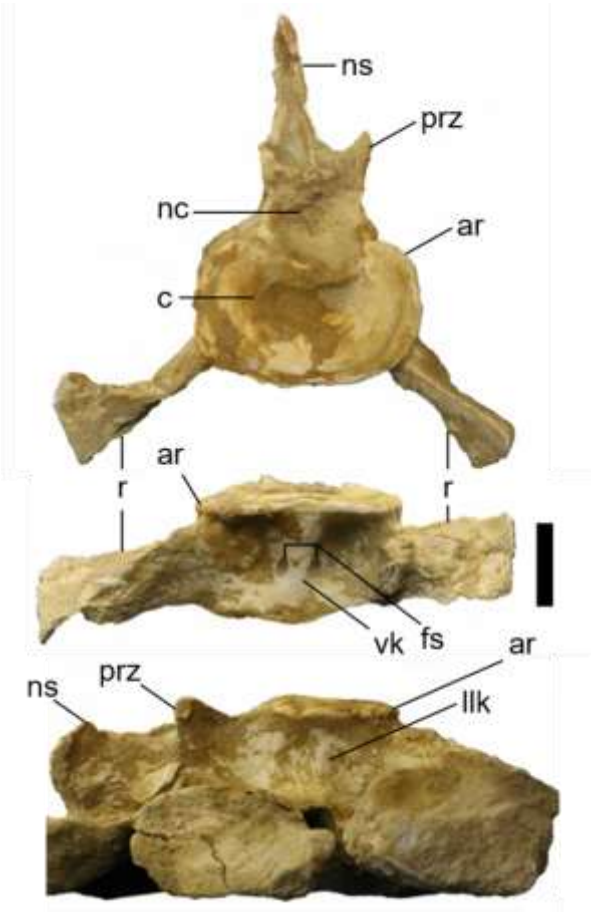

Figure 5.8.5. Anterior, ventral, and right lateral views of 'anterior cervical vertebra' 2 from *C. mukulu* (MGUAN PA278). Scale is 2 cm.

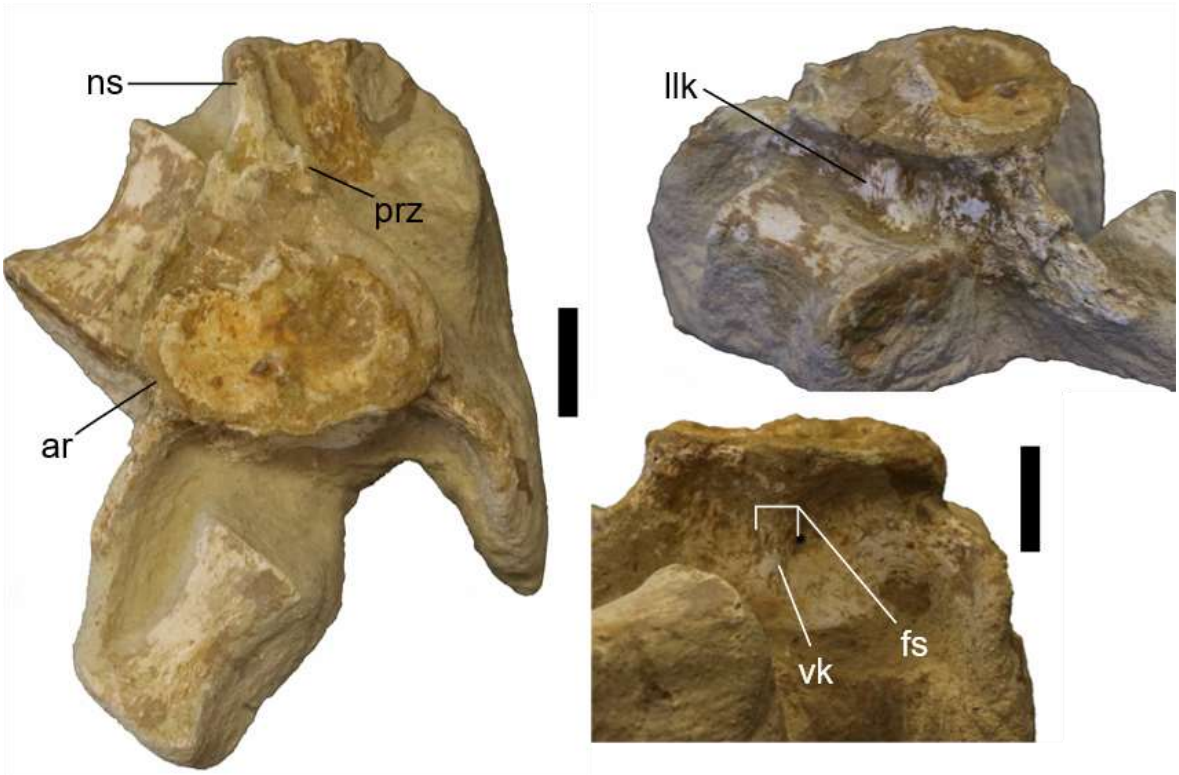

Figure 5.8.6. Left side: Anterior view of ‘anterior cervical vertebra’ 4 from *C. mukulu* (MGUAN PA278); right side: top: oblique view with lateral longitudinal keel visible; bottom: ventral view. Scale is 2 cm.

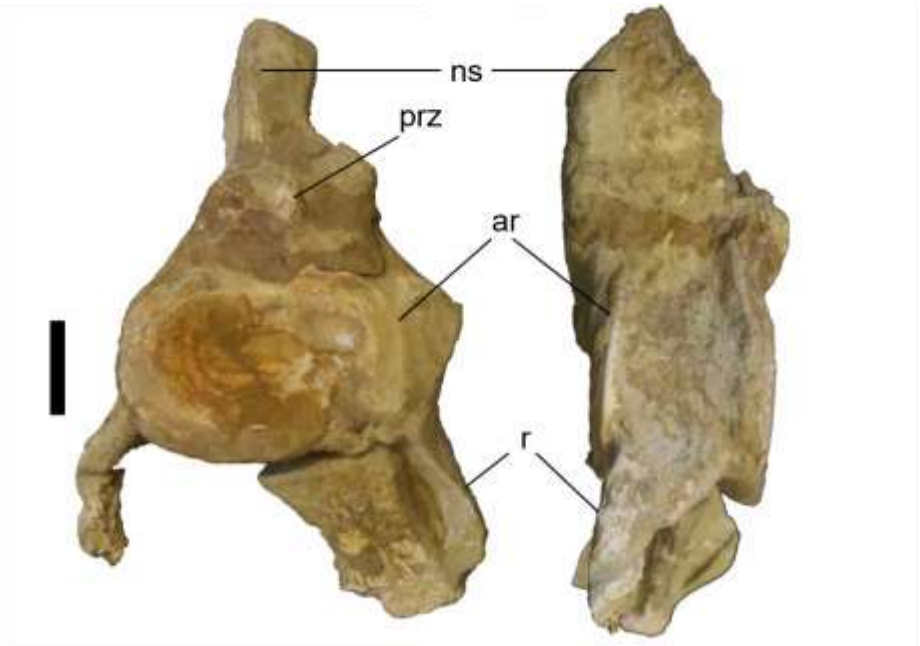

Figure 5.8.7. Anterior and right lateral view of ‘anterior cervical vertebra’ 6 from *C. mukulu* (MGUAN PA278). Scale is 2 cm.

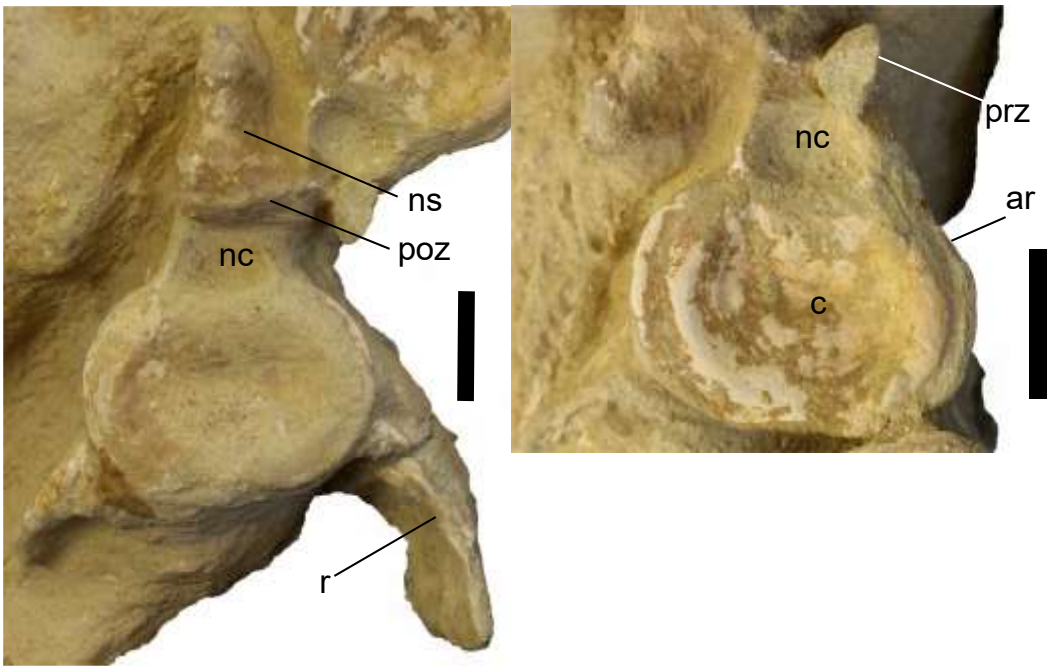

Figure 5.8.8. Left side: 'anterior cervical vertebra' 5 from *C. mukulu* (MGUAN PA278) in posterior view; right side: 'anterior cervical vertebra 3' in anterior view. Scale is 2 cm.

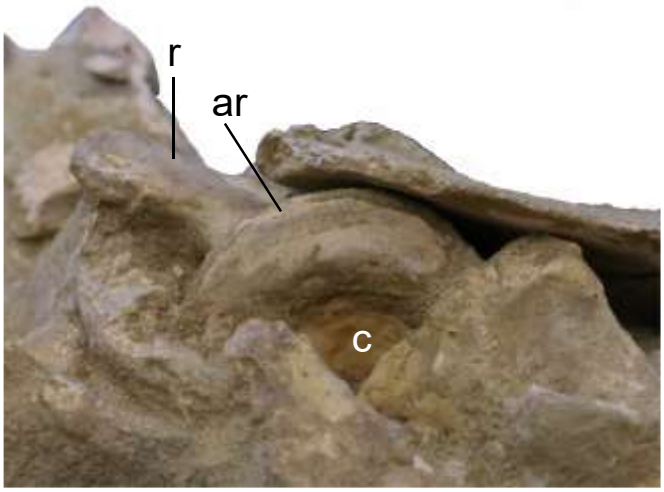

Figure 5.8.9. Exposed view of 'anterior cervical' 7 from *C. mukulu* (MGUAN PA278).

In the more proximal cervical vertebrae, the dorsal surface of the prezygapophyses from the proximal cervical vertebrae form a smooth concave articular facet to receive the postzygapophyses, however, the sharp ridge that extended between the prezygapophyses in the anterior cervical vertebrae is absent in the proximal cervical vertebrae. The postzygapophyses of 'proximal cervical vertebra 2' are exposed, and these processes are narrow and completely merge with each other medially and with the neural spine dorsally (figure 5.8.9.3.). The articular facet of the postzygapophyses in 'proximal cervical vertebra 2' forms a smooth convex surface on the ventral side. The exposed postyzgapophyses of the proximal cervical vertebrae extend beyond the posterior articular facet of the centra. The neural arches are narrow relative to the width of the proximal cervical vertebrae; this is a common elasmosaurid plesiosaurian character (Benson and Druckenmiller, 2014). Both the anterior and proximal cervical vertebrae of MGUNA PA278 exhibit ribs that are curved inward, to where the distal ends are facing medially (5.8.9.1.).

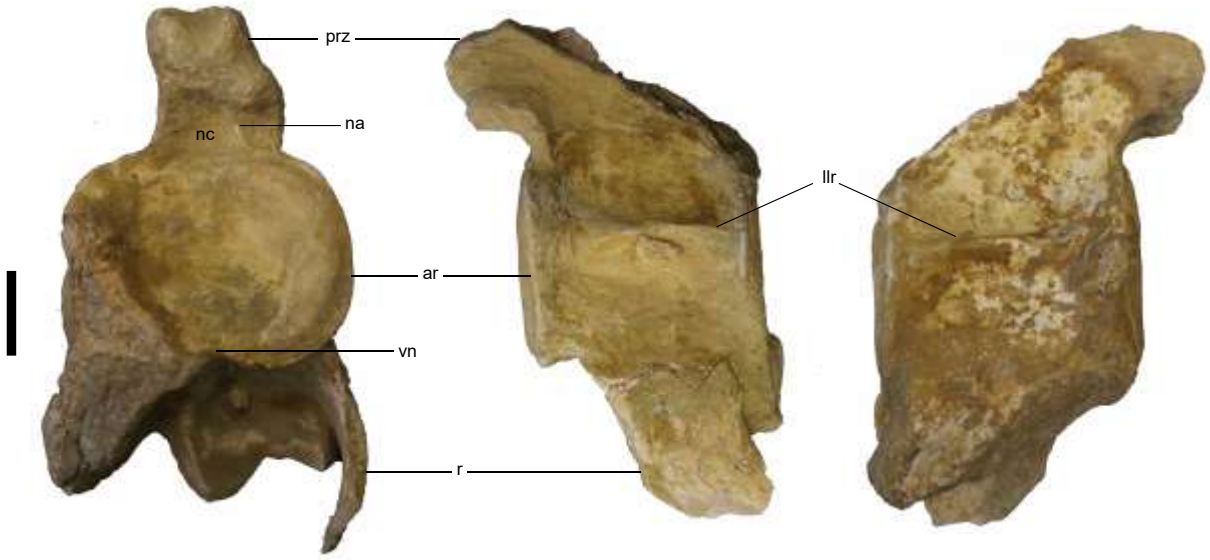

Figure 5.8.9.1. Anterior, left lateral, and right lateral view of 'proximal cervical vertebra' 1 from *C. mukulu* (MGUAN PA278). Scale is 2 cm.

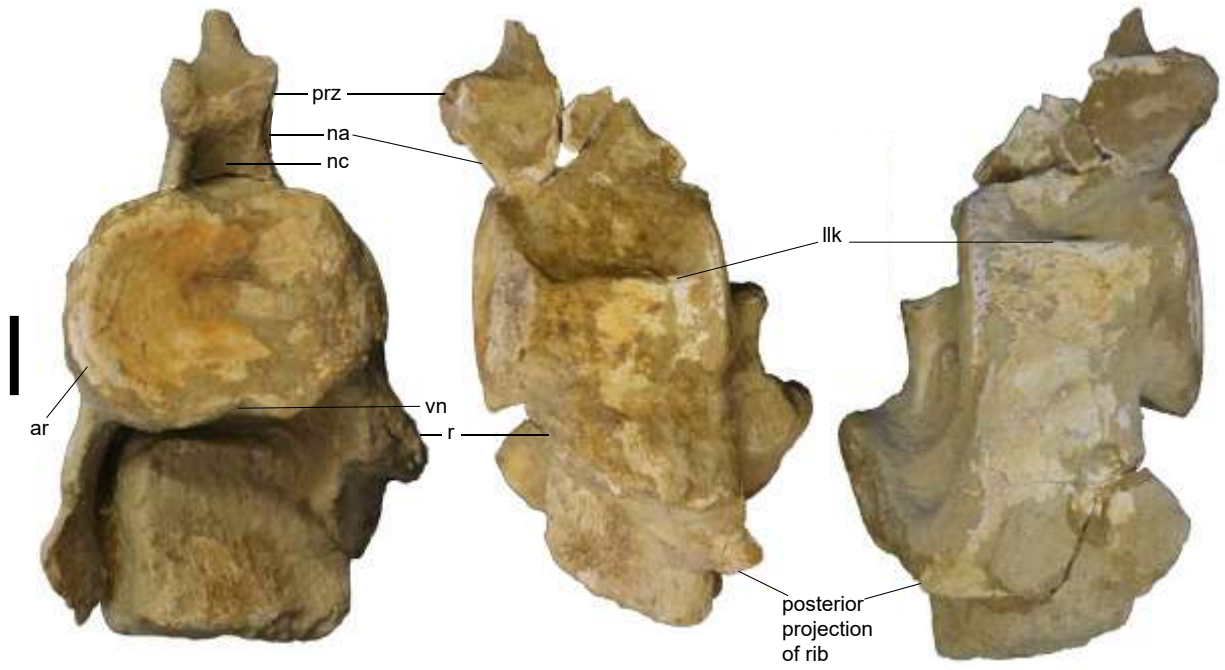

Figure 5.8.9.2. Anterior, left lateral, and right lateral views of ‘proximal cervical vertebra’ 2 from *C. mukulu* (MGUAN PA278). Scale is 2 cm.

Figure 5.8.9.3. ‘proximal cervical vertebra’ 2 attached to neural spine from *C. mukulu* (MGUAN PA278). Note the anterior projection at the apex of the neural spine, a shared autapomorphy with *C. mukulu* holotype. This feature would have extended further, as the anterior margin is broken. Scale is 5 cm.

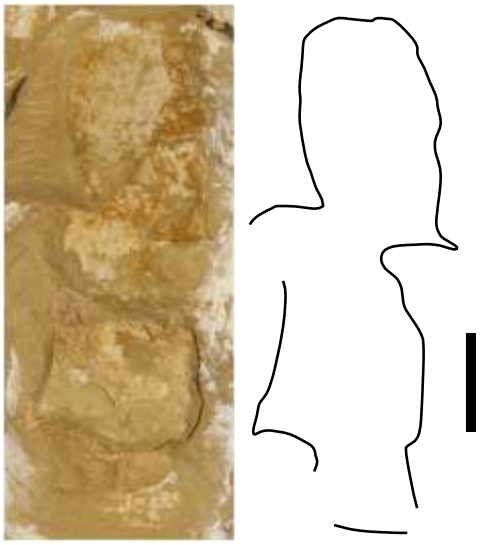

Figure 5.8.9.4. ‘Proximal cervical vertebra’ 3 in left lateral view from *C. mukulu* (MGUAN PA278). Note the lack of an anterior or posterior projection at the apex of the neural spine. Scale is 5 cm.

Table 4. Centrum dimensions for ten out of the at least fifteen postaxial cervical vertebrae associated with MGUAN PA278. Note: only vertebrae that were prepared or CT scanned were available for measuring. Thus, the position of the vertebrae labeled here are ordered relative to other prepared vertebrae, and do not reflect the real position of the vertebra within the cervical column. L = length; W = width; H = height.

Vertebrae dimensions of MGUAN PA278	L	W	H
anterior cervical vertebra 1	30.04 mm	44.08 mm	31.4 mm
anterior cervical vertebra 2	29.69 mm	54.11 mm	37.46 mm
anterior cervical vertebra 3	35.6 mm	51.14 mm	38.17 mm
anterior cervical vertebra 4	34.79 mm	51.51 mm	38.94 mm
anterior cervical vertebra 5	30.79 mm	56.3 mm	42.95 mm
anterior cervical vertebra 6	39.58 mm	61.87 mm	45.72 mm
anterior cervical vertebra 7	47.68 mm	61.99 mm	42.58 mm
proximal cervical vertebra 1	61.16 mm	70.63 mm	53.41 mm
proximal cervical vertebra 2	58.10 mm	80.54 mm	58.53 mm
proximal cervical vertebra 3	85.40 mm	NA	84.60 mm

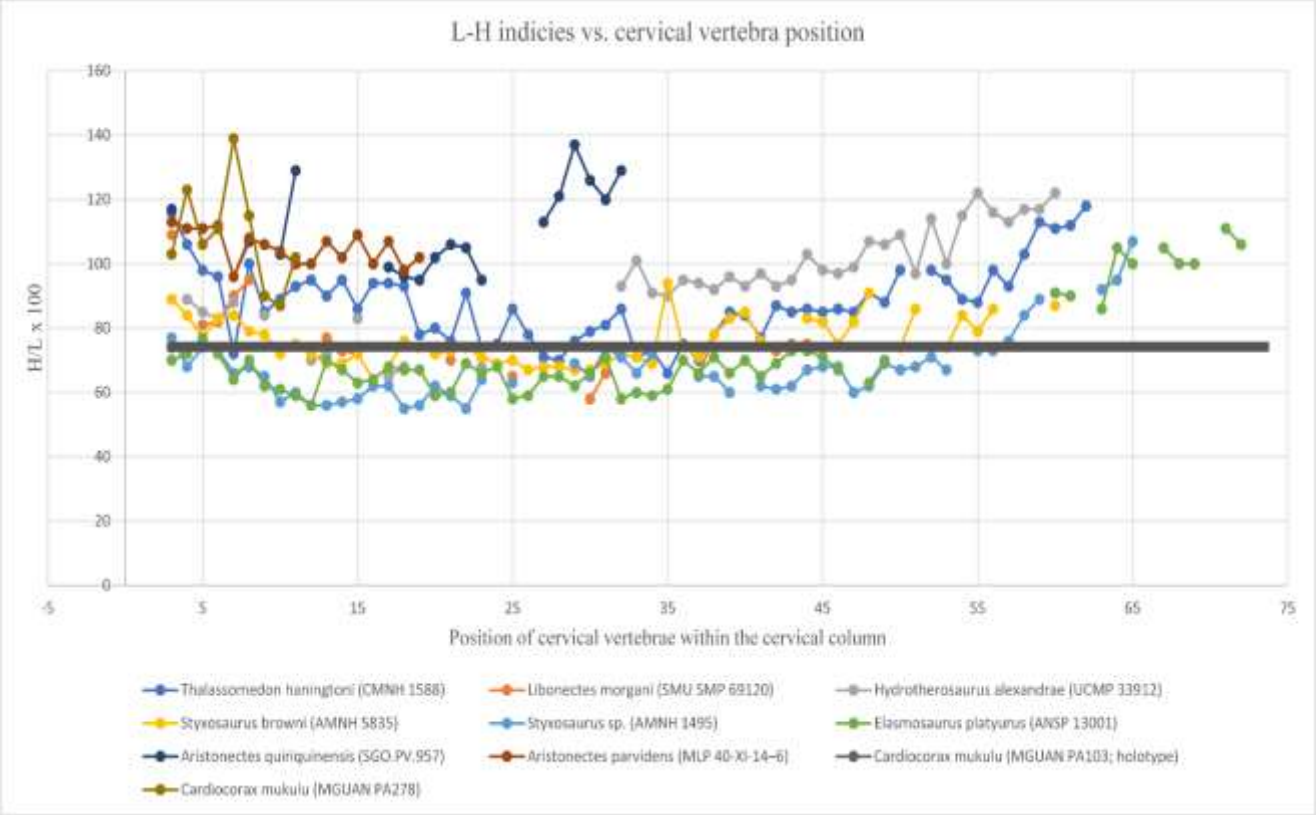

Figure 5.8.9.5. Above: Graph showing height indices (Welles, 1952) versus position within the cervical column. The horizontal grey bar represents the H index (calculated by dividing height of centrum by its length and then multiplying by 100) of the fifth cervical vertebra in the vertebrae series from MGUAN PA103 (height: 77.75 mm, length: 105.41 mm), which overlaps with middle cervical vertebrae from other '*Cimoliasaurus*'-grade elasmosaurids (*T. haningtoni*, *L. morgani*, and *H. alexandrae*), indicating that the cervical vertebra series from MGUAN PA103 is likely from the middle region of the cervical column and not the posterior end. Measurements of centra from *Styxosaurus* sp. (AMNH 1495) and *S. browni* come from Otero (2016); centra measurements of *T. haningtoni*, *L. morgani*, and *H. alexandrae* come from Welles (1943); dimensions of cervical centra of *E. platyurus* comes from Sachs (2005a); dimensions of cervical centra from *A. quiriquinensis* and *A. parvidens* come from Otero et al., (2014a) and O'Gorman (2015), respectively.

The morphology of the neural spines is difficult to assess as most are obscured by matrix. However, the anterior margin of the neural spine in several anterior cervical vertebrae is straight, and not sinusoidal, as in 'proximal cervical vertebra' 2 (Figure 5.8.5., 5.8.6., 5.8.7., and 5.8.9.3.). The neural spine of 'proximal cervical vertebra' 2 is mediolaterally compressed and 'blade-like' (figure 5.8.9.3.). The apex of the neural spine is flat, without evidence of any inclination along the dorsal margin. The anterior margin of the neural spine also presents a noticeable anterior projection that is smoothly convex in outline and transitions to a concave preaxial margin in lateral view near the base of the neural spine (figure 5.8.9.3.). The anterior projection seen in the mid-cervical vertebra of MGUAN PA278 (figure 5.8.9.3.)

would have extended even further than what is preserved, as the process is partly broken and worn along its anterior margin. The posterior margin of the neural spine in 'proximal cervical vertebra' 2 is damaged (figure 5.8.9.3.). Thus, MGUAN PA278 shares what Araújo et al., 2015a consider an autapomorphy with *C. mukulu*: an anterior projection of the neural spine. The cervical vertebra that exhibits these traits in MGUAN PA278 is located more anteriorly than in the 'posterior cervical vertebrae' of the holotype of *C. mukulu* (MGUAN PA103) based on the larger length and height dimensions of the centra from MGUAN PA103 (Figure 5.8.9.5.). The cervical vertebrae series of MGUAN PA103, despite being identified as 'posterior' cervical vertebrae in Araújo et al., (2015a) exhibit several traits that suggest a more anterior position, likely in the middle region of the cervical column. In terms of morphology, posterior cervical vertebrae in elasmosaurid plesiosaurians typically lack a lateral keel on the centrum, exhibit platycoelous articular facets, and lack the constriction circumscribing the articular facets of the centrum (Araújo et al., 2015b; Sato, 2002). Araújo et al., (2015a) describe the vertebrae in the preserved series with all three of the aforementioned traits but assign the vertebrae to the posterior region of the cervical column. The last cervical vertebra in the series from MGUAN PA103 exhibits a constriction around the articular rim of the posterior facet, and a clear lateral ridge (Figure 5.8.9.6.). The second cervical vertebra in the series also exposes a lateral ridge (figure 5.8.9.6.).

The height index (height/length x 100; Welles, 1943, O'Gorman, 2016) of the fifth cervical in the series of MGUAN PA103 (centrum length: 105.41mm; centrum height: 77.75 mm) is most consistent with a mid-cervical vertebra in other '*Cimoliosaurus*-grade' elasmosaurid taxa, such as *T. haningtoni*, *L. morgani*, and *H. alexandrae* (Otero, 2016) (Figure 5.8.9.5.). MGUAN PA278 and MGUAN PA103 exhibit cervical vertebrae that do not conform to the elongated 'can'-shaped vertebrae of Elasmosaurines (=Styxosaurines) that characterizes several western interior basin elasmosaurids (Otero, 2016). The taxa *T. ponteixensis*, *E. platyurus*, *A. vanderveldi*, *S. snowii*, *S. browni*, and AMNH 1495 (Styxosaurus sp.) all exhibit the elongated condition of the cervical vertebrae (Sato, 2003; Sachs, 2005; Kubo et al., 2012; Otero, 2016; M.M. pers. obs.). The dimensions of the centra in MGUAN PA278 and MGUAN PA103 are also distinguishable from the anteroposteriorly abbreviated condition of aristonectines (Araújo et al., 2015b). Rather, the height and length of the preserved cervical vertebrae in MGUAN PA278 and MGUAN PA103 are closer to being sub-equal ('*Cimoliosaurus* condition' in Otero, 2016) as in *L. morgani*, *H. alexandrae*, *T. haningtoni*, *F. suzukii*, and *C. colombiensis* (Welles, 1943; Welles, 1949; Welles, 1962; Sato et al., 2006).

Thus, the morphology of the exposed centra and the height index of the exposed fifth cervical vertebra from MGUAN PA103 places the vertebrae series of this specimen in the mid-cervical region of the cervical column. As in MGUAN PA278, these mid-cervical vertebrae exhibit neural spines with anterior projections near the apex of the neural spine. Thus, a functional definition for mid-cervical vertebrae in *C. mukulu* (MGUAN PA103 and MGUAN PA278) could be the presence of these projections on the neural spines.

'Proximal cervical vertebra' 3 in MGUAN PA278 exhibits lacks an articular rim around the exposed anterior articular facet, unlike the anterior cervical vertebrae and 'proximal cervical vertebrae' 1 and 2 (figure 5.8.9.4.). The anterior and posterior margins of the neural spine from 'proximal cervical vertebra' 3 are smoothly convex. The height and length of the centrum of 'proximal cervical vertebra' 3 are greater than that of 'proximal cervical vertebra' 1 and 2 and provide 'posterior cervical vertebra' 3 with an H index of 99 (Table 4). This would plot 'posterior cervical vertebra' 3 as a posterior-mid or posterior cervical vertebra for '*Cimoliasaurus*'-grade elasmosaurids (*T. haningtoni* and *H. alexandrae*). True posterior cervical vertebrae, with the lack of a lateral longitudinal keel at mid-height on the centrum, a lack of a ventral keel on the median central surface of the centra, platycoelous articular facets of the centra, and unfused cervical rib facets on the ventrolateral surface of the centra are exhibited in MGUAN PA271, another elasmosaurid plesiosaurian specimen from Bentiaba that is referable to *C. mukulu* (Williston, 1903; Carpenter, 1996; Sato, 2002; Sato, 2005; Kubo et al., 2012; Araújo et al., 2015b) (Figure 5.8.9.7.). Note that in this specimen, the anterior and posterior projections of the neural spines are no longer present. Rather, the anterior and posterior margins are straight (Figure 5.8.9.7.).

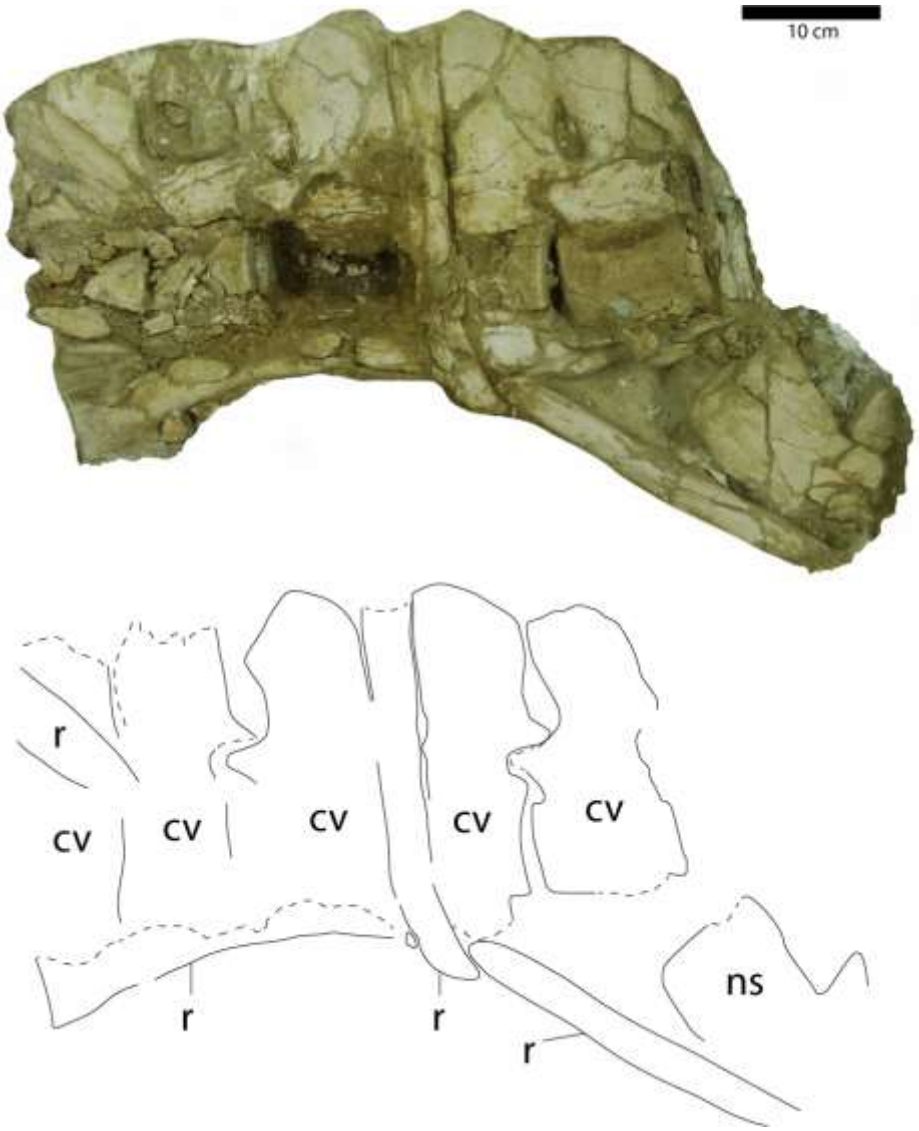

Figure 5.8.9.6. Middle cervical vertebrae series from the holotype of *C. mukulu* (MGUAN PA103).

Figure 5.8.9.7. Posterior cervical vertebrae from a fourth specimen of *C. mukulu* (MGUAN PA271) in left lateral view.

Ribs

In MGUAN PA278, two rib fragments are preserved and are slightly crushed. The body of a pectoral or dorsal rib is preserved although fragmented across three blocks (Figure 4.1.3. and 4.1.4.). A fragment from a second rib is also preserved (Figure 5.8.9.8.). The ribs appear to be compressed mediolaterally.

Figure 5.8.9.8. Rib fragment associated with *Cardiocorax mukulu* (MGUAN PA278).

Appendicular skeleton

Elements from the appendicular skeleton of MGUAN PA278 remain mostly unprepared. Descriptions are made where possible in the exposed elements. Appendicular bones are spread out onto three different blocks, with none of the elements in articulation, except for a set of seven phalanges in close association.

Propodial element

The propodial element of MGUAN PA278 is exposed in dorsal view, with the dorsal half of the proximal end caved in (Figure 5.9.1.). The head of the propodial is embedded in matrix is preserved, but the tuberculum is weathered away. Deposits of salt crystals line the exposed trabeculae of the caved-in tuberculum. The propodial is mostly covered in a calcareous residue on the external surface of the bone. No fracturing or distortion is observable across the exposed surface of the propodial. The propodial is oriented straight without an observable dorsal or ventral curvature. The transition from the proximal end of the propodial toward the distal end is constricted at the diapophysis. The preaxial and postaxial borders of the diapophysis are straight and sub-parallel but widen toward the distal end. The distal end of the propodial is substantially wider than the shaft and is covered along the dorsal surface by rugose, sub-parallel ridges. The ridges become smooth and flatten toward the diapophysis. The propodial is proximodistally short and robust, reflective of elasmosaurid affinities.

Figure 5.9.1. Dorsal view of propodial associated with *Cardiocorax mukulu* (MGUAN PA278).

Fibulare

A fibulare is identified from one of the preserved tarsal elements associated with MGUAN PA278 (Figure 5.9.2.). The element is slightly crushed dorsoventrally, with cracks running throughout the visible surface but is overall well preserved. The fibulare measures 67.0 mm along its proximodistal axis and is 50.8 mm in width across the proximodistal midsection. The texture of the exposed surface is smooth at the center but becomes more rugose near the margins. The fibulare is 28.5 mm thick along the exposed, non-crushed, proximal margin. Five discrete articular facets are observable: two along the proximal margin, one straight facet medially, and two on the distal margin. The lateral border is smoothly concave and would have contributed to part of the posterior margin of the paddle.

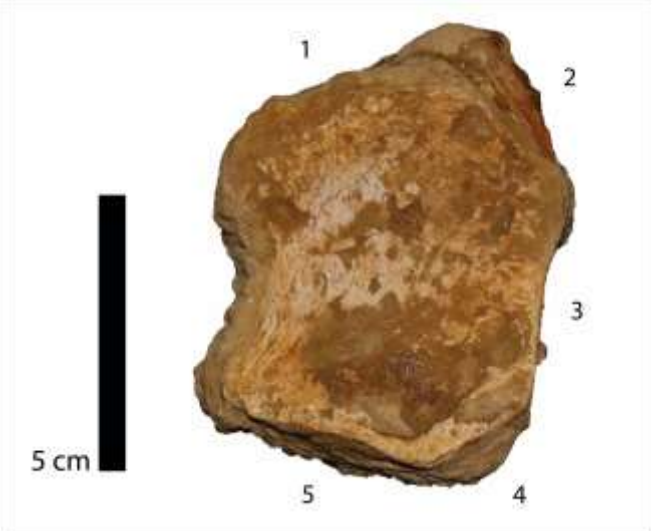

Figure 5.9.2. Fibulare of *C. mukulu* (MGUAN PA278) with number of facets indicated.

Distal tarsal element

A distal tarsal element remains joined to the ventral side of a cervical vertebra in MGUAN PA278 (Figure 5.9.3.). The element presents a rectangular outline in dorsoventral view, with sediment obscuring much of the surface. The exposed bone surface is rugose. Dorsoventrally, the element is thick and tapers toward its posterior margin.

Figure 5.9.3. Distal tarsal element of *C. mukulu* (MGUAN PA278) in dorsoventral view (top) and lateral view (bottom).

Phalanges

The phalanges exhibit the classic plesiosaurian spool shape with wide distal ends and a constricted mid-section (Figure 5.9.4.). There is a total of 33 phalanges associated with MGUAN PA278. The texture of the mid-section of the phalanges is smooth but the distal ends are rugose with low ridges of bone that run sub-parallel to each other. The distal and proximal articular facets of the phalanges are flat with no foramina present. The phalanges are slightly compressed along the dorsal-ventral axis. There is an association between seven phalanges that are in near articulation with each other, all other phalanges are scattered throughout the specimen blocks. Length and width dimensions of the exposed phalanges indicate a short and 'robust' morphology, where the proximodistal length is less than twice as long as the anteroposterior width (Benson & Druckenmiller, 2014).

Figure 5.9.4. Partly articulated phalanges of *C. mukulu* (MGUAN PA278). In the top right of the figure the phalanges have been replaced by carbonate.

Phylogenetic analysis

We utilize recent iterations of the Benson and Druckenmiller (2014) matrix (Sachs et al., 2015; Serratos et al., 2017; Allemand et al., 2017; Otero et al., 2018, and O'Gorman 2020) in this study to test the evolutionary relationship of MGUAN PA278 and the *C. mukulu* hypodigm (created from a composite of character scores from MGUAN PA278, MGUAN PA103, and MGUAN PA270) with other plesiosaurians . These matrices take into account elasmosaurid taxa from a broad stratigraphic range, new characters, and updated character scores for elasmosaurid taxa. The methodologies of Serratos et al., (2017), Otero et al., (2018), and O'Gorman (2020) were tested for replicability before adding MGUAN PA278 and the *C. mukulu* hypodigm.

When replicating the methodology of Serratos et al., (2017), differences in the resulting consensus trees in our analysis using TnT v.1.5 and that of Serratos et al., (2017) with PAUP*4.0b10 after pruning of wildcard taxa were evident. Serratos et al., (2017) ran a parsimony ratchet analysis (Nixon, 1999) with the software PAUP*4.0b10 (Swofford, 2010), implemented with PAUPRat (Sikes and Lewis, 2001). The ratchet analysis of Serratos et al., (2017) using PAUP*4.0b10 resulted in 95 MPTs (most parsimonious trees), a tree length of 1450, and the following statistics: CI: 0.2705, RI: 0.6839. After implementing ratchet analysis in TnT v.1.5 (Goloboff and Catalano, 2016), our analysis yielded 149 MPTs, length: 1449; CI: 0.274, RI: 0.684, and RCI: 0.187. Serratos et al., (2017) subsequently applied TBR branch swapping until more than 75,000 trees were recovered, and the resulting consensus tree produced a large unresolved polytomy formed by taxa from Leptocleidia and Elasmosauridae. The same result followed using TBR branch swapping in our analysis using TnT v.1.5. Serratos et al., (2017) identified wildcard taxa manually by observing the set of MPTs and running an Adams consensus. Wildcard taxa using TnT v.1.5 were identified with the command 'pcrprune' which indicated *E. australis*, *E. platyurus*, and *F. suzukii* as wildcard taxa at several different nodes. The same taxa were recovered by Serratos et al., (2017) as wildcard taxa. Pruning of *E. platyurus* and *F. suzukii* however resulted in differences between our strict reduced consensus tree topology and that of Serratos et al., (2017). In both our analysis and Serratos et al., (2017) pruning *E. australis* produced greater resolution, with Leptocledia being a distinct group from Elasmosauridae, and the Speeton clay plesiosaurian being the sister taxon to all other elasmoaurid plesiosaurians. Pruning of *E. platyurus* followed by *F. suzukii* further resolved elasmosaurid interrelationships by resolving the large polytomy to elucidate more inclusive clades of Elasmosaurinae and Aristonectinae in Serratos et al. (2017) (Figure 6.1.). However, in our analysis with TnT v.1.5 the large polytomy within Elasmosauridae persisted and is comprised of two clades: one formed by *A. parvidens*, *A. quiriquinensis*, *K. katiki*, a second clade formed by *N. bradti* (MOR 3072), '*Hydralmosaurus*' *serpentinus* (=*Styxosaurus* sp.), and *S. snowii*, with all other elasmosaurid

plesiosaurians forming a polytomy with these two clades; Speeton clay plesiosaurian, *W. betsynichollsae* and *C. colombiensis* were recovered as basal elasmosaurids (Figure 6.2.). A bremer index of 1 was recovered for Elasmosauridae in our analysis after removal of *E. platyurus*, *E. australis*, and *F. suzukii*.

Adding MGUAN PA278 to the matrix of Serratos et al., (2017) with ratchet analysis and TBR swapping and pruning of wildcard taxa *E. platyurus*, *E. australis*, and *F. suzukii* does not improve resolution within Elasmosauridae (99,999 MPTs, CI: 0.272, RI: 0.684, RCI: 0.186, length: 1461) (Figure 6.3.). The CI, RI, and RCI were calculated after keeping 10 MPTs (keep 10 command in TnT) because the high number of retained trees (99,999 MPTs) caused an error in calculation; this command was used for all subsequent analyses where the number of recovered MPTs made calculation of CI, RI, and RCI difficult. MGUAN PA278 joins a large polytomy with other elasmosaurid plesiosaurians, although *Z. oceanis* is recovered as the sister taxon to Aristonectinae, previously *Z. oceanis* was within the large polytomy of elasmosaurid plesiosaurians before the inclusion of MGUAN PA278, and *Gronausaurus wegneri* was recovered in a polytomy with Leptocleidia and Elasmosauridae. Bootstrap analysis returned a score of 12 for Elasmosauridae and 44 for the large polytomy of all elasmosaurid plesiosaurians other than, Speeton Clay plesiosaurian, *W. betsynichollsae*, and *C. colombiensis*. A bremer index of 3 was recovered for Elasmosauridae after pruning *E. platyurus*, *E. australis*, and *F. suzukii*. Adding the *C. mukulu* hypodigm does not significantly improve resolution in the consensus tree (99,999 MPTs, CI: 0.27, RI: 0.683, RCI: 0.185; length: 1469). Wildcard taxa *E. platyurus*, *E. australis*, and *F. suzukii* were pruned again. *T. ponteixensis* and *A. vanderveldi* form a clade within the large polytomy of elasmosaurid plesiosaurians, *L. atlasense* is recovered as the sister taxon of Elasmosaurinae, and surprisingly *Gronausaurus wegneri* (a Leptocleidian in the previous analysis) is recovered as a basal elasmosaurid. A bremer index of 3 was recovered for Elasmosauridae and the large polytomy containing *C. mukulu*; Elasmosauridae was recovered with a bootstrap value of 12, and the large elasmosaurid polytomy returned a bootstrap value of 42 (Figure 6.4.).

In replicating the methods of Otero et al., (2018), 38,999 trees were retained in our traditional search, and Otero et al., (2018) recovered over 5,000 MPTs (1,000 Wagner trees and 1,000 trees to save per replication). In the analysis of Otero et al., (2018), Speeton Clay Plesiosaurian and GWUU A3B2 are reported as wildcard taxa. However, Speeton Clay Plesiosaurian and GWWU A3B2 in our analysis were not recovered as wildcard taxa. Rather, 3 nodes are gained when pruning *E. carinognathus*, and 1 node is gained when pruning *A. zealandiensis*. Otero et al., (2018) removed Speeton Clay Plesiosaurian and GWUU A3B2 a priori before running further analyses. Removing taxa a priori because they are wildcard taxa does not necessarily improve a phylogeny to reflect real evolutionary relationships, as it is deleting data. To replicate the results of Otero et al., (2018), we were consistent with the methodology of the

authors by removing Speeton Clay Plesiosaurian and GWUU A3B2 a priori. When a traditional search was run with the remaining taxa (1,000 Wagner trees; 1,000 trees to save per replication) a large polytomy was recovered for Elasmosauridae that included a clade composed of Aristonectinae and Elasmosaurinae, a second clade composed of CM Zfr 115, *H. alexandrae*, and *F. suzukii*, with all other elasmosaurid taxa recovered within the polytomy (24,000 MPTs, CI: 0.276, RI: 0.676, RCI: 0.186, length: 1511) (Figure 6.5.) Our topology is in stark contrast to the more resolved results of Otero et al., (2018) (Figure 6.6.). Introducing MGUAN PA278 to the matrix only places this specimen within the large polytomy. Interestingly, the original matrix, before the removal of Speeton Clay Plesiosaurian and GWUU A3B2 recovered a topology that was nearly identical to Otero et al., (2018). The only differences being, in our analysis, the taxa GWWU A3 B2, Speeton Clay Plesiosaurian, *W. betsynichollsae*, *E. carinognathus*, and *C. colombiensis* form a polytomy along with a clade that includes the rest of Elasmosauridae, a polytomy is formed by *L. morgani*, a clade composed of *H. alexandrae* and *F. suzukii*, and a second clade including all other derived elasmosaurids, and lastly, CM Zfr 115 was recovered in our analysis as the sister taxon to Aristonectinae. We thus decided to test the phylogenetic relationship of MGUAN PA278 and the *C. mukulu* hypodigm with Speeton Clay Plesiosaurian and GWWU A3B2 included, as these taxa resolved some of the interrelationships in our analysis. Pruning "*E. carinognathus"* (*E. carinognathus* is a junior synonym of *E. australis*, although Otero et al., 2018 use *E. carinognathus* as their taxonomic unit) resulted in better resolution of basal elasmosaurids in the consensus tree, thus "*E. carinognathus"* was pruned in subsequent analyses with the Otero et al., (2018) matrix (Figure 6.7.).

The matrix of Otero et al., (2018) with the addition of MGUAN PA278 returns a consensus tree (45,000 MPTs) with MGUAN PA278 included in a polytomy formed by *T. haningtoni*, *T. keyesi*, *L. morgani*, a clade composed of *H. alexandrae* and *F. suzukii*, and a second clade that includes Elasmosaurinae and Aristonectinae (CI: 0.271, RI: 0.671, RCI: 0.182; length: 1537) (Figure 6.8.). A bremer index of 1 supports the clade Elasmosauridae. Bootstrap analysis provided a score of 16 for Elasmosauridae and 31 for the polytomy that includes MGUAN PA278. When the hypodigm of *C. mukulu* is added to the matrix of Otero et al., (2018), the taxon is returned as the sister taxon of *L. morgani* (23,000 MPTs, CI: 0.27, RI: 0.67, RCI: 0.181, length: 1546) (Figure 6.9.). Elasmosauridae is recovered with a bremer index of 1 and a bootstrap value of 11. The clade uniting *L. morgani* and *C. mukulu* recovered a bremer index of 1 and a bootstrap value of 17. Comparatively, Elasmosaurinae was recovered with a bootstrap value of 85 and a bremer index of 3, and Aristonectinae received a bootstrap value of 96, and a bremer index of 5. The clade formed by *L. morgani* and *C. mukulu* is supported by a unique combination of plesiomorphic and apomorphic character states from the matrix of Otero et al., (2018): ch.63.0, an absence of a notochordal pit on the occipital condyle; ch.80.1, basisphenoid (or

parabasisphenoid) does not contribute to the basioccipital; ch.122.0, retroarticular process of the mandible is oriented posterodorsally; ch.209.1, shape of anterior process of the coracoid is anteroposteriorly long and transversely narrow. These character states are widely dispersed throughout the taxa included in the matrix of Otero et al., (2018) (modified from Benson and Druckenmiller, 2014) with ch.63.0 being present in 10/38 scorable taxa, ch.80.1 being present in 9/24 scorable taxa, ch.122.0 being present in 37/53 scorable taxa, and ch.209.1 being present in 15/45 scorable taxa.

C. mukulu is diagnosed by a unique combination of plesiomorphies and apomorphies in the taxon matrix of Otero et al., (2018): ch.13.1, the alveolar margin of upper jaw in lateral view is undulating or 'scalloped'; ch.52.0, anterior extension of the parietal extends to the level of the temporal bar; ch.61.1, dorsal portion of the posterior margin of the squamosal is inflected abruptly anterodorsally; ch.98.0, the pterygoids form a loose, overlapping contact with the basicranium; ch.132.1, heterodont posterior premaxillary dentition, reduced distalmost alveolus; ch.136.1, an absence of enamel 'striations'; ch.165.1, the presence of a rounded median ventral keel on the cervical centra; ch.207.2, posterolateral cornua of the coracoid extend lateral to the glenoid. These characters however are also widely dispersed within different clades of Plesiosauria; ch.13.1 occurs in 23/61 scorable taxa, ch.52.0 occurs in 25/50 scorable taxa, ch.61.1 in 18/57 scorable taxa, ch.98.0 occurs in 7/39 scorable taxa, ch.132.1 in 15/54 scorable taxa, ch.136.1 in 50/63 scorable taxa, ch.165.1 in 8/72 scorable taxa, and ch.207.2 in 11/41 scorable taxa. This suggests a high degree of homoplasy in the characters used for diagnosis of *C. mukulu*. It appears that ch.98.0 may be a secondarily acquired plesiomorphic trait, as it is shared by the pistosaurids *Yunguisaurus liae*, *Pistosaurus*, and *Augustasaurus hagdorni*, along with aristonectines: *A. quiriquinensis*, *M. seymourensis*, and *A. zealandiensis*. The presence of this same character state in *C. mukulu* may suggest a secondary expression of this character state in Elasmosauridae. *C. mukulu* can be differentiated from all other elasmosaurid plesiosaurians in the taxon matrix of Otero et al., (2018) based on the lateral extension of the cornua of the coracoids beyond the glenoid of pectoral girdle (ch.207.2). The last character that can be reliably used to differentiate *C. mukulu* from nearly all other taxa of Elasmosauridae within the taxon dataset of Otero et al., (2018) is the anterior extension of the parietal until the temporal bar (Ch.52.0), which is present only in one other elasmosaurid (*C. colombiensis*). Examination of other elasmosaurid taxa via literature review and collection visits by M.M. suggests that character states ch.13.1, ch.61.1, ch.132.1, ch.136.1, and ch.165.2 may have been scored incorrectly by Otero et al., (2018) and this is reviewed in more detail within the discussion of this work.

The most recent elasmosaurid-focused dataset is that of O'Gorman (2020), with the highest number of elasmosaurid taxa used so far for any matrix (28 elasmosaurid plesiosaurians). Replicating the methodology of O'Gorman (2020) (traditional search) recovered the exact same topology as that of

O'Gorman (2020), along with the same statistical output (CI: 0.28, RI: 0.687). Our analysis yielded one less step in the length of the consensus tree (1516) and only 70 MPTs as opposed to 130 MPTs in O'Gorman (2020) (1,000 Wagner trees additive sequences). In our analysis we identified the elasmosaurid taxa MLP 99-XII 1-5 and *A. quiriquinensis* as wildcard taxa, while O'Gorman (2020) also recovered MLP 99-XII 1-5 as a wildcard taxon, in addition to *A. zealandensis*. Interestingly, inclusion of MGUAN PA278 or the *C. mukulu* hypodigm into the matrix of O'Gorman (2020) collapses the clade Cryptocledia. It should be noted that the bremer indicies for Elasmosauridae and Xenopsaria in the analysis of O'Gorman (2020) are 1 and 2, respectively. Thus, these two clades were unstable before including the new specimen of MGUAN PA278 or the hypodigm. Interestingly, Inclusion of our character scores for MGUAN PA103 (holotype of *C. mukulu*) recovered the specimen in a polytomy at the base of Elasmosauridae (Figure 6.9.1.). Thus, differences reflected in the character scores for MGUAN PA103 are resulting in a basal placement for this specimen of *C. mukulu.*

Evaluation of character scores, their taxonomic distribution, and importance concerning the diagnosis of *C. mukulu* and the clade of *C. mukulu* and *L. morgani* is attempted for data sets that provide resolution. Data sets that resulted in large polytomies and unclear phylogenetic affinities for *C. mukulu* were not evaluated for their character scores. Additionally, running a phylogenetic analysis using the matrix of Otero et al., (2018) with MGUAN PA278 and MGUAN PA103 as separate terminal taxa results in a large polytomy at the base of Elasmosauridae: (MGUAN PA103, MGUAN PA278, *T. keyesi*, *T. haningtoni*, *L. morgani*, (*H. alexandrae*, *F. suzukii*), (Elasmosaurinae, Aristonectinae)). The only characters that MGUAN PA278 and MGUAN PA103 share are those in the cervical vertebrae, thus there are few diagnostic characters available that could unite these two specimens into a single clade. Additionally, the characters in the cervical vertebrae of MGUAN PA278 and MGUAN PA103 are widely distributed within elasmosaurid plesiosaurians.

Introducing the hypodigm of *C. mukulu* into the matrix of Sachs et al., (2015) (an iteration from the matrix of Benson and Druckenmiller, 2014) which included revised character scores for *L. morgani*, recovered *C. mukulu* again as the sister taxon to *L. morgani* after running a traditional search with TBR swapping (1,000 Wagner trees; 1,000 trees saver per replication; 46,000 MPTs, CI: 0.290, RI: 0.656, RCI: 0.190, length: 1,351) (Figure 6.9.2.). Sachs et al., (2015) utilized a ratchet analysis in PAUP*4.0b10 with the random number of seed set to 'seed = 0' and 'wtmode = uniform'; ratchet implementation by Sachs et al., (2015) underwent 200 iterations followed by a heuristic search. To just test the relationship of *C. mukulu* to other elasmosaurids plesiosaurians in the Sachs et al., (2015) matrix, we applied a traditional search with TBR swapping. The clade formed by *C. mukulu* and *L. morgani* returned a bremer index of 1, and was united by combination of three characters: Ch.92.0 (pterygoids do not separate vomers along

midline), Ch.133.1 (maxillary dentition is heterodont), and Ch.165.1 (median ventral surface of cervical vertebrae bears a rounded midline ridge). These characters are widely dispersed within Elasmosauridae.

The possible evolutionary relationship between *C. mukulu* and *L. morgani* was tested again by including the *C. mukulu* hypodigm into the matrix of Allemand et al., (2017), which included three OTUs diagnosed as *Libonectes*: the holotype of *L. morgani* (SMU SMP 69120), *L. atlasense* (SMNK-PAL 3978), and a third OTU diagnosed as *L. morgani* by Allemand et al., (2017), SMNS 81783. The *C. mukulu* hypodigm was returned in a polytomy along with the three *Libonectes* OTUs (49,000 MPTs, CI: 0.286, RI: 0.659, RCI: 0.188, length: 1,370) (Figure 6.9.3.). The polytomy formed by the three *Libonectes* OTUs and the *C. mukulu* hypodigm returned a bremer index of 1 and a bootstrap value of 13; Elasmosauridae returned a bremer index of 1 and a bootstrap value of 8. The presence of heterodont maxillary dentition ch.133.1 (Benson and Druckenmiller, 2014) is the single synapomorphy supporting the association between the *Libonectes* OTUs and *C. mukulu*. This character is however widespread throughout Elasmosauridae and is not reliable for diagnosis.

A new character is added to the parent matrix of Benson and Druckenmiller, 2014: ch.271; basisphenoid/ parabasisphenoid, length of sella turcica is equal or subequal to its width (0); length of sella turcica is at least 1.5x longer than its width (1). *C. mukulu* and *L. morgani* both share the derived character state where the sella turcica is at least 1.5x as long as its width. All other plesiosaurians, including aristonectine elasmosaurid plesiosaurians, exhibit a sella turcica with a width approximately equal to its length. Few taxa can be scored for this character, and the addition of the new character to the matrix of Otero et al., (2018) does not change the topology of the consensus tree from that of the addition of the hypodigm of *C. mukulu* (Figure 6.9.).

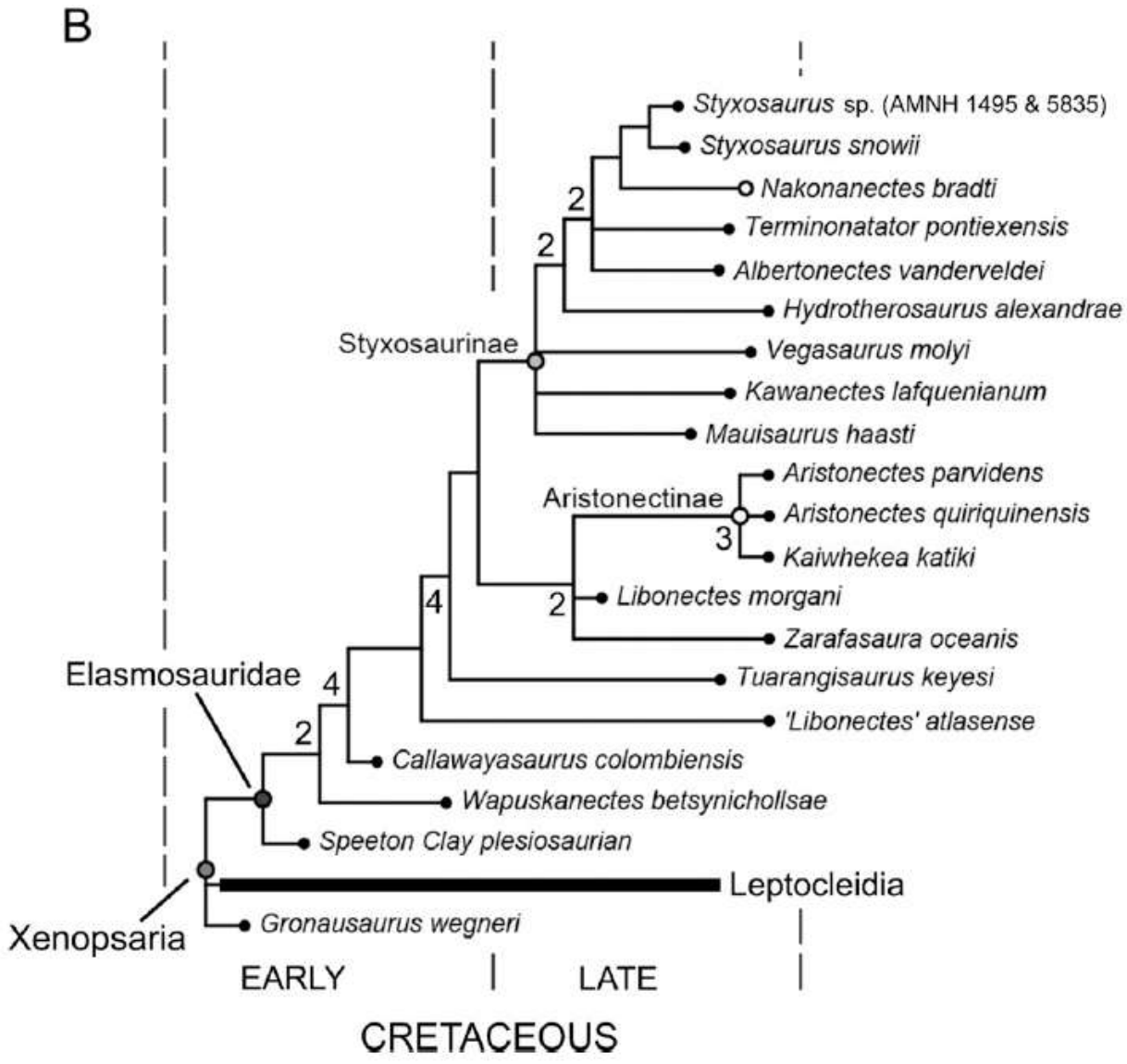

Figure 6.1. The phylogeny produced by Serratos et al., (2017) after removal of 'wildcard' taxa. Figure 15B from Serratos et al., (2017).

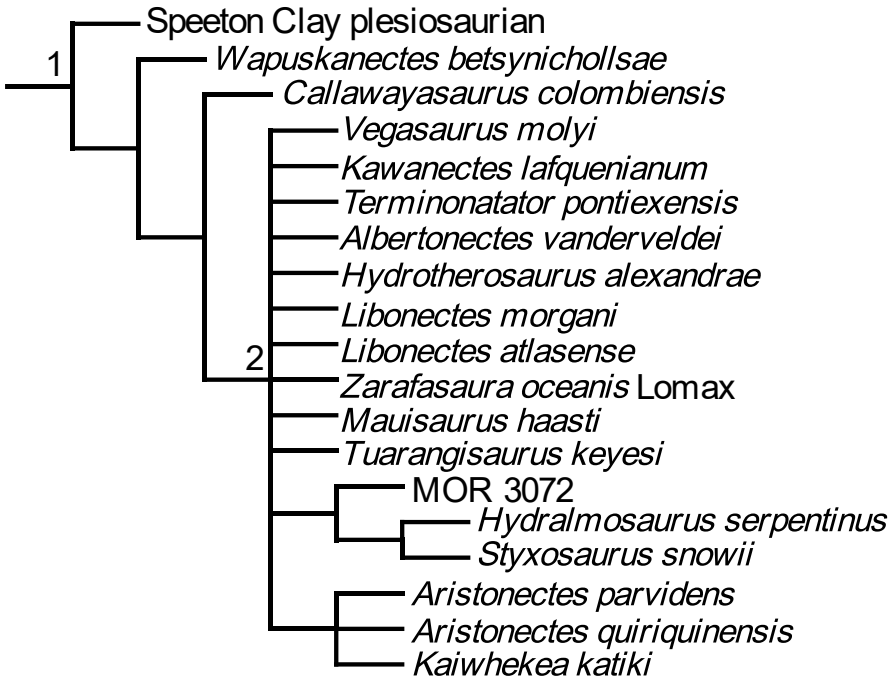

Figure 6.2. Consensus tree from matrix of Serratos et al., (2017) after replicating methodology.

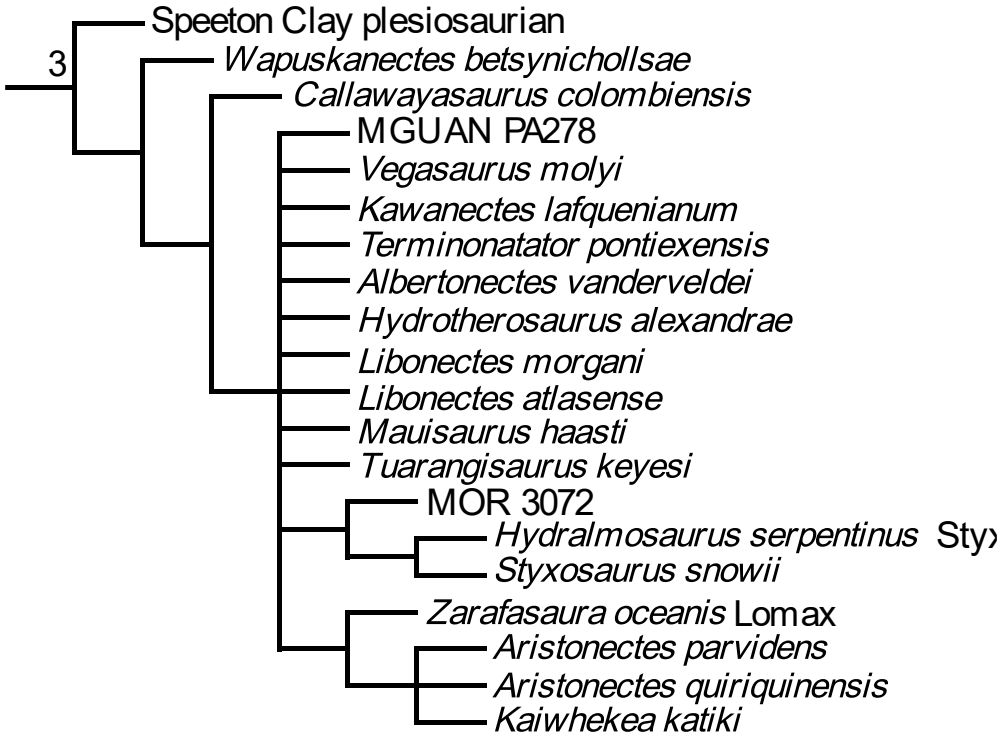

Figure 6.3. Consensus tree of matrix from Serratos et al., (2017) with MGUAN PA278 included.

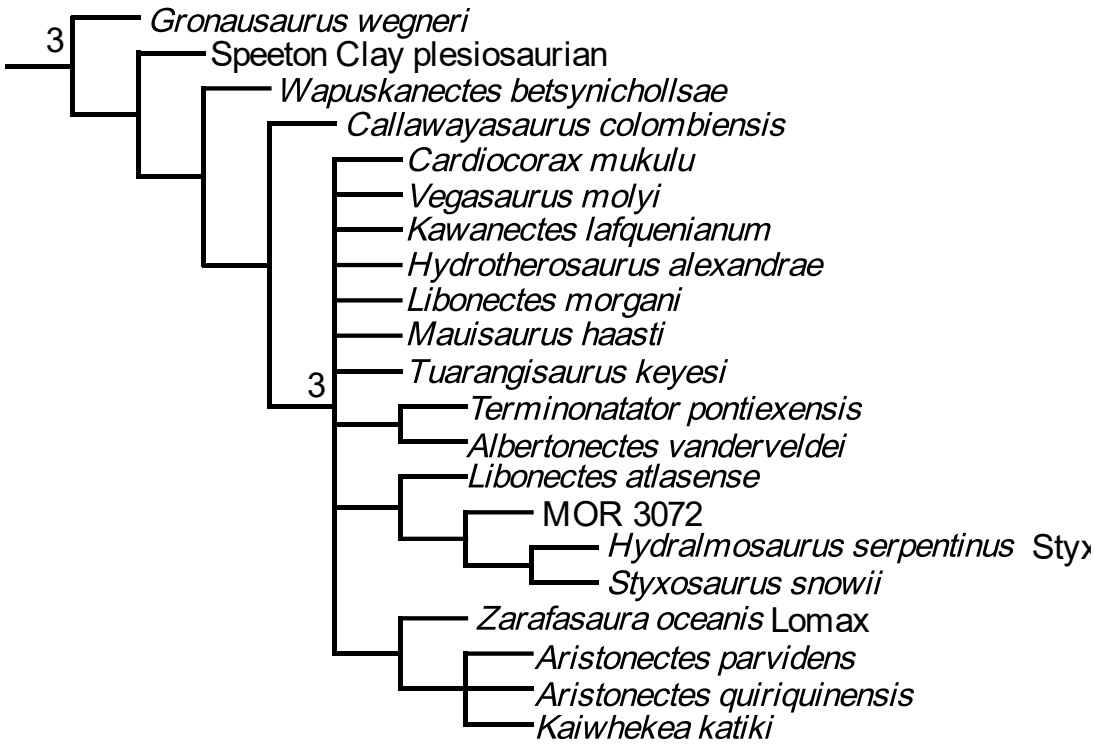

Figure 6.4. Consensus tree of matrix from Serratos et al., (2017) with the *C. mukulu* hypodigm.

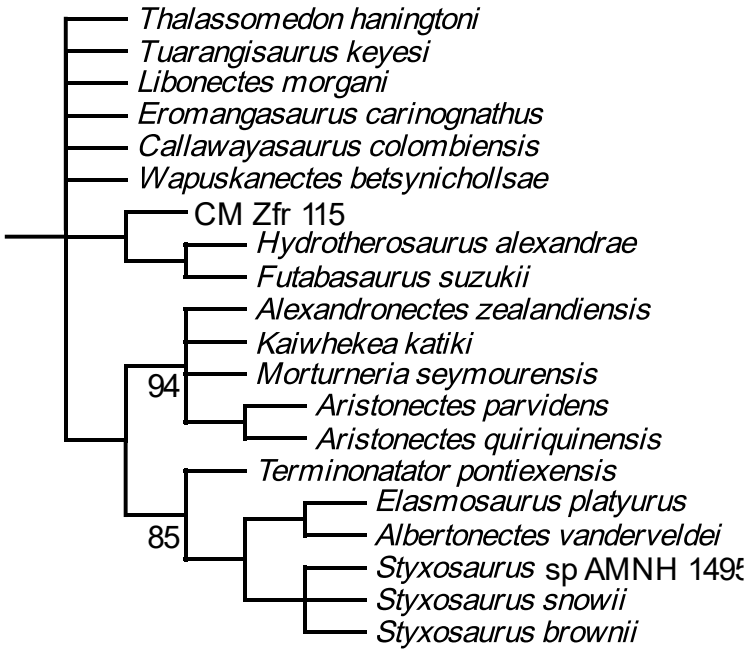

Figure 6.5. Replicated consensus tree of matrix from Otero et al., (2018). There was an error in bremer calculation.

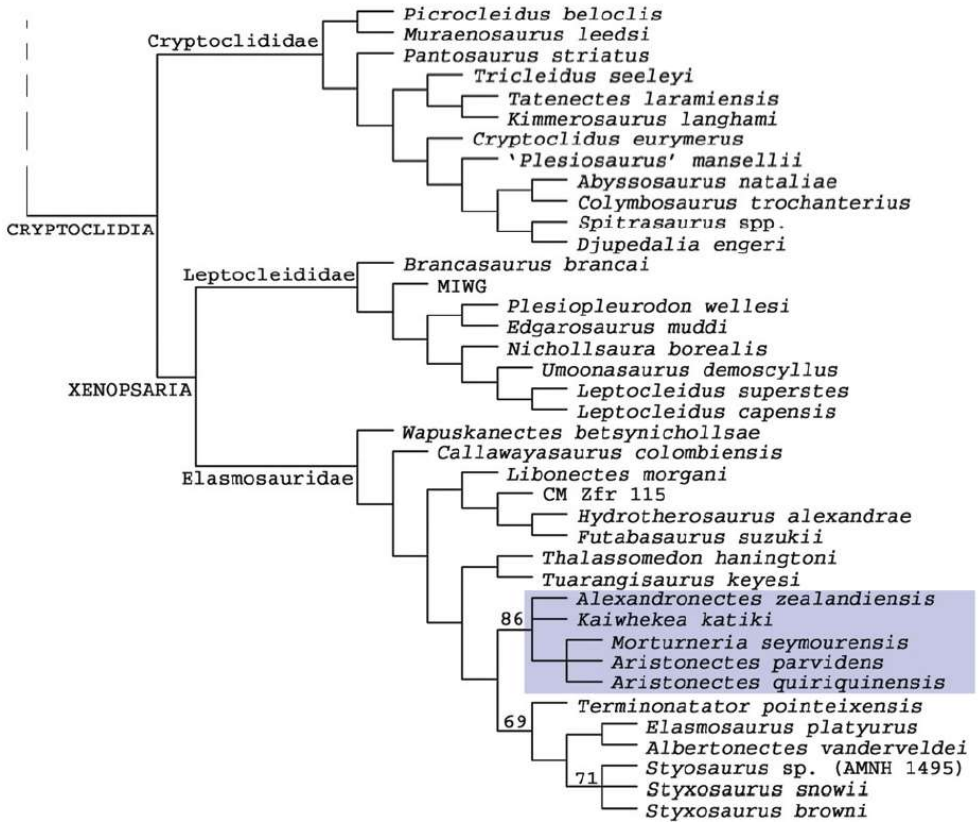

Figure 6.6. Consensus tree of matrix from Otero et al., (2018) (Figure 12).

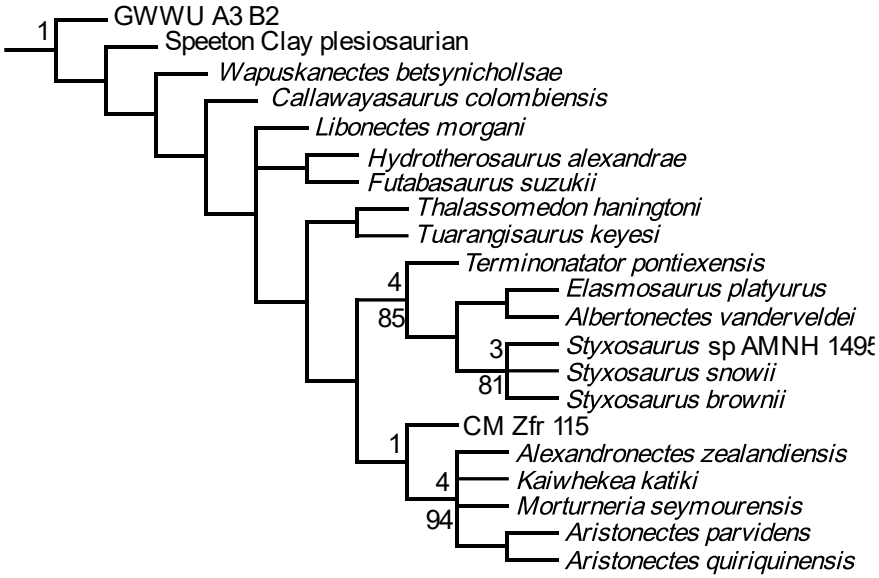

Figure 6.7. Consensus tree of matrix from Otero et al., (2018) with *E. carinognathus* pruned.

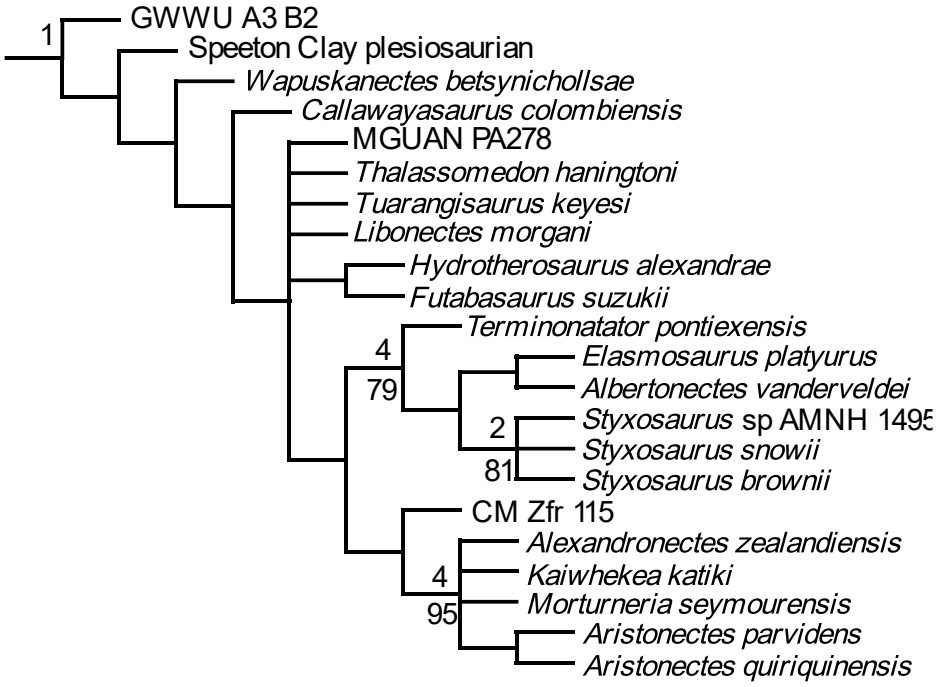

Figure 6.8. Consensus tree of matrix from Otero et al., (2018) with MGUAN PA278.

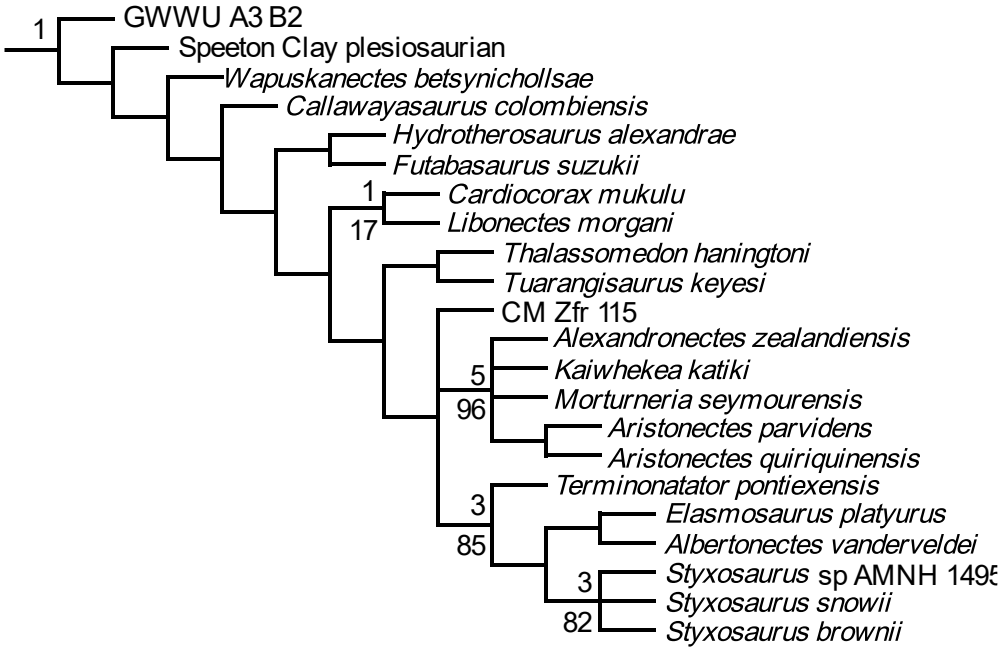

Figure 6.9. Consensus tree of matrix from Otero et al., (2018) with *C. mukulu* hypodigm included.

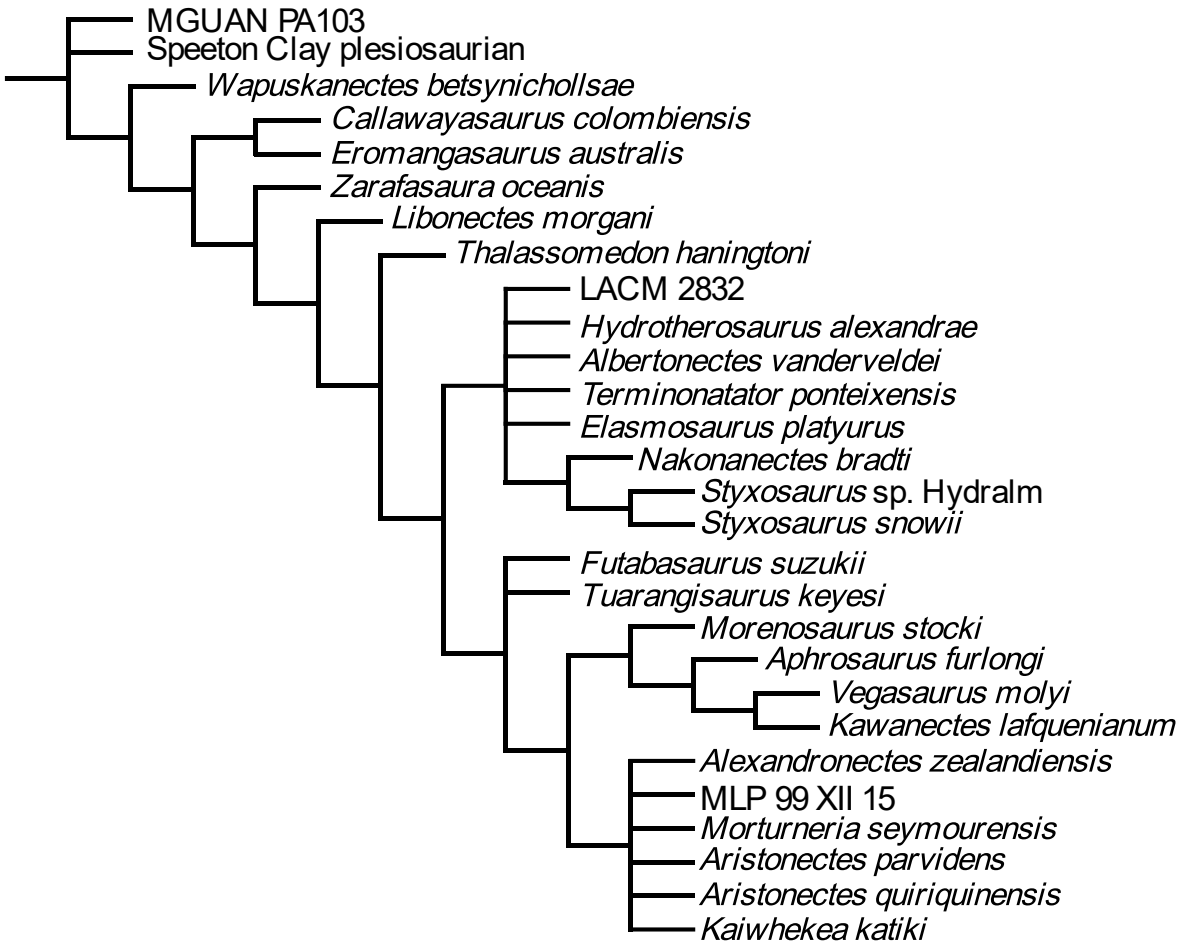

Figure 6.9.1. Consensus tree of matrix from O'Gorman (2020) with MGUAN PA103 included. An error from converting the NEXUS file of the matrix from O'Gorman (2020) to a TNT file prevented calculation of bremer indices. All bootstrap values were <50.

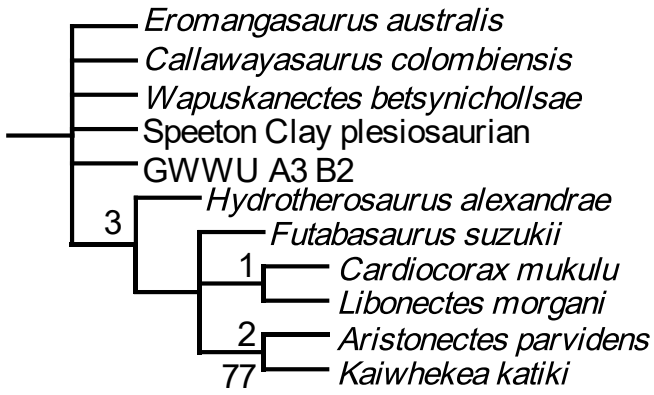

Figure 6.9.2. Consensus tree of matrix from Sachs et al., (2015) with *C. mukulu* hypodigm included.

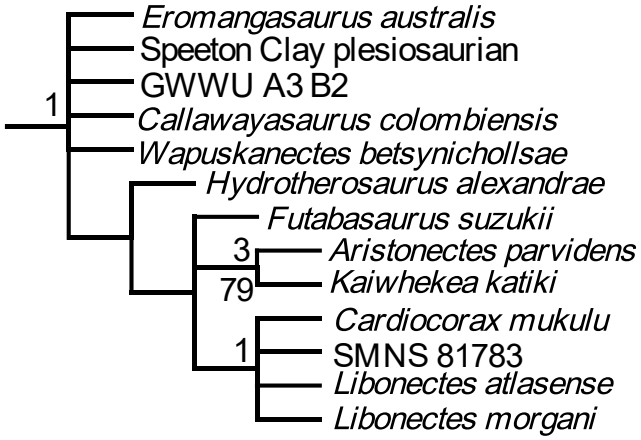

Figure 6.9.3. Consensus tree of matrix from Allemand et al., (2017) with *C. mukulu* hypodigm included.

Discussion

Amended diagnosis of *Cardiocorax mukulu* with comments on MGAUN PA103

MGUAN PA278 exhibits a suite of traits that make its diagnosis to Elasmosauidae unequivocal. Unambiguous characters diagnosing MGUAN PA278 to Elasmosauridae include: lateral ridge on anterior cervical vertebrae (Druckenmiller & Russel, 2008; Ketchum & Benson, 2010), closed pineal foramen (Ketchum & Benson, 2010), premaxilla excluded from border of internal nares (O'Keefe, 2001), vomer extends posterior to internal nares (O'Keefe, 2001), number of cervical rib heads reduced to one (O'Keefe, 2001); combined width of cervical zygapophyses distinctly narrower than centrum (Druckenmiller & Russel, 2008; Otero, 2016); absence of anterior interpterygoid vacuity (Vincent et al., 2011), a massive femur (Kubo et al., 2012), and cervical vertebrae with a ventral notch giving the cervical vertebrae a bilobed articular facet (Otero, 2016).

MGUAN PA278 shares with the holotype of *C. mukulu* (MGUAN PA103) a single apomorphy: cervical neural spines nearly touch its adjacent neural spines. This character state is designated to the 'posterior' cervical vertebrae of MGUAN PA103 in Araújo et al., (2015a), however, as demonstrated in figure 5.8.9.5. and mentioned in the description of MGUAN PA278, the cervical series of MGUAN PA103 is likely from the mid-cervical region and not the posterior end. The morphological condition of the neural spines that allows for near contact between adjacent neural spines is derived from anterior and posterior projections along the anterior and posterior margins of the neural spines. Araújo et al., (2015a) state that a posterior projection of the neural spine is shared between *C. mukulu* and *C. colombiensis*, however the anterior projection of the neural spine is autapomorphic for *C. mukulu*. Thus, a more appropriate wording for this character state follows: middle cervical neural spines exhibit a sinusoidal outline along the anterior margin in lateral view. *Kaiwhekea katiki* also exhibits a sinusoidal outline along the anterior margin of the cervical neural spines (Cruickshank and Fordyce, 2002; O'Gorman, 2020 supp. material.). Thus, this character is not considered an autapomorphy in this work. *C. mukulu* and *K. katiki* are however readily distinguishable by characters in the cranium (ex. tooth count).

Araújo et al., (2015a) mention an angled apex of the 'posterior' cervical vertebrae as another autapomorphy for *C. mukulu*. Close inspection of the cervical vertebra series shows considerable damage along the apices of the neural spines, altering its morphology (Figure 5.8.9.6.). The dorsal inclination of the dorsal border in the 'posterior' cervical vertebrae may have been the result of fracturing along the margins of the neural spines. Secondly, there is a well-preserved neural spine offset from the cervical series in figure 2 of Araújo et al., (2015a) that exhibits a dorsal margin that is flat and not inclined. This better-preserved neural spine may be more representative of the natural condition of the neural spines

before breakage. Thus, an angled apex of the cervical vertebrae is considered dubious and is not included in the revised diagnosis of *C. mukulu*.

Araújo et al., (2015a) state as another autapomorphy for *C. mukulu*: "transversely broad neural spines: length of base of neural spines slightly smaller to centrum length". This statement seems to be confusing transversal width for anteroposterior length. The neural spines of the cervical vertebrae in MGUAN PA103 seem to be more blade-like and exhibit a broad anteroposterior base that is nearly equal in length to the centrum. Mid-cervical neural spines with a base nearly equal to the length of the centrum is observable in other elasmosaurid plesiosaurians (*Styxosaurus* sp. (AMNH 1495), *S. snowii* (KUVP 1301), *T. haningtoni*) (Otero, 2016; Sachs et al., 2018; M.M. pers. obs.). The width of the neural arch relative to the width of the centrum is difficult to determine in MGUAN PA103, given the current state of the specimen. A middle cervical vertebra preserved with MGUAN PA278 exhibits a mediolaterally compressed neural spine. Thus, the above mentioned autapomorphy from Araújo et al., (2015a) is not included in the revised diagnosis.

The anterior cervical vertebra associated with MGUAN PA103 is morphologically indiscriminate from the anterior cervical vertebrae of MGUAN PA278. In both specimens, the anterior cervical vertebrae are amphicoelous to sub-amphicoelous and exhibit a thickened articular rim constricted by a shallow depression. The articular facets are binocular in outline, and a prominent ventral keel is situated between oval foramina subcentralia, located within concavities on the ventral surface. The neural arch of the anterior cervical vertebra of MGUAN PA103 is not preserved. Another specimen diagnosed as *C. mukulu*, MGUAN PA270 (figure 11 of Mateus et al., 2012), preserves a femur that is also morphologically indiscriminate from what is visible in MGUAN PA278. The shared autapomorphy between MGUAN PA278 and the holotype of *C. mukulu* (MGUAN PA103) in addition to the morphological overlap between the two specimens strongly suggests that MGUAN PA278 is diagnosable to the taxon, *Cardiocorax mukulu* Araújo et al., (2015a). With the addition of a specimen that includes a nearly complete cranium, new characters with taxonomic utility can distinguish *C. mukulu* from other elasmosaurid plesiosaurians.

Cranial elements contributing to the formation of the orbit are of diagnostic value and may differentiate between different species within Elasmosauridae. This same conclusion was noted by O'Keefe (2001) more broadly for differentiating taxa within Plesiosauria and O'Gorman et al., 2017b (table 1 in O'Gorman et al., 2017b) for elasmosaurid plesiosaurians. *T. haningtoni* may be diagnosable by the lack of contact between the prefrontal and the external nares, and *S. snowii* may be diagnosable by the absence of a maxillary bar in lateral view (Figure 5.2.8. and 5.2.9.1.). In MGUAN PA278, the maxilla forms a broad ventral, anteroventral and anterior margin for the orbit. The most conspicuous feature of the

maxilla is a semi-vertical ramus that significantly contributes to the anterior margin of the orbit. This high bar formed by the maxilla is immediately distinguishable from *T. haningtoni*, which presents a maxilla with a very low dorsal process, and *S. snowii* with essentially no maxillary bar. The maxillary bar of MGUAN PA287 is similar to that of *L. morgani* (SMU SMP 69120), *L. atlasense* (the dorsal bar of the maxilla in the Moroccan *L. morgani*, SMNS 81783, is difficult to distinguish), *N. bradti*, and *T. keyesi* (Sachs and Kear, 2017; Serratos et al., 2017; O'Gorman et al., 2017b). The maxillary bar of *S. browni* is difficult to assess without a detailed description of the cranium but appears to be shorter than the maxillary bar of MGUAN PA278. Sato (2003) does not identify any contribution from the maxilla onto the preorbital bar in *T. ponteixensis*. *K. katiki* is distinct from all known elasmosauirds in possessing exceptionally high and slender maxillary bars, strongly curved posterodorsally (Cruickshank and Fordyce, 2002). The contribution of the maxilla to the preorbital bar in *E. australis* and *C. colombiensis* is difficult to assess due to crushing (Welles, 1962; Kear, 2005a; M.M. pers. obs.).

The overall number of canals piercing the exoccipital-opisthotic may be informative taxonomically. It is curious however that the number of nerve canals piercing the braincase of three different *L. morgani* specimens (SMU SMP 69120, SMNS 81783, and D1-8213) all vary (Carpenter, 1997; Allemand et al., 2017; Allemand et al., 2018). The taxonomic implications of this for the referred *L. morgani* specimens will not be commented on here, however the number of cranial nerve openings for any given species should be consistent, aside from occasional instances of asymmetry (Chatterjee and Small, 1989). Reporting a different number of cranial nerve openings in the exoccipital-opisthotic for different specimens of the same species (*L. morgani*) may indicate an interpretational error. MGUAN PA278 exhibits three clear openings on the lateral and medial side of the exoccipital-opisthotic, one for the jugular canal (IX-XI) and two for the hypoglossal nerves (XII). It should be noted that due to the rareness of elasmosaurid basicrania, the number of cranial canals that diagnose any given taxon, may prove to be more widespread in other species, with new discoveries. Thus, three cranial nerve openings in the exoccipital-opisthotic is a tentative diagnosis for the elasmosaurid, *C. mukulu*.

Tooth count has been used to distinguish elasmosaurid taxa (*E. platyurus*, *S. snowi*, *T. ponteixensis*, *A. parvidens*, *T. keyesi*, *K. katiki*, *E. australis*) (Sachs, 2005a; Sachs et al., 2018; Sato, 2003; Gasparini, 2003; O'Gorman et al., 2017b; Cruickshank & Fordyce, 2002; Kear, 2005). MGUAN PA278 unambiguously possesses five premaxillary alveoli, as is common in elasmosaurid plesiosaurians, 17 maxillary alveoli, and at least 20 dentary alveoli. *L. morgani* (SMU SMP 69120) possesses 14 in the right maxilla and 13 in the left maxilla, with 18 alveoli in both rami of the mandible; 15 alveoli are present in the left maxilla of SMNS 81783 (*L. morgani*), with approximately 16 alveoli in the dentary; 18 alveoli are present in the left dentary of D1-8213 (*L. morgani*) (Carpenter, 1997; Allemand et al., 2017; Allemand et

al., 2018; M.M. pers. obs.). *L. atlasense* provides a count of 14 maxillary alveoli, with 16 alveoli on the right dentary and 15 on the left dentary, according to Sachs & Kear (2017). Although, Buchy (2005) counted 17 alveoli on the right dentary and 16 on the left for *L. atlasense*. A maxillary tooth count for *S. snowii, S. browni*, and *T. haningtoni* is ambiguous due to the state of preservation. It is likely that the exact alveoli count of *S. snowii* is more than reported counts (15 from Otero, 2016, 10 from Sachs et al., 2018, and at least 15 from M.M. pers obs.). The upper tooth row is partly obscured by the dentition from the lower tooth row in *S. snowii* and it is likely that the true number of maxillary alveoli cannot be discerned without a CT scan. 15 discernable complete and fragmented maxillary teeth, in addition to obscured alveoli in the upper tooth row, would provide *S. snowii* with a similar tooth count to MGUAN PA278 (17). In *T. haningtoni* (UNSM 50132) most of the maxillary alveoli are obscured by overlap of the dentary. 17 dentary teeth are observable in the left (less obscured) dentary of *S. snowii*, with 16 observable dentary teeth on the right side (Sachs et al., (2018) count 18 on the left dentary), 18 in the left dentary of *T. haningtoni* (UNSM 50132) (only observable side), while *S. browni* possesses an indiscernible number of dentary teeth (figure 7 of Otero, 2016). *N. bradti* exhibits 14 teeth in the maxillae and 19 alveoli on the left dentary and 18 on the right (Serratos et al., 2017). The tooth counts of *A. parvidens* and *A. quiriquinensis* are particularly high amongst elasmosaurids (at least 50 in the dentaries of *A. quiriquinensis* and at least 50 maxillary teeth, 13 premaxillary teeth, and 65 dentary alveoli in *A. parvidens*) (Gasparini, 2003; Otero et al., 2014; O'Gorman, 2015).

Obscured upper and lower tooth rows, intraspecific variation, and a varying number of teeth between the left and right maxillae and dentaries in the same individual (SMU SMP 69120) may render maxillary and dentary tooth count an unreliable autapomorphy for most elasmosaurid taxa. Aristonectine elasmosaurids are unique in having a particularly high tooth count relative to other elasmosaurids (50 or more alveoli). However, having a definitive number of upper and lower tooth row alveoli is rare given the preservation quality of most elasmosaurid crania and mandibles, and the number of maxillary and dentary teeth in *C. mukulu* (MGUAN PA278) can distinguishes it from several elasmosaurid taxa. MGUAN PA278 and *T. keyesi* may share the exact same number of premaxillary, maxillary and dentary alveoli (O'Gorman et al., 2017b). O'Gorman et al., (2017b) reports five premaxillary alveoli, an estimate of 17 maxillary alveoli and an unambiguous count of 21 alveoli on the dentary.

In view of the palate, *C. mukulu* exhibits internal nares that create an ellipsoidal outline in palatal view. The internal nares are formed by the vomer anteriorly and medially, the maxilla laterally, with a small contribution from the palatine posteriorly. The internal nares in most known elasmosaurid plesiosaurians is tear-drop shaped, with a pinched anterior margin and a more rounded posterior margin. In *C. mukulu*, the internal nares form near perfect ovals, with well-rounded anterior and posterior

margins. The internal nares of *Z. oceanis* are difficult to assess due to taphonomic distortion, and *T. ponteixensis* may also exhibit internal nares with an ellipsoidal shape (Sato, 2003; Vincent et al., 2011). The morphology of the internal nares in *T. keyesi* are ambiguous, as are the elements that contribute to its formation (O'Gorman et al., 2017b).

The absence of medial contact between the pterygoids ventral to the basioccipital is distinct from all other elasmosaurids, except for those within Aristonectinae. In MGUAN PA278 the pterygoids remain separated, with the long ventral keel of the parasphenoid extending onto almost the posterior margin of the basioccipital. This condition is in stark contrast to *L. morgani* (SMU SMP 69120 & D1-8213; the posterior extent of the pterygoids in SMNS 81783 is damaged), and *C. colombiensis* which exhibit a medial pterygoid symphysis posterior to the interpterygoid vacuity. The lack of contact between the pterygoids in *C. mukulu* is convergent with aristonectines (*A. zealandensis*, *A. quiriquinensis*, and *M. seymourensis*). Otero et al., (2016) report the lack of a pterygoid symphysis as a possible synapomorphy for these Weddelian Province taxa, but this character is also present in *C. mukulu*, a non-arsitonectine elasmosaurid. The palate area of elasmosaurid plesioaurians is rarely unobscured or well-preserved, making comparative studies of this area challenging.

A character that was revealed by the phylogenetic analyses incorporating *C. mukulu* with the matrix of Otero (2016) and Otero et al., (2018) that is useful for diagnosis concerns the lateral extension of the cornua of the coracoids extending beyond the glenoid of the pectoral girdle. This apomorphy is also shared with *C. colombiensis*, *Aphrosaurus furlongi* Welles, 1943, and *Alzadasaurus pembertoni* Welles and Bump 1949 (SDSM 451; synonymized to *S. snowii* by Carpenter, 1999).

Regarding the holotype of *C. mukulu* (MGUAN PA103), this specimen was redescribed, with two notable differences regarding the pectoral girdle from the original description (Araújo et al., 2015a). In view of the pectoral girdle, the interclavicle is identified as being directly adjacent to the clavicle by Araújo et al., (2015a). Close examination of the interclavicle and clavicle contact margin identified a more extensive contact between these two elements, with the interclavicle forming a more extensive anterior contact with the clavicle than what is figured in figure 3 of Araújo et al., (2015a) (figure 7.1.). A second feature of the pectoral girdle from MGUAN PA103 concerns the inferred presence of a median pectoral bar by Araújo et al., (2015a). In figure 3A of Araújo et al., (2015a) the scapula is not rotated to its natural position. However, rotation of this element does not complete a pectoral bar (Figure 7.2.). There also appears to be no articular facets on the preglenoid projections of the coracoids, or on the posterior projections of the scapula. This changes the character scoring for the presence of this feature in the matrix of Benson & Druckenmiller (2014). Almost all autapomorphic characters from the pectoral girdle, as first described from Araújo et al., 2015a, were retained as these characters are distinguishable

from other elasmosaurid taxa. The medial contact between the entire medial margins of the clavicles in *C. mukulu* (MGUAN PA103) may also be shared with *C. colombiensis*. Thus, complete median contact between the clavicles was designated in this work as a shared derived character in the diagnosis.

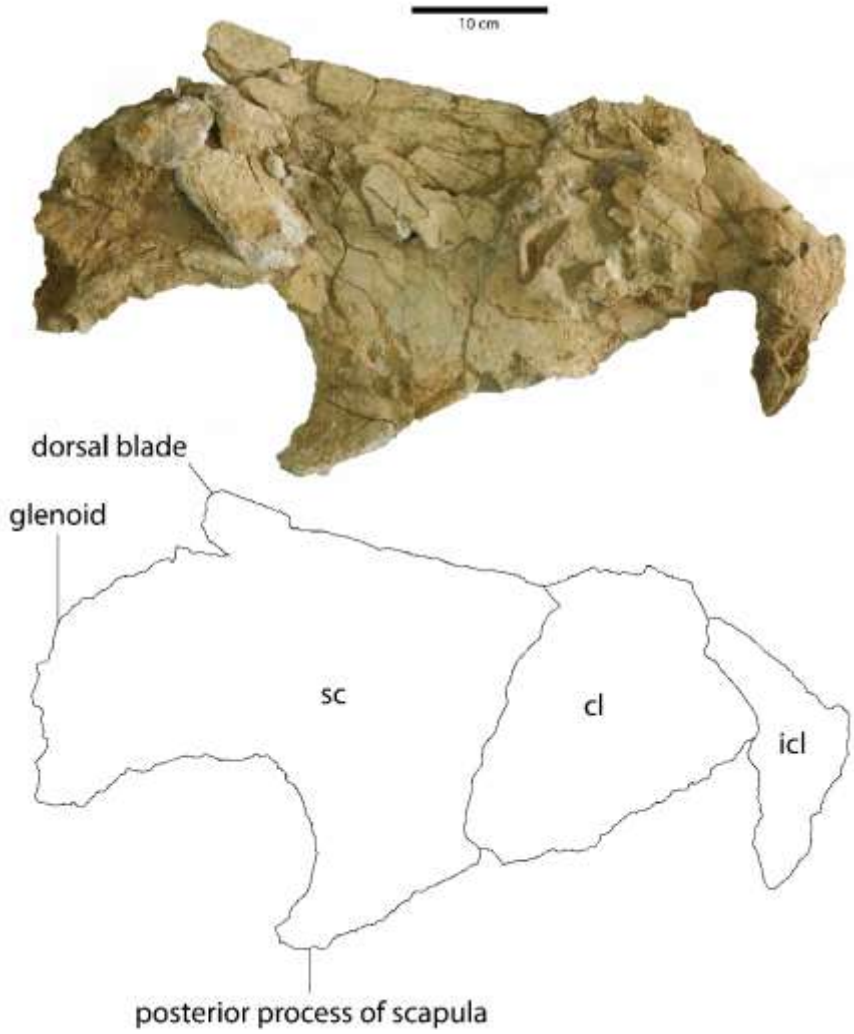

Figure 7.1.1. Left scapula, left clavicle, and interclavicle from the holotype of *Cardiocorax mukulu* (MGUAN PA103) in dorsal view.

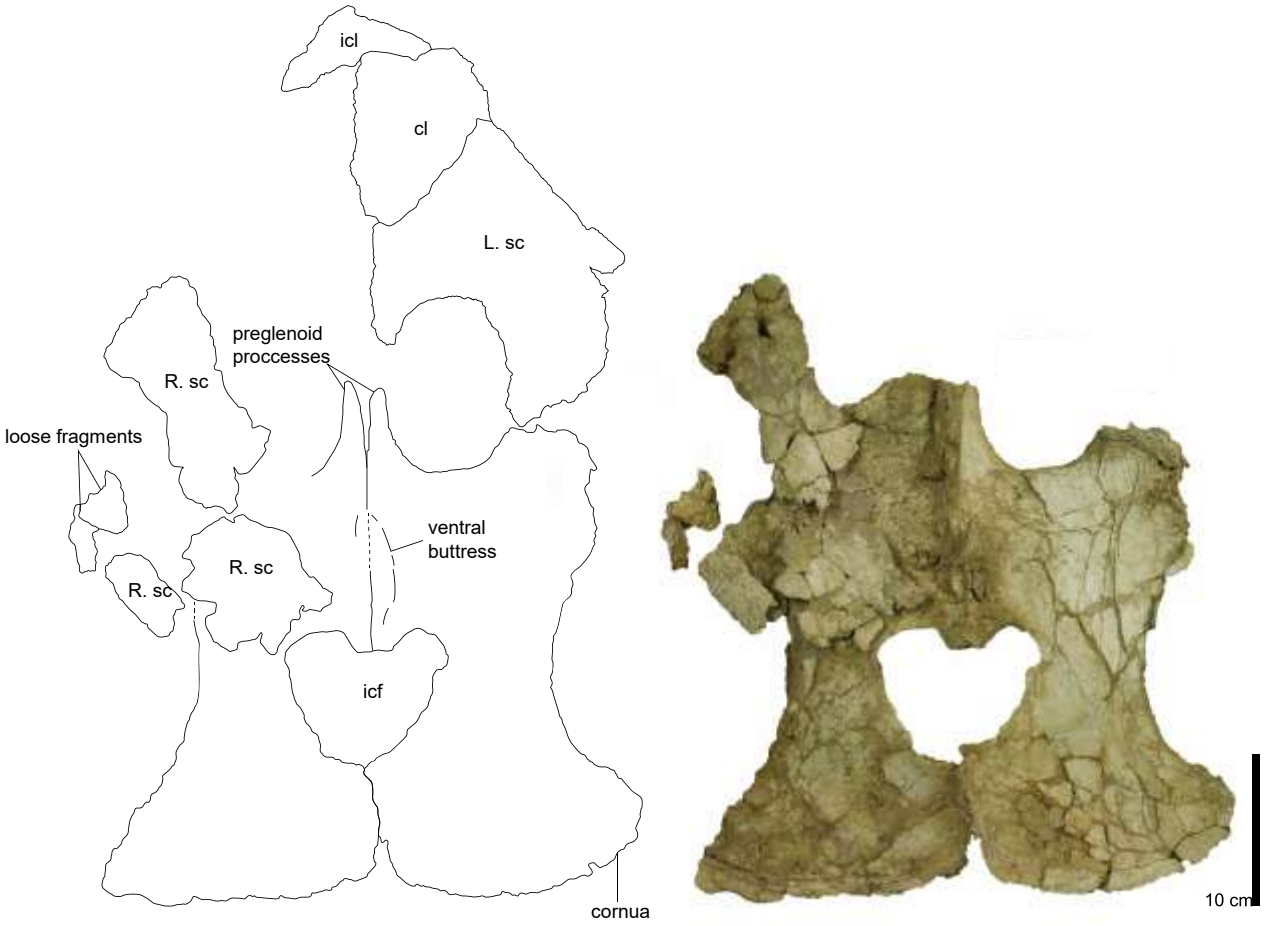

Figure 7.1.2. Pectoral girdle of *Cardiocorax mukulu* holotype (MGUAN PA103) in ventral view. Note the absence of the pectoral bar.

Phylogenetic affinity of *Cardiocorax mukulu*

The assignment of *C. mukulu* as a basally branching taxon outside of Elasmosaurinae and Aristonectinae is congruent with observed elasmosaurid comparative anatomy. The cranial anatomy of *C. mukulu* is clearly distinct from that of aristonectines, but similar to the general morphotype exhibited by elasmosaurines, and elasmosaurids outside of Elasmosaurinae, such as *T. haningtoni*, *L. morgani*, and *L. atlasense* (Sachs and Kear, 2017). The cervical vertebrae of *C. mukulu* fall into the '*Cimaliosaurus*'-grade, as in *Libonectes*, *T. haningtoni*, *C. colombiensis*, *H. alexandrae*, and *F. suzukii*, where length of the centra is not significantly greater or smaller than the width (Welles, 1943; Sato et al., 2006; Otero, 2016) (Figure 6.2.1.).

The character scores for taxa that were studied first-hand by M.M. (*S. snowii*, *C. colombiensis* and *T. haningtoni*) do not agree with all the character scores provided in the matrices of Otero (2016), Serratos et al., (2017), Otero et al., (2018), and O'Gorman (2020). Revised scoring for these taxa are provided in the supplementary data, but an exhaustive review of each character change is not provided, but it is of note that a thorough understanding of elasmosaurid plesiosaurian anatomy needs to be understood to avoid incorrect character scoring which are influencing phylogenies. The character states that distinguished *C. mukulu* from other elasmosaurid plesiosaurians in the matrices of Otero (2016) and Otero et al., (2018) are more widespread within Elasmosauridae. Ch13.1 is also present in *T. haningtoni*, *C. colombiensis*, and *L. morgani*; ch.61.1 is present in *L. morgani*, *S. snowii*, and *T. haningtoni*, and ch132.1 is present in *S. snowii*. Ch136.1 may be scored incorrectly in Otero (2016) and Otero et al., (2018); the presence of enamel 'striations' or grooves were originally scored by Benson and Druckenmiller (2014) only for the taxa *Augustasaurus hagdonri* and *Bobosaurus forojuliensis*, while all other taxa were scored for an absence of enamel 'striations'. Otero et al., (2018) score multiple elasmosaurid taxa as 136.0. Scoring for ch.165 appears to be in a confused state across Benson and Druckenmiller (2014), Sachs et al., (2015), Otero (2016), Serratos et al., (2017), Otero et al., (2018) and O'Gorman (2020). The character states for ch.165 are rather straight-forward as stated in the parent matrix, Benson and Druckenmiller (2014). Cervical centra, median ventral surface: approximately flat or convex (0); bears a rounded midline ridge (1); or bears a sharp keel (2). Benson and Druckenmiller (2014) score all their elasmosaurid plesiosaurian cervical vertebrae as 165.0 despite a clear ventral ridge/keel present on the ventral surface of the cervical centra. Sachs et al., (2015) correctly score *L. morgani* as 165.1 in their matrix and do not simply assign all the elasmosaurid plesiosaurians in their matrix as 165.0. Serratos et al., (2017) however retain a score of 165.0 for all their elasmosaurid taxa, except for *E. platyurus* and MOR 3072 (*N. bradti*). Otero (2016) scores ch.165 as 165.0 for all elasmosaurid taxa in their taxon matrix except for *S. snowii* and AMNH 1495 (165.1). Otero et al., (2018) score ch.165 as

165.0 for all elasmosaurid taxa except for taxa referable to *Styxosaurus*. O'Gorman (2020) scores ch.165 as 165.1 for all the elasmosaurid taxa in his matrix. Sachs et al., (2018) from their redescription of *S. snowii* scored ch.165 as 165.2. It can be noted that some of the newest matrices did not incorporate changed character states. This is just one example of confusion surrounding a particular character in the elasmosaurid plesiosaurian literature. Mistakes and incorrect character scoring affect the resulting diagnoses of taxa in a given cladogram. There is also the issue of morphological variation within a single individual that makes certain characters difficult to score with the Benson and Druckenmiller (2014) character matrix. An example of this is again ch.165, as O'Gorman (2020) reports that the shape of the keel is dependent upon the region of the cervical column.

The anatomy of elasmosaurid plesiosaurians needs to be better understood to allow for more consistent and accurate scoring. This is a conclusion echoing previous phylogenetic studies of elasmosaurids (Vincent et al., 2011; Serratos et al., 2017; Sachs et al., 2018). It can be hypothesized however that *C. mukulu* is an Early Maastrichtian representative of a basally branching group of elasmosaurids outside of the most derived clade formed by Aristonectinae and Elasmosaurinae. The results of this analysis contrast with that of Araújo et al., (2015a), which found *C. mukulu* to be the sister taxon of *S. snowii* after inputting MGUAN PA103 into the dataset of Ketchum and Benson (2010). Increased taxon datasets, discoveries of new specimens, the addition of new elasmosaurid-specific character states, and revised character scores of historic specimens have since provided more up-to-date matrices for phylogenetic analysis of elasmosaurid plesiosaurians (Benson and Druckenmiller, 2014; Otero, 2016; Serratos et al., 2017; Otero et al., 2018; O'Gorman, 2020). Thus, our results using these matrices are reflective of the most recent understanding of elasmosaurid systematics.

The matrices that provided the best resolution in our phylogenetic analyses (Sachs et al., 2015; Allemand et al., 2017; Otero et al., 2018) suggest a possible evolutionary relationship between *C. mukulu* and *L. morgani*. However, *L. morgani* specimens are Cenomanian- lower Turonian in age and this represents a substantial time gap in the '*Libonectes-Cardiocorax*' clade, as *C. mukulu* is recovered from Lower Maastrichtian outcrops of Bentiaba (Welles, 1949; Araújo et al., 2015a; Sachs and Kear, 2017; Allemand et al., 2017). Additionally, there are few elasmosaurid taxa that are more derived than the most basal members of Elasmosauridae (*C. colombiensis* and *E. australis*) that are also outside of Elasmosaurinae and Aristonectinae to compare with *C. mukulu* in the mentioned matrices. Thus, a bias in the data may be producing a clade composed of *Libonectes* and *Cardiocorax*. There is a Maastrichtian-aged elasmosaurid from New Zealand (Cm Zfr 145) that exhibits a pectoral girdle that is morphologically similar to that of *C. mukulu* (MGUAN PA103) (Hiller and Mannering, 2005; figure 7; Michael Polcyn, pers. comm. April, 2020). It is also worth commenting that the pectoral girdle of *L. morgani* (now

represented as a sketch from Welles, 1949 as the original girdle material is lost) is also similar to *C. mukulu* based on the narrow and elongated morphology of preglenoid processes, lateral extent of coracoid cornua at the level of the pectoral glenoid or beyond the glenoid, and the posteromedial projection of the coracoids into the intercoracoid foramen (Ricardo Araújo pers. comm. May, 2020). A close phylogenetic association between *L. morgani* and *C. mukulu* would indicate a southward migration of basal Northern Hemisphere elasmosaurids during the opening of the South Atlantic. If Cm Zfr 145 is closely related to *C. mukulu* based on characters of the pectoral girdle, then this may indicate a dispersal of this lineage to Australasia. Comparing the hypotheses of dispersal for the *Libonectes-Cardiocorax* lineage to other Cretaceous marine reptiles (mosasaurs and turtles) can provide insight toward dispersal patterns in the South Atlantic, however, this goes beyond the scope of this thesis.

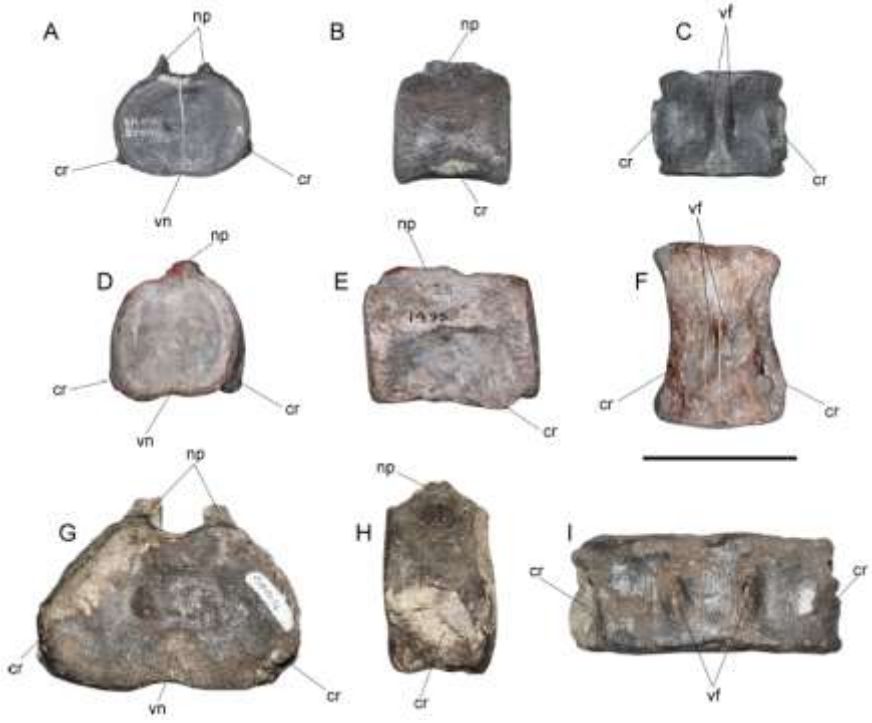

Figure 7.2.1. The three cervical vertebra morphotypes of Elasmosauridae. Top row: the '*Cimoliasaurus*'-grade cervical centrum of AMNH 2554 (holotype of the *nonmen dubium* '*Cimoliasaurus magnus*) in (A) anterior, (B) lateral, and (C) ventral views. Middle row: The elongated morphology typical of Elasmosaurine (Sxyosaurine) elasmosaurids cervical centra; AMNH 1495 (*Styxosaurus* sp.) cervical centrum in (D) anterior, (E) lateral, and (F) ventral views. Bottom row: the anteroposteriorly abbreviated cervical centrum typical of Aristonectine elasmosaurids; isolated centrum (SGO.PV.96) in (G) anterior, (H) lateral, and (I) ventral views. Figure 15 from Otero (2016).

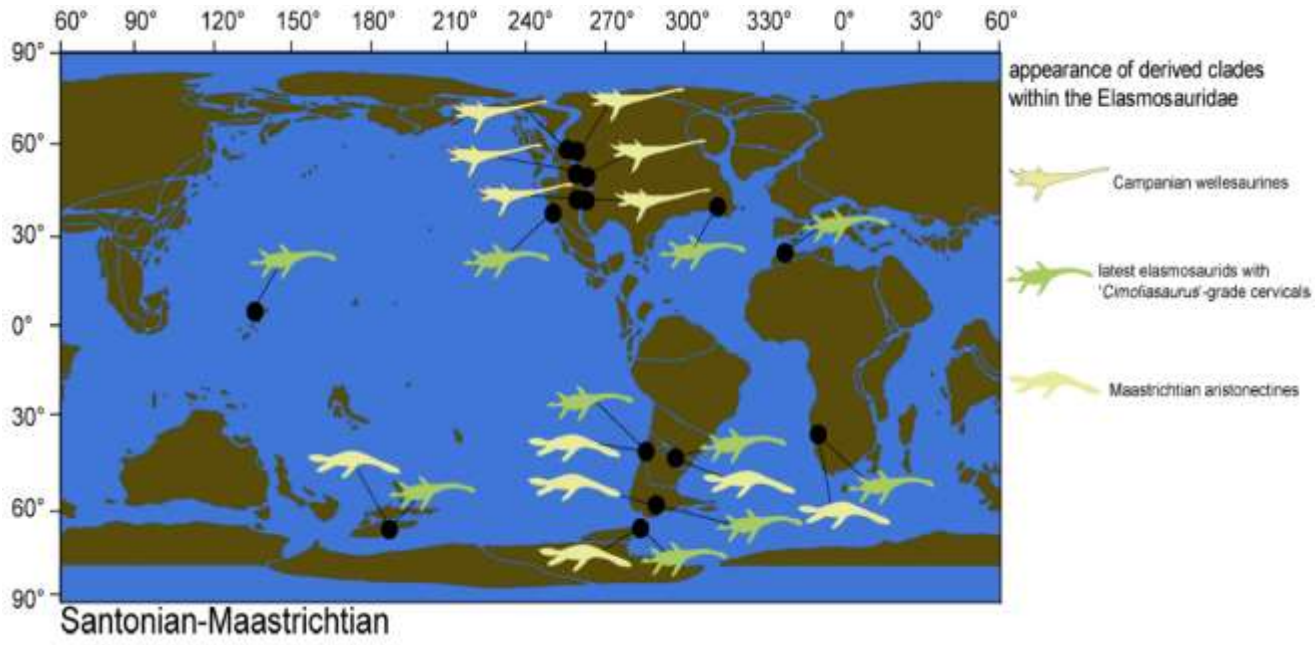

Figure 7.2.2. Biogeographic distribution of the three elasmosaurid morphotypes in the Late Cretaceous (Santonian-Maastrichtian). Wellesaurines are synonymous with Elasmosaurines. Modified from figure 17 of Otero (2016).

Sensory adaptations of *Cardiocorax mukulu*

Modern imaging technology has allowed for visualization of the braincase and endosseous labyrinth in both extant and fossil specimens. Imaging technology coupled with software capable of creating three-dimensional digital endocasts of soft-tissue organs/ structures has allowed for the morphological description of soft parts of the anatomy of extinct taxa (Dufeau & Witmer, 2015; Porter & Witmer, 2015; Allemand et al., 2017; Neenan et al., 2017). However, the assumptions involved with interpretation of endocasts from the braincase and endosseous labyrinth to infer sensory capabilities and behavior need to be addressed.

As noted by Dickson et al., (2017), a large body of research on mammalian taxa has established a relationship between the structure of the semicircular canals and sensitivity of the vestibular system, locomotor behavior, agility and speed (Hullar, 2006; Yang and Hullar, 2007; Spoor et al., 2007; Georgi, 2008; Malinzak et al., 2012; Billet et al., 2012; Schutz et al., 2014; Ifediba et al., 2017). However, comparative studies between the structure and function of the vestibular system in reptiles remains less studied (Sipla, 2007, Georgi & Sipla, 2009; Boistel et al., 2011; Yi & Norell, 2015). Dickson et al., (2017) found that the ecological niche of the *Anolis* taxa was the most important covariate of the morphology of the semicircular canals. However, the proportions of the cranium, the size of the semicircular canals, and phylogenetic legacy also correlate with morphology of the semicircular canals.

Second, there is a question as to how accurate 3D segmentation of the cavities of the braincase or endosseous labyrinth reflect the real morphology of the soft tissue (Evers et al., 2019). The study by Evers et al., (2019) examined the segmented brain and corresponding braincase of the modern turtle, *Trachemys scripta*, and found that the space inside the braincase is a poor proxy for brain morphology. With respect to the semicircular canals, Evers et al., (2019) found, using *T. scripta* as a study taxon, that the endosseous labyrinth provides a much larger representation of the cross-section of the membranous semicircular canals, the posterior and lateral endosseous canals only partly reflected the actual orientation of the membranous canals, and the anterior endosseous canal was the most accurate representation of the anterior membranous canal. Although the size of the membranous canals is not accurately reflected by the endosseous labyrinth, the general morphology of the vestibular system is preserved. Evers et al., (2019) found the endosseous labyrinth reflects the arc length of the membranous anterior semicircular canal well. The ampullae appear to be defined less so by the enlarged ventral margin of the endosseous labyrinth (Evers et al., 2018).

With the above issues and assumptions concerning the accuracy of interpreting behavior/ ecology and the real morphology of the membranous semicircular canals based on casts from segmented fossil specimens, it should be noted that the endosseous labyrinth digital cast from MGUAN PA278 is just an approximation of the membranous vestibular system. With that said, the digital endosseous cast of MGUAN PA278 exhibits a highly compact morphology similar to *L. morgani*, but unlike any other Sauropterygian (Neenan et al., 2017; Allemand et al., 2017). The maximum height of the crus communus does not extend much further dorsally than the dorsal apices of the ampullae (Figure 5.9.1.). The anterior and posterior semicircular canals are wide, with a short and atrophied lateral semicircular canal that is almost absorbed into the lateral surface of the endosseous labyrinth. Thus, the endrosseous labyrinth clearly exhibits a low aspect ratio (dorsoventral height relative to anteroposterior length). It has been hypothesized that endosseous labyrinths with a low aspect ratio are correlated with adaptations to swimming in a pelagic environment (Neenan et al., 2017). This association is consistent with other plesiosaurians; in general, the morphology of the endosseous labyrinth is related to depth of water in the animal's environment (Neenan et al., 2017). However, this hypothesis does not always hold true, as wide semicircular canals have been reported in the terrestrial turtle, *Indotestudo elongata* (Evers et al., 2019).

Another aspect of the sensory system of *C. mukulu* of note is the snout, highly innervated by the trigeminal nerve. The surface of the premaxillae exhibits a dense network of branching at the surface of the bone. This condition is found across not only elasmoaurid plesiosaurians, but also in pliosaurids (Foffa et al., 2014). A dense network of nerves near the surface of the snout may have been of function concerning prey acquisition, specifically changes in water pressure near the snout, indicating the location of food, similar to modern crocodilians (George and Holliday, 2013). Thus, interpretation of the morphology of the endosseous labyrinth coupled with the branching pattern of the trigeminal nerve on the surface of the snout suggest that *C. mukulu* may not have been actively chasing its prey. Preying on large schools of fish, where the confusion of a feeding frenzy may allow for fish to get close enough to catch, or feeding in depths of low visibility (or at night) may have allowed for a large-bodied plesiosaur to get within striking range of prey items, with a highly sensitive snout capable of detecting where prey items are before striking.

Conclusion

MGUAN PA278 includes a nearly complete cranium with a mandible and represents the most complete skull of an elasmosaurid from Sub-Saharan Africa. This new specimen shares with the holotype of *Cardiocorax mukulu* (MGUAN PA103) a sinusoidal outline along the anterior margin of the mid-cervical vertebra neural spines. Overlapping skeletal material between specimens MGUAN PA278 and MGUAN PA103 is morphologically indistinguishable. Thus, MGUAN PA278 represents a new specimen of the elasmosaurid species, *C. mukulu*, from the same locality where the holotype (MGUAN PA103) and another referable specimen of *C. mukulu* (MGUAN PA270) were excavated (Mateus et al., 2012; Araújo et al., 2015a). A new combination of apomorphies from the cranium adds to the diagnosis of *C. mukulu*, and a reanalysis of the skeletal material from the holotype of *C. mukulu* clarifies the anatomy of the pectoral girdle. Phylogenetic analysis of the new specimen places *C. mukulu* as a more basal elasmosaurid taxon, outside of the Elasmosaurinae + Aristonectinae clade. The compact morphology of the endossesous labyrinth digital cast suggests a pelagic lifestyle for *C. mukulu*.

Bibliography

Ala, M. A. and Selley, R. C. 1997. The western African coastal basins. In *African Basins* (Sedimentary Basins of the World, 3). (eds Selley, R. C. and Hsu, K.J.). pp. 173-186. Elsevier Science, Saint Louis, Missouri.

Albrecht, P.W. 1976. The cranial arteries of turtles and their evolutionary significance. *Journal of Morphology* 149, 159-182. DOI: 10.1002/jmor.1051490203

Allemand., R., Bardet, N., Houssaye, A., and Vincent, P. 2017. Virtual reexamination of a plesiosaurian specimen (Reptilia, Plesiosauria) from the Late Cretaceous (Turonian) of Goulmima, Morocco, using computed tomography, *Journal of Vertebrate Paleontology*, DOI: 10.1080/02724634.2017.1325894

Allemand., R., Bardet, N., Houssaye, A., and Vincent, P. 2018. New plesiosaurian specimens (Reptilia, Plesiosauria) from the Upper Cretaceous (Turonian) of Goulmima (Southern Morocco). *Cretaceous Research* 82, 83-98.

Allemand., R., Houssaye, A., Bardet, N., and Vincent, P. 2019. Endocranial anatomy of plesiosaurians (Reptilia, Plesiosauria) from the Late Cretaceous (Turonian) of Goulmima (Southern Morocco). *Journal of Vertebrate Paleontology*, DOI: 10.1080/02724634.2019.1595636.

Andrews, C.W. 1910. *A Catalogue of the Marine Reptiles of the Oxford Clay, Part I*. British Museum (Natural History), London.

Andrews, C.W., 1911. Description of a new plesiosaur (*Plesiosaurus capensis*, sp. nov.) from the Uitenhage Beds of Cape Colony. *Annals of the South African Museum* 1, 309–322.

Andrews, C. W. 1913. *A Catalogue of the Marine Reptiles of the Oxford Clay, Part II*. British Museum (Natural History), London.

Antunes, M.T. 1961. Sur la faune de Vertébrés du Crétacé de Iembe (Angola). Comptes Rendus de l'Académie des Sciences, Paris, 253, 513-514.

Antunes, M.T. 1964. O Neocretácico e o Cenozóico do litoral de Angola. Junta de Investigações do Ultramar 27, 1-257.

Antunes, M.T. 1970. Paleontologia de Angola. Curso de Geologia do Ultramar. Junta de Investigações do Ultramar. Lisboa, II.

Arambourg, C., 1952. Les vertébrés fossiles des gisements de phosphates (Maroc–Algérie–Tunisie). Notes et Mémoires du Service géologique du Maroc 92, 1–372.

Araújo, R., M.J. Polcyn, M.J., Schulp, A.S., Mateus, O., Jacobs, L.L., Gonçalves, A.O., and Morais, M.-L. 2015a. A new elasmosaurid from the early Maastrichtian of Angola and the implications of girdle morphology on swimming style in plesiosaurs. *Netherlands Journal of Geosciences* - Geologie en Mijnbouw, Available on CJO 2015, DOI:10.1017/njg.2014.44

Araújo, R., Polcyn, M.J., Lindgren, J., Jacobs, L.L., Schulp, A.S., Mateus, O., Gonçalves, O., and Morais, M.-L. 2015b. New aristonectine elasmosaurid plesiosaur specimens from the Early Maastrichtian of Angola and comments of paedomorphism in plesiosaurs. *Netherlands Journal of GeoSciences*, Available on CJO 2015, DOI:10.1017/njg.2014.43

Averianov, A.O., and Popov, V.K. 2005. The First Plesiosaur from the Primorye Krai. *Doklady Biological Sciences*, 401, 104-106.

Bakker, R. T. 1993. Plesiosaur extinction cycles - Events that mark the beginning, middle and end of the Cretaceous. In Evolution of the western interior basin, *Geological Association of Canada Special Paper* 39, 641–664.

Bardet, N., Godefroit, P., and Sciau, J. 1999. A new elasmosaurid plesiosaur from the Lower Jurassic of Southern France. *Palaeontology* 42(5), 927-952.

Bardet, N., and X. Pereda Suberbiola. 2002. Marine reptiles from the Late Cretaceous phosphates of Joran. Palaeobiogeographical implications. *Geodiveritas* 24, 831-839.

Bardet, N., Pereda, Suberbiola X., and Jalil, N.-E. 2003. A new polycotylid plesiosaur from the Late Cretaceous (Turonian) of Morocco. *Comptes Rendus Paleo* 2, 307–315.

Bardet, N., Fernández, M., García-Ramos, J.C., Suberbiola, X.P., Piñuela, L., Ruiz-Omeñaca, J.I., and Vincent, P. 2008. A Juvenile Plesiosaur from the Pliensbachian (Lower Jurassic) of Asturias, Spain. *Journal of Vertebrate Paleontology* 28(1), 258-263.

Bardet, N., Segura, M., and Pérez-García, A. 2018. A plesiosaur (Reptilia, Sauropterygia) from the Cenomanian (Late Cretaceous) of Algora (Guadalajara Province, Central Spain). *Cretaceous Research*, DOI: 10.1016/j.cretres.2018.05.006.

Baumel, J.J., and Witmer, L.M. 1993. Osteologia. In *Handbook of Avian Anatomy Nomina Anatomica Avium* 2nd edition (eds Baumel, J.), pp. 45-133. Cambridge, MA.

Benson, R.B.J., Evans, M., and Druckenmiller, P.S. 2012. High Diversity, Low Disparity and Small Body Size in Plesiosaurs (Reptilia, Sauropterygia) from the Triassic– Jurassic Boundary. *PLoS ONE* 7(3): e31838. DOI:10.1371/journal.pone.0031838

Benson, R.B.J., and Druckenmiller, P.S. 2014. Faunal turnover of marine tetrapods during the Jurassic-Cretaceous transition. *Biological Reviews* 89, 1-23.

Benton, M.J. 1985. Classification and phylogeny of the diapsid reptiles. *Zoological Journal of the Linnean Society* 84, 97-162.

Benton, M.J., Bouaziz, S., Buffetaut, E., Martill, D., Ouaja, M., Soussi, M., and Trueman, C. 2000. Dinosaurs and other fossil vertebrates from fluvial deposits in the Lower Cretaceous of Southern Tunisia. *Palaeogeography, Palaeoclimatology, Palaeoecology* 157(3-4), 227-246.

Benton. M.J. 2015. *Vertebrae Palaeontology*. 4th ed., Oxford, Wiley-Blackwell.

Berezin, A.Y. 2011. A new plesiosaur of the family aristonectidae from the early cretaceous of the center of the Russian platform. *Paleontological Journal* 45, 648-660.

Berezin, A.Y. 2018. Craniology of the Plesiosaur *Abyssosaurus nataliae* Berezin (Sauropterygia, Plesiosauria) from the Lower Cretaceous of the Central Russian Platform. *Paleontological Journal* 52, 328-341.

Billet, G., Hautier, L., Asher, R.J., Schwarz, C., Crumpton, N., Martin, T, and Ruf, I. 2012. High morphological variation of vestibular system accompanies slow and infrequent locomotion in three-toed sloths. *Proceedings of the Royal Society* B 279, 3932–3939, DOI:10.1098/rspb.2012.1212

Blainville, H.D. 1835. Description de quelques espèces de reptiles de la Californie précédé de l'analyse d'un system general d'Erpétologie et d'Amphibiologie. *Nouvelles Annales du Museum National d'Histoire Naturelle, Paris*. 233-296.

Boistel, R., Herrel, A., Lebrun, R., Daghfous, G., Tafforeau, P., Losos, J.B., and Vanhooydonck, B. 2011. Shake rattle and roll: the bony labyrinth and aerial descent in squamates. *Integrative and Comparative Biology* 51, 957–968, DOI:10.1093/icb/icr034

Bond, G. 1978. Evidence for late Tertiary uplift of Africa relative to North America, South America, Australia, and Europe. *Journal of Geology* 86, 47-65.

Brognon, G. P. and Verrier, G. V. 1966a. Tectonique et sedimentation dans le basin du Cuanza (Angola). *Serviços de Geologia e Minas de Angola Boletim* 11, 5-90.

Brognon, G. P. and Verrier, G. V. 1966b. Oil and geology in Cuanza Basin of Angola. *American Association of Petroleum Geologists Bulletin* 50, 108-158.

Brown, D.S., 1981. The English Upper Jurassic Plesiosauroidea (Reptilia) and a review of the phylogeny and classification of the Plesiosauria. *Bulletin of the British Museum (Natural History) Geology Series* 35, 253-344.

Buchy, M.-C., Metayer, F., and Frey, E., 2005. Osteology of *Manemergus anguirostris* n. gen. et sp., a new plesiosaur (Reptilia, Sauropterygia) from the Upper Cretaceous of Morocco. *Palaeontographica, Abteilung* A 272, 97–120

Buchy, M.-C., 2006. An Elasmosaur (Reptilia: Sauropterygia) from the Turonian (Upper Cretaceous) of Morocco. *Carolinea* 63, 5–28.

Buffetaut, E. 1987. *A Short History of Vertebrate Paleontology*. Croom Helm, Australia. Croom Helm, Ltd.

Cabrera, A. 1941. Un plesiosaurio nuevo del Creticeo del Chubut. *Revista del Museo de La Plata* 2, 113-130.

Carpenter, K. 1996. A review of short-necked plesiosaurs from the Cretaceous of the Western Interior, North America. *Neues Jahrbuch f¨ur Geologie und Paläontologie, Abhandlungen* 201, 259–287.

Carpenter, K. 1997. Comparative cranial anatomy of two North American Cretaceous plesiosaurs. In *Ancient Marine Reptiles* (eds Callaway, J. M. and Nicholls, E.), pp. 191–213. Academic Press, San Diego.

Carpenter, K. 1999. Revision of North American elasmosaurs from the Cretaceous of the Western Interior. *Paludicola* 2, 148–173.

Chatterjee, S., Small, B.J. 1989. New plesiosaurs from the Upper Cretaceous of Antarctica. *Geological Society London Special Publications* 47 (1), 197- 215.

Choffat, P. 1905. Contributions a la Connaisance Géologique des Colonies Portugaises D'Afrique II. Nouvelles Donnees Sur la Zone Littorale D'Angola. Lisbonne, Imprimerie de L'Académie Royale des Sciences, 31-88.

Consoli, C.P., adn Stilwell, J.D. 2009. Late Cretaceous reptiles (Elasmosauridae and Mosasauridae) of the Chatham Islands, New Zealand. *Cretaceous Research* 30, 991-999.

Conybeare, W.D. 1822. Additional notices on the fossil genera Ichthyosaurus and Plesiosaurus. *Transactions of the Geological Society of London* 2(1), 103-123.

Conybeare, W.D. 1824. On the discovery of an almost perfect skeleton of the Plesiosaurus. *Transactions of the Geological Society of London* 2(1), 382-389.

Cooper, 2003. Upper Cretaceous (Turonian-Coniacian) Ammonites from São Nicolau, Angola. *Annals of the South African Museum*, 89- 144.

Cope, E. D. 1868. Remarks on a new enaliosaurian, Elasmosaurus platyurus. *Proceedings of the Academy of Natural Sciences of Philadelphia* 1868, 92-93.

Cope, E.D., 1869. Synopsis of the extinct Batrachia and Reptilia of North America. *Transactions of the North American Philosophical Society* 14, 1-252.

Cragin, F.W. 1888. New or Little Known Saurian from the Benton of Kansas. *American Geologist* 2, 404-407.

Cruickshank, A.R.I., 1997. A Lower Cretaceous pliosauroid from South Africa. *Annals of the South African Museum* 105, 207–226.

Cruickshank, A.R.I., Fordyce, R.E., and Long, J.A. 1999. Recent developments in Australasian sauropterygian paleontology (Reptilia: Sauropterygia). *Records of the Western Australian Museum* 57, 201- 205.

Cruickshank, A.R.I., and Fordyce, R.E. 2002. A New Marine Reptile (Sauropterygia) from New Zealand: Further Evidence for a Late Cretaceous Austral Radiation of Cryptoclidid Plesiosaurs. *Palaeontology*, 45(3), 557-575.

Dames, W. 1895. Die Plesiosaurier der su¨ddeutschen Liasformation. Physikalische und Mathematische Abhandlungen der ko¨niglichen Akademie der Wissenschaften zu Berlin, 1895, 1–83.

Dartevelle, E. and Casier, E. (1943-59). Les poisons fossiles du Bas-Congo et des régions voisines. *Annales du Musée Royale du Congo Belge*, 11, 1-3.

Davidson, J.P., and Everhart, M.J. 2018. The Mystery of *Elasmosaurus platyurus* Cope 1868- Where is the rest of the specimen? *Transactions of the Kansas Academy of Science*, 121(3-4), 335-345.

De la Beche, H.T. and W.D. Conybeare. 1821. Notice of the discovery of a new fossil animal, forming a link between the *Ichthyosaurus* and the crocodile, together with general remarks on the osteology of *Ichthyosaurus*. *Transactions of the Geological Society of London* 5, 559-594.

DeLair, J. B. 1959. The Mesozoic reptiles of Dorset, Part 2. *Proceedings of the Dorset Natural History and Archeaological Society* 80, 52–90.

Dickson B.V., Sherratt E., Losos J.B., and Pierce S.E. 2017 Semicircular canals in Anolis lizards: ecomorphological convergence and ecomorph affinities of fossil species. *Royal Society Open Science* 4: 170058. http://dx.doi.org/10.1098/rsos.170058

Dortangs, R.W., Schulp, A.S., Mulder, E.W.A., Jagt, J.W.M., Peeters, H.H.G., de Graaf, D.T. 2002. A large new mosasaur from the Upper Cretaceous of the Netherlands. *Netherlands Journal of Geosciences/ Geologie en Mijnbouw* 81(1), 1-8.

Dragonfly 3.6 [Computer software]. Object Research Systems (ORS) Inc, Montreal, Canada, 2018; software available at http://www.theobjects.com/dragonfly.

Druckenmiller, P.S. 2002. Osteology of a new plesiosaur from the lower Cretaceous (Albian) Thermopolis shale of Montana. *Journal of Vertebrate Paleontology* 22 (1), 29-42.

Druckenmiller, P.S. and Russell, A.P. 2008. A phylogeny of Plesiosauria (Sauropterygia) and its bearing on the systematic status of Leptocleidus Andrews, 1922. *Zootaxa* 1863, 1-120.

Druckenmiller, P.S., Knutsen, E. 2012. Phylogenetic relationships of Upper Jurassic (Middle Volgian) plesiosaurians (Reptilia: Sauropterygia) from the Agardhfjellet Formation of central Spitsbergen, Norway. *Norsk Geologisk Tidsskrift* 92 (2&3), 277-284.

Dufeau, D.L., and Witmer, L.M. 2015. Ontogeny of the Middle-Ear Air-Sinus System in *Alligator mississippiensis* (Archosauria: Crocodylia). *PLoS ONE* 10(9): e0137060, DOI:10.1371/journal.pone.0137060.

Ebersole, J.A., Dean, L.S. 2013. The History of Late Cretaceous Vertebrate Research in Alabama. *Bulletin of the National Museum of Alabama* 31(1), 3- 45.

Evans, M. 2012. A new genus of plesiosaur (Reptilia: Sauropterygia) from the Pliensbachian (Early Jurassic) of England, and a phylogeny of the Plesiosauria. Doctoral dissertation, University of Leicester, Leicester, England.

Evers, S.W., Neenan, J.M., Ferreira, G.S., Werneberg, I., Barrett, P.M., and Benson, R.B.J. 2019. Neurovascular anatomy of the protostegid turtle *Rhinochelys pulchriceps* and comparisons of membranous and endosseous labyrinth shape in an extant turtle. *Zoological Journal of the Linnean Society* 187, 800–828.

Fischer, V., Benson, R.B.J., Zverkov, N.G., Stenshin, I.M., Uspensky, G.N., Druckenmiller, P.S. 2017. Plasticity and Convergence in the Evolution of Short-Necked Plesiosaurs. *Current Biology* 27(11), 1667-1676.

Gaina, C., Torsvik, T.H., van Hinsbergen, D.J.J., Medvedev, S., Werner, S.C. and Labails, C. 2013. The African Plate: A history of oceanic crust accretion and subduction since the Jurassic. *Tectonophysics* 606, 4-25.

Gasparini, Z., N. Bardet, J. E. Martin, and M. Fernandez. 2003. The elasmosaurid plesiosaur *Aristonectes Cabrera* from the latest Cretaceous of South America and Antarctica. *Journal of Vertebrate Paleontology* 23(1), 104–115.

Gasparini, Z.B., Salgado, and L., Casadío, S. 2003. Maastrichtian plesiosaurs from northern Patagonia. *Cretaceous Research* 24, 157-170.

Gasparini, Z., Salgado, L., and Parras, A. 2007. Late Cretaceous plesiosaurs from northern Patagonia, Argentina. *Geological Journal* 42 (2), 185- 202.

George, I.D., and Holliday, C.M. 2013. Trigeminal Nerve Morphology in *Alligator mississippiensis* and Its Significance for Crocodyliform Facial Sensation and Evolution. *The Anatomical Record* 296 (4), 670-680.

Georgi J.A. 2008. Semicircular canal morphology as evidence of locomotor environment in amniotes. PhD Dissertation, Stony Brook University, New York, NY, USA.

Georgi, J.A, Sipla, J.S. 2009. Comparative and functional anatomy of balance in aquatic reptiles and birds. In *Sensory evolution on the threshold: adaptations in secondarily aquatic vertebrates* (eds JGM Thewissen, N Sirpa), pp. 98. Berkley, CA: University of California Press.

Gerrard, I. and Smith, G. C. 1982. Post-Paleozoic succession and structure of the southwestern African continental margin. In *Studies in Continental Margin Geology* (eds Watkins, J.S. and Drake, C.L.). pp. 49-74. *American Association of Petroleum Geologists Memoir* 34.

Goloboff, P.A., and Catalano, S.A. 2016. TNT version 1.5, including a full implementation of phylogenetic morphometrics. *Cladistics* 32 (3), 221-334.

Groβmann, F., 2007. Preliminary description and phylogenetic position of a new plesiosaur (Reptilia: Sauropterygia) from the Toarcian of Holzmaden, Germany. *Journal of Paleontology* 78, 973–988.

Hector, J. 1874. On the fossil reptiles of New Zealand. *Transactions of the New Zealand Institute* 6, 333-358.

Hiller, N. and Mannering, A.A. 2005. A new elasmosaurid plesiosaur (Sauropterygia) from the Upper Haumerian (Maastrichtian) of the South Island, New Zealand. *Memoirs of the Queensland Museum* 51 (1): 000-000. Brisbane, ISSN 0079-8835.

Huene, F. von 1921. Ein Plesiosaurier-Rest aus dem untersten Lias Wu¨rttembergs. Centralblatt fu¨r Mineralogie, Geologieund Paläontologie, Abteilung, B, 1921, 401–405.

Hullar TE. 2006 Semicircular canal geometry, afferent sensitivity, and animal behavior. *Anatomical Record Part A: Discoveries in Molecular, Cellular, and Evolutionary Biology* 288, 466–472, DOI:10.1002/ar.a.20304

Ifediba MA, Rajguru SM, Hullar TE, and Rabbitt RD. 2007. The role of 3-canal biomechanics in angular motion transduction by the human vestibular labyrinth. *Annals of Biomedical Engineering* 35, 1247–1263, DOI:10.1007/s10439-007-9277-y

Jacobs, L.L., Mateus, O., Polcyn, M.J., Schulp, A.S., Antunes, M.T., Morais, M.L. and Da Silva Tavares, T. 2006. The occurrence and geological setting of Cretaceous dinosaurs, Mosasaurs, Plesiosaurs, and Turtles from Angola. *Journal of the Paleontological Society of Korea*, 22 (1), 91-110.

Jacobs, L.L., Mateus, O., Polcyn, M.J., Schulp, A.S., Scotese, C.R., Goswami, A., Ferguson, K.M., Robbins, J.A., Vineyard, D.P. and Neto, A.B. 2009a. Cretaceous paleogeography, paleoclimatology, and amniote biogeography of the low and mid-latitude South Atlantic Ocean. *Bulletin of the Geological Society of France* 180(4), 333-341.

Jacobs, L.L., Polcyn, M.J., Mateus, O., Schulp, A. and Neto, A.B. 2009b. The Cretaceous Skeleton Coast of Angola. *Journal of Vertebrate Paleontology*, 29 (3), 121A.

Jacobs, L.L., Polcyn, M.J., Mateus, O., M.J., Schulp, Gonçalves, O.A., and Morais, M.L. 2016. Post-Gondwana Africa and the vertebrate history of the Angolan Atlantic Coast. *Memoirs of Museum Victoria* 74, 343–362.

Kear, B. P. 2002a. Darwin Formation (Early Cretaceous, Northern Territory) marine reptile remains in the South Australian Museum. *Records of the South Australian Museum* 35, 33–47.

Kear, B.P. 2002b. Reassessment of the Early Cretaceous plesiosaur *Cimoliasaurus maccoyi* Etheridge, 1904 (Reptilia, Sauropterygia) from White Cliffs, New South Wales. *Australian Journal of Zoology* 50, 671–685.

Kear, B.P. 2003. Cretaceous marine reptiles of Australia: a review of taxonomy and distribution. *Cretaceous Research* 24, 277-303.

Kear, B.P. 2004. Biogeographic and biostratigraphic implications of Australian Mesozoic marine reptiles. *Australian Biologist* 17, 4–22.

Kear, B.P. 2005a. A new elasmosaurid plesiosaur from the Lower Cretaceous of Queensland, Australia. *Journal of Vertebrate Paleontology* 25(4), 792-805.

Kear, B.P. 2005b. Marine reptiles from the Lower Cretaceous (Aptian) of White Cliffs, southeastern Australia: implications of a highlatitude cold-water assemblage. *Cretaceous Research* 26, 769– 782.

Kear, B.P. 2006. Marine reptiles from the Lower Cretaceous of South Australia: Elements of high-latitude cold-water assemblage. *Palaeontology* 49(4), 837- 856.

Kear, B.P. 2007. Taxonomic clarification of the Australian elasmosaurid genus *Eromangasaurus*, with reference to other austral elasmosaur taxa. *Journal of Vertebrate Paleontology*, 27 (1), 241-246, DOI: 10.1671/0272-4634(2007)27[241:TCOTAE]2.0.CO;2

Kear, B.P., Rich, T., Ali, M.A., and Almufareeh, Y. 2008. Late Cretaceous (Campanian-Maastrichtian) marine reptiles from the Adaffa Formation, NW Saudia Arabia. *Geological Magazine* 145(5), 648-654.

Kear, B.P. 2016. Cretaceous marine amniotes of Australia: perspectives on a decade of research. *Memoirs of Museum Victoria* 74, 17-28.

Kellner, A.W.A., Simões, T.R., Riff, D., Grillo, O., Romano, P., Paula, H., Ramos, R., Carvalho, M., Sayão, J., Oliveira, G., and Rodrigues, T. 2011. The oldest plesiosaur (Reptilia, Sauropterygia) from Antarctica. *Polar Research* 30 (7265), pp. 1- 6, DOI: 10.3402/polar.v30i0.7265

Ketchum, H., and Benson, R.B.J. 2010. Global interrelationships of Plesiosauria (Reptilia, Sauropterygia) and the pivotal role of taxon sampling in determining the outcome of phylogenetic analyses. *Biological Reviews* 85, 361-392. DOI: 10.1111/j.1469-185X.2009.00107.x

Ketchum, H.F., and Benson. R.B.J. 2011. A new pliosaurid (Sauropterygia, Plesiosauria) from the Oxford Clay Formation (Middle Jurassic, Callovian) of England: Evidence for a gracile, longirostrine grade of Early-Middle Jurassic pliosaurids. *Special Papers in Palaeontology* 86 109–129.

Knutsen, E.M., Druckenmiller, P.S., and Hurum, J.H. 2012a. A new species of *Pliosaurus* (Sauropterygia: Plesiosauria) from the Middle Volgian of central Spitsbergen, Norway. *Norwegian Journal of Geology* 92,.235-258. Trondheim 2012, ISSN 029-196X.

Knutsen, E.M., Druckenmiller, P.S., and Hurum, J.H. 2012b. A new plesiosauroid taxon (Reptilia - Sauropterygia) from the Agardhfjellet Formation (Middle Volgian) of central Spitsbergen, Norway. *Norwegian Journal of Geology* 92, 213- 234.Trondheim 2012, ISSN 029-196X

Kubo, T., Mitchell, M.T., Henderson, D.M. 2012. *Albertonectes vanderveldi*, a new elasmosaur (Reptilia, Sauropterygia) from the Upper Cretaceous of Alberta, *Journal of Vertebrate Paleontology* 32 (3), 557-572.

Lapão, L.J.P. 1972. Carta Geológica: Folha nº 184-Novo Redondo. Direcção Provincial dos Serviços de Geologia e Minas, Luanda, 1-58.

Lazo, D.G., and Cichowolski, M. 2003. First plesiosaur remains from the Lower Cretaceous of the Neuquén Basin, Argentina. *Journal of Paleontology* 77 (4), pp. 784- 789.

Lee, M.S.Y. 2013. Turtle origins: insights from phylogenetic retrofitting and molecular scaffolds. *Journal of Evolutionary Biology* 26 (12), 2729-2738.

Leidy, J., 1851. [Descriptions of a number of fossil reptilian and mammalian remains]. *Proceedings from the Philadelphia National Academy of Science* 5, 325- 327.

Liebe L., and Hurum J.H. 2012. Gross internal structure and microstructure of plesiosaur limb bones from the Late Jurassic, central Spitsbergen. *Norwegian Journal of Geology* 92, 285-309.

Liu, J., Rieppel, O., Jiang, D.-Y., Aitchison, J.C., Motani, R., Zhang, Q.-Y., Zhou, C.-Y., and Sun, Y.-Y. 2011. A new pachypleurosaur (Reptilia: Sauropterygia) from the Lower Middle Triassic of southwestern China and the phylogenetic relationships of Chinese pachypleurosaurs. *Journal of Vertebrate Paleontology* 31(2), 292–302.

Lomax, D.R., and Wahl, W.R. 2013. A new specimen of the elasmoaurid plesiosaur *Zarafasaura oceanis* from the Upper Cretaceous (Maastrichtian) of Morocco. *Paludicola* 9(2), 97-109.

Lunde, G., Aubert, K., Lauritzen, O., and Lorange, E. 1992. Tertiary uplift of the Kwanza Basin in Angola; pp. 99-117 in Curnelle, R. (ed.), *Géologie Africaine: Colloque de Stratigraphie et de Paléogéographie des Bassins Sédimentaires Ouest-Africains*. Recuell des Communications, 6-8 May 1991, Libreville, Gabon.

Maisch, M.W., and Matzke, A.T. 2000. The Ichthyosauria, Stuttgarter Beiträge zur Naturkunde Serie B (Geologie und Paläontologie) 298, 1-159.

Maisey, J. G. 2000. Continental break up and the distribution of fishes of western Gondwana during the Early Cretaceous. *Cretaceous Research* 2, 281-314.

Malinzak, M.D., Kay, R.F., and Hullar, T.E. 2012 Locomotor head movements and semicircular canal morphology in primates. *Proceedings of the National Academy of Sciences of the United States of America* 109 (44), 17914-17919.

Martin, J.E., Sawyer, J.F., and Reguero, M., Case, J.A. 2007. Occurrence of a young elasmosaurid plesiosaur skeleton from the Late Cretaceous (Maastrichtian) of Antarctica. U.S. Geological Survey and The National Academies; USGS OF-2007-1047, Short Research Paper 066, DOI:10.3133/of2007-1047.srp066erica 109 (17), 914–17 919. (DOI:10.1073/pnas.1206139109)

Marton, L. G., Tari, G. C. and Lehman, C. T. 2000. Evolution of the Angolan passive margin, West Africa, with emphasis on post-salt structural styles. In *Geology and Geophysics of Continental Margins.* (eds Mohriak, W. U. and Talwani, M.). pp. 129-149. American Geophysical Union Geophysical Monographs 115

Marzola, M., Mateus, O., Milàn, J. and Clemmensen, L.B. 2018. A review of Palaeozoic and Mesozoic tetrapods from Greenland. © 2018 by Bulletin of the Geological Society of Denmark 66, 21–46. ISSN 2245-7070. (www.2dgf.dk/publikationer/bulletin).

Mateus, O., Polcyn, M.J., Jacobs, L.L., Araújo, R., Schulp, A.S., Marinheiro, J., Pereira, B. and Vineyard, D., 2012. Cretaceous amniotes from Angola: dinosaurs, pterosaurs, mosasaurs, plesiosaurs, and turtles. *V Jornadas Internacionales sobre Paleontolog´ıa de Dinosaurios y su Entorno* 71-105.

Mateus, O., Callapez, P.M., Polcyn, M.J., Schulp, A.S., Gonçalves, A.O., and Jacobs, L.L. 2019. "The Fossil Record of Biodiversity in Angola Through Time". Ch. 4 in *Biodiversity of Angola Science & Conservation: A Modern Synthesis*, edited by Brian J. Huntley, Vladmir Russo, Fernanda Lages, and Nuno Ferrand.

Muller, M. 1994. Semicircular duct dimensions and sensitivity of the vertebrate vestibular system. *Journal of Theoretical Biology*. 167, 239–256.

Müller, J. 2004. The relationships among diapsid reptiles and the influence of taxon selection. In *Recent Advances in the Origin and Early Radiation of Vertebrates* (eds Arratia, G., Wilson, M.V.H., Cloutier, R.). pp. 379-408. Verlag Dr. Freidrich Pfeil, München.

Nascimento, J.P. 1898. Exploraçâo Geographica e Mineralogica no Districto de Mossamedes em 1894-1895. Lisbon, TYP. da companhia nacional editora, 6-110.

Neenan, J.M., Reich, T., Evers, S.W., Druckenmiller, P.S., Voeten, D.F.A.E., Choiniere, J.N., Barrett, P.M., Pierce, S.E., and Benson, R.B.J. 2013. Evolution of the Sauropterygian Labyrinth with Increasingly Pelagic Lifestyles. *Current Biology* l https://doi.org/10.1016/j.cub.2017.10.069

Neto, M. 1960. Novidades paleontológicas. *Boletim dos Serviços Geológicos e Mineiros de Angola* 2, 73

Neto, M. 1964. O sedimentar costeiro de Angola. Algumas notas sobre o estado actual do seu conhecimento. Curso de Geologia do Ultramar. Junta de Investigações do Ultramar 2, 193-232.

Nixon, K.C. 1999. The Parsimony Ratchet, a new method for rapid parsimony analysis. *Cladistics* 15, 407-414.

Noè, L.F., Liston, J., and Evans, M. 2003. The first relatively complete exoccipital–opisthotic from the braincase of the Callovian pliosaur, *Liopleurodon*. *Geological Magazine* 140, 479–486.

Nurnberg, D., and Muller, D. 1991. The tectonic evolution of the South Atlantic from the late Jurassic to present. *Tectonics* 191, 27-53.

Nyblade, A. A. and Robinson, S. W. 1994. The African superswell. *Geophysical Research Letters* 21, 765-768.

Obata, I., Matsukawa, M., Shibata, K. 2007. Geological age and environments of the plesiosaurs and the mosasaurs from Japan. In: Jubilee Publication in Commemoration of Professor Kameis's 80th Birthday. Office of the Jubilee Events in Commemoration of Professor Kamei's 80th Birthday, Tokyo, 155-177.

Ogg, J.G., and Smith, A.G. 2004. The geomagnetic polarity time scale. In *A Geologic Time Scale* (eds Gradstein, F., Ogg, J. and Smith, A.). pp. 63-86. Cambridge University Press.

O'Gorman, J.P., and Varela, A.N. 2010. The oldest lower Upper Cretaceous plesiosaurs (Reptilia, Sauropterygia) from Southern Patagonia, Argentina. *Ameghiniana: Revista de la Asociasión Paleontologica Argentina* 47 (4), 448- 459.

O'Gorman, J.P., Lazo, D.G., Luci, L., Cataldo, C.S., Schwarz, E., Lescano, M., and Aguirre-Urreta, M.B. 2015. New plesiosaur records from the Lower Cretaceous of Neuquén Basin, west-central Argentina, with an updated picture of occurrences and facies relationships. *Cretaceous Research* 56, 372- 387

O'Gorman, J.P. 2015a. New insights on the *Aristoneces parvidens* (Plesiosauria, Elasmosauridae) holotype: New on an old specimen. *Ameghiniana*, DOI: 10.5710/AMGH.24.11.2015.2921

O'Gorman, J.P. 2015b. *Vegasaurus molyi*, gen. et sp. nov. (Plesiosauria, Elsmosauridae), from the Cape Lamb Member (lower maastrichtian) of the Snow Hill Island Formation, Vega Island, Antarctica, and remarks on Weddellian Elasmosauridae. *Journal of Vertebrate Paleontology* 35:3, e931285, DOI: 10.1080/02724634.2014.931285

O'Gorman, J.P. 2016. A Small Body Sized Non-Aristonectine Elasmosaurid (Sauropterygia, Plesiosauria) from the Late Cretaceous of Patagonia with comments on the relationships of the Patagonian and Antarctic Elasmosaurids. *Ameghiniana* 53(3), 245- 268.

O'Gorman, J.P. and Coria, R.A. 2016. A new elasmosaurid specimen from the upper Maastrichtian of Antarctica: new evidence of a monophyletic group of Weddellian elasmosaurids. *Alcheringa: An Australasian Journal of Palaeontology* 41(2), 240-249, DOI:10.1080/03115518.2016.1224318

O'Gorman, J.P., Panzeri, K.M., Fernández, M.S., Santillana, S., Moly, J.J., and Reguero, M. 2017a. A new elasmosaurid from the upper Maastrichtian López de Bertodano Formation: new data on weddellonectian diversity. *Alcheringa: An Australasian Journal of Palaeontology*, 42(4), 575-586, DOI: 10.1080/03115518.2017.1339233

O'Gorman, J.P., Otero, R.A., Hiller, N., Simes, J., and Terezow, M. 2017b. Redescription of *Tuarangisaurus keyesi* (Sauropterygia; Elasmosauridae), a key species from the uppermost Cretaceous of the Weddellian Province: Internal skull anatomy and phylogenetic position. *Cretaceous Research* 71, 118- 136.

O'Gorman, J.P., Santillana, S., Otero, R., and Reguero, R. 2019a. A giant elasmosaurid (Sauropterygia: Plesiosauria) from Antarctica: New information on elasmosaurid body size diversity and aristonectine evolutionary scenarios. *Cretaceous Research* 102, 37-58.

O'Gorman, J.P., Otero, R., Reguero, M., and Gasparini, Z. 2019b. Cretaceous Antarctic plesiosaurs: stratigraphy, systematics and paleobiogeography. *Advances in Polar Sciences* 30(3), 210-227, DOI: 10.13679/j.advps.2018.0049

O'Gorman, J.P. 2020. Elasmosaurid phylogeny and paleobiogeography, with a reappraisal of *Aphrosaurus furlongi* from the Maastrichtian of the Moreno Formation. *Journal of Vertebrate Paleontology*, DOI: 10.1080/02724634.2019.1692025.

O'Keefe, F.R. 2001. A cladistic analysis and taxonomic revision of the Plesiosauria (Reptilia: Sauropterygia). *Acta Zoologica Fennica* 213, 1-63.

O'Keefe, F.R. 2002. The evolution of plesiosaur and pliosaur morphotypes in the Plesiosauria. *Paleobiology* 28, 101-112.

O'Keefe, F.R., and Wahl., W. 2003. Preliminary report on the osteology and relationships of a new aberrant cryptocleidoid plesiosaur from the Sundance Formation, Wyoming. *Paludicola* 4, 48-68.

O'Keefe, F.R. 2004. Preliminary description and phylogenetic position of a new plesiosaur (Reptilia: Sauropterygia) from the Toarcian of Holzmaden, Germany. *Journal of Paleontology* 78, 973-988.

O'Keefe, F.R, and Hiller, N. 2006. Morphologic and ontogenetic patterns in elasmosaur neck length, with comments on the taxonomic utility of neck length variables. *Paludicola* 5, 206-229.

O'Keefe, F.R. 2006. Neoteny and plesiomorphic condition of the plesiosaur basicranium. In *Amniote Paleobiology* (eds Carrano, M.T., Gaudin, T.J., Blob, R.W., and Wible, J.R.). pp. 391-409. Chicago, IL: University of Chicago Press.

O'Keefe, F.R., and Street, H.P. 2009. Osteology of the cryptocleidoid plesiosaur *Tatenectes laramiensis*, with comments on the taxonomic status of the Cimoliasauridae. *Journal of Vertebrate Paleontology* 29(1), 48-57.

O'Keefe, F.R., Otero, R.A., Soto-Acuña, S., O'Gorman, J., Godfrey, S.J., and Chatterjee, S. 2017. Cranial anatomy of Morturneria seymourensis from Antarctica, and the evolution of filter feeding in plesiosaurs of the Austral Late Cretaceous. *Journal of Vertebrate Paleontology*, DOI: 10.1080/02724634.2017.1347570

Oman, C. M., Marcus, E. N., and Curthoys, I. S. 1987. The influence of the semicircular canal morphology on endolymph flow dynamics. *Acta Otolaryngologica* 103, 1–13.

Otero, R.A., Soto-Acuña, S., and Rubilar-Rogers, D. 2012. A postcranial skeleton of an elasmosaurid plesiosaur from the Maastrichtian of central Chile, with comments on the affinities of Late Cretaceous plesiosauroids from the Weddellian Biogeographic Province. *Cretaceous Research* 37, pp. 89- 99.

Otero, R.A., Soto-Acuña, S., O'Keefe, F.R., O'Gorman, J.P., Stinnesbeck, W., Suárez, M.E., Rubilar-Rogers, D., Salazar, C., and Quinzio-Sinn, L.A. 2014a. *Aristonectes quiriquinensis*, sp. nov., A New Highly Derived Elasmosaurid from the Upper Maastrichtian of Central Chile. *Journal of Vertebrate Paleontology*, 34(1), 100-125.

Otero, R.A., Soto-Acuña, S., Vargas, A.O., and Rubilar-Rogers, D. 2014b. A new postcranial skeleton of an elasmosaurid plesiosaur from the Upper Cretaceous of central Chile and reassessment of *Cimoliasaurus andium* Deecke. *Cretaceous Research* 50, pp. 318- 331.

Otero, R.A., Soto-Acuña, S., Oyarzún J.L. 2015. New elasmosaurids (Plesiosauria, Sauropterygia) from the Late Cretaceous of the Magallanes Basin, Chilean Patagonia: evidence of a faunal turnover during the Maastrichtian along the Weddelian Biogeographic Province. *Andean Geology* 42, 237-267.

Otero, R.A. 2016. Taxonomic reassessment of *Hydralmosaurus* as *Styxosaurus*: new insights on the elasmosaurid neck evolution throughout the Cretaceous. *PeerJ* 4:e1777; DOI: 10.7717/peerj.1777

Otero, R.A., O'Gorman, J.P., Hiller, N., O'Keefe, F.R., and Fordyce, E.R. 2016. *Alexandronectes Zealandiensis* gen. et sp. nov., a new aristonectine plesiosaur from the lower Maastrichtian of New Zealand. *Journal of Vertebrate Paleontology*. DOI: 10.1080/02724634.2015.1054494.

Otero R.A., Soto-Acuña, S., and O'Keefe, F.R. 2018. Osteology of *Aristonectes quiriquinensis* (Elasmosauridae, Aristonectinae) from the upper Maastrichtian of central Chile. *Journal of Vertebrate Paleontology*, DOI: 10.1080/02724634.2017.1408638

Otero, R.A., O'Gorman, J.P., Moisley, W.L., Terezow, M., and McKee, J.A.W. 2018. A juvenile *Tuarangisaurus keysi* Wiffen and Moisley 1986 (Plesiosauria, Elasmosauridae) from the Upper Cretaceous of New Zealand, with remarks on its skull anatomy. *Cretaceous Research* 85, 214- 231.

Owen, R., 1860. On the orders of fossil and recent Reptilia and their distribution in time. *Report of the British Association for the Advancement of Science* 29, 153-166.

Pahlu, D.J., and Sheil, C.A. 2013. Anatomy of the Fully Formed Chondrocranium of *Emydura subglobosa* (Chelidae): A Pleurodiran Turtle. *Journal of Morphology* 274, 1-10.

Páramo, M.E., Gómez-Perez, M., Noé, L.F., Etayo- Serno. F. 2016. *Stenorhynchosaurus munozi*, gen. et sp. nov. a new pliosaurid from the Upper Barremian (Lower Cretaceous) of Villa de Leiva, Columbia, South America. *Revista de la Academia Columbiana de Ciencias Exactas, Fisícas y Naturales* 40 (154), pp. 84-103.

Páramo, M. E., Benavides, C.D., and Gutiérrez, I.E. 2018. A new large Pliosaurid from the Barremian (Lower Cretaceous) of Sáchica, Boyacá, Colombia. *Earth Sciences Research Journal* 22, pp. 223-238. DOI: 10.15446/esrj.v22n4.69916.

Parámo, M.E., O'Gorman, J.P., Gasparini, Z., Padilla, S., and Parra-Ruge, M.L. 2019. A new late Aptian elasmosaurid from the Paja Formation, Villa de Leiva, Columbia. *Cretaceous Research* 99, 30- 40.

Persson, P. O. (1963). A revision of the classification of the Plesiosauria with a synopsis of the stratigraphical and geographical distribution of the group. *Lunds Universitets Årsskrift*, series 2 (59), 1–60.

Polcyn, M. J., Jacobs, L.L., Schulp, A.S. and Mateus, O. 2010. The North African mosasaur *Globidens phosphaticus* from the Maastrichtian of Angola. *Historical Biology* 22, 175-185.

Porter W.R., and Witmer L.M. 2015. Vascular Patterns in Iguanas and Other Squamates: Blood Vessels and Sites of Thermal Exchange. *PLoS ONE* 10(10): e0139215, DOI:10.1371/journal.pone.0139215

Quesada, J.M., Pérez-García, A., Gasulla, J.M., Ortega, F. 2019. Plesiosauria remains from the Barremian of Morella (Castellón, Spain) and first identification of Leptocleididae in the Iberian record. *Cretaceous Research* 94, 8-24, DOI: 10.1016/j.cretres.2018.10.010

Rabinovich, R., Hanan, H., Schudack, M., Schudack, U., Ashckenanzi-Polivoda, S., and Rogolsky, G. 2014. A late Cretaceous elasmosaurid of the Tethys Sea margins (southern Negev, Israel) and its palaeogeographic reconstruction. *Netherlands Journal of Geosciences*, DOI: 10.1017/njg.2014.26

Reyment, R. A. and Dingle, R. V. 1987. Palaeogeography of Africa during the Cretaceous Period. *Palaeogeography, Palaeoclimatology, Palaeoecology* 59, 93-116.

Rieppel, O. 1989. A new pachypleurosaur (Reptilia: Sauropterygia) from the Middle Triassic of Monte San Giorgio, Switzerland. *Philosophical Transactions of the Royal Society of London* B 323, 1-73.

Rieppel, O. 1994. *Osteology of Simosaurus gaillardoti and the relationships of stem-group Sauropterygia* (Reptilia, Diapsida). *Fieldiana (Geology) New Series* 28, 1-85.

Rieppel, O. 1999. Phylogeny and paleobiogeography of Triassic Sauropterygia: problems solved and unresolved. *Palaeogeography, Palaeoclimatology, Palaeoecology* 153, 1–15.

Rieppel, O., Reisz, R., 1999. The Origin and early evolution of turtles. *Annual Review of Ecology and Systematics* 30, 1-22.

Robinson, J.A., 1975. The locomotion of plesiosaurs. *Neues Jahrbuch f¨ur Geologie und Paläontologie, Abhandlungen* 149, 286-332.

Romer, A.S. and Lewis, A.D. 1959. A mounted skeleton of the giant plesiosaur *Kronosaurus*. *Breviora* 112, 1- 15.

Romer, A.S. 1976. *The osteology of the reptiles*. Chicago: University of Chicago Press.

Sachs, S., 2005a. Redescription of *Elasmosaurus platyurus* Cope 1868 (Plesiosauria: Elasmosauridae) from the Upper Cretaceous (lower Campanian) of Kansas, USA. *Paludicola* 5, 92–106.

Sachs, S. 2005b. *Tuarangisaurus australis* sp. nov. (Plesiosauria: Elasmosauridae) from the Lower Cretaceous of Northeastern Queensland, with additional notes on the phylogeny of Elasmosauridae. *Memoirs of the Queensland Museum* 50 (2), 425- 440. Brisbane. ISSN 0079-8835.

Sachs, S., Kear, B.J., and Everhart, M.J. 2013. Revised Vertebral Count in the ‘‘Longest-Necked Vertebrate’’ *Elasmosaurus platyurus* Cope 1868, and Clarification of the Cervical-Dorsal Transition in Plesiosauria. *PLoS ONE* 8(8) e70877, DOI:10.1371/journal.pone.0070877

Sachs, S., and Kear, B. P. 2015. Postcranium of the paradigm elasmosaurid plesiosaurian *Libonectes morgani* (Welles, 1949). *Geological Magazine* 152, 694–710.

Sachs, S., Hornung, J.J., and Kear, B.P. 2016a. Reapprasial of Europe’s most complete Early Cretaceous plesiosaurian: *Brancasaurus brancai* Wegner, 1914 from the “Wealden facies” of Germany. *PeerJ* 4: e2813 https://doi.org/10.7717/peerj.2813

Sachs, S., Lindgren, J., Kear, B.P. 2016b. Re-description of *Thalassomedon haningtoni*- an elasmosaurid from the Cenomanian of North America. In 5th Triennial Mosasaur Meeting- A Global Perspective on Mesozoic Marine Amniotes- Abstracts and Program, pp. 38-40.

Sachs, S., Hornung, J.J., and Kear, B.P. 2017. A new basal elasmosaurid (Sauropterygia: Plesiosauria) from the Lower Cretaceous of Germany, *Journal of Vertebrate Paleontology*, 37(4), e1301945, DOI: 10.1080/02724634.2017.1301945

Sachs, S., Kear, B.P. 2017. Redescription of the elasmosaurid plesiosaurian *Libonectes atlasense* from the Upper Cretaceous of Morocco. *Cretaceous Research* 74, 205- 222.

Sachs, S., Lindgren, J., and Kear, B.P. 2018. Reassessment of the *Styxosaurus snowii* (Williston, 1890) holotype specimen and its implications for elasmosaurid plesiosaurian interrelationships, *Alcheringa: An Australian Journal of Palaeontology*, DOI: 10.1080/03115518.2018.1508613

Sahagian, D. 1988. Epeirogenic motions of Africa as inferred from Cretaceous shoreline deposits. *Tectonics* 7:125-138.

Sato, T., and Storrs, G. 2000. An early polycotylid plesiosaur (Reptilia: Sauropterygia) from the Cretaceous of Hokkaido, Japan. *Journal of Paleontology* 74 (5), 907- 914.

Sato, T. 2002. Description of plesiosaurs (Reptilia: Sauropterygia) from the Bearpaw Formation (Campanian–Maastrichtian) and a phylogenetic analysis of the Elasmosauridae. PhD thesis, University of Calgary.

Sato, T., 2003. *Terminonatator ponteixensis*, a new elasmosaur (Reptilia; Sauropterygia) from the Upper Cretaceous of Saskatchewan. *Journal of Vertebrate Paleontology* 23, 89–103.

Sato, T. 2005. A new polycotylid plesiosaur (Reptilia: Sauropterygia) from the Upper Cretaceous Bearpaw Formation in Saskatchewan, Canada. *Journal of Paleontology* 79, 969-980.

Sato, T., Hasegawa, Y., and Manabe, M. 2006. A new elasmosaurid plesiosaur from the upper Cretaceous of Fukushima, Japan. *Palaeontology* 49 (3), 467-484.

Sato, T., and Wu, X. 2011. Braincase of a Polycotylid Plesiosaur (Reptilia: Sauropterygia) from the Upper Cretaceous of Manitoba, Canada. *Journal of Vertebrate Paleontology* 31 (2), 313-329.

Sato, T., Konishi, T., Hirayama, R., and Caldwell, M.W. 2012. A Review of the Upper Cretaceous marine reptiles from Japan. *Cretaceous Research* 37, 319-340.

Schulp, A.S., Polcyn, M.J., Mateus, O., Jacobs, L.L., Morais, M.L. and Tavares, T. da S. 2006. New mosasaur material from the Maastrichtian of Angola, with notes on the phylogeny, distribution and paleoecology of the genus *Prognathodon*, 57-67 in: Schulp, A.S., (ed.), *On Maastricht Mosasaurs*. *Publicaties van het Natuurhistorisch Genootschap in Limburg*, 45.

Schulp, A.S., Polcyn, M.J., Mateus, O., Jacobs, L.L. and Morais, M.L. 2008. A new species of *Prognathodon* (Squamata, Mosasauridae) from the Maastrichtian of Angola, and the affinities of the mosasaur genus *Liodon*. Proceedings of the Second Mosasaur Meeting Hays, Kansas, 1-12.

Schulp, A.S., Polcyn, M.J., Mateus, O. and Jacobs, L.L. 2013. Two rare mosasaurs from the Maastrichtian of Angola and the Netherlands. *Netherlands Journal of Geosciences* 92(1), 3-10.

Schumacher, B.A., and Everhart, M.J. 2005. A Stratigraphic and Taxonomic review of *Plesiosaurs* from the old "Fort Benton Group" of Central Kansas: A New Assessment of Old Records. *Paludicola* 5(2), 33-54.

Schutz H, Jamniczky HA, Hallgrimsson B, and Garland T. 2014. Shape-Shift: semicircular canal morphology responds to selective breeding for increased locomotor activity. *Evolution* 68, 1–39, DOI:10.5061/ dryad.3sv4p

Sennikov, A.G, and Arkhangelsky, M.S. 2010. On a Typical Jurassic Sauropterygian from the Upper Triassic of Wilczek Land (Franz Josef Land, Arctic Russia). *Paleontological Journal* 44(5), 567–572.

Serratos, D.J. Druckenmiller, P., and Benson, R.B.J. 2017. A new elasmosaurid (Sauropterygia, Plesiosauria) from the Bearpaw Shale (Late Cretaceous, Maastrichtian) of Montana demonstrates multiple evolutionary reductions of neck length within Elasmosauridae. *Journal of Vertebrate Paleontology* 37, e1278608

Shannon, L.V. (1985): The Benguela ecosystem Part I. Evolution of the Benguela, physical features and processes. *Oceanography and Marine Biology Annual Reviews*, 23, 105-182.

Shimada, K., Tsuihiji, T., Sato, T. and Hasegawa, Y. 2010. A remarkable case of a shark-bitten elasmosaurid plesiosaur. *Journal of Vertebrae Paleontology* 30(2), 592-597.

Sikes, D.S., and Lewis, P.O. 2001. Beta Software, Version 1. PAUPRat: PAUP Implementation of the Parsimony Ratchet. Distribution by the authors. Department of Ecology and Evolutionary Biology, University of Connecticut, Storrs, Connecticut.

Sipla J.S. 2007. The semicircular canals of birds and non-avian theropod dinosaurs. Stony Brook, NY: Stony Brook Univ.

Smith, A.S., and Dyke, G.J. 2008. The skull of the giant predatory pliosaur *Rhomaleosaurus cramptoni*: implications for plesiosaur phylogenetics. *Naturwissenschaften* 95, 975- 980, DOI 10.1007/s00114-008-0402-z

Smith, A.S., and Vincent, P. 2010. A new genus of pliosaur (Reptilia: Sauropterygia) from the Lower Jurassic of Holzmaden, Germany. *Palaeontology* 53 (5), 1049-1063.

Smith, A.S., Araújo, R., and Mateus, O. 2012. A new plesiosauroid from the Toarcian (Lower Jurassic) of Alhadas, Portugal. *Acta Palaeontologica Polonica* 57 (2), 257–266.

Smith, A.S., and Araújo, R. 2017. *Thaumatodracon wiedenrothi*, a morphologically and stratigraphically intermediate new rhomaleosaurid plesiosaurian from the Lower Jurassic (Sinemurian) of Lyme Regis. *Palaeontographica, Abteilung A: Palaeozoology- Stratigraphy* 308(4-6), 89-125.

Spoor F, Garland T, Krovitz G, Ryan TM, Silcox MT, and Walker A. 2007 The primate semicircular canal system and locomotion. *Proceedings of the National Academy of Sciences of the United States of America* 104(10), 808–10 812, DOI:10.1073/pnas.0704250104

Standlee, L. A., Brumbaugh, W. D. and Cameron, N. R. 1992. "Controlling factors in the initiation of the South Atlantic Rift system", 141-152 in Curnelle, R. (ed.), *Géologie Africaine: Colloque de Stratigraphie et de Paléogéographie des Bassins Sédimentaires Ouest-Africains*. Recuell des Communications, 6-8 May 1991, Libreville, Gabon.

Storrs, G.W. 1991. Anatomy and Relationships of *Corosaurus alcovensis* (Diapsida: Sauropterygia) and the Triassic Alcova Limestone of Wyoming. *Peabody Museum Bulletin* 19(2), 1-151.

Strganac, C., Jacobs, L.L., Ferguson, K.M., Polcyn, M.J., Mateus, O., Schulp, A.S., Morais, M.L. and Gonçalves, A.O. 2014. Carbon isotope stratigraphy, magnetostratigraphy, and 40Ar/39Ar age of the Cretaceous South Atlantic coast, Namibe Basin, Angola. *Journal of African Earth Sciences* 99, 452-462.

Strganac, C., Jacobs, L.L., Polcyn, M.J., Mateus, O., Myers, T.S., Salminen, J., May, S.R., Araújo, R., Ferguson, K.M., Gonçalves, A.O., Morais, M.L., Schulp, A.S., and Tavares, T.S. 2015. Geological setting and paleoecology of the Upper Cretaceous Bench 19 Vertebrate Bonebed at Bentiaba, Angola. *Netherlands Journal of Geosciences*, 121-136.

Sues, H. 1987. Postcranial skeleton of Pistosaurus and interrelationships of Sauropterygia (Diapsida). *Zoological Journal of the Linnean Society* 90, 109-131.

Sues, H. 2019. *The Rise of Reptiles: 320 Million Years of Evolution*. Baltimore, Johns Hopkins University Press, DOI:10.1353/book.67468. 15-21.

Tarlo, L. B. (1960). A review of the upper Jurassic pliosaurs. *Bulletin of the British Museum (Natural History), Geology Series* 4, 147–189.

Taylor, M. I 992a. Taxonomy and taphonomy of *Rhomaleosaurus zetlandicus* (Plesiosauria, Reptilia) from the Toarcian (Lower Jurassic) of the Yorkshire coast. *Yorkshire Geological Society Proceedings* 49:49-55.

Taylor, S., and A. Cruickshank. 1993. Cranial anatomy and functional morphology of *Pliosaurus brachyspondylus* (Reptilia: Plesiosauria) from the Upper Jurassic of Westbury, Whitshire. *Philosophical Transactions of the Royal Society of London* B 341, 399-418

Taylor, M.A. 1997. *Before the Dinosaur: The Historical Significance of the Fossil Marine Reptiles*. In *Ancient Marine Reptiles*, edited by Jack M. Callaway and Elizabeth L. Nicholls. San Diego, Academic Press.

Thulborn, T., and S. Turner. 1993. An elasmosaur bitten by a pliosaur. *Modern Geology* 18, 489–501.

Torrens, H.S. 1995. Mary Anning (1799-1847) of Lyme: “the greatest fossilist the world ever knew”. *British Journal for the History of Science* 28, 257-284.

Utsunomiya, S. 2019. Oldest Elasmosauridae (Plesiosauria) in East Asia from the Upper Cretaceous Goshoura Group, Shishijima Island, Southwestern Japan. *Bulletin of the Osaka Museum of Natural History* 73, 23-35.

Vincent, P. and Taquent. P. 2010. A plesiosaurs specimen from the Lias of Lyme Regis: the second ever discovered plesiosaurs by Mary Anning. *Geodiversitas* 32(3), 377-399.

Vincent, P., Bardet, N., Suberbiola, X.P., Bouya, B., Amaghzaz, M., Meslouh, S. 2011. *Zarafasaura oceanis*, a new elasmosaurid (Reptilia: Sauroperygia) from the Maastrichtian Phosphates of Morocco and the palaeobiogeography of latest Cretaceous plesiosaurs. *Gondwana Research* 19, pp. 1062- 1073.

Vincent, P., Bardet, N., Houssaye, A., Amaghzaz, M., and Meslouh, S. 2013. New plesiosaur specimens from the Maastrichtian Phosphates of Morocco and their implications for the ecology of the latest Cretaceous marine apex predators. *Gondwana Research* 24(2), 796-805.

Voeten, D.F.A.E., Reich, T., Araújo, R, and Scheyer, T.M. 2018. Synchrotron microtomography of a *Nothosaurus marchicus* skull informs on nothosaurian physiology and neurosensory adaptations in early Sauropterygia. *PLoS ONE* 13(1): e0188509. https://doi.org/10.1371/journal.pone.0188509

Wegner T.H. 1914. *Brancasaurus brancai* n. g. n. sp., ein Elasmosauride aus dem Wealden Westfalens. In *Frestschrift für Wilhelm Branca zum* 70. Geburtstage 1914. Leipzig: Borntraeger, 235-305.

Welles, S. P. 1943. Elasmosaurid plesiosaurs with description of new material from California and Colorado. *Memoirs of the University of California* 13, 125–254.

Welles, S.P. 1949. A new elasmosaur from the Eagle Ford Shale of Texas. Part I. Systematic description. *Fondren Science Series* 1, 1–28.

Welles, S.P. 1952. A Review of the North American Cretaceous Elasmosaurs. *University of California Publications in Geological Sciences*, 47-143.

Welles, S.P., and Bump, J.D. 1949. *Alzadasaurus pembertoni*, A new elasmosaur from the Upper Cretaceous of South Dakota. *Journal of Vertebrate Paleontology* 23(5), 521-535.

Welles, S. P. 1962. A new species of elasmosaur from the Aptian of Colombia and a review of the Cretaceous plesiosaurs. *University of California Publications in Geological Sciences* 44, 1–96.

Werner, C., and Bardet, N. 1996. New record of elasmosaurs (Reptilia, Plesiosauria) in the Maastrichtian of the Western Desert of Egype. *Berliner geowissenschaften Abhandlungen*, E18, 335-341.

White, T. E. (1940). Holotype of *Plesiosaurus longirostris* Blake and classification of the Plesiosaurs. *Journal of Paleontology* 14, 451–467.

Wiffen, J., and Moisley, W.L. 1986. Late Cretaceous reptiles (Families Elasmosauridae and Pliosauridae) from the Mangahouanga Stream, North Island, New Zealand, *New Zealand Journal of Geology and Geophysics*, 29:2, 205-252, DOI: 10.1080/00288306.1986.10427535

Wiffen, J., De Buffr´enil, V., De Ricql`es, A. and Mazin, J.-M., 1995. Ontogenetic evolution of bone structure in Late Cretaceous Plesiosauria from New Zealand. *Geobios* 28, 625-640.

Williston, S.W. 1890. A new plesiosaur from the Niobrara Cretaceous of Kansas. *Transactions of the Kansas Academy of Sciences* 12, 174-178.

Williston, S.W. 1903. North American plesiosaurs. Part 1. Publication n. 73, Field Columbian Museum, 3-77.

Williston, S.W. 1906. North American plesiosaurs, *Elasmosaurus*, *Cimoliasaurus*, and *Polycotylus*. *American Journal of Science* (4), 21, 221-236.

Williston, S. W. 1907. The skull of *Brachauchenius*, with observations on the relationships of the plesiosaurs. *Proceedings of the U. S. National Museum* 32, 477–489.

Williston, S.W., Moodie, R.L. 1913. A new plesiosaurian genus from the Cretaceous of Kansas. *Bulletin of Geological Society of America* 24, 120-121 (abstract)

Williston, S.W. 1914. *Water reptiles of the past and present*. Chicago, University of Chicago Press.

Williston, S.W., Moodie, R.L. 1917. *Ogmodirus martini*, a new plesiosaur from the Cretaceous of Kansas. *Kansas University Science Bulletin* 10, 61-73.

Williston, S.W. 1925. *The osteology of the reptiles*. Edited by William K. Gregory. Cambridge, Harvard University Press.

Witmer, L.M., and Ridgely, R.C. 2009. New insights into the brain, braincase, and ear region of *Tyrannosaurus* (Dinosauria, Theropoda), with implications for sensory organization and behavior. *The Anatomical Record* 292, 1266-1296.

Yang A, and Hullar TE. 2007. Relationship of semicircular canal size to vestibular-nerve afferent sensitivity in mammals. *Journal of Neurophysiology* 98, 3197–3205, DOI:10.1152/jn.00798.2007

Yi H, and Norell MA. 2015. The burrowing origin of modern snakes. *Science Advances* 1, 1–5. DOI:10.1126/sciadv.1500743

Zinmeister, W.J. 1979. Biogeographic significance of the late Mesozoic and early Tertiary molluscan faunas of Seymour Island (Antarctic Peninsula) to the final breakup of Gondwanaland. In *Historical Biogeography, Plate Tectonics and the Changing Environment*. (eds Gray, J. and Boucot, A.J.). pp. 349-355. Proceedings of the Thirty-seventh Annual Biology Colloquium and Selected Papers 27. Ohio State University. Institute of Polar Studies, Columbus, OH.

Zverkov, N.G., Averianov, A.O., and Popov, E.V. 2017. Basicranium of an elasmosaurid plesiosaur from the Campanian of European Russia. Alcheringa: *An Australasian Journal of Palaeontology*, DOI: 10.1080/03115518.2017.1302508

Annex I: centrum measurements for elasmosaurids used to calculate H-I index

T. haningtoni (CMNH 1588) measurements from Welles (1943)

cervical vertebra number	L	W	H	HI
3	38	41	44	116
4	47	55	50	106
5	44	55	43	98
6	47	67	45	96
7	54	60	39	72
8	46	70	46	100
9	54	67	46	85
10	56	68	50	89
11	54	67	50	93
12	57	63	54	95
13	58	67	52	90
14	57	74	54	95
15	65	75	56	86
16	62	79	58	94
17	63	83	59	94
18	72	82	67	93
19	80	80	62	78
20	79	82	63	80
21	87	85	66	76
22	87	87	79	91
23	97	86	72	74
24	97	87	73	75
25	90	90	77	86
26	95	84	74	78
27	103	83	73	71
28	105	100	73	70
29	104	95	79	76
30	105	93	83	79
31	105	?85	?85	81
32	110	90	95	86
33	115	97	82	71
34	117	103	85	73
35	123	102	81	66
36	118	102	88	75
37	122	109	85	70
38	125	113	97	78
39	123	112	105	85
40	122	110	102	84
41	137	134	105	77
42	127	137	110	87
43	132	143	112	85
44	129	142	111	86
45	134	142	114	85
46	131	145	116	86
47	137	151	117	85
48	140	155	127	91
49	135	163	119	88
50	130	160	127	98
51	NA	160	117	
52	120	172	117	98
53	130	165	124	95
54	140	167	124	89
55	136	165	119	88
56	130	183	128	98
57	136	180	126	93
58	123	170	127	103
59	115	170	130	113
60	113	185	125	111
61	110	188	123	112
62	110	192	130	118

L. morgani (SMU SMP 69120) measurements from Welles (1949)

cervical vertebra number	L	W	H	HI
3	22	42	32	109
4	35	45		
5	37	54	?30	81
6	39	54	?32	82
7	41	53	?37	90
8	44	55	42	95
9	45	55	NA	
10	49	60	NA	
11	50	57	NA	
12	52	62	NA	
13	52	63	?40	77
14	55	?65	40	73
15	58	65	42	72
16	61	65	NA	
17	64	67	42	66
18	57		NA	
19	65	67	NA	
20	70		NA	
21	67	77	47	70
22	73		NA	
23	NA	24	NA	
24	77		NA	
25	80	82	52	65
26	82	79	NA	
27	85	85	55	65
28	87	82	NA	
29	92	88	NA	
30	95	93	?55	58
31	95	NA	63	66
32	102	NA	NA	
33	102	NA	NA	
34	100	91	70	70
35	101	100	NA	
36	100	105	NA	
37	110	105	72	65
38	102	107	80	78
39	105	112	NA	
40	104	112	NA	
41	105	120	NA	
42	106	117	77	73
43	107	117	80	75
44	110	121	82	75
45	110	121	NA	
46	110	120	NA	
47	110	120	NA	
48	110	125	NA	
49	NA	125	?90	
50	105	NA	NA	
51	110	NA	NA	
52	115	NA	NA	
53	105	NA	NA	
54	115	NA	NA	
55	110	NA	NA	
56	112	NA	NA	
57	110	NA	NA	
58	NA	NA	NA	
59	102	NA	NA	
60	95	NA	NA	
61	102	NA	NA	
62	98	NA	NA	

H. alexandrae (UCMP 33912) measurements from Welles (1943)

cervical vertebra number	L	W	H	HI
3	34	45	NA	
4	37	46	33	89
5	39	38	33	85
6	42	44	35	83
7	41	NA	36	88
8	43	NA	NA	
9	43	NA	36	84
10	48	NA	NA	
11	47	NA	NA	
12	50	56	35	70
13	53	55	38	72
14	57	NA	NA	
15	58	60	48	83
16	61	NA	NA	
17	63	NA	41	65
18	63	NA	43	68
19	64	NA	NA	
20	65	NA	39	60
21	68	NA	NA	
22	69	NA	NA	
23	73	74	50	68
24	NA	75	49	
25	76	79	NA	
26	76	78	NA	
27	73	76	NA	
28	81	82	NA	
29	78	NA	NA	
30	83	NA	NA	
31	83	NA	NA	
32	87	86	81	93
33	87	95	88	101
34	87	90	79	91
35	88	80	79	90
36	86	89	82	95
37	87	94	82	94
38	90	92	83	92
39	91	96	87	96
40	92	90	86	93
41	89	87	86	97
42	95	76	88	93
43	94	92	89	95
44	91	101	94	103
45	93	93	91	98
46	95	101	92	97
47	94	103	93	99
48	90	91	96	107
49	89	110	94	106
50	88	108	96	109
51	96	95	93	97
52	87	104	99	114
53	99	108	99	100
54	89	119	102	115
55	86	114	105	122
56	91	116	106	116
57	91	118	103	113
58	88	117	103	117
59	87	116	102	117
60	88	110	107	122
61	89	120	98	
62	89	117	104	

Styxosaurus sp. (AMNH 1495) measurements from Otero (2016)

cervical vertebra number	L	W	H	HI
3	40	46	35	89
4	41	46	35	84
5	44	49	34	77
6	45	50	37	83
7	46	50	38	84
8	47	51	37	79
9	53	51	42	78
10	51	50	39	72
11	56	52	42	75
12	57	55	41	72
13	61	?55	42	69
14	57	57	40	69
15	64	60	46	72
16	70	63	45	64
17	74	60	50	68
18	72	63	54	76
19	74	64	55	74
20	79	66	57	72
21	78	66	57	73
22	81	65	60	74
23	85	67	60	71
24	88	69	61	69
25	88	72	62	70
26	93	71	62	67
27	94	77	64	68
28	96	76	66	68
29	98	76	66	67
30	99	77	67	67
31	100	80	69	69
32	101	85	73	72
33	104	85	74	71
34	109	90	75	69
35	89	94	83	94
36	109	101	81	74
37	111	110	79	71
38	113	110	88	78
39	113	113	?93	83
40	114	?112	?97	85
41	107	114	82	76
42	NA	NA	NA	
43	NA	NA	NA	
44	112	119	93	83
45	118	111	?97	82
46	132	123	?99	75
47	115	117	94	82
48	112	124	102	91
49	113	124	?	
50	127	127	94	74
51	108	119	93	86
52	112	127	NA	
53	120	134	89	74
54	106	124	89	84
55	123	126	96	79
56	108	122	93	86
57	NA	122	101	
58	NA	NA	NA	
59	NA	NA	NA	
60	116	128	102	87
61	NA	NA	NA	
62	NA	128	NA	
63	NA	NA	104	

S. browni (AMNH 5385) measurements from Otero (2016)

cervical vertebra number	L	W	H	HI
3	38	41	30	77
4	42	40	28	68
5	45	38	34	74
6	43	40	32	73
7	50	40	33	66
8	49	43	33	68
9	51	46	33	65
10	54	48	31	57
11	57	48	34	60
12	58	52	32	56
13	61	49	34	56
14	62	51	36	57
15	64	54	38	58
16	61	55	38	62
17	66	54	41	62
18	68	60	37	55
19	68	57	38	56
20	69	61	43	62
21	71	56	?42	59
22	71	67	39	55
23	73	65	46	64
24	79	63	NA	
25	80	63	50	63
26	NA	NA	NA	
27	?83	NA	NA	
28	87	83	NA	
29	89	76	?62	69
30	95	?84	?62	65
31	94	NA	?69	74
32	90	NA	64	71
33	94	NA	62	66
34	100	NA	72	72
35	NA	NA	NA	
36	105	86	NA	
37	103	89	?67	65
38	98	?92	64	65
39	102	100	62	60
40	107	86	NA	
41	107	?104	66	62
42	115	?102	?70	61
43	111	93	69	62
44	117	100	79	67
45	116	?100	79	68
46	116	106	79	68
47	118	109	71	60
48	117	111	72	62
49	114	107	78	69
50	117	117	79	67
51	116	120	79	68
52	116	126	82	71
53	119	?125	?80	67
54	119	113	NA	
55	115	132	84	73
56	116	128	84	73
57	111	133	84	76
58	108	139	91	84
59	105	139	93	89
60	NA	NA	NA	
61	101	NA	NA	
62	103	NA	NA	
63	104	139	95	92
64	99	143	94	95
65	96	158	103	107

E. platyurus (ANSP 10081) measurements from Sachs (2005)

cervical vertebra number	L	W	H	HI
3	4	4	3	70
4	4	4	3	72
5	4	4	3	77
6	4	4	3	72
7	5	4	3	64
8	5	3	3	70
9	5	4	3	62
10	5	4	3	61
11	6	5	4	59
12	6	4	3	56
13	5	4	4	70
14	6	5	4	67
15	6	5	4	63
16	6	5	4	64
17	6	5	4	68
18	6	5	4	67
19	6	6	4	67
20	7	5	4	59
21	7	7	4	60
22	7	5	5	69
23	7	6	5	66
24	8	6	5	68
25	8	6	5	58
26	8	6	5	59
27	8	6	5	65
28	8	6	5	65
29	9	6	5	62
30	9	6	6	66
31	9	7	6	71
32	9	7	5	58
33	10	6	6	60
34	10	6	6	59
35	10	6	6	61
36	9	6	6	70
37	9	7	6	66
38	11	6	8	71
39	10	7	7	66
40	10	6	7	70
41	11	6	7	65
42	11	6	7	69
43	11	8	8	73
44	11	7	8	73
45	11	7	8	71
46	12	7	8	67
47	12	NA	NA	
48	12	6	8	63
49	12	7	8	70
50	NA	NA	9	
51	11	NA	NA	
52	12	NA	NA	
53	NA	7	9	
54	11	NA	NA	
55	11	NA	NA	
56	12	NA	NA	
57	12	NA	NA	
58	12	NA	NA	
59	11	NA	NA	
60	11	10	10	91
61	11	10	10	90
62	11	NA	NA	
63	11	11	9	86
64	10	12	10	105
65	11	11	11	100
66	10	NA	NA	
67	10	13	10	105
68	10	13	10	100
69	10	13	10	100
70	9	NA	NA	
71	9	12	10	111
72	9	12	9	106

Aristonectes parvidens (MLP 40-XI-14-6) measurements from O'Gorman (2016)

cervical vertebra number	L	W	H	HI
3	40	58	45	113
4	44	60	49	111
5	46	69	51	111
6	49	70	55	112
7	52	68	50	96
8	51	75	55	108
9	52	71	55	106
10	52	72	54	104
11	55	78	55	100
12	56	87	56	100
13	56	91	60	107
14	56	86	57	102
15	55	90	60	109
16	68	95	68	100
17	58	99	62	107
18	63	97	62	98
19	63	99	64	102

Aristonectes quiriquinensis (SGO.PV.957) measurements from Otero et al., (2014b)

cervical vertebra number	L	W	H	HI
3	46	?67	?54	117
4	52	NA	NA	
5	NA	NA	NA	
6	NA	NA	NA	
7	57	75	55	96
8	55	77	58	107
9	NA	77	NA	
10	56	NA	58	103
11	51	?79	?66	129
12	NA	NA	NA	
13	NA	NA	NA	
14	NA	NA	NA	
15	NA	NA	91	
16	NA	NA	89	
17	82	?91	?81	99
18	84	?95	81	96
19	83	?99	79	95
20	?80	NA	?82	102
21	?78	NA	?82	106
22	?76	NA	?81	105
23	?84	NA	?79	95
24	74	NA	NA	
25	NA	NA	NA	
26	NA	NA	NA	
27	85	NA	?96	113
28	83	?113	?100	121
29	83	?121	?113	137
30	?83	?134	?105	126
31	?86	?134	?102	120
32	?87	?129	?111	129
33	88	NA	NA	
34	?79	NA	NA	
35	87	NA	NA	
36	88	NA	NA	
37	NA	NA	NA	

Cardiocorax mukulu (MGUAN PA278 and MGUAN PA103 measured by M.M. Measurements of centra were rounded up to the ones place to be consistent with measurements of centra taken by other authors. There is no articulated cervical series associated with MGUAN PA278. Cervical vertebra are assigned a position based on their location relative to each other in order to get a general idea of the HI index for cervical vertebrae associated with *C. mukulu*.

C. mukulu (MGUAN PA278)				
cervical vertebra number	L	W	H	HI
1	30	44	31	103
2	30	54	37	123
3	36	51	38	106
4	35	52	39	111
5	31	56	43	139
6	40	62	46	115
7	48	62	43	90
8	61	71	53	87
9	58	81	59	102
C. mukulu (MGUAN PA103)	L	W	H	HI
mid-cervical	105	NA	78	74

Annex II:

Character scores for matrix of Sachs et al., (2015), Otero (2016), Allemand et al., (2017), and Otero et al., (2018)

Cardiocorax mukulu (PA278)
000010??11??10201?200?00200?00??001?00010011????0?20??1?1?00110?00??1?2010???0?10?221100
10100010?002?1201???2001???101??000????0001110011001??1?11021????111?2?3202210111??0100?
??0??????????????????????????????1

Cardiocorax mukulu (PA103)
??
??111???3?0??10??????1?0????????????????
??????2001100112021100l0?11001011??0???111??????00????30?10???????1?1??1?1???????

Cardiocorax mukulu (PA270)
??
??
??0??0???10??2?1??????????1??12??

Cardiocorax mukulu hypodigm (MGUAN PA103, MGUAN PA278, MGUAN PA270)
000010??11??10201?200?00200?00??001?00010011????0?20??1?1?00110?00??1?2010???0?10?221100
10100010?002?1201???2001???101??000????0001110011001??1?11021???[12]111?2?3202210111??01
00????????????????????2001100112021100l0?11001011??0???111??????0001?030?10??2?1??1?1??1?
11??12?1

C. colombiensis (UCMP 38349) skull scores
000010?1?1?010[12]000?00?0020??00?100??0001001010000?2010111001010?0?1???2010????11??22?
??????????0?12???200?????1?01??0??20????????01?1001??0????????????????????????????????????
??

T. haningtoni (UNSM 50132) skull and cervical vertebrae series
0?0010?0????10211220020020?0001?000100010011???0?321?11110??11????????????????????????????
??????????????????????????010???00???????0??10011?0???1?110?10?6211?022320?200111010?000???
??

S. snowii (KUVP 1301)
0?0010?0?1?0102?122002002O?0001?001?00010011???1?32??11111??11????????????????????????????
??????????????????2??10[01]110112000?122?001110011001????111??0??211?1??3?022201???1???0??
??

Character scores for Serratos et al., (2017) matrix

Cardiocorax mukulu hypodigm (MGUAN PA103, MGUAN PA278, MGUAN PA270)
000010??11??10201?200?00200?00??001?00010011????0?20??1?1?00110?00??1?2010???0?10?221100
10100010?002?1201???2001???101??000????0001110011021??1?11021???[12]111?2?3202210111??01
00??????????????????????2001100112021100l0?11001011??0???111??????0001?030?10??2?1??1?1??1?
11??12?1

Cardiocorax mukulu (MGUAN PA278)
000010??11??10201?200?00200?00??001?00010011????0?20??1?1?00110?00??1?2010???0?10?221100
10100010?002?1201???2001???101??000????0001110011021??1?11021????111?2?3202210111??0100?
??0??????????????????????????1

Character scores for O'Gorman (2020) matrix

Cardiocorax mukulu hypodigm (MGUAN PA103, MGUAN PA278, MGUAN PA270)
000010??11??10201?200?00200?00??001?00010011????0?20??1?1?00110?00??1?2010???0?10?221100
10100010?002?1201???2002???101??000????0001110011021??1?11021???[12]111?3?3202210111??02
00??????????????????????2001100112023100l0?11001011??0???111??????0001?030?10??2?0??1?1??1??
1??12?10100??100?0?0

Cardiocorax mukulu (MGUAN PA278)
000010??11??10201?200?00200?00??001?00010011????0?20??1?1?00110?00??1?2010???0?10?221100
10100010?002?1201???2002???101??000????0001110011021??1?11021????111?3?3202210111??0200?
??0??????????????????????????10
100???00?0?0

Cardiocorax mukulu (MGUAN PA103)
??
??111???3?0??10??????1?0????????????????
??????2001100112021100l0?11001011??0???111??????00????30?10???????1?1??1?1?????????????100
?0?0

Annex III:

New character for Benson and Druckenmiller, 2014 matrix

Character 271: Basisphenoid/ parabasisphenoid, length to width ratio of sella turcica (see Zverkov et al., 2017): length of sella turcica is approximately equal to its width (0); length of the sella turcica is at least 1.5 x greater than its width (1) (new character) *taxa scored from supplementary of Zverkov et al., (2017) and available literature.

C. mukulu: 1 *T. seeley*: 0

L. morgani: 1 *M. leedsi*: 0

T. keyesi: 0 *S. guilelmiimperatoris*: 0

A. quriquiensis: 0 *T. hawkinsii*: 0

E. muddi: 0 *B. brancai*: 0

Annex IV: OBJ file of *Cardiocorax mukulu* (MGUAN PA278) digital model